University of Southampton

Faculty of Engineering and Physical Sciences

Chemistry

Synthesis and Spectroscopy of Lanthanide Halide and High Oxidation State Early Transition Metal Complexes with Neutral Donor Ligands

by

Robert David Bannister

Thesis for the degree of Doctor of Philosophy

September 2019

University of Southampton

Abstract

Faculty of Engineering and Physical Sciences

Cehmistry

Thesis for the degree of Doctor of Philosophy

Synthesis and Spectroscopy of Lanthanide Halide and High Oxidation State Early Transition Metal Complexes with Neutral Donor Ligands

by

Robert David Bannister

The reaction of phosphine oxide ligands ($dppmO_2$, $dppeO_2$ or PPO_2) with $LnCl_3$, LnI_3 or $LnCl_3/[NH_4][PF_6]$ (Ln = La or Lu) are used to investigate the effect of varying metal ion radius, counter ion and ligand architecture on resulting metal complexes. The phosphine oxide ligand, $dppmO_2$, is coordinated to a range of lanthanide halides in order to further illustrate the effect of the lanthanide contraction on the coordination of this bidentate phosphine oxide.

The first examples of divalent lanthanide halide complexes (SmI_2, EuI_2, $EuBr_2$ or YbI_2) bearing phosphine oxide ligands ($OPPh_3$ or $OPMe_3$) have been isolated and characterised. The species are characterised by elemental analysis, infrared spectroscopy, UV-vis spectroscopy and $^{31}P\{^1H\}$ NMR spectroscopy. The solid state structures of $[EuBr_2(OPPh_3)_4]$ and $[EuI_2(OPPh_3)_4]$ were obtained. The products are readily oxidised to form $[LnX_2(OPR_3)_4]^+$, with $[EuI_2(OPPh_3)_4][I_3]$ being confirmed by crystallographic analysis.

A family of lanthanide (II) halide macrocyclic complexes are synthesised by the controlled addition of the macrocycle ligand to the lanthanide halide (YbI_2, EuI_2, $EuBr_2$, SmI_2). The use of mixed donor macrocyclic ligands allows for the rare coordination of soft thio- or seleno-ether groups to coordinate to hard Ln(II) metal centres.

The coordination chemistry of two series of complexes derived from $TaOCl_3$ and $TaSCl_3$ with neutral N-donor and O-donor ligands is explored. The complexes are synthesised by the addition of $O(SiMe_3)_2$ or $S(SiMe_3)_2$ to $TaCl_5$ respectively followed by the addition of the relevant neutral ligands. The complexes were characterised by ^1H and $^{31}P\{^1H\}$ NMR spectroscopy, infrared spectroscopy, elemental analysis and single crystal X-ray diffraction where possible. The crystal structures of the distorted octahedral $[TaOCl_3(1,10\text{-phen})]$, $[TaSCl_3(1,10\text{-phen})]$, $[TaOCl_3\{o\text{-}C_6H_4(P(O)Ph_2)_2\}]$, $[TaSCl_3(OPPh_3)_2]$, $[TaSCl_3\{Ph_2P(O)CH_2CH_2P(O)Ph_2\}]$ and $[TaSCl_3(MeCN)_2]$ are reported. The complexes are compared to their niobium analogues and appear to be significantly less robust and more readily hydrolysed in solution.

A series of tantalum thio-chloride complexes featuring a range of neutral chalcogenoether ligands of the form, $RE\{CH_2\}_nER$ (E = S or Se), are described. Low pressure chemical vapour deposition experiments to establish the suitability of selected candidates, as precursors, to form thin films of TaS_2 were explored, but proved unsuccessful.

Table of Contents

Table of Tables

Table of Figures

Table of Schemes

Research Thesis: Declaration of Authorship

Print name:	Robert David Bannister
Title of thesis:	Synthesis and Spectroscopy of Lanthanide Halide and High Oxidation State Early Transition Metal Complexes with Neutral Donor Ligands

I declare that this thesis and the work presented in it are my own and has been generated by me as the result of my own original research.

I confirm that:

1. This work was done wholly or mainly while in candidature for a research degree at this University;
2. Where any part of this thesis has previously been submitted for a degree or any other qualification at this University or any other institution, this has been clearly stated;
3. Where I have consulted the published work of others, this is always clearly attributed;
4. Where I have quoted from the work of others, the source is always given. With the exception of such quotations, this thesis is entirely my own work;
5. I have acknowledged all main sources of help;
6. Where the thesis is based on work done by myself jointly with others, I have made clear exactly what was done by others and what I have contributed myself;
7. Parts of this work have been published as:-

"Diphosphine dioxide complexes of lanthanum and lutetium – The effects of ligand architecture and counter-anion", Robert D. Bannister, William Levason, Gillian Reid, Wenjian Zhang, *Polyhedron*, 2017, **133**, 264-269.

"Tertiary phosphine oxide complexes of lanthanide diiodides and dibromides", Robert D. Bannister, William Levason, Mark E. Light, Gillian Reid, *Polyhedron*, 2018, **154**, 259-262.

"Complexes of $TaOCl_3$ and $TaSCl_3$ with Neutral N- and O-donor ligands – synthesis, properties and comparison with the niobium analogues" – Robert D. Bannister, William Levason, Mark E. Light, Gillian Reid, Wenjian Zhang, *Polyhedron*, 2019, **167**, 1-10.

"Chalcogenoether complexes of tantalum(V) sulphide trichloride – synthesis, properties and structures", Robert D. Bannister, William Levason, Gillian Reid, Fred Robinson, *Polyhedron*, 2019, **169**, 129-134.

Signature: Date: 06/09/2019

Acknowledgements

Firstly, I would like to thank Prof. Gill Reid and Prof. Bill Levason. I have been incredibly lucky to have you as my supervisors. Your passion, knowledge and enthusiasm has made these four years an incredible experience, and I will always be grateful for your support.

Many thanks to Fred Robinson, whose experience, and knowledge was fundamental to the work on the CVD experiments and characterisation. You were incredibly patient and always positive and I am extremely grateful for your help. Thanks to Dr. Mark Light and Dr. Wenjian Zhang who's help with solving particularly difficult crystal structures has been invaluable. Also, thanks to Dr. Peter Norton and Dr. Graham Tizzard for all their help and guidance. Crystallography has quickly become my favourite area of Chemistry in no small part due to all your support and assistance. My special thanks to Dr. Victoria Greenacre, for your help on countless occasions. You have endured a near endless torrent of questions and requests and I'm not sure how I'd have made it through this year without your support.

I would like to thank my project student, Bethany Paul, who developed a range of $[Mg(OPR_3)]^{2+}$ complexes which aided my understanding of the divalent lanthanide work. I really enjoyed working alongside you and hope you look back on the year fondly. Also, I would like to acknowledge the work of Callum Waller, who carried out preliminary reactions towards the $[TaOCl_3(L\text{-}L)]$ complexes developed herein.

Thanks to the Reid group, both current and past members. It has been an incredible experience working with you all. I hope those of you that remain enjoy your time at Southampton and that you make new members feel as welcome and at home as I have felt in this group.

I would like to thank EPSRC for funding this work and thanks to the University of Southampton for providing incredible facilities, it has been a pleasure and a privilege to study here.

Finally, I would like to thank my family. I would not be where I am today if it were not for your love and support. I love you all dearly and I'm forever grateful for the opportunities you have given me.

Definitions and Abbreviations

1,10-phen	1,10-phenanthroline
2,2’-bipy	2,2’-bipyridine
br	Broad
Bu	Butyl
cat	Catalytic
Cp	Cyclopentadiene
Cp*	Pentamethylcyclopentadiene
CVD	Chemical Vapour Deposition
d	Doublet (Describing an NMR resonance)
dppe	bis(diphenylphosphino)ethane
$dppeO_2$	bis(diphenylphosphino)ethane dioxide
dppm	bis(diphenylphosphino)methane
$dppmO_2$	bis(diphenylphosphino)methane dioxide
EDX	Energy-dispersive X-ray Spectroscopy
Et	Ethyl
fac	Facial
GIXRD	Grazing incidence X-ray diffraction
hfa	1,1,1,5,5,5-hexafluoro-2,4-pentanedione
HMPA	Hexamethylphosphoramide
HSAB	Hard soft acid base theory
IR	Infrared spectroscopy
Ln	Lanthanide
LPCVD	Low pressure chemical vapour deposition
m	Medium (Describing infrared band)
m	Multiplet (Describing an NMR resonance)
Me	Methyl
MeCN	Acetonitrile
mer	meridional
MRI	Magnetic resonance imaging
NMR	Nuclear magnetic resonance
OTf	Triflate ($CF_3SO_3^-$)

Ph	Phenyl
PPO_2	bis(diphenylphosphino)benzene dioxide
PXRD	Powder X-ray diffraction
s	Singlet (Describing an NMR resonance)
s	Strong (Describing infrared band)
SEM	Scanning electron microscopy
t	Triplet (Describing an NMR resonance)
THF	Tetrahydrofuran
UV vis	UV visible spectroscopy
w	Weak (Describing infrared band)
XRD	X-ray diffraction

Chapter 1 Introduction

The work in this thesis is concerned with developing new coordination chemistry of the hard Ln(III) (Chapter 2), Ln(II) (Chapter 3) ions with a range of phosphine oxide and macrocyclic ligands bearing hard and soft donor atoms, and high oxidation state Ta(V) oxide halide and thiohalide complexes with hard phosphine oxide and immine ligands (Chapter 4) and soft thioethers, selenoethers and phosphines (Chapter 5). This introduction serves to give a general background into some of the main aspects of the chemistry for the work described herein. A more specific overview of the background literature is presented at the start of each chapter, and these will refer back to this chemistry where appropriate.

1.1 Hard Soft Lewis Acids and Bases

The hard soft acid base (HSAB) theory was proposed in 1963 and is one of the fundamental principles of inorganic chemistry.[1] It categorises chemical species as either hard or soft acids or bases depending on a number of properties, described below, and states that hard acids prefer to bind to hard bases and soft acids preferentially bind to soft bases. The theory uses the Lewis definition of acids and bases, i.e. a Lewis acid is any substance which can accept a pair of nonbonding electrons and a Lewis base is any substance which can donate a pair of nonbonding electrons.[2] As such Lewis acids are commonly referred to as acceptors, while Lewis bases are referred to as donors.

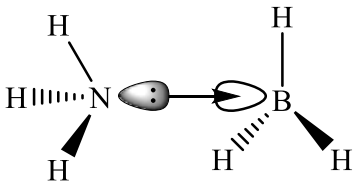

Figure 1.1. A simplified acid base reaction using an electron poor Lewis acid, BH_3, and an electron rich Lewis base, NH_3, to form an adduct.[3]

Hard acids and bases have relatively small atomic or ionic radii, high oxidation states and are not particularly polarisable. They show a preference for electrostatic bonding. Examples of

hard acids include early transition metals, the f- and s-block metals, and hard bases include fluoride ions, water, alcohols and ethers. Soft acids and bases have larger atomic or covalent radii, low or zero oxidation states and are highly polarisable. They show a preference for covalent bonding. Examples of soft acids include late transition metal ions such as silver(I), gold(II), mercury(I) and platinum and soft bases include chalcogenoethers, phosphines and carbon monoxide.[4] The hard and soft descriptions are not related to the relative strength of an acid or base; soft bases can be weak or strong bases and hard acids can be weak or strong acids. This is by no means a conclusive explanation of bonding and there are many examples of soft Lewis base donors coordinated to hard Lewis acid acceptors.[5–7] It has become an area of interest within the literature to discover the limits of this theory and understand the characteristics of the bonds that are at the limits. This work will study interactions between hard Lewis bases, particularly phosphine oxides, and hard Lewis acids, for example high oxidation state early transition metals like tantalum, Ta(V), and the lanthanide series. It will also at some soft Lewis bases, such as thioethers, with Ta(V), a hard Lewis acid. Due to the weak nature of these interactions, soft Lewis bases coordinated to hard Lewis acids are commonly displaced by hard donor solvents, water or oxygen donors and as such reactions need to be performed in weakly coordinating solvents under rigorously dry and inert conditions.

1.2 Lanthanide Chemistry

In the past the lanthanides were often overlooked due to their general inability to access oxidation states other than +3. However, with the discovery of new applications for lanthanides, such as single molecular magnets,[8–10] in catalysis,[11–13] and as MRI contrast agents (due to their luminescent properties and paramagnetism),[14–16] interest in the lanthanides has increased significantly. Due to their varying size and, therefore, charge density, their chemistry can be quite specifically tuned to their required use.

Table 1.1. The lanthanides alongside their atomic electron configuration.[17]

Element (Symbol)	Atomic Number	Electron Configuration
Lanthanum (La)	57	$[Xe]5d^{1}6s^{2}$
Cerium (Ce)	58	$[Xe]4f^{1}5d^{1}6s^{2}$
Praseodymium (Pr)	59	$[Xe]4f^{3}6s^{2}$
Neodymium (Nd)	60	$[Xe]4f^{4}6s^{2}$
Promethium (Pr)	61	$[Xe]4f^{5}6s^{2}$
Samarium (Sm)	62	$[Xe]4f^{6}6s^{2}$
Europium (Eu)	63	$[Xe]4f^{7}6s^{2}$
Gadolinium (Gd)	64	$[Xe]4f^{7}5d^{1}6s^{2}$
Terbium (Tb)	65	$[Xe]4f^{9}6s^{2}$
Dysprosium (Dy)	66	$[Xe]4f^{10}6s^{2}$
Holmium (Ho)	67	$[Xe]4f^{11}6s^{2}$
Erbium (Er)	68	$[Xe]4f^{12}6s^{2}$
Thulium (Th)	69	$[Xe]4f^{13}6s^{2}$
Ytterbium (Yb)	70	$[Xe]4f^{14}6s^{2}$
Lutetium (Lu)	71	$[Xe]4f^{14}5d^{1}6s^{2}$

It is true that the chemistry of the lanthanides is dominated by the +3 oxidation state, owing to the fact that the fourth ionization energy of these systems is greater than the sum of the first three ionization energies, meaning that any energy regained from bond formation to ligands is often not enough to overcome such a large ionization energy.

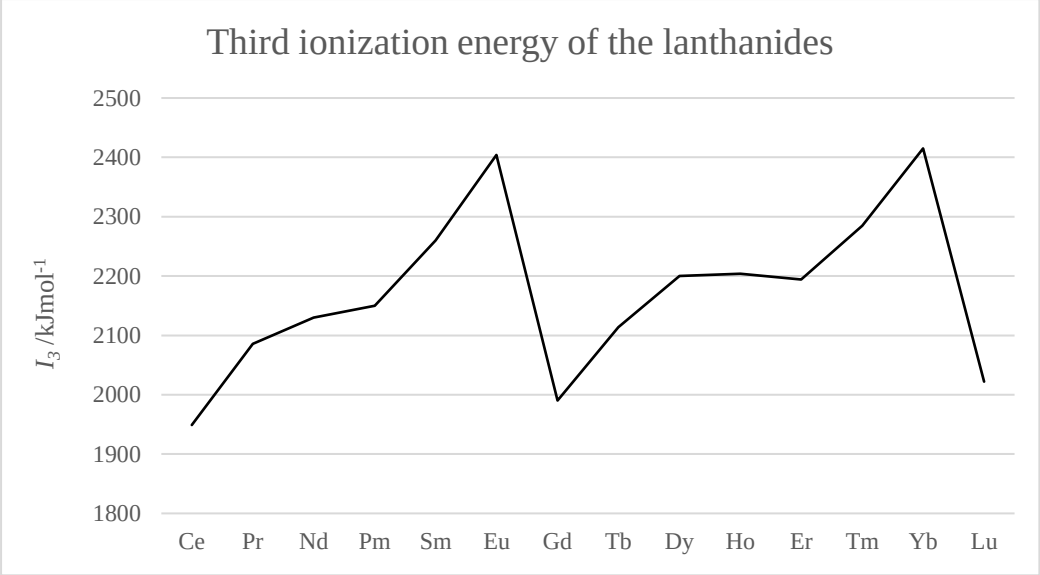

Figure 1.1. A graph plotting the third ionization energies of the lanthanides.[17]

As shown in Figure 1.2, the third ionisation energy for europium and ytterbium are comparatively very high, and also followed by a sharp drop at gadolinium and lutetium. This is because europium(II) has half filled f-orbitals, [Xe]4f^7 and ytterbium(II) has filled f-orbitals, [Xe]4f^{14}. Considering the more stable electronic configurations of Eu(II) and Yb(II) it is easy to see how these systems lend themselves well to a 2+ configuration, as indeed do samarium and thulium.[18] Similarly, the low third ionization energy of cerium explains why the 4+ oxidation state is much more readily accessible for cerium than for any of the other lanthanides. Although the 2+ oxidation state is accessible for these metals they are still readily oxidised to the 3+ state, and great care needs to be taken to avoid air, moisture or strongly coordinating solvents. A review of the relevant literature of divalent lanthanide chemistry is given in Chapter 3.

The variation in ionic radius, which steadily decreases across the lanthanide series, by 0.2 Å from lanthanum (r = 2.07 Å) to lutetium (r = 1.87 Å),[19,20] is probably one of the most widely acknowledged trends in this part of the periodic table. This effect is called the lanthanide contraction, i.e. the rapid contraction of atomic and ionic radii of the lanthanides across the series in a greater than expected decrease. This results from the 4f electrons having a very poor ability to shield the valence electrons from the nuclear charge of the atom, pulling the 6s electrons towards the nucleus. The lanthanide contraction is widely viewed as the main component of lanthanide coordination chemistry. Coordination is largely driven by electrostatic interactions and steric effects often dictate molecular geometries, so it follows that as you go across the series, the smaller size of the 3+ ion often results in smaller coordination

numbers. As the lanthanides generally adopt a 3+ oxidation state and this is spread across a smaller metal centre, there is an increase in charge density along the group, therefore lutetium is a harder Lewis acid than lanthanum.

The lanthanides, scandium and yttrium collectively are commonly described as the 'rare earth' elements, despite their relative abundance being high. Comparisons to scandium, yttrium and less commonly group 1, 2 are made when studying the lanthanides.[21,22] This is due to their hard nature and preference for oxygen donor ligands, their lability in solution and, in the case of yttrium (r = 1.90 Å), its ionic radius which is similar to that of later lanthanides such as thulium (r = 1.90 Å) or holmium (r = 1.92 Å).[19] Examples of group 1, 2 and 3 metals are also occasionally surveyed in this work as comparisons to lanthanide complexes are relevant due to their comparable hard nature. Even though they are often listed with and compared to the transition metals, Sc and Y, the lanthanides are completely unique in their chemistry. The only other series with valence f-orbitals, the actinides, display wildly different chemical properties compared to the lanthanides. The actinides display a much greater range of oxidation states, especially in the early part of the series. Due to their much larger atomic masses and high atomic numbers, the actinides are radioactive and they are also far less abundant than the lanthanides, in fact only thorium, protactinium and uranium occur naturally. Their larger size also means they are more susceptible to relativistic expansion and destabilisation of the 5f orbitals. Relativistic effects are extremely important when understanding the chemistry of heavy elements. As the mass of the nucleus increases the 1s electrons increase in velocity, which in turn increases their relativistic mass. This increase in mass leads to a contracting of the 1s orbital leading to an energetic stabilisation. As the 1s orbital contracts, it causes a contraction and stabilisation of the other s orbitals in the atom. By contrast, valence d and f orbitals are expanded and destabilised as the s orbital is contracted, due to an increased shielding of the nucleus by outer core s and p electrons. This is referred to as indirect relativistic orbital expansion. This orbital expansion is sufficient to alter the chemistry of the actinides when compared to the smaller lanthanides, which do not experience relativistic effects to the same extent. It also means the 5f orbitals are more available for bonding than the contracted 4f orbitals in the lanthanides and so bonds are often more covalent in character.[17]

1.3 High Oxidation State Complexes of Niobium and Tantalum

The group V metals, niobium and tantalum, are often discussed simultaneously due to their similar chemical properties, and as such, here M refers to both Nb and Ta unless specified otherwise. This similarity in chemical behaviour is due to their very similar atomic radii, Nb (r = 1.64 Å) and Ta (r = 1.70 Å),[19] due to the lanthanide contraction.[23] These metals exhibit a range of formal oxidation states, ranging from –III to +V.[24] There has been an increased development of Group V, specifically niobium and tantalum, chemistry over the last 15 years which can be attributed to their uses as superconductors, alongside advances in anhydrous techniques. Their high melting point and resistance to corrosion[23,25] also gives them a wide range of uses in the chemical, automotive, aerospace and medicinal industries, amongst others.[26] The coordination chemistry of these metals largely revolves around the metal halides, due to their commercial availability. Niobium and tantalum pentahalides, MX_5, are known for all halides, with bromide, chloride and iodide forming the dimeric M_2X_{10} and fluoride forming a tetramer, M_4F_{20}, Figure 1.3.[27] They are formed by the direct high temperature reaction of the elemental metal with the appropriate halide, in an inert atmosphere. The metal centres also readily react with oxygen to form M_2O_5, a compound which is inert and insoluble in most common solvents.[28] Due to the rapid formation of these oxides, the coordination chemistry of tantalum and niobium are underrepresented in the literature.

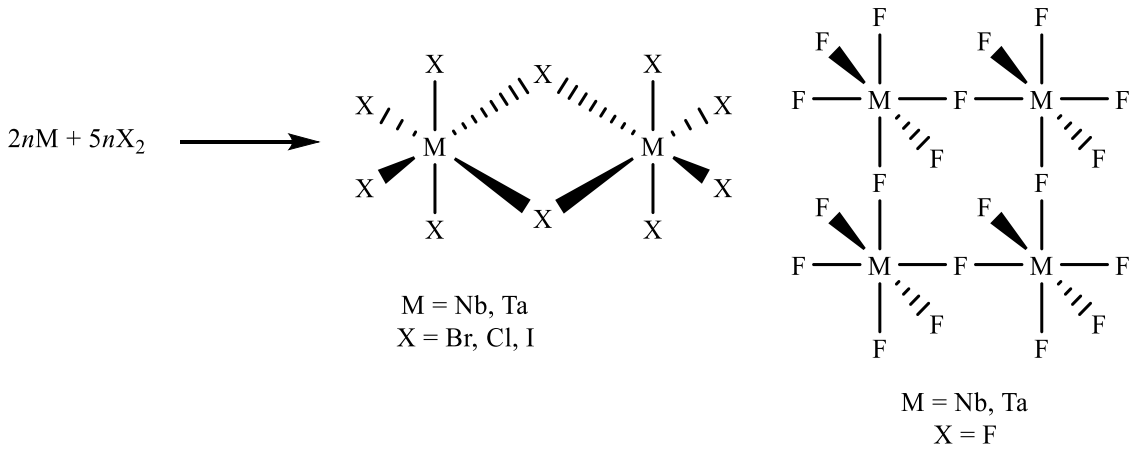

Scheme 1.1. Synthesis of niobium and tantalum halides. (n = 1 for X = Cl or Br and n = 2 for X = F).[27]

The polynuclear MX_5 unit is readily broken up upon the addition of a range of ligands and the outcome of these reactions is highly variable depending on the metal halide, the ligand and the reaction conditions. The complexes $[TaF_5(Me_2Se)]$, $[NbCl_4\{Me_2P(CH_2)_2PMe_2\}_2][NbCl_6]$, $[NbF_4(Me_2S)_4][NbF_6]$ and $[(TaCl_5)_2\{o\text{-}C_6H_4(CH_2SEt)_2\}]$ all show the variable nature of these complexes and are described in more detail in Chapter 5.

These metal halides are often a starting point of various precursors which are useful for materials chemistry, for example transition metal dichalcogenides, ME_2 (M = Nb or Ta; E = S or Se). Although transition metal dichalcogenides can be readily synthesised from their respective elements while heating, often they exhibit unique properties when formed as 2D layers. They are commonly referred to as 'inorganic graphene' and they have uses in areas such as optoelectronics, sensors, energy storage devices and electrocatalysis.[29–31] Popular methods of formation for these thin films include exfoliation of bulk samples, or chemical vapour deposition (CVD) from single or dual source precursors, Section 1.5. These transition metal dichalcogenides stack with strong bonds across the plane, but weak interactions between layers, much like graphite. They form bulk crystals on the surface of a substrate in a variety of polymorphs caused by different stacking orders. The polymorphs are named according to the crystal system, not the geometry of the species, and the number of packing layers.[32] For example three polymorphs of NbS_2 are known, 1T,[33] 2H[33] and 3R[34] (T = tetragonal, H = hexagonal, R = rhombohedral). The niobium metal centres are octahedral in the 1T system, and trigonal prismatic in the 2H and 3R. The packing of these polymorphs is particularly important as it affects the properties of the thin films. For example, 2H-$NbSe_2$ is a superconductor but 3R-$NbSe_2$ is not.[35]

1.4 Ligand Types

1.4.1 Neutral Tertiary Phosphines

Although this work deals with phosphines primarily as a starting material for producing the related phosphine oxide, they are themselves an extremely versatile and common ligand type. Phosphines, PR_3, utilise a lone pair for bonding and use a range of alkyl or aryl R groups for steric and electronic tuning. Alkyl phosphines are more difficult to handle and are more readily oxidised in air than their aryl analogues, however, they are stronger donors.[36] They exist as pyramidal structures, although they can undergo pyramidal inversion it is a much higher energy process, than in their isoelectronic amine analogues, and so is rarely observed.[37] They readily form multidentate species, such as dppm, *bis*(diphenylphosphino)methane, which allows for further tuning of the properties of the Lewis base. The benefit of using these multidentate ligands is that the chelate effect aids the formation and the stability of the complex. Phosphines are classed as soft Lewis bases and as such preferentially coordinates to soft Lewis acids, although there are a number of examples of them forming bonds with hard Lewis acids.[38–40] Phosphines are useful as the NMR active nuclei (^{31}P) provides a spectroscopic handle which is highly sensitive to its chemical environment, and as such can be used to demonstrate successful coordination of the ligand, which is of particular importance in the absence of other spectroscopic techniques.

The three R groups on the phosphine can be used to tune the electronic and steric properties of the ligand. Bulky R groups can lead to steric clashing and prevent coordination. The method typically used to quantify the steric properties of a phosphine ligand is by its 'cone angle'. While the cone angle can be easily measured from solid state structural data, it can also be calculated to a reasonable degree of accuracy where there is no available crystal structure. The Tolman cone angle, θ, can be calculated without a crystal structure, and is defined as the apex angle of a cylindrical cone formed by a point 2.28 Å from the centre of the phosphorus atom, which just touches the van der Waals radii of the outermost atoms, Figure 1.3.[41] The 2.28 Å represents an idealised M-P bond length (originally for platinum metal complexes) and wider cone angles represent a larger steric bulk. For bidentate ligands, the cone angle is derived from the outer non-bridging substituents and the bisector of the P–M–P angle.

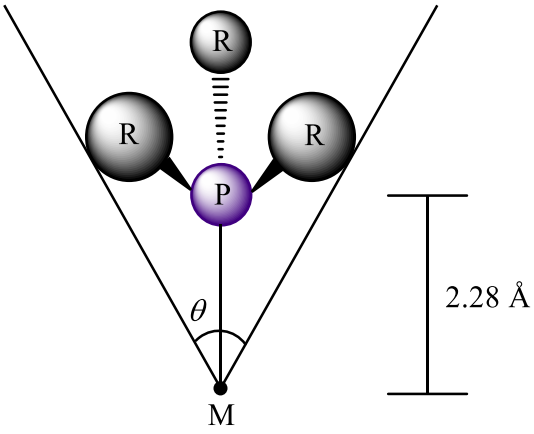

Figure 1.3. Tolman cone angle.[41]

This model has its limitations and has been found to generally underestimate the steric demands of the ligand, largely due to the assumptions present in the calculation.[42] In the absence of structural data, the calculation allows for a reasonable approximation suitable for determining trends within coordination chemistry as these cone angles serve primarily to show a trend of increasing steric bulk. Chelating phosphines also have a 'bite angle' which is important when choosing a suitable ligand system. This bite angle is the P-M-P angle, which is dictated by the constraints imposed by the backbone of the ligand, steric repulsion between the substituents and the steric and the electronic properties of the Lewis acid. In general, bidentate phosphines which coordinate to form a five-membered coordination ring are the most stable. This is because it gives the closest bite angle to 90˚ which is beneficial for both octahedral and square planar complexes.[43]

It has been shown that for monodentate phosphines, the chemical shift of a free phosphine in solution, δF, and the change in chemical shift upon coordination to a metal centre, Δ, are directly related as shown in Equation 1.1. As such the chemical shift of a complex can be predicted with a high accuracy, provided enough data about analogues are known.[44,45]

$$\Delta = A\delta F + B$$

Equation 1.1. The chemical shift of a phosphine ligand upon coordination. A and B are constants dependant on the ligand.[44–46]

Given the speed and effective cost of NMR experiments, this is an extremely powerful method of helping to determine the structure of a species. This direct relation, however, is not

applicable to bidentate phosphines. This is due to the ring contribution, Δ_R, which is defined as the difference between the coordination chemical shift, Δ, of a *cis*-disubstitued phosphine complex and the coordination chemical shift of the analogous phosphorus in a chelate complex. Table 1.2 shows the change in chemical shift from free ligand, Δ, for three chelating phosphines compared to a *cis*-disubstituted phosphine complex, $[Me_2Pt(PPh_2Me)_2]$, and the ring contribution for each of them.[46] Some approximation is required, of course, since there is no way to find an exact match of chelate and *bis*-monodentate ligand complexes.

Table 1.2. A demonstration of the ring contribution of three different samples of varying ring coordination size.[46]

Complex	Chelate ring size	Δ	Δ_R
$[Me_2Pt(PPh_2Me)_2]$	0	+34.4	N/A
$[Me_2Pt(Ph_2PCH_2PPh_2)]$	4	-17.4	-51.9
$[Me_2Pt\{Ph_2P(CH_2)_2PPh_2\}]$	5	+67.7	+33.3
$[Me_2Pt\{Ph_2P(CH_2)_3PPh_2\}]$	6	-20.5	-14.0

Complexes which have a 5-membered chelate ring show large positive ring contributions and so spectroscopic resonances tend to be found much further downfield than analogous complexes with 4 or 6 membered chelate rings.[47] Although the exact origin of the ring contribution is not clear, its existence and the resulting downfield shift specifically for 5-membered chelate rings is a widely observed phenomena.[38,48,49]

As the phosphines used in this work are primarily as a precursor for the bidentate phosphine oxide ligands, and these phosphines are commercially available, the synthesis of bidentate tertiary phosphines is mostly beyond the scope of this study. However, one method of synthesis for these phosphines is via the reduction of the appropriate phosphine oxide. Given the strength of the phosphine oxide bond (Section 1.4.2.1), powerful nonselective reductants, such as $LiAlH_4$, $HSiCl_3$ or Si_2Cl_6 are necessary for the reduction.[50]

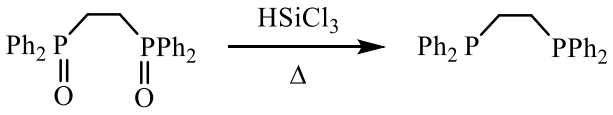

Scheme 1.2. Reduction of dppeO₂ to dppe in THF.[51]

1.4.2 Phosphine Oxides

1.4.2.1 Bonding

The P=O bond occurs in a vast number of compounds and is one of the most common functional groups. It is a very stable bond, with a dissociation energy of 589 kJ/mol,[52] and as such phosphine oxides, $R_3P=O$, are themselves stable molecules, much more so than their phosphine counterparts.[50] Phosphines can be oxidised by a range of oxidising agents and as expected, due to their inherent stability, phosphine oxides require very strong reducing agents for the reversal of this reaction to the appropriate phosphine. Their behaviour is largely contrasting to the phosphines from which they are derived, owing to the nature of the hard oxygen donor atom, which results in phosphine oxides being classified as hard bases. It is a stark difference to the structurally similar amines, which are oxidised only with powerful oxidising agents, while amine oxides are readily reduced. Phosphine oxides are often unwanted side products in phosphine coordination chemistry. However, they are, themselves, an extremely useful and versatile series of ligands. The ability to change the substituents and, in the case of bidentate ligands, the linking backbone gives an incredible level of control over the steric and electronic effects of the ligand system. Due to the extremely extensive range of P=O containing compounds, this work will focus primarily on tertiary phosphines and phosphine oxides and in the case of monodentate phosphine oxides, the substituents will all be the same in order to remove the possibility of a chiral centre.

The very nature of the phosphorus bond with oxygen has been the subject of much debate throughout its history. Early literature often described the bond as $R_3P\rightarrow O$, implying a dative bond, with the lone pair of the phosphorus filling the 'octet' of electrons on the oxygen atom. This discussion developed into the description of the bond as a formal double bond, $R_3P=O$, owing to the availability of the vacant d-orbitals of the phosphorus atom allowing for 'back-bonding' from a pair of electrons from oxygen. This would explain the differences in oxygen affinity, between phosphorus and nitrogen, as the d-orbitals would not be accessible for such 'back-bonding' in an $R_3N=O$ species. This double bond is not comparable to a C=C double bond as it does not undergo the same addition reactions to give stable adducts. There is a range of structural evidence for this multiple bond such as the d(P-O) internuclear distance of these species. For example, in H_3NO, the d(N-O) is 1.38 Å which is typical of an N-O single bond. However, the d(P-O) in H_3PO is 1.47Å. This is much shorter than the average 1.60 Å for a P-O-P single bond unit, (the average bond length, d(P-O) in the bridging molecule, containing only P-O-P units, P_4O_{10} is 1.63 Å). It was argued that the bond could, therefore, be viewed as

a double bond or even a partial triple bond.[53] Representation of the P-O bond as a formal double bond, however, is potentially problematic in part due to its clear differences from that of other double bonds, C=C or C=O for example. A range of theoretical studies show that the d-orbital has no role in the formation of valence electrons.[54] An explanation, provided by Kutzelnigg, suggests the lone pair on the oxygen atom instead 'backbonding' into the antibonding orbitals of the R_3P unit. The d-orbital, instead of being directly involved in the bonding, polarizes the other existing valence orbitals to allow for the backbonding.[53]

Another representation of the phosphorus-oxygen bond is that of an ionic component, R_3P^+-O^-. The regular σ bond causes a strong ionic charge on each atom, which then strengthens and shortens the P-O bond, giving the effect of a multiple bond.[55,56] This is important, for example, in lanthanide bonding where coordination is nearly exclusively the result of static interactions. Not only would a formally charged oxygen be more favourably coordinated by the positively charged lanthanide metal centre, but the positively charged phosphorus would be repelled leading to an Ln-O-P bond angle of nearing 180, ignoring any steric effects.[57]

The precise nature of this bond is still open to some debate, and recent works estimate the PO bond order to be ~ 1.5.[58] However it is most commonly referred to in the literature as P=O with the understanding that the bond is more complex in nature. The P=O bond exhibits a strong dipole moment and readily forms complexes with hard Lewis acids and hydrogen bond donors, unlike the soft phosphines.

Much like phosphines, phosphine oxides have similar steric concerns, due to the three substituents on the phosphorus atom. The steric properties of bidentate phosphine oxides do differ from bidentate phosphines in that coordination rings are inherently larger. The insertion of an oxygen into each M-P bond means a five-membered coordination ring is no longer achievable. An ethylene carbon backbone leads to a seven-membered coordination ring, and this can mean that polymerisation *via* the bridging of two metal centres is favourable over chelation.[59]

1.4.2.2 Synthesis

There are a number of strategies for the formation of phosphine oxides from their respective phosphines. A commonly used preparation for aryl-phosphine oxides uses aqueous H_2O_2 as an oxidising agent, Scheme 1.3.[60,61]

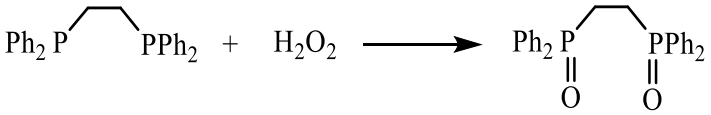

Scheme 1.3. Synthesis of dppeO_2 via the addition of H_2O_2 to dppe.[60,61]

However, hydrogen peroxide can be explosive, as demonstrated by the co-crystallisation of a small amount of H_2O_2 with a phosphine oxide product while drying which resulted in a violent detonation,[62] and so alternative routes are desirable, such as the addition of $Ph_2P(O)H$ to ethyne or 1,2-dichloroethane, Scheme 1.4. Unfortunately, these methods can lead to impure products and low yields.

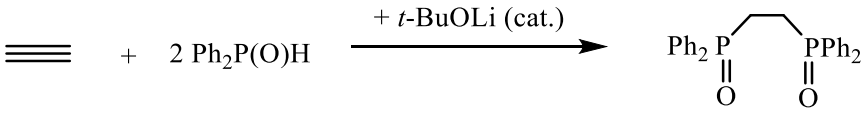

Scheme 1.4. Base-catalysed double addition of $Ph_2P(O)H$ to ethyne to form dppeO_2.[63]

Halogenation of the phosphine followed by hydrolysis readily leads to the phosphine oxide and as such, rigorously dry glassware and solvents are employed to prevent this. Later transition metals can also promote oxidation of aryl-phosphines, likely through metal-dioxygen intermediate complexes. Reactions of a range of aryl phosphines with tin (IV) iodide in dry air or O_2, in dichloromethane, have been shown to catalytically convert the phosphine into the appropriate phosphine oxide cleanly and in quantitative yields, Scheme 1.5.

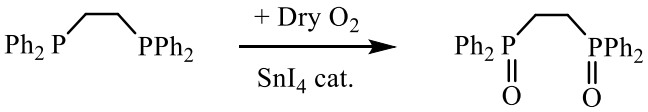

Scheme 1.5. Synthesis of bis-(diphenylphosphino)ethane dioxide by oxidation of the ligand catalysed by SnI_4.[62]

1.4.3 Macrocycles

1.4.3.1 Macrocyclic effect

Macrocycles are defined as large cyclic molecules containing, usually, three or more donor atoms which can form coordinate bonds with a metal centre. A great amount of interest in the field was generated with the work of Pedersen in 1967 on the synthesis of a series of crown ethers. The group synthesised 49 different macrocyclic compounds varying both in size and number of ethereal O-donor atoms.[64] Due to the long IUPAC names these molecules have, a

method of nomenclature has been derived to easily describe them. The crown ethers are oxygen donor macrocycles named as such: X-crown-Y, where X denotes the number of atoms in the macrocyclic ring and Y denotes the number of oxygen donors. The most common of these being 18-crown-6, which contains 18 atoms in the ring and 6 oxygen donor atoms. Replacing two of the oxygen donor atoms for selenium, for example, gives [18]aneO_4Se_2, which follows a similar naming convention, where pendant chains (if present) are named first, then the ring size, followed by the contained donor atoms in alphabetical order. This naming convention will be used throughout this work.

Macrocycles are incredibly versatile ligands, allowing for the specific tuning of a range of factors. Everything from pendant chains, to the ring / hole size to the donor atoms can be changed. It allows for an incredible level of control over a ligand environment. Initial interest in these molecules was in their synthesis, being able to produce such large rings in such a specific fashion and in such high yield. As interests shifted towards their coordination chemistry it was noted that complexes were kinetically and thermodynamically more stable than analogous compounds with non-cyclic ligands. This is because macrocyclic complexes benefit from the macrocyclic effect, which significantly increases the thermodynamic driving force for binding these ligands to metal centres. It is well established that multidentate ligands form more stable compounds than their monodentate counterparts due to an increased entropic stability, this is known as the chelate effect. Macrocycles, however, form more stable complexes than open chain multidentate ligands as they are pre-organised for binding to a metal centre. Unlike the chelate effect, the macrocyclic effect does not have a common origin solely in its entropic term, though there is an entropic element to the macrocyclic effect. There is also an additional energetic contribution due to the preorganised nature of the rings meaning there are no additional strains introduced upon coordination. While it is not possible to ascribe a single origin to the effect, although the resulting stability has been experimentally observed.[65]

The ability to replace donor atoms allows for mixed donor macrocyclic ligands, ligands which contain more than one type of donor atoms, combining two or more different bonding preferences. One example is named above, [18]aneO_4Se_2, which contains four oxygen donor atoms and two selenium donor atoms, Figure 1.4. The oxygen donor atoms preferentially bind to a hard Lewis acid metal centre causing a close proximity of the very soft selenium donors to the metal centre, leading to soft donor - hard acceptor interactions.

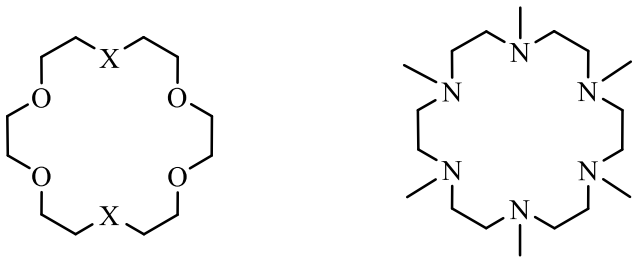

X = O; 18-crown-6
X = NH; [18]aneN_2O_4
X = S; [18]aneO_4S_2
X = Se; [18]aneO_4Se_2

Me_6[18]aneN_6

Figure 1.4. The macrocyles used in this work.

It is easy to envisage macrocyclic complexes as an equatorial ring, with the donor atoms in a coplanar arrangement. This is sometimes the case, and depends somewhat on the flexibility of the ring. However, it is not always the case that hole size directly correlates to metal ion discrimination. Due to the flexibility of the large rings, the selectivity of macrocycles is instead dictated by the stability of the conformers of the macrocycle.[65–67] An extreme example of this is shown in a macrocyclic sodium complex, Figure 1.5. Homoleptic octathia coordination of a macrocycle to a sodium ion gives [Na([24]aneS_8)][BArF].[68] The hole size is clearly too large for the metal centre, so instead of wrapping around it, the macrocycle is distorted, to allow each of the donor atoms to interact with the metal centre.

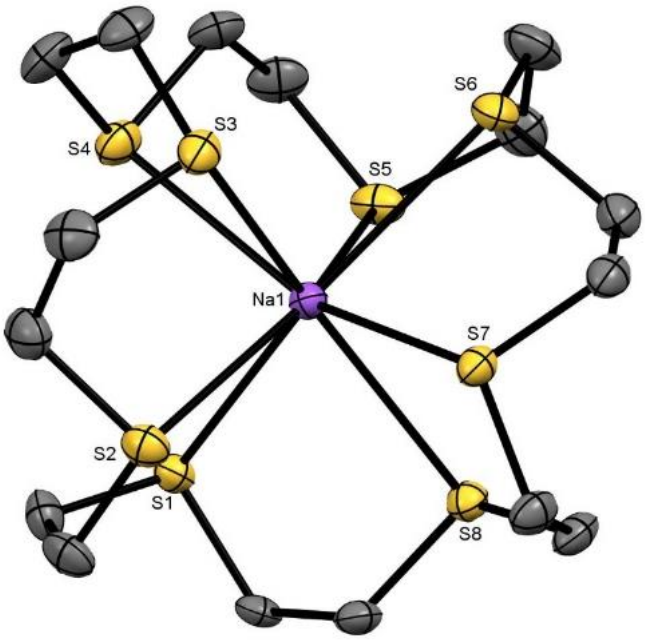

Figure 1.5. A crystal structure of the cation of [Na([24]aneS$_8$][BArF] showing homoleptic octathioether macrocyclic coordination to Na$^+$.[68]

The remarkable eight-coordination complex is the first example of a very hard group 1 metal macrocycle complex containing only S donors in the macrocycle. Examples of mixed donor macrocycles on divalent lanthanides,[69] group 1,[70] group 2,[71,72] and early transition metals[73] have also been demonstrated.

The way in which a macrocyclic ligand coordinates to the metal centre is important for the rate of formation of these complexes. In general, macrocyclic complexes form slower than their open-chain analogues. They form following the Eigen-Wilkins mechanism, an associative substitution, followed by an interchange process, with one of the donor atoms within the macrocycle replacing one of the other ligands. This is repeated until all of the donor atoms are coordinated to the metal centre. Unlike open chain ligands, in which the first step is most often rate determining, any of these steps can be rate determining. It is dependent on the flexibility of the macrocyclic ligand, and its ability to 'stretch' around the metal centre. Unlike open-chain ligands, macrocyclic ligands cannot freely rotate to position the next donor atom next to the metal centre, and instead must rely on high energy conformations leading to higher energy barriers. It is for this reason that, once coordinated, these complexes are so stable. Removal of a macrocyclic ligand requires a stepwise 'peeling off' of the donors.

1.4.3.2 Synthesis

It is also pertinent to discuss the synthesis of macrocyclic complexes, which can often be challenging in itself. The synthesis of large macrocycles generally involves one or two long carbon chains with reactive groups on each end. Different methods can be employed to bring these chains together and replace the leaving group with a linker atom. This is generally performed by one of two different methods, templated and non-templated synthesis. Non-templated synthesis uses dilute solutions of the long chains to promote cyclisation, Figure 1.6. Templated synthesis uses a central atom that the long chain is wrapped around, usually a metal centre, which pre-organises the starting materials in such a way that cyclisation is favoured over polymerisation, Figure 1.7.

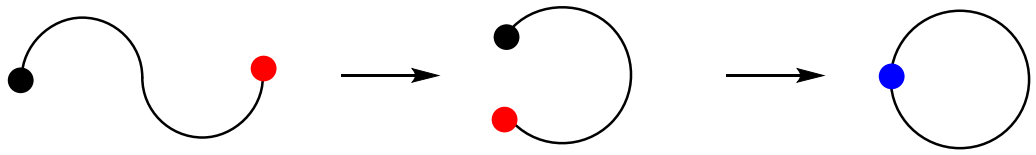

Figure 1.6. The visual representation of the synthesis of a macrocycle via high dilution or disguised dilution synthesis.

Non-templated macrocycle synthesis often uses large volumes of solvent, in high dilution syntheses, and is less environmentally friendly. It is also more likely to lead to smaller or larger macrocycles than the desired product, or oligomers and polymers can be formed. High dilution experiments can take days of stirring, very slow addition of reactants, maintaining consistent concentration of the starting material can be experimentally challenging. Another method similar to this is called disguised dilution, whereby one of the reactants is very poorly soluble in the selected solvent system. Minimal amounts of that reactant will dissolve into the solvent at any given time again, allowing for an increased chance of cyclisation instead of polymerisation.[74] An example of a high dilution reaction can be seen below, Scheme 1.6.

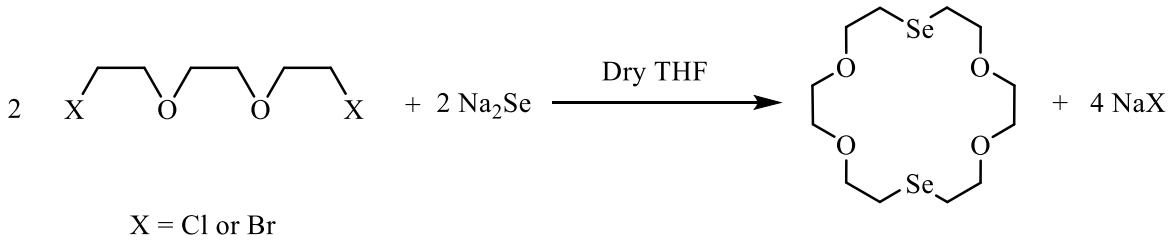

Scheme 1.6. Synthesis of [18]aneO$_4$Se$_2$ via the high dilution reaction of Na$_2$Se with 1,2-bis(2-chloroethoxy)ethane.[75]

A further problem that arises from these reactions is that often the reactants are highly moisture sensitive and so rigorous anhydrous conditions are required to be maintained in large quantities of solvent for long periods, often days, at a time. In addition to this, even by avoiding polymerisation, the addition of the reactants can lead to several products in the form of different ring sizes. The reaction in Scheme 1.6 shows only the [2+2] product, [18]aneO_4Se_2, however, the reaction also yields the [1+1] product [9]aneO_2Se.[75]

Instead of high dilution, a template can often be used to give specific ring sizes in increased yields. The condensation of $Cl(CH_2)_2O(CH_2)_2Cl$ with $HO(CH_2)_2O(CH_2)_2OH$ can give rise to many different products including the oligomer, the [1+1] product (12-crown-4) and the [2+2] product (24-crown-12). In a scenario whereby only one of these macrocycles is desired, the addition of different bases can be used to ensure an increased yield of a specific product. For example, the addition of LiH produces the smaller [1+1] product, whereas the addition of NaOMe produces the larger [2+2] product. While the advantages of this method are obvious, the disadvantages include that the products formed will usually contain the metal coordinated to the macrocycle and extracting the free ligand from these systems is challenging, especially if the ligand systems are particularly fragile. In some cases the desired metal can be coordinated either by using the metal centre as the template, or by a metal exchange reaction if possible. However, more common methods of liberating the free macrocycle include harsh reaction conditions which can fragment the ligand.[65]

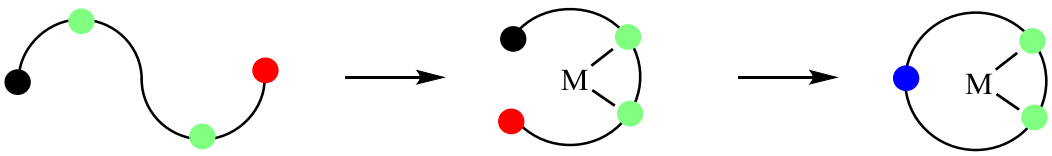

Figure 1.7. The visual representation of the templated synthesis of a macrocycle.

1.4.4 Chalcogens

1.4.4.1 Chalcogenoether bonding

Chalcogenoethers (ER_2; E = S, Se or Te) are a series of ligands using S, Se and Te donor atoms. Thioethers are soft Lewis bases and the ligands get softer as you go down the group. The coordination of these ligands to transition metals has been the focus of much attention over the last 20 years.[76,77] Although similar in some ways to the group 15 donors, (such as phosphines), the group 16 chalcogenoethers do not have the same sort of steric hindrances, with only two substituents per chalcogen. This means the electronic factors involved with these ligands are much more important. The neutral chalcogenoether, ER_2, has two lone pairs of electrons on the donor atom. One pair typically forms a σ-bond with a σ-acceptor with the second lone pair remaining non-bonding. Examples of the second lone pair bridging two metal species are known, such as $[Ta_2Cl_4(S^nBu_2)_2(\mu\text{-}Cl)_2(\mu\text{-}S^nBu_2)]$, Figure 1.8.[78]

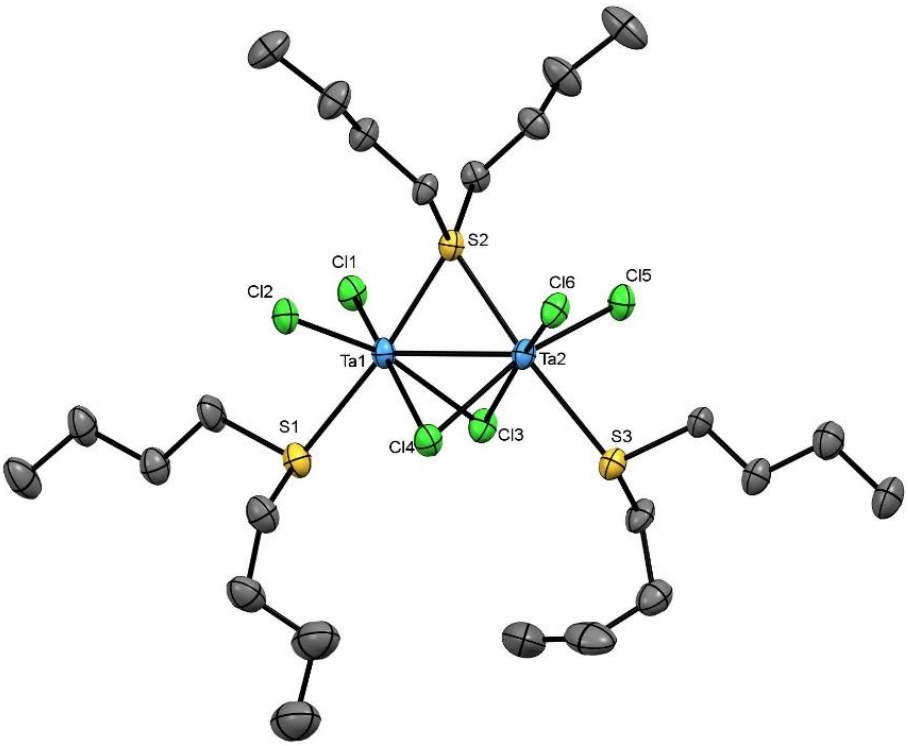

Figure 1.8. The structure of $[Ta_2Cl_4(S^nBu_2)_2(\mu\text{-}Cl)_2(\mu\text{-}S^nBu_2)]$ showing a bridging monodentate thioether.[78]

Upon descending Group 16, the increased shielding from the nucleus means the valence electrons of tellurium are much more diffuse than in those for sulfur, and as such tellurium is much softer than sulfur. Owing to poor orbital overlap between the valence shell of tellurium and the valence shell of carbon, telluroether ligands are particularly unstable and so complexes using these ligands are much less common. The diffuse orbitals also interact poorly with the contracted orbitals of hard high oxidation state early transition metals. As such they will be addressed in this work, where appropriate, but are not the primary focus.

Although chalcogenoethers can carry two differing R groups, upon coordination to a metal centre the species becomes chiral. This is avoided in this work by using the same R groups on monodentate ligands. The bidentate species, $RE(CH)_xER$, fundamentally have differing substituents on the chalcogen atoms. Coordination to a metal centre, therefore, gives rise to a *meso* form and a pair of *DL* diastereoisomers, Figure 1.9. While these often form mononuclear species, there are also examples of bidentate chalcogenoethers acting as bridging ligands between two metal centres, these are discussed in Chapter 5. The interconversion of diastereoisomers by pyramidal inversion can be rapid, but is often observed in NMR experiments cooled to low temperatures.[76,79–82] Factors affecting the rate of this pyramidal inversion include the metal centre and oxidation state of the metal, the chalcogen, the ligands *trans* to the chalcogens, the substituent on E and the chelate ring size.[76]

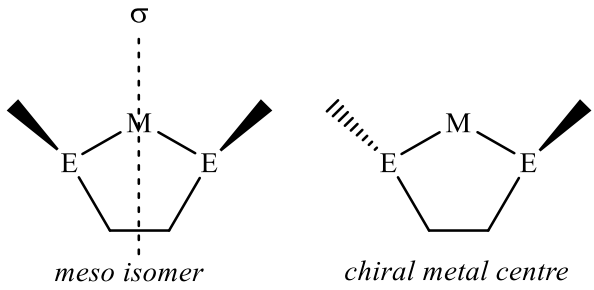

Figure 1.9. A visual representation of a meso isomer (left) and chiral metal centre forming one of a pair of D/L stereoisomers.

1.4.4.2 Chalcogenide Ions as Ligands

This work also deals with chalcogenide ions, E^{2-}, as electron rich ligands. Terminal coordination of chalcogens occurs mostly in early transition metal complexes in high oxidation states, though they can exist also as bridging ligands. Examples include tetrahedral anions ME_4^{n-} (M = V, Nb or Ta, n = 3; M = Mo or W, n = 2) but also the cluster anions $[M_6S_{17}]^{4-}$ (M = Nb or Ta), showing the versatility of the sulfide ligands. The ability to form bridging species

increases down the group as selenium and tellurium have larger ionic radii. Chalcogenohalides are known for a range of transition elements,[83,84] although their coordination chemistry is less explored than that of the corresponding metal halides or metal oxy-halides.[24] This work will focus specifically on $NbSCl_3$ and $TaSCl_3$, and a review of their coordination chemistry is discussed in Chapters 4 and 5. Several synthetic routes to $NbSCl_3$ and $TaSCl_3$ have been described, alongside their analogous bromides. They are formed by reacting the relevant metal halide with a chalcogen source, such as H_2S,[85] Sb_2S_3[86,87] or $S(SiMe_3)_2$[88,89] in a non-competitive solvent. Chalcogenides are good ligands for single source CVD precursors as they increase the ratio of chalcogen to metal within the precursor, as described in Section 1.5.2.

1.4.4.3 Synthesis of Chalcogenoethers

As with many of the ligand systems described here, there are an extensive range of ligands of this type and several synthetic routes to reach them. A number of more common simple monodentate thioethers such as Me_2S, $^nBu_2S$ and Ph_2S are commercially available. However, given the volatility and stench of some of the thioethers, and their niche uses, many have to be prepared. $MeSCH_2CH_2SMe$ (dithiahexane) can be prepared from the addition of methyl iodide to the dithiol, $HSCH_2CH_2SH$, in the presence of a base, Scheme 1.7.[61]

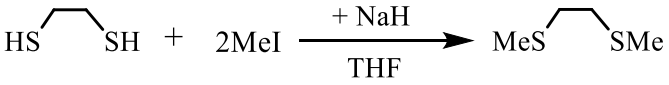

Scheme 1.7. Synthesis of $MeSCH_2CH_2SMe$.[61]

A similar method can be used to synthesise ^{i}PrSCH2CH2S^{i}Pr, instead using two molar equivalents of 2-propanethiol and a dihaloalkane, for example $BrCH_2CH_2Br$, to add the substituents to the ethylene linker, Scheme 1.8.[90] Most bidentate thioethers with aliphatic backbones can also be produced by a similar attack of RS^- on the appropriate haloalkane, including the thioethers used in this work, $RS(CH_2)_nSR$ (n = 2, R = Me, ^{i}Pr or Ph; n = 3, R = Me or ^{n}Bu).[76] Both thiols and disulfides are commonly commercially available starting materials.

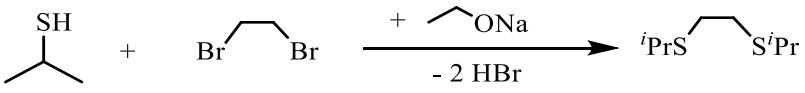

Scheme 1.8. Synthesis of ^{i}PrSCH$_2$CH$_2$S^{i}Pr.[90]

Synthesis of the aryl thioethers can be a little more complicated. Initial synthetic methods were performed by the reaction of the appropriate copper thiolate with dihalobenzene in quinolone / pyridine.[91] This method avoids the use of high temperatures and particularly reactive substances.[92,93] However, reaction yields are variable and copper reagents can be difficult to work with. Testaferri *et al.* developed a synthetic method using the reaction of halobenzenes with Me_2CHSNa in HMPA to give *o*-$C_6H_4(SCMe_2)_2$, Scheme 1.9.[94] This can be converted to *o*-$C_6H_4(SMe)_2$ or *o*-$C_6H_4(SH)_2$ *via* the addition of excess sodium and either MeI or HCl respectively. This synthetic route not only eliminates the need for a copper thiolate reagent, but can also produces the ligand in good yield. Direct formation of the methylthio- or ethylthio-benzenes requires careful control of the reaction conditions as the initially formed products further react with excess RSNa to give the respective aromatic thiols.[95]

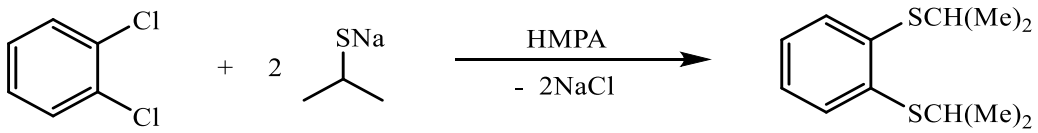

Scheme 1.9. Synthesis of o-$C_6H_4(SCHMe_2)_2$ in HMPA. Formation of the respective methyl thiol analogues can be formed via the addition of MeI or HCl to the final product.[94]

Selenols, RSeH, are not commercially available, likely because of their poor stability, and as such the selenoethers are often prepared from the addition of a dihalo-alkane to a combination of elemental selenium and a lithium reagent in THF, Scheme 1.10.[96]

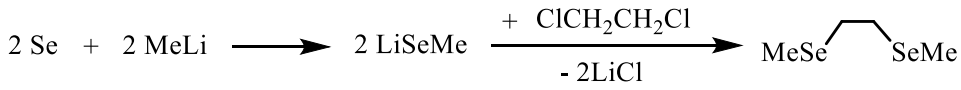

Scheme 1.10. Synthesis of $MeSeCH_2CH_2SeMe$ from MeLi and selenium.[96]

Selenoethers are often prepared from the addition of a halo-alkane to a combination of elemental selenium and a lithium reagent in THF, Scheme 1.11.[96] Monodentate selenoethers, R_2Se, can be made similarly,[76] and the more common ligands, such as Me_2Se, Et_2Se and Ph_2Se, are commercially available. Although other synthetic methods are available, this is a more convenient synthetic method for the synthesis of $MeSeCH_2CH_2SeMe$ than the alternatives. These include forming NaSeMe in liquid ammonia to add to a haloalkane,[97] the addition of

Me_2Se_2 to a haloalkane in the presence of KOH at high temperatures,[98] or bubbling ethene through a solution of Me_2Se_2, in the presence of $SnCl_4$.[99]

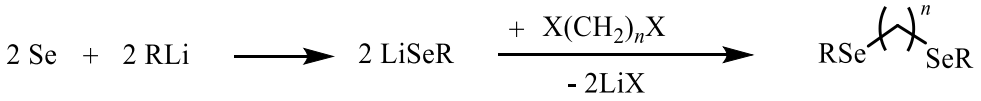

Scheme 1.11. General synthetic method for $RSe(CH_2)_nSeR$ from RLi, elemental selenium and a halo-alkane in a THF solution.[96]

Bidentate tellurides have proven much more difficult to synthesise, owing to the poor orbital overlap between tellurium and carbon. This poor orbital overlap means telluroethers are often oxygen sensitive, unlike the analogous selenoethers or thioethers which are air stable.[77] Tellurium also forms very weak bonds with hydrogen, resulting in tellurols being very poor reagents. Due to their sensitivity, coupled with their malodorous nature, they are less extensively researched than thioethers and selenoethers.[7,77] Dimethyl telluride can be synthesised similarly to the analogous selenoether, *via* formation of the MeTeLi species, addition of excess MeI followed by dealkylation with PPh_3.[76]

The synthesis of the bidentate species, $RTe(CH_2)_nTeR$, have proven much more difficult than for the thio- or selenoethers, and species are only known for certain values of *n*. Attempts to form $MeTe(CH_2)_2TeMe$, through a preparation similar to the synthesis of $MeSe(CH_2)_2SeMe$, (Scheme 1.11), at -198 ˚C, result in Me_2Te_2 and ethene.[100,101] The synthesis of $RTeCH_2TeR$ (R = Me, Et, ^{i}Pr, ^{n}Bu, Ph etc.) are known and these can be synthesised via the addition of RTeTeR to a haloalkane in the presence of a base. When reacting $X(CH_2)_3X$ with RTeTeR at room temperature olefins are produced, although reactions at low temperatures give high yields of $RTe(CH_2)_3TeR$.[100]

1.4.5 Pyridyl ligands

Both 2,2'-bipyridine, (bipy), and 1,10-phenanthroline, (phen), are hard Lewis bases. They are chemically quite similar, however, phen is a more rigid ligand than bipy, pre-organised for bonding due to the aryl backbone. They coordinate to most transition metals, and bind *via* both σ donating nitrogen atoms. Bipy is commonly depicted with its nitrogen atoms in a *cis* formation, however, its lowest energy conformation is with the nitrogen atoms in a *trans* position and as such is not pre-organised for coordination.[102] Despite the aryl backbone in phen providing a better steric configuration for coordination, it is a weaker donor than bipy. Both species form stable five-membered coordination rings with most metals on the periodic table.

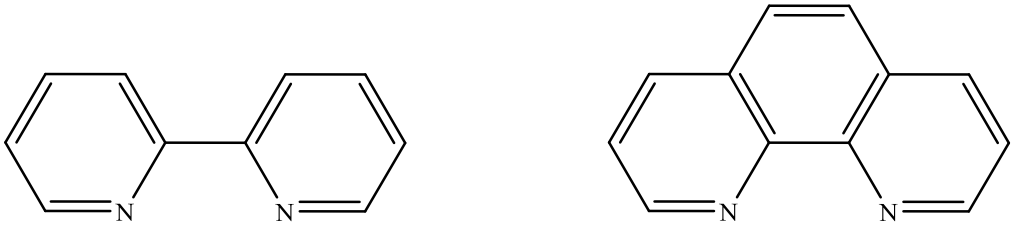

2,2'-bipyridine *1,10-phenanthroline*

Figure 1.10. The structures of 2,2'-bipy and 1,10-phen.

1.5 Chemical Vapour Deposition

1.5.1 Deposition Experiments

Chemical vapour deposition is a technique used to coat a substrate with 2D films of a desired material. For example, layered transition metal dichalcogenides ME_2 (M = Nb, Ta, V, W, Mo etc; E = S, Se or Te) are inorganic analogues of graphene, and their band gaps and other properties can be tuned by varying the chalcogen or the metal. Applications of these dichalcogenide thin films include spintronics, sensors, magnetic materials, optoelectronics and electrocatalysis.[29,30,103–105] The production of thin films of these materials is of particular importance since this maximises the anisotropy of the electrical or magnetic properties when compared to the bulk properties.[106] Chemical vapour deposition is a thermally driven technique which involves the decomposition of a precursor containing the desired elements. The products are then formed on a heated surface from the elements of the precursor. The advantage of using chemical vapour deposition over other methods of deposition is the ability to form very thin films. The method of CVD used in this project is Low Pressure Chemical Vapour Deposition, LPCVD, in which deposition are performed under vacuum and precursors are decomposed with heat. An example of a common CVD set up can be seen below, Figure 1.11.

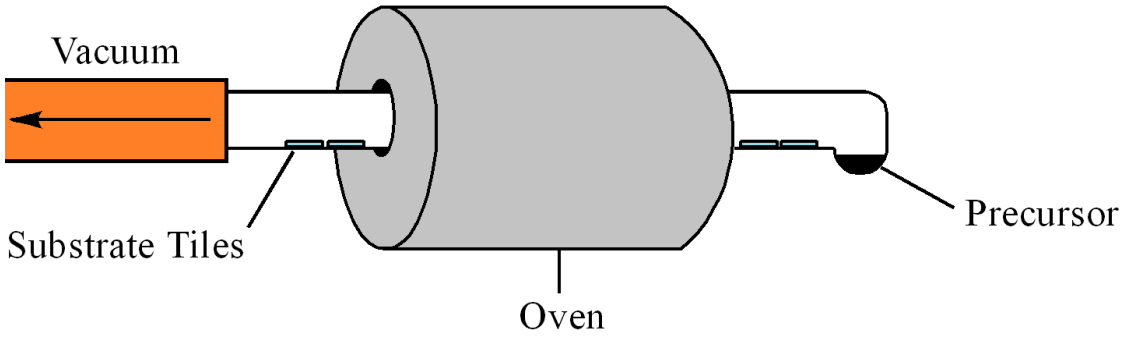

Figure 1.11. A typical set up for LPCVD. The precursor is loaded into the tube and stored in the bulb on the right. Substrates are placed inside the tube at either end of the tube furnace. The arrow represents a vacuum as this is a closed system under vacuum.

1.5.2 Precursors

Chemical vapour deposition experiments can be performed using either single source or multi-source precursors, Figure 1.13. Single source precursors contain all the components of the target phase within a single covalent, molecular or coordination complex, ideally for this work, with a suitable ratio of M:E atoms (M= metal and E = chalcogenide). In contrast dual or multisource precursors consist of separate molecules, each providing one of the target elements in smaller molecules.

As single source precursors contain all the required atoms in a single compound, they tend to have higher molecular weights than dual-source precursors, this leads to greater stability than but also means they are less volatile, this is especially true with heavier atoms, (precursors involving selenium or tantalum for example), as higher temperatures are required to volatilise the sample.

The specialised nature of these compounds means they are generally not commercially available and therefore require synthesis. Dual or multi-source precursors consists of lighter, more volatile molecules which are generally commercially available, however, the lower molecular weights result in them being less stable, therefore they are often more toxic and pyrophoric. There are also engineering controls to consider for multisource precursors in order to deliver multiple precursors in the heated chamber in a controlled fashion

To ensure minimal impurities in the thin films, precursors are designed to have facile decomposition pathways, forming volatile by-products. For example, alkyl chains, commonly ethyl or butyl groups, are often employed to stabilise the precursors, as these can undergo β-hydride elimination, (Figure 1.12) to facilitate the removal of gaseous ethene or butene.

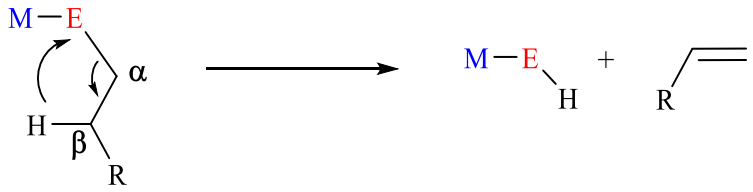

Figure 1.12. A diagram showing β-hydride elimination pathway.

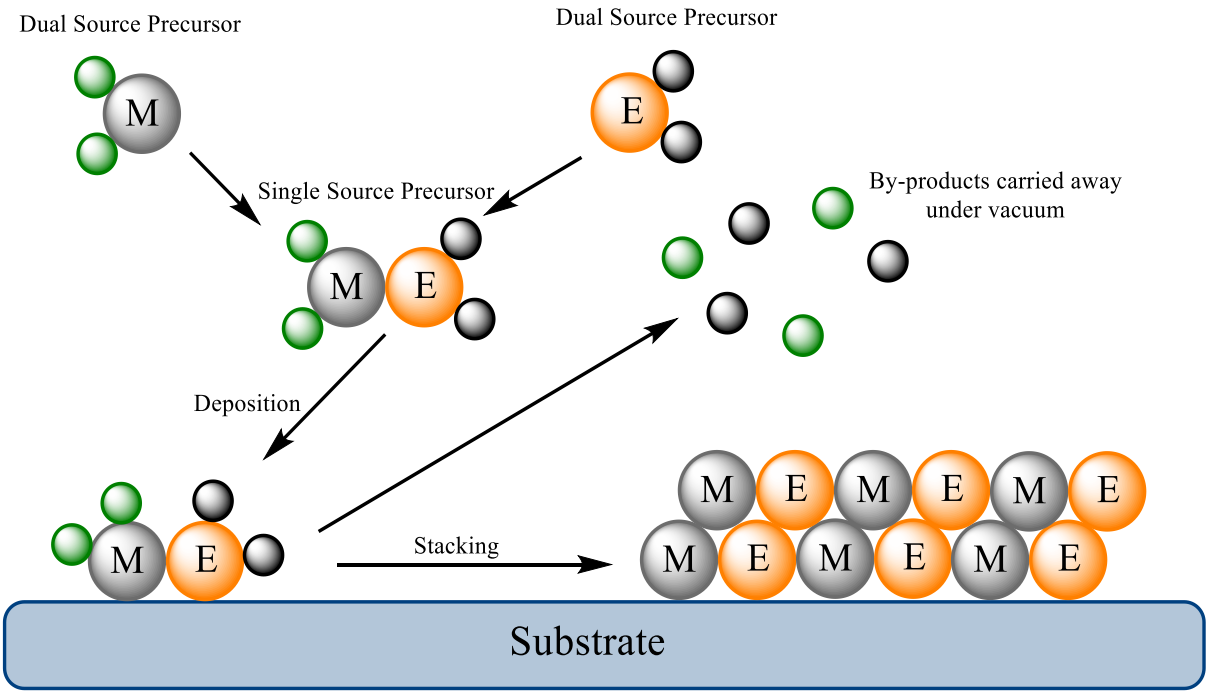

Figure 1.13. Deposition of a thin film of a desired material onto a substrate via a single source or dual source precursor.[106]

1.6 Analytical Techniques

1.6.1 Infrared Spectroscopy

Bonds have specific vibrational energies and definite vibrational transitions. When infrared radiation of quantised energy, corresponding to a discrete vibrational level of a bond, is absorbed the bond begins to vibrate. This absorption can be measured against a pre-recorded background, leading to an IR spectrum. Infrared spectroscopy is a useful, cheap and fast method of characterisation, and is used for identifying key functional groups or types of bonds in a species. Key vibrational bands lie in the 'fingerprint' region (1500 – 200 cm^{-1}). This technique is useful for showing coordination of ligands, as functional groups such as P=O which show characteristic peaks at ≈ 1100 cm^{-1}, and shift upon coordination to a metal centre. It can also be used to show the presence or absence of certain solvents, for example water has very large broad bands at 3500 – 3300 cm^{-1} and a band at 1650 cm^{-1}. The presence of Ta=S (500 - 520 cm^{-1}) or a Ta=O (920 – 940 cm^{-1}) stretches are important for showing the incorporation of the terminal bond. Metal halide bonds, M-X, have characteristic stretches between 200 and 600 cm^{-1} and can provide information about the symmetry of the molecule with group theory. For example, this work contains many octahedral complexes with three coordination sites occupied by chlorides and three occupied by other atoms, which can be represented as L and the molecule represented by MCl_3L_3. The geometry could be *facial* or *meridional*. *Fac* complexes, of the form MCl_3L_3, exhibit a C_{3v} symmetry and are expected to show two IR active M-X bands (a_1 + e), whereas *mer* complexes exhibit C_{2v} symmetry and thus are expected to show three IR active M-X bands ($2a_1$ + b_1). Some care must be taken as solid state effects and intermolecular interactions can cause a broadening of peaks such that bands coincide with other bands. Lanthanide halide stretches are often observed at values below 200 cm^{-1} which is beyond the range of the equipment available,[107,108] as such these are not assigned in this work and single crystal X-ray diffraction, where possible, provides a better technique for confirming the presence of halides in the metal coordination sphere. Infrared spectra are collected as Nujol Mulls over the range of 4000 – 200 cm^{-1} using CsI disks, as samples are air and moisture sensitive, and the mull will help to protect them. CsI disks are also not IR active above 200cm^{-1} so do not interfere with the spectra of the samples.

1.6.2 NMR Spectroscopy

Many of the other analytical techniques described here are used for analysing a species in the solid state, however, metal complexes can often behave differently in solution. Nuclear Magnetic Resonance Spectroscopy (NMR Spectroscopy) is an extremely powerful tool, most commonly used for analysing molecular systems in the solution state. It can provide information about geometries, symmetry and stoichiometry. It is complementary to techniques such as single crystal XRD as it provides information about the species in a dynamic environment, but cannot provide structural data such as bond lengths and angles. NMR spectroscopy can be used to probe an extensive range of nuclei. The properties of the relevant NMR active nuclei are shown below, Table 1.3.

Table 1.3. Nuclear properties of the relevant NMR active nuclei.[109]

Nucleus	Spin	Abundance (%)	MHz
^{1}H	1/2	100	100
^{31}P	1/2	100	40.48
^{33}S	3/2	0.76	7.67
^{77}Se	1/2	7.58	19.07
^{125}Te	1/2	6.99	31.54

NMR spectroscopy is commonly used to observe the difference in the chemical shift from free ligand to coordinated ligand. ^{1}H NMR spectroscopy is particularly useful for bidentate ligands, as many of the species in this work contain asymmetric metal complexes, and the inequivalence of the donor atoms leads to inequivalent protons on the backbone of the ligand. For example, one of the advantages in using ^{1}H NMR spectroscopy within this work is that at low temperatures it is used to identify DL and *meso* isomers trapped by slow pyramidal inversion causing a separation of resonances.

The ^{31}P isotope is 100% abundant, spin 1/2 and has a relatively high receptivity and as such is a widely used nuclei for NMR spectroscopic studies. Unfortunately, in the case of paramagnetic systems, ^{1}H NMR spectra can be complicated and uninformative, and a multinuclear approach is required to identify a compound. This work deals with phosphorus proton decoupled NMR spectroscopic experiments, denoted as $^{31}P\{^{1}H\}$ NMR spectroscopy. There is no coupling from the phosphorus to other nuclei in any of the species and so by removing any proton coupling simplifies the spectrum and allows the direct study of the position of the free phosphorus ligand and the chemical shift once the ligand is coordinated to a metal centre can be observed. Due to

the sensitivity of the chemical shift the free phosphine ligands used in this work (dppm, dppe and *o*-($C_6H_4P_2Ph_2$)) can be easily distinguished from the corresponding phosphine oxides and these shifts are also very different from those of the metal phosphine oxide complexes.

Although sulfur contains a spin active nuclei, ^{33}S, sulfur NMR is relatively uncommon. This is due to ^{33}S being spin 3/2 and so quadrupolar relaxation and a low receptivity, means only highly symmetrical compounds are suitable for running ^{33}S NMR experiments. As such it is not used as a spectroscopic handle in this work. However, ^{77}Se has a spin 1/2 and a susceptibility of 2.98 relative to ^{13}C, so despite its relatively low abundance, 7.58 %, $^{77}Se\{^1H\}$ experiments are quick and informative. This makes it an ideal nuclei for the determination of successful coordination to a metal centre. Continuing down group 16, tellurium has two NMR active nuclei, ^{123}Te and ^{125}Te. ^{125}Te is more receptive than ^{77}Se, it has spin 1/2 and a similar natural abundance and so in principle it is a good nuclei for NMR spectroscopy. However, given tellurium has poor orbital overlap with carbon, it is less useful as a ligand in the systems used in this work.[109]

Paramagnetism plays an important role in lanthanide systems and due to their paramagnetic properties they are often used as shift reagents for deconvoluting complex peak patterns. Complexes such as *tris*-(2,2,6,6-tetramethylhepta-3,5-dionato)-europium (III) ($Eu(tmhd)_3$), Figure 1.14, can be added to solutions of complex organic species.[110–112] The effect of the unpaired electron causes a shift of the resonances. The observed chemical shift is affected by the number of unpaired electrons on the lanthanide centre used and therefore different metal centres will give rise to vastly different chemical shifts. The change in these chemical shifts is not always linear or proportional to the number of unpaired electrons, an increase in the number of unpaired electrons does not mean an increase in the chemical shift. Another interesting feature of lanthanide paramagnetism in ^1H NMR spectroscopy is that, although it leads to significant shifts of the proton resonances, it often does not lead to significant peak broadening, therefore splittings can still be observed. This is why lanthanide complexes make good shift reagents. These lanthanide shift reagents briefly interact with the organic compounds resulting in a small change in chemical shift. In the lanthanide phosphine oxide systems described within this work, ligands are directly coordinated to the metal centre and they are more greatly affected by the unpaired electrons in the lanthanide metal centre, leading to broader peaks and much larger changes in the chemical shift. In the lanthanide phoshine oxide complexes, phosphorus atoms are separated from the metal centre by two bonds (Ln-O-P) and so experience significant shifts and peak broadening. The $^{31}P\{^1H\}$ NMR spectra are still important as they provide information about other possible species in solution, such as *tris* or *tetrakis* products. Also upon

oxidation the metal centre loses an unpaired electron and this leads to a significant effect in the position of the observed resonance, so the spectra are used to show product degradation.

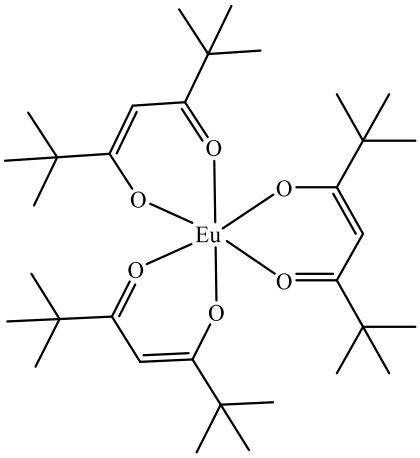

Figure 1.14. Tris-(2,2,6,6-tetramethylhepta-3,5-dionato)-europium (III), a shift reagent.[110]

The paramagnetic shift of lanthanide systems can be attributed the interaction of the spin active nuclei on the ligand to the electronic spin of the unpaired electron in the lanthanide ion. This interaction can be separated into two components, the Fermi-contact shift (often referred to as the contact-shift) which is a contact shift through bonds and the pseudo-contact shift (also called the dipolar shift) which is a contact shift through space.[113] The Fermi-contact shift is an effect originating from the delocalisation of unpaired electron spin from the lanthanide ion onto the NMR active nucleus, transferred through chemical bonds. The spin active nuclei couples with the unpaired electron on the lanthanide ion. The rapid rate of relaxation of the electron spin is much faster than that of nuclear spin relaxation and this causes a broadening of the resonance rather than an expected doublet. The collapsing of the doublet into a broad singlet comes at a weighted average caused by the two resonances not being of equal intensity, this causes a significant chemical shift in the spectrum. It stands to reason that this effect is less impactful the further from the lanthanide metal centre the nucleus is, and the effect on the nuclei gets weaker the more bonds away from the unpaired electrons the nuclei are. The pseudo-contact shift is derived from anisotropy in the magnetic susceptibility of axially-symmetric lanthanide complexes when the unpaired is treated as a geometrical point. The anisotropy of the paramagnetic centre complements that of the instrument's magnet. If the susceptibility was not anisotropic the value of dipolar coupling with the nucleus would average to zero. The magnitude of the pseudo-contact shift is proportional to r^{-3}, where r is the distance between the metal centre and the nucleus.[109,114–117]

In summary, paramagnetic lanthanide metal centres cause a large change in chemical shift and broadening of resonances in NMR spectra, especially when ligands are coordinated directly to the metal centre. The nuclei are less affected the further from the unpaired electron (in the lanthanide) they are, both with regards to through-space interactions and in the number of bonds between them. The NMR spectra of lanthanide complexes, particularly of those in Chapter 3 of this work, contain $^{31}P\{^{1}H\}$ NMR resonances which are shifted significantly from their expected values, some are relatively broad, but the spectra are still significant in terms of the chemical information they provide.

1.6.3 Single Crystal X-ray Diffraction

Single crystal X-ray diffraction (XRD) is an extremely powerful tool which allows for probing the atomic arrangement of a crystal. Bond lengths and angles can be calculated to a high degree of accuracy. The technique is dependent on the successful growth of high-quality single crystals. Crystals can be grown by several different methods, such as the slow cooling of a concentrated solution, the slow evaporation of solvent from a solution of a product, vapour diffusion or layered solvent diffusion. The slow precipitation of a compound using these techniques, allows for the formation of regularly repeating units which make up a crystalline solid.

Crystal lattices are highly ordered structures, built by regularly repeating units along principal directions in three-dimensional space. The smallest group of atoms or molecules which can be used to form these units, repeating only by translational symmetry, is the unit cell. This is made up of asymmetric units, which are the smallest unit of volume that contain all the structural information required that, by an application of the symmetry operations, can reproduce the unit cell. This unit cell is a parallelepiped with six lattice parameters, lengths of a, b and c and angles α, β and γ. Based on these values, crystal symmetry is divided into seven types called crystal systems.

Table 1.4. Crystal systems.[118]

Crystal System	Unit cell parameters
Triclinic	$a \neq b \neq c$, $\alpha \neq \beta \neq \gamma \neq 90°$
Monoclinic	$a \neq b \neq c$, $\alpha = \gamma = 90°$, $\beta \neq 90°$
Orthorhombic	$a \neq b \neq c$, $\alpha = \beta = \gamma = 90°$
Rhombohedral	$a = b = c$, $\alpha = \beta = \gamma \neq 90°$
Tetragonal	$a = b \neq c$, $\alpha = \beta = \gamma = 90°$
Hexagonal	$a = b \neq c$, $\alpha = \beta = 90°$, $\gamma \neq 120°$
Cubic	$a = b = c$, $\alpha = \beta = \gamma = 90°$

In an X-ray diffraction experiment, X-rays are fired at the crystal at the angle of incidence, θ_i, and diffract at an angle of reflection, θ_r, whereby θ_i is equal to θ_r. Whether a spot is observed by the detector is dependent on whether it abides by Bragg's Law, Equation 1.2. Under the conditions where Bragg's law is satisfied, atoms are such a distance apart whereby the X-rays are diffracted at such an angle that they produce constructive interference (when two waves are in phase), Figure 1.15, and so are observed by the detector. For a single measurement the angle of incidence, θ, is constant, and the distance between atomic planes is a property of the crystal. The wavelength, λ, is dependent on the X-ray source (e.g. molybdenum, silver or copper). Given so many of these values are constant, for a single incident angle, only a few reflections will satisfy Bragg's law. The crystal is, therefore, rotated to change the angle of incidence and another measurement is taken, offering a new set of reflections, which appear as spots on the image generated by the detector. Once a number of these images has been generated at a number of different angles, the 2D images can be used to determine the unit cell parameters. The intensity of the spots can be used to determine the position of the electron density within the unit cell. This electron density map can be used to identify the atoms and determine their relative positions in space.

$$n\lambda = 2d\sin\theta$$

Equation 1.2. Bragg's law, n = integer, λ = wavelength, θ = angle of incidence.

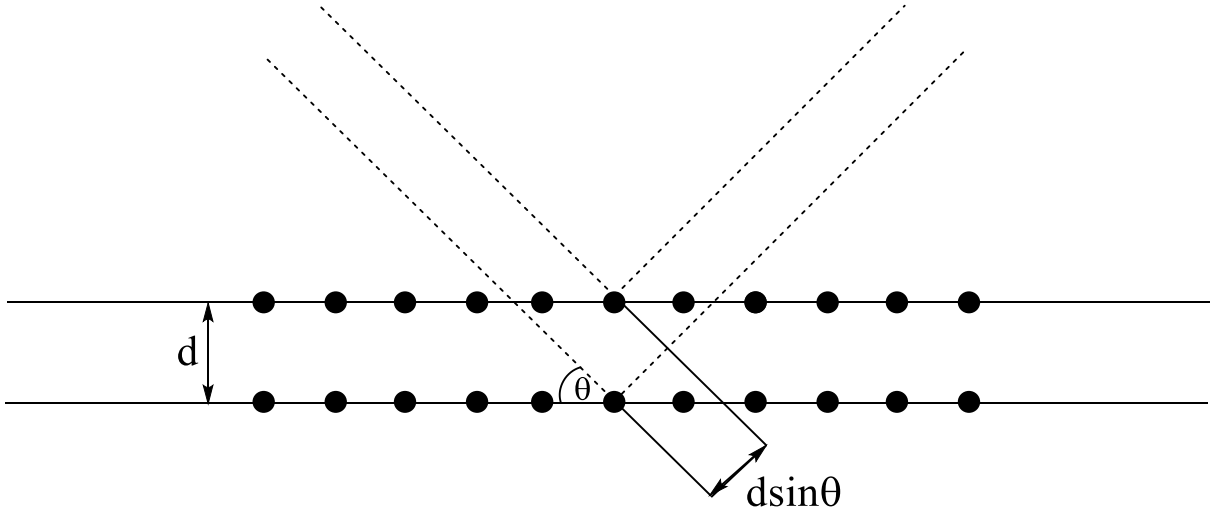

Figure 1.15. A representation of Bragg's law.[119]

Single crystal XRD is a vital tool within inorganic chemistry to provide structural data, when other spectroscopic probes are unavailable. However, it does have its limitations. Analysis tends to be performed only on one crystal and so may not be representative of the bulk product. High crystal quality is extremely important for accurate structural data, but this can be very difficult to obtain for some systems, particularly labile systems. Disorder in a crystal can make structural solution difficult and even disordered solvent can lead to inaccuracies in bond lengths and angles of the complex. There are many types of disorder, which result from the individual unit cells within a crystal lattice not being completely identical. Dynamic disorder, caused by differences in bond lengths as they vibrate, bend and stretch, is overcome by running the experiment at low temperature (100 K). Static disorder, which is caused by the random variation of the position of atoms within the crystal, leads to partially occupied atom sites which can be modelled during the refinement process. One of the common causes of disorder in this work is the presence of disordered solvent within the lattice. The crystallised lanthanide complexes (Chapters 2 and 3) have large solvent accessible voids. As there is no single preferred orientation for the solvent molecules to fill this void, unit cells contain solvent in varied orientations, and this can be difficult to model absolutely. These different forms of disorder are discussed throughout this work in relation to specific examples. The use of Single crystal XRD cannot, therefore, be used in isolation, but must be used in conjunction with additional techniques for more accurate and reliable data.

1.6.4 Elemental Analysis

Elemental (combustion) analysis is most commonly used to determine the carbon, hydrogen and, where applicable, nitrogen percentages of these systems in the solid state. These elements are selected because the analysis is quick and inexpensive whilst offering a lot of information about the purity of the sample. Where single crystal X-ray diffraction can be useful in determining the exact composition of a single crystal, elemental analysis can be used to show the bulk has the same elemental make up as the single crystal. The elemental analyses within this work consist entirely of CHN analysis, whereby a small amount of the sample is burnt in an excess of oxygen and the resulting CO_2, H_2O and N_2 formed are trapped and used to calculate the percentage of C, H and N in the bulk sample. It is useful for determining sample purity and can be used in addition with other techniques to show the presence of any trace impurities or solvent retention.

1.6.5 UV Visible Spectroscopy

Ultraviolet-visible (UV vis) spectroscopy is a simple method for observing the absorption of electromagnetic radiation in the UV and visible regions. It is a useful technique as it is quick and inexpensive to run, it is a non-destructive technique and it can be performed on gas, solution or solid-state samples. In a general experiment, a beam of incident radiation is split in two, with one passing through the beam and the other passed through a reference. The resulting beams are compared at a detector and the absorption is displayed as a function of wavelength. The intensity of absorption is measured as the absorbance and can be related to the molar concentration of the absorbing species using the Beer Lambert Law, Equation 1.3.[120]

$$A = -\log\left(\frac{I}{I_0}\right) = \varepsilon l c$$

Equation 1.3. Beer Lambert Law.[120] *A = absorbance, ε = molar absorptivity, l = path length and c = concentration of the sample.*

UV vis spectroscopy is often used for probing ligand-ligand, metal-metal and charge transfer transitions. Ligand-ligand transitions occur primarily in organic ligands containing π systems, such as aromatic groups. Metal localised transitions occur mostly in transition metals with partially filled d-orbitals. In an octahedral species, the d-orbital splits into the t_{2g} and e_g orbitals. Excitation of an electron would promote it from the t_{2g} orbital to the e_g orbital. This d-d transition is spin forbidden by both the Laporte Rule ($g \rightarrow u$) and often the $\Delta I = \pm 1$ selection

rule, meaning transitions must occur between levels with two different symmetry and must change orbital angular momentum. Due to being spin forbidden, these are usually weak transitions. They are sometimes observed due to vibronic coupling, especially in distorted octahedral systems, in which a molecular vibration lowers the symmetry around the metal centre and one of the metal's orbitals symmetry more similarly resembles that of a p-orbital. The transition then resembles that of a d→p transition, which is not spin forbidden, and is observed. This vibronic coupling requires from a significant interaction between the d orbitals of the metal and the p orbitals from the ligand. Transition metals also benefit from charge transfer bands, either ligand to metal or metal to ligand, both are often extremely intense (depending on symmetry selection rules) and can come in both the UV and the visible range, giving transition metal complexes very intense colours.[120]

In this work UV vis spectroscopy is used observe f→d transitions in the divalent lanthanides. The lanthanides in the 3+ oxidation state show primarily f→f transitions which are very weak due to being spin forbidden. The lanthanides also do not benefit from vibronic coupling in the way d→d transitions often do, as the 4f orbitals are not as shielded from the nucleus as the d orbitals are, and as such are much more contracted and do not have the same interaction with the surrounding ligands. Due to the lack of interaction between these orbitals, charge transfer transitions are not observed. This leads to the trivalent lanthanide compounds being mostly white or pale in colour. However, in 2+ species, the 4f orbitals are destabilised, with respect to those in 3+ species, and so lie closer in energy to the 5d orbitals, allowing for f→d transitions. These transitions often occur in the visible region and the species are therefore often brightly coloured.[17,121–124]

1.6.6 Thin Film Analysis

Upon successful deposition of a thin film onto a substrate, several techniques can be employed to determine the composition of the thin film. These include grazing incidence X-ray diffraction (GIXRD), scanning electron microscopy (SEM) and energy dispersive X-ray spectroscopy (EDX).

Similar to single crystal XRD, grazing incidence X-ray diffraction (GIXRD) involves firing an X-ray beam at a sample and measuring the diffraction pattern. However, as it is optimised to analyse thin films and small quantities of sample, high angles of incidence would likely penetrate all the way through the sample and show diffraction caused only by the substrate the thin films are on. Instead incident angles of 1˚ or lower are used and the detector moves around

the sample, rather than the source. This limits the number of angles available to rotate around, unlike for single crystal which can rotate around 3 axes, to give a complete sphere. Instead patterns are used for determining a unit cell, often of a known compound, to determine if a desired product has been deposited. The process is very similar to powder X-ray diffraction, (PXRD). However, unlike PXRD, due to stacking in a preferred orientation, intensities of peaks are more representative of a crystalline solid even if they cannot be used to determine structural information, and are not consistent with the intensities of bulk PXRD patterns.[125,126]

Scanning electron microscopy (SEM) uses a narrowly focussed beam of electrons which hit the surface of a sample, under vacuum. When the electrons hit the sample, they produce backscattered electrons (which bounce off the surface) and secondary electrons (which excite the electrons in the inner shells of the atoms). The reflected beams are then imaged by detectors. SEM allows for high resolution images to be taken at magnifications much larger than an optical microscope would allow for. It is useful for looking at the surface of thin films to see the morphology of the film. SEM samples need to be conductive otherwise electrons gather on the surface of the sample, interacting with the beam, resulting in blurred images. Non-conductive samples can still be imaged, but require coating in a metal surface (such as gold or aluminium).[127] Samples in this work were conductive and as such did not require such coating.

Energy dispersive X-ray spectroscopy (EDX) is a fast method of chemical characterisation and can be performed with very small amounts of sample. The thin film is hit with an electron beam which excites the electrons in the inner shells of atoms on the surface. The electron emits X-rays as it relaxes back into a lower energy shell. This X-ray is of a characteristic wavelength, depending on the element. Elements lighter than sodium can be identified but are unquantifiable due to low fluorescence yield. Unfortunately, their absorption peaks often overlap with peaks from heavier elements and EDX is unable to distinguish between overlapping peaks when the energies of two X-rays are very similar. For example, Mo L_α (2.293 eV) is almost equivalent to the energy of S K_α (2.306 eV) and so these peaks overlap.[128]

1.7 Aims

The objectives of this thesis are:

- To develop new coordination chemistry of hard Ln(III) (Chapter 2) and Ln(II) (Chapter 3) ions with a range of phosphine oxide ligands. This study of trivalent lanthanide metal complexes will utilise bidentate phosphine oxides, with a focus on the effects of varying the metal ion (and as a result, the size of the metal ion), the counter ion and the ligand architecture on the resulting structure. The study of divalent lanthanide metal complexes will employ the monodentate ligands $OPMe_3$ and $OPPh_3$, to synthesise the first examples of divalent lanthanide phosphine oxide complexes.
- To synthesise a family of SmI_2, EuI_2 and YbI_2 macrocyclic complexes (Chapter 3). A range of mixed donor macrocycles, [18]aneO_4X_2 (X = NH, S, Se), 18-crown-6 and Me_6[18]aneN_6 will be used to study the effects of varying the donor atoms on the macrocyclic ligand.
- To study the first series of tantalum oxychloride and thiochloride coordination complexes of the form $[TaECl_3(L\text{-}L)]$ or $[TaECl_3(L)_2]$ (E = O or S) and to explore their properties (Chapter 4).
- To explore the chemistry of series of tantalum thiochloride complexes with soft donor thio- and selenoethers (Chapter 5). These compounds have potential uses in chemical vapour deposition and successfully synthesised precursor targets would be tested in CVD experiments in attempts to deposit thin films of TaE_2.

1.8 References

1 R. G. Pearson, *J. Am. Chem. Soc.*, 1963, **85**, 3533–3539.

2 G. N. Lewis, *Valence and The Structure of Atoms and Molecules*, Chemical Catalogue Company, New York, 1923.

3 R. G. Pearson, *J. Chem. Educ.*, 1968, **45**, 581–597.

4 D. F. Shriver, P. W. Atkins, T. L. Overton, J. P. Rourke, M. T. Weller and F. A. Armstrong, in *Inorganic Chemistry*, ed. W. H. Freeman & Co, Oxford University Press, Oxford, 4th edn., 2003, pp. 125–138.

5 J. Burt, W. Levason and G. Reid, *Coord. Chem. Rev.*, 2014, **260**, 65–115.

6 W. Levason, F. M. Monzittu and G. Reid, *Coord. Chem. Rev.*, 2019, **391**, 90–130.

7 W. Levason, S. D. Orchard and G. Reid, *Coord. Chem. Rev.*, 2002, **225**, 159–199.

8 P. Zhang, L. Zhang and J. Tang, *Dalton Trans.*, 2015, **44**, 3923–3929.

9 H. Wang, B.-W. Wang, Y. Bian, S. Gao and J. Jiang, *Coord. Chem. Rev.*, 2016, **306**, 195–216.

10 D. N. Woodruff, R. E. P. Winpenny and R. A. Layfield, *Chem. Rev.*, 2013, **113**, 5110–5148.

11 M. Szostak, N. J. Fazakerley, D. Parmar and D. J. Procter, *Chem. Rev.*, 2014, **114**, 5959–6038.

12 B. T. Kilbourn, *J. Less Common Met.*, 1986, **126**, 101–106.

13 R. Häner, J. Hall and G. Rihs, *Helv. Chim. Acta*, 1997, **80**, 487–494.

14 S. Zhang, P. Winter, K. Wu and A. D. Sherry, *J. Am. Chem. Soc.*, 2001, **123**, 1517–1518.

15 M. J. Allen, *Synlett*, 2016, **27**, 1310–1317.

16 S. Aime, D. D. Castelli, S. G. Crich, E. Gianolio and E. Terreno, *Acc. Chem. Res.*, 2009, **42**, 822–831.

17 N. Kaltsoyannis and P. Scott, *The f elements*, Oxford University Press, Oxford, 1999.

18 M. N. Bochkarev, *Coord. Chem. Rev.*, 2004, **248**, 835–851.

19 B. Cordero, V. Gómez, A. E. Platero-Prats, M. Revés, J. Echeverría, E. Cremades, F. Barragán and S. Alvarez, *Dalton Trans.*, 2008, 2832–2838.

20 P. Pyykkö, *Chem. Rev.*, 1988, **88**, 563–594.

21 M. J. D. Champion, P. Farina, W. Levason and G. Reid, *Dalton Trans.*, 2013, **42**, 13179–13189.

22 J. Fawcett and A. W. G. Platt, *Polyhedron*, 2003, **22**, 967–973.

23 L. G. Hubert-Pfalzgraf, in *Encyclopedia of Inorganic Chemistry: Niobium & Tantalum*, eds. R. B. King, R. H. Crabtree, C. M. Lukehart, D. A. Atwood and R. A. Scott, American Cancer Society, 2006, pp. 1–24.

24 T. Waters and A. G. Wedd, in *Comprehensive Coordination Chemistry II - 4.5 Niobium and Tantalum*, eds. J. A. McCleverty and T. J. Meyer, Elsevier, Amsterdam, 2004, pp. 241–312.

25 S. B. Lyon, in *Shreir's Corrosion*, eds. B. Cottis, M. Graham, R. Lindsay, S. Lyon, T. Richardson, D. Scantlebury and H. Stott, Elsevier BV, Oxford, 2009, pp. 2135–2150.

26 A. Agulyansky, in *Chemistry of Tantalum and Niobium Fluroide Compounds*, ed. A. Agulyansky, Elsevier, Amsterdam, 2004, pp. 1–10.

27 N. N. Greenwood and A. Earnshaw, in *Chemistry of the Elements*, eds. N. N. Greenwood and A. Earnshaw, Elsevier, 1997, vol. 108, pp. 976–1001.

28 F. Marchetti and G. Pampaloni, *Chem. Commun.*, 2012, **48**, 635–653.

29 M. Chhowalla, Z. Liu and H. Zhang, *Chem. Soc. Rev.*, 2015, **44**, 2584–2586.

30 M. Chhowalla, H. S. Shin, G. Eda, L.-J. Li, K. P. Loh and H. Zhang, *Nat. Chem.*, 2013, **5**, 263–75.

31 J. Liu and X. W. Liu, *Adv. Mater.*, 2012, **24**, 4097–4111.

32 T. Heine, *Acc. Chem. Res.*, 2015, **48**, 65–72.

33 C. J. Carmalt, T. D. Manning, I. P. Parkin, E. S. Peters and A. L. Hector, *J. Mater. Chem.*, 2004, **14**, 290.

34 B. Morosin, *Acta Crystallogr.*, 1974, **B30**, 551–552.

35 M. B. Alemayehu, M. Falmbigl, K. Ta and D. C. Johnson, *Chem. Mater.*, 2015, **27**,

2158–2164.

36 A. J. Kendall and D. R. Tyler, *Dalton Trans.*, 2015, **44**, 12473–12483.

37 J. H. Downing and M. B. Smith, in *Comprehensive Coordination Chem II - 1.12 Phosphorus Ligands*, eds. J. A. McCleverty and T. J. Meyer, Elsevier Pergamon, Oxford, 2003, pp. 253–296.

38 M. Carravetta, M. Concistre, W. Levason, G. Reid and W. Zhang, *Chem. Commun.*, 2015, **51**, 9555–9558.

39 M. Carravetta, M. Concistre, W. Levason, G. Reid and W. Zhang, *Inorg. Chem.*, 2016, **55**, 12890–12896.

40 W. Levason, F. M. Monzittu, G. Reid and W. Zhang, *Chem. Commun.*, 2018, **54**, 11681–11684.

41 C. A. Tolman, *Chem. Rev.*, 1977, **77**, 313–348.

42 J. A. Bilbrey, A. H. Kazez, J. Locklin and W. D. Allen, *J. Comput. Chem.*, 2013, **34**, 1189–1197.

43 P. W. N. M. Van Leeuwen, P. C. J. Kamer, J. N. H. Reek and P. Dierkes, *Chem. Rev.*, 2000, **100**, 2741–2769.

44 B. E. Mann, C. Masters and B. L. Shaw, *J. Chem. Soc.*, 1971, 1104–1106.

45 B. E. Mann, C. Masters and B. L. Shaw, *J. Chem. Soc. Dalton Trans.*, 1970, 704–708.

46 P. E. Garrou, *Chem. Rev.*, 1981, **81**, 229–266.

47 S. Hietkamp, D. J. Stufkens and K. Vrieze, *J. Organomet. Chem*, 1976, **122**, 419–428.

48 P. Kapoor, R. Kapoor, D. D. Pathak and G. Gaur, *Inorganica Chim. Acta*, 1986, **112**, 153–157.

49 W. Levason, M. E. Light, G. Reid and W. Zhang, *Dalton Trans.*, 2014, **43**, 9557–9566.

50 L. D. Quinn, *A guide to organophosphorus chemistry*, John Wiley & Sons, Inc., New York, 2000.

51 L. C. Baldwin and M. J. Fink, *J. Organomet. Chem*, 2002, **646**, 230–238.

52 Y.-R. Luo, *Comprehensive Handbook of Chemical Bond Energies*, Taylor & Francis Group, 2007.

53 W. Kutzelnigg, *Angew. Chemie Int. Ed. English*, 1984, **23**, 272–295.

54 D. G. Gilheany, *Chem. Rev.*, 2002, **94**, 1339–1374.

55 D. B. Chesnut and A. Savin, *J. Am. Chem. Soc.*, 1999, **121**, 2335–2336.

56 D. B. Chesnut, *J. Am. Chem. Soc.*, 1998, **120**, 10504–10510.

57 A. W. G. Platt, *Coord. Chem. Rev.*, 2017, **340**, 62–78.

58 N. De Silva, F. Zahariev, B. P. Hay, M. S. Gordon and T. L. Windus, *J. Phys. Chem. A*, 2015, **119**, 8765–8773.

59 Z. Spichal, M. Necas and J. Pinkas, *Inorg. Chem.*, 2005, **44**, 2074–2080.

60 M. J. Petersson, W. A. Loughlin and I. D. Jenkins, *Chem. Commun.*, 2008, 4493–4494.

61 F. T. Schevenels, M. Shen and S. A. Snyder, *J. Am. Chem. Soc.*, 2017, **139**, 6329–6337.

62 W. Levason, R. Patel and G. Reid, *J. Organomet. Chem*, 2003, **688**, 280–282.

63 A. Yoshimura, Y. Saga, Y. Sato, A. Ogawa, T. Chen and L. B. Han, *Tetrahedron Lett.*, 2016, **57**, 3382–3384.

64 C. J. Pedersen, *J. Am. Chem. Soc.*, 1967, **89**, 7017–7036.

65 E. Constable, *Coordination Chemistry of Macrocyclic Compounds*, Oxford University Press, Oxford, 1999.

66 R. D. Hancock, *Pure Appl. Chem.*, 1986, **58**, 1445–1452.

67 K. Bowman-James, *Encyclopedia of Inorganic and Bioinorganic Chemistry: Macrocyclic Ligands*, John Wiley & Sons, Ltd., 2006.

68 M. J. D. Champion, J. M. Dyke, W. Levason, M. E. Light, D. Pugh, H. Bhakhoa, L. Rhyman, P. Ramasami and G. Reid, *Inorg. Chem.*, 2015, **54**, 2497–2499.

69 P. N. Bartlett, M. J. D. Champion, M. E. Light, W. Levason, G. Reid and P. W. Richardson, *Dalton Trans.*, 2015, **44**, 2953–2955.

70 M. J. D. Champion, W. Levason, D. Pugh and G. Reid, *Dalton Trans.*, 2015, **44**, 18748–18759.

71 P. Farina, W. Levason and G. Reid, *Dalton Trans.*, 2013, **42**, 89–99.

72 W. Levason, D. Pugh, J. M. Purkis and G. Reid, *Dalton Trans.*, 2016, **45**, 7900–7911.

73 W. Levason and G. Reid, *J. Chem. Res.*, 2002, **2**, 467–472.

74 W. Levason, S. D. Orchard and G. Reid, *Chem. Commun.*, 2001, **837**, 427–428.

75 M. J. Hesford, W. Levason, M. L. Matthews and G. Reid, *Dalton Trans.*, 2003, **14**, 2852–2858.

76 W. Levason and G. Reid, eds. J. A. McCleverty and T. J. Meyer, Elsevier Pergamon, Oxford, 2003, pp. 391–398.

77 Y.-P. Chang, W. Levason and G. Reid, *Dalton Trans.*, 2016, **15**, 18393–18416.

78 S. L. Benjamin, Y.-P. Chang, M. Huggon, W. Levason and G. Reid, *Polyhedron*, 2015, **99**, 230–237.

79 S. L. Benjamin, A. Hyslop, W. Levason and G. Reid, *J. Fluor. Chem.*, 2012, **137**, 76–83.

80 M. Jura, W. Levason, R. Ratnani, G. Reid and M. Webster, *Dalton Trans.*, 2010, **39**, 883–891.

81 S. G. Murray and F. R. Hartley, *Chem. Rev.*, 1981, **81**, 365–414.

82 R. Hart, W. Levason, B. Patel and G. Reid, *J. Chem. Soc. Dalt. Trans.*, 2002, 3153–3159.

83 M. J. Atherton and J. H. Holloway, *Adv. Inorg. Radiochem.*, 1979, **22**, 171–198.

84 D. A. Rice, *Coord. Chem. Rev.*, 1978, **25**, 199–227.

85 B. Siewert, G. Koellner, K. Ruhlandt-Senge, F. Schmock and U. Müller, *Z. Anorg. Allg. Chem.*, 1991, **593**, 160–168.

86 G. W. A. Fowles, R. J. Hobson, D. A. Rice and K. J. Shanton, *J. Chem. Soc., Chem. Commun.*, 1976, 552–553.

87 I. Nowak, E. M. Page, D. A. Rice, A. D. Richardson, R. J. French, K. Hedberg and J. S. Ogden, *Inorg. Chem.*, 2003, **42**, 1296–1305.

88 Y.-P. Chang, A. L. Hector, W. Levason and G. Reid, *Dalton Trans.*, 2017, **46**, 9824–9832.

89 R. D. Bannister, W. Levason, G. Reid and F. Robinson, *Polyhedron*, 2019, **169**, 129–

134.

90 E. D. Brown, S. M. Iqbal and L. N. Owen, *J. Chem. Soc.*, 1966, 415–419.

91 F. R. Hartley, S. G. Murray, W. Levason, H. E. Soutter and C. A. McAuliffe, *Inorganica Chim. Acta*, 1979, **35**, 265–277.

92 J. D. Baleja, *Synth. Commun.*, 1984, **14**, 215–218.

93 S. Oae, K. Shinhama and Y. Hae Kim, *Bull. Chem. Soc. Jpn.*, 1980, **53**, 2023–2026.

94 F. Maiolo, L. Testaferri, M. Tiecco and M. Tingoli, *J. Org. Chem.*, 1981, **46**, 3070–3073.

95 L. Testaferri, M. Tingoli and M. Tiecco, *J. Org. Chem.*, 1980, **45**, 4376–4380.

96 D. J. Gulliver, E. G. Hope, W. Levason, S. G. Murray, D. M. Potter and G. L. Marshall, *J. Chem. Soc. Perkin Trans. II*, 1984, 429–434.

97 E. W. Abel, K. Kite, K. G. Orrell and V. Sik, *J. Chem. Soc. Dalton Trans.*, 1981, 2439–2446.

98 N. V. Russavskaya, V. A. Grabel'nykh, E. P. Levanova, E. N. Sukhomazova, L. V. Klyba, E. R. Zhanchipova, A. A. Tatarinova, A. V. Elaev, E. N. Deryagina, N. A. Korchevin and B. A. Trofimov, *Russ. J. Org. Chem.*, 2006, **42**, 652–658.

99 B. Hermans, N. Colard and L. Hevesi, *Tetrahedron Lett.*, 1992, **33**, 4629–4632.

100 E. G. Hope, T. Kemmltt and W. Levason, *Organometallics*, 1987, **6**, 206–207.

101 D. Selvakumar, R. Singh, M. Nasim and G. N. Mathjr, *Phosphorus. Sulfur. Silicon Relat. Elem.*, 2001, **172**, 247–259.

102 L. L. Merritt and E. Schroeder, *Acta Crystallogr.*, 1956, **9**, 801–804.

103 Q. Xiang, J. Yu and M. Jaroniec, *J. Am. Chem. Soc.*, 2012, **134**, 6575–6578.

104 K. Lee, R. Gatensby, N. McEvoy, T. Hallam and G. S. Duesberg, *Adv. Mater.*, 2013, **25**, 6699–6702.

105 K. Xu, P. Chen, X. Li, C. Wu, Y. Guo, J. Zhao, X. Wu and Y. Xie, *Angew. Chemie Int. Ed.*, 2013, **52**, 10477–10481.

106 A. C. Jones and M. L. Hitchman, *Chemical Vapour Deposition - Chapter 1*, The Royal Society of Chemistry, 2009.

107 G. Oczko, L. Macalik, J. Legendziewicz and J. Hanuza, *J. Alloys Compd.*, 2004, **380**, 327–336.

108 C. M. Schurz and T. Schleid, *J. Solid State Chem.*, 2010, **183**, 2253–2260.

109 J. Mason, *Multinuclear NMR*, Plenum Press, New York, 1987.

110 C. C. Hinckley, *J. Am. Chem. Soc.*, 1969, **91**, 5160–5162.

111 B. D. Flockhart, *C R C Crit. Rev. Anal. Chem.*, 1976, **6**, 69–130.

112 V. S. Sastri, J.-C. Bünzli, V. R. Rao, G. V. S. Rayudu and J. R. Perumareddi, in *Modern Aspects of Rare Earths and Their Complexes*, eds. V. S. Sastri, J.-C. Bünzli, V. R. Rao, G. V. S. Rayudu and J. R. Perumareddi, Elsevier, Amsterdam, 2003, pp. 779–843.

113 C. N. Rellley, B. W. Good and R. D. Allendoerfer, *Anal. Chem.*, 1976, **48**, 1446–1458.

114 E. A. V. Ebsworth, D. W. H. Rankin and S. Craddock, *Structural Methods in Inorganic Chemistry*, Blackwell Scientific Publications Ltd., Edinburgh, 1987.

115 D. W. H. Rankin, N. Mitzel and C. Morrison, *Structural Methods in Molecular Inorganic Chemistry*, John Wiley & Sons, Inc., 2013.

116 B. Bleaney, *J. Magn. Reson.*, 1972, **8**, 91–100.

117 A. J. Pell, G. Pintacuda and C. P. Grey, *Prog. Nucl. Magn. Reson. Spectrosc.*, 2019, **111**, 1–271.

118 D. F. Shriver, P. W. Atkins, T. L. Overton, J. P. Rourke, M. T. Weller and F. A. Armstrong, in *Inorganic Chemistry*, ed. W. H. Freeman & Co, Oxford University Press, Oxford, 4th edn., 2003, pp. 72–73.

119 D. F. Shriver, P. W. Atkins, T. L. Overton, J. P. Rourke, M. T. Weller and F. A. Armstrong, in *Inorganic Chemistry*, ed. W. H. Freeman & Co, Oxford University Press, Oxford, 4th edn., 2003, pp. 169–172.

120 D. F. Shriver, P. W. Atkins, T. L. Overton, J. P. Rourke, M. T. Weller and F. A. Armstrong, in *Inorganic Chemistry*, ed. W. H. Freeman & Co, Oxford University Press, Oxford, 4th edn., 2003, pp. 173–177.

121 R. D. Bannister, W. Levason, M. E. Light and G. Reid, *Polyhedron*, 2018, **154**, 259–262.

122 N. B. Mikheev, S. A. Kulyukhin, A. N. Kamenskaya, I. A. Rumer and N. A. Konovalova, *Radiochemistry*, 2004, **46**, 521–535.

123 E. Rogers, P. Dorenbos, J. T. M. De Haas and E. Van Der Kolk, *J. Phys.: Condens. Matter*, 2012, **24**, 275502 (5pp).

124 O. Yoshihiro and I. Toshiyuki, *Inorganica Chim. Acta*, 1988, **144**, 143–146.

125 G. Renaud and A. Barbier, ed. D. P. Woodruff, Elsevier Ltd., 2001, vol. 9, pp. 256–300.

126 O. Sakata and M. Nakamura, in *Surface Science Techniques*, eds. G. Bracco and B. Holst, Springer Berlin Heidelberg, Berlin, 2013, vol. 51, pp. 165–190.

127 D. F. Shriver, P. W. Atkins, T. L. Overton, J. P. Rourke, M. T. Weller and F. A. Armstrong, in *Inorganic Chemistry*, ed. W. H. Freeman & Co, Oxford University Press, Oxford, 4th edn., 2003, pp. 646–651.

128 S. Ebnesajjad, *Handbook of Adhesives and Surface Preparation - 4. Surface and material characterization techniques*, William Andrew Publishing, 2nd edn., 2011.

Chapter 2 Trivalent Lanthanide Phosphine Oxide Complexes

2.1 Introduction

Work towards complexes of lanthanide phosphine oxide complexes has often focused on monodentate phosphine oxide ligands coordinated to lanthanide triflates, nitrates and carboxylates, with work on complexes of lanthanide halides being more infrequent. This chapter aims to explore the chemistry of a range of bidentate phosphine oxide ligands with the less explored lanthanide (III) halides and the effect of differing counter ions. A range of ligand architectures are employed to show the effects of varying backbone flexibility. A range of lanthanides are used to explore the differences along the series and how they are affected by the lanthanide contraction. Finally, the effect of varying the counter ion is probed, including using the very weakly coordinating anion $[PF_6]^-$.

2.1.1 Lanthanide Coordination Chemistry

The coordination chemistry of the lanthanides is often viewed as very similar across the series. The common narrative is that upon coordination, the lanthanide ions only have access to the 3+ oxidation state and form bonds with as many ligands as can be accommodated within the coordination sphere, with steric effects being the dominant factor in any bonding. However, in practice, the trends within the lanthanides turn out to be quite unpredictable, with subtle differences in their coordination chemistry. As described previously, the range of possible applications for lanthanide complexes is vast, ranging from catalysis,[1,2] to single molecule magnets,[3,4] to MRI relaxation agents.[5–7] These uses rely on very specific lanthanides with very specific ligand systems. Differences in ionic radius due to the lanthanide contraction (Chapter 1) result in an increased charge/radius ratio along the series, which can have profound effects on their coordination properties. These differences are subtle, but can lead to unexpected deviations from the expected trend of a smaller ionic radius leading to a lower coordination number.[8–10] This suggests that the observed differences are not simply the result of steric effects.

Work on lanthanide phosphine oxide complexes can be separated into those formed with monodentate ligands, such as $OPMe_3$[11,12] and more commonly $OPPh_3$[13–16] and those formed with higher denticity ligands, such as $dppmO_2$, $dppeO_2$ and PPO_2 described here. Lanthanide complexes formed with monodentate phosphine oxides, mainly focused on $OPPh_3$, have been

widely explored and are reviewed in Section 3.1. Work towards lanthanide complexes bearing bi- or multi-dentate phosphine oxide ligands is a more neglected field, though more recently has been demanding attention. These will be the focus of the study for this chapter.

Lanthanide complexes are prone to retain variable amounts of solvent or water in the crystal lattice, which are not removed by prolonged drying *in vacuo*, a consequence of the large voids produced by the bulky asymmetric ligands.[9,17] Although these often non-stoichiometric solvates make only small differences to the micro-analytical results, they are often evident in the spectroscopic data and in the X-ray crystal structures, where they are typically difficult to model. It is even more important to be specific in the description of the identification of products for lanthanides. The lanthanide ions are notoriously labile and ligands rapidly dissociate or exchange in solution, with one species often precipitating out of a solution. Due to this, it is often the case that the solid state data does not accurately portray the systems in solution and so it is important to take care when analysing lanthanide complexes. The metal centres are often paramagnetic and as such, only limited information can be obtained from NMR studies. As described, bonding is primarily ionic and in solution ligands are often rapidly exchanging. As the lanthanides are most stable in the +3 oxidation state, these species are typically much less air and moisture sensitive than the divalent lanthanide systems.

2.1.2 Bidentate lanthanide phosphine oxide species

Due to the bonding in these systems primarily consisting of electrostatic interactions, they are extremely sensitive to the reaction conditions. The metal centre, temperature, solvent system, ligand, stoichiometry and importantly counter ion are all important factors in the outcome of reactions.

A good example of the impact these factors can have is demonstrated by the reaction of various lanthanide nitrates with differing ratios of *bis*(diphenylphosphino)methane dioxide, $dppmO_2$, which form a variety of structures. Using a 1 : 1.5 molar ratio of metal : $dppmO_2$, the complexes $[Ln(NO_3)_2(dppmO_2)_2][Ln(NO_3)_4(dppmO_2)]$ (Ln = Pr, Eu) are formed.[18]

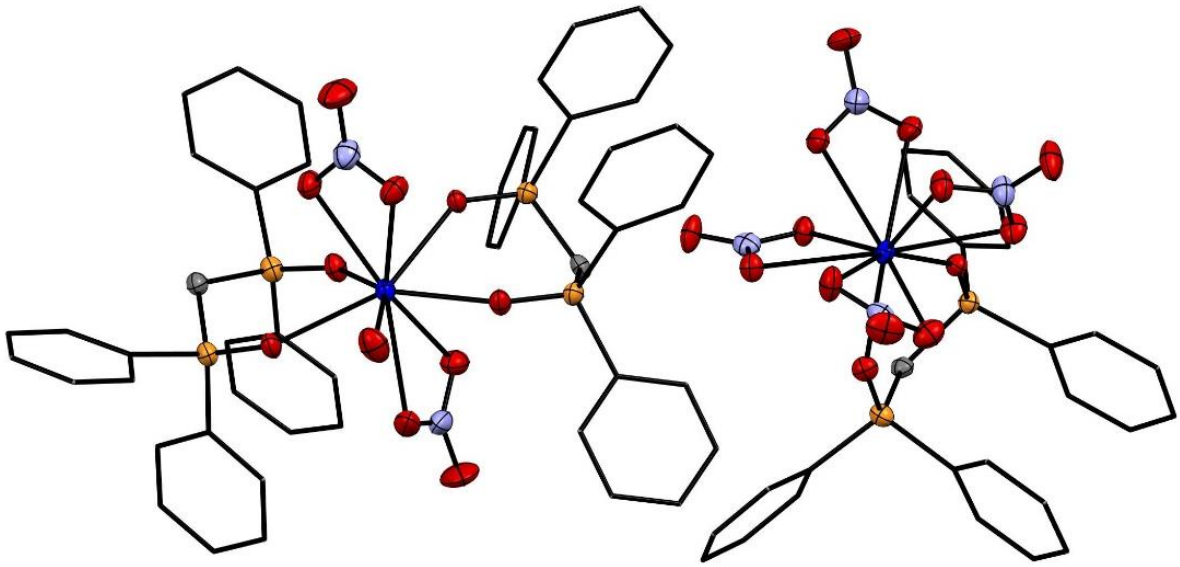

Figure 2.1 View of the crystal structure of [Pr(NO$_3$)$_4$(dppmO$_2$)][Pr(NO$_3$)$_2$(dppmO$_2$)$_2$(H$_2$O)] with hydrogen atoms omitted and phenyl rings depicted as wire frames for clarity.[18]

When using two or more equivalents of dppmO$_2$, two different structures were obtained, as shown by single crystal X-ray analysis; the neutral ten-coordinate [Ln(NO$_3$)$_3$(dppmO$_2$)$_2$] complex, where Ln = La, Ce, and the nine-coordinate ionic complex, [Ln(NO$_3$)$_2$(dppmO$_2$)$_2$(H$_2$O)][NO$_3$], for the smaller lanthanides (Ln = Nd, Gd, Ho).[18] The formation of this six-membered chelate ring is energetically favourable. In these systems the NO_3^- anion is hydrogen bonded to the coordinated water. Interestingly, these systems adopt a *pseudo-cis* conformation, unlike the monodentate phosphine oxide systems which generally prefer a *trans* geometry.[14,15,17] On heating the solid white compounds at 150 ˚C, they become yellow in colour. These yellow powders were washed with water and the resulting solid analysed as Ln(NO$_3$)$_3$L$_3$(H$_2$O)$_2$. Structural data from crystals grown from the gadolinium and ytterbium species confirmed them to be of the form [Ln(NO$_3$)(dppmO$_2$)$_3$][NO$_3$]$_2$, with residual solvent molecules in the lattice. These solid state structures also contain six-membered chelate rings.

Lanthanide salts with weakly coordinating anions tend to expel the anion in favour of the bidentate dppmO$_2$ ligand. The reaction of an aqueous solution of [Eu(ClO$_4$)$_3$] with an ethanolic solution of excess dppmO$_2$ formed the complex [Eu(dppmO$_2$)$_4$][ClO$_4$]$_3$·2H$_2$O, with the Eu^{3+} metal centre present in an eight coordinate distorted square antiprismatic geometry.[19] The reaction of one equivalent of La(OTf)$_3$ (OTf = CF$_3$SO$_3$) with two equivalents of dppmO$_2$ produces a similar cation in complex [La(dppmO$_2$)$_4$][OTf]$_3$·1.5H$_2$O, which has been confirmed

crystallographically. The analogous reactions using the much smaller lutetium(III) ion, on the other hand, results in only three ligands coordinating to the metal centre, which also retains a coordinated water molecule; $[Lu(dppmO_2)_3(H_2O)][OTf]_3$ adopts a seven coordinate pentagonal bipyramidal geometry with the $dppmO_2$ ligands chelating.[20]

In discussing the synthesis of the triflate salts, $[La(dppmO_2)_4][OTf]_3{\cdot}1.5H_2O$ and $[Lu(dppmO_2)_3(H_2O)][OTf]_3$,[20] Platt compares the six membered chelate ring to that formed by the *tris*-chelated ion $[Na(dppmO_2)_3]Br{\cdot}3H_2O$. Here the six-membered ring adopts a 'chair'-like geometry, however, in the triflate examples, the bidentate ligands form a more flattened ring with the metal centre, as shown in Figure 2.2, which Platt attributes to a greater positive charge on the metal ion repelling the more positive phosphorus and balancing this effect against the conformational stability of the ring.

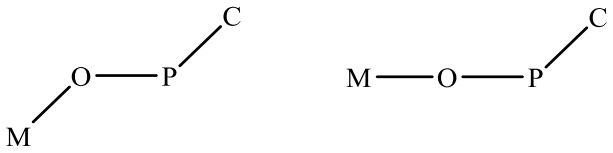

Figure 2.2. A diagram showing exaggerated M-O-C bond angles in $[Na(dppmO_2)_3]^+$ cations and the $[Ln(dppmO_2)_x]^{3+}$ cations.[20,21]

A series of complexes based upon $Eu(hfa)_3$ (hfa = $CF_3COCHCOCF_3^-$) with $dppmO_2$, PPO_2 and 1,3-bis(diphenylphosphino)benzene, *m*-$C_6H_4\{P(O)Ph_2\}_2$, have been characterised, producing $[Eu(hfa)_3(dppmO_2)]$, $[Eu(hfa)_2(PPO_2)_2][hfa]$, and a polymeric $[Eu(hfa)_3(m\text{-}C_6H_4\{P(O)Ph_2\}_2)]_n$.[22] The two mononuclear species exhibit an eight coordinate *anti*-symmetrical square antiprism geometry around the europium centre. Interestingly, when *m*-$C_6H_4\{P(O)Ph_2\}_2$ is used instead of the *ortho*- substituted analogue, the europium still coordinates two ligands, but forms an eight-coordinate polymeric structure whereby all three hfa ligands are still coordinated and each PPO_2 ligand bridges separate metal centres. This further highlights the directing influence the backbone of the diphosphine dioxide has upon the complexes formed in this less well studied area of the periodic table. With its rigid *o*-phenylene backbone, PPO_2 is somewhat preorganised towards chelation and formation of a mononuclear complex, whereas the bite angle of the *meta*-disubstituted analogue is more suited to bridging two metal centres. Though these species have been structurally characterised within the work, no crystallographic information is available in the CCDC and no cifs are provided with the

paper. There were no other examples of a crystallographically authenticated lanthanide complexes with PPO_2 in the literature.[17]

A series of polymeric structures of the form $[LnX(dppeO_2)_{1.5}]_n$ (Ln = Pr, Nd, Sm, Dy; X = NO_3, Ln = Nd, Gd; X = Cl) have been synthesised using gel diffusion and solvothermal reactions. These layered coordination polymers formed three different two-dimensional lattice architectures described as 'bricks', 'parquets' and 'distorted honeycombs', Figure 2.3. Characterisation of all of these species was primarily based on the solid state structural data, owing to their insolubility in most organic solvents. Though infrared spectroscopy and elemental analysis are provided, the main area of focus is on the crystal structures.

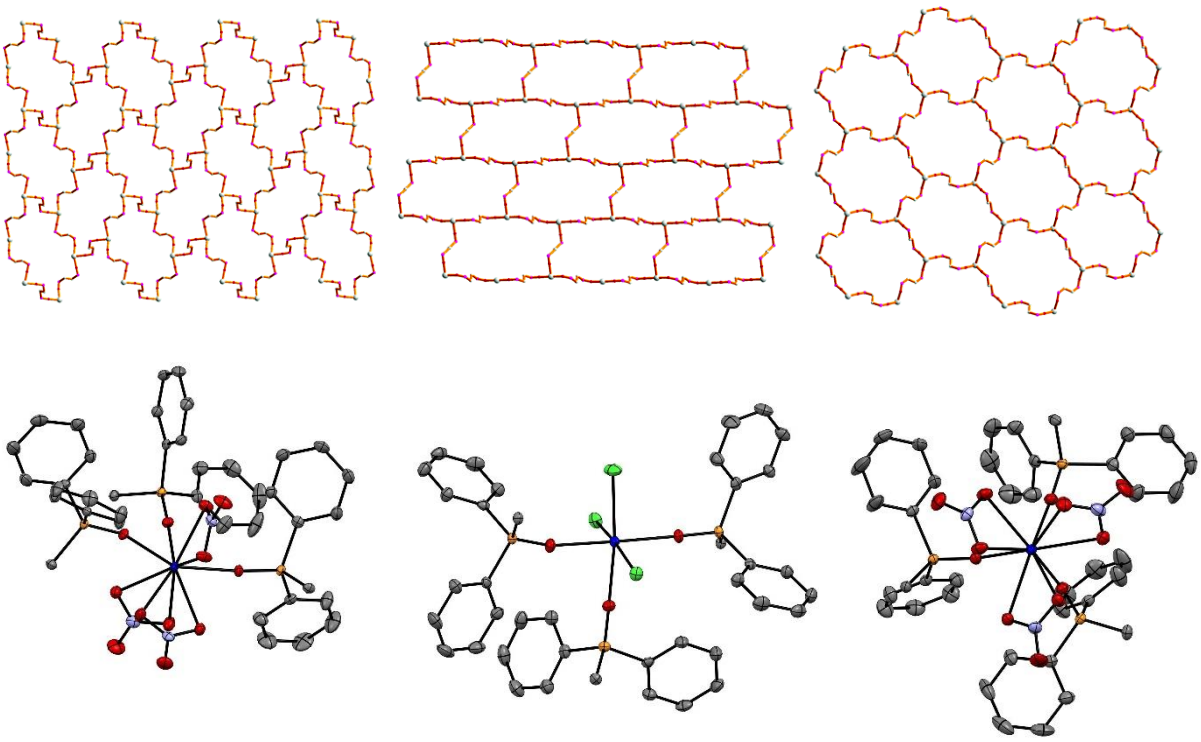

Figure 2.3. Crystal structures of the repeating unit of $[NdCl_3(dppeO_2)_{1.5}]_n$ (middle) and two different structures of $[Nd(NO_3)_3(dppeO_2)_{1.5}]_n$ (left and right) each below a simplified 2D lattice image of the three different polymeric architectures, from left to right: parquet floor, brick wall and honeycomb.[23] *Adapted with permission from Z. Spichal, M. Necas and J. Pinkas, Inorg. Chem., 2005,* ***44****, 2074–2080. Copyright 2005 American Chemical Society.*

The polymeric complexes, $[LnCl_3(dppeO_2)_{1.5}]_n$ (Ln = Nd, Gd), were synthesised by the addition of two equivalents of $dppeO_2$ with one equivalent of the lanthanide trichloride in methanol in a stainless steel reactor under solvothermal conditions. Single crystal X-ray diffraction analysis of the resulting crystals showed these complexes adopt the 'brick'

architecture, with a six-coordinate octahedral metal centre and each ligand coordinating to two metal centres. Reactions of hydrated $[Ln(NO_3)_3]$ (Ln = Pr, Nd, Sm, Dy) with $dppeO_2$ in identical conditions also led to a two-dimensional polymeric lattice, of the form $[Ln(NO_3)_3(dppeO_2)_{1.5}]_n$. However, the larger, lighter $[Ln(NO_3)_3]$ (Ln = Pr, Nd) nodes lead to a distortion of the brick like architecture, the polymeric structures of $[Pr(NO_3)_3(dppeO_2)_{1.5}]_n$ and $[Nd(NO_3)_3(dppeO_2)_{1.5}]_n$ resembling a parquet floor or herringbone pattern, as described by the authors. Finally, $[Sm(NO_3)_3(dppeO_2)_{1.5}]_n$ and $[Dy(NO_3)_3(dppeO_2)_{1.5}]_n$ also form brick structures, however unlike the chlorides which form clear rectangular units, distortion leads to a more square-shaped structure. The structures of these are much closer to that of the 'brick' architecture than the 'parquet' architecture, however, the tiles are more distorted than in the chloride structures and are much closer to square in shape. All of these structures show a *meridional* isomer, with the chlorides adopting an octahedral geometry and the nitrates a pseudo-octahedral geometry.

Two polymeric lanthanide phosphine oxide compounds were obtained by layering solutions of one equivalent of the hydrated lanthanide nitrates (Pr and Nd), in a gel formed from polyethylenoxide, ethanol and dichlorethane, with $dppeO_2$ in the same gel mixture. This was left to stand for 2-4 weeks at room temperature until a crystalline solid formed $[Ln(NO)_3(dppeO_2)_{1.5}]_n$, of which, the crystal structure displayed a different type of ligand architecture, 'distorted honycomb', Figure 2.3. The hexagonal tiles are formed due to the 9-coordinate pseudo-octahedral species instead adopting a *facial* isomer. In a similar fashion, two compounds were made by layering a solution of one equivalent of a hydrated lanthanide salt ($Pr(NO_3)_3$ and $Dy(NO_3)_3$) with two equivalents of $dppeO_2$ in methanol. This led to the formation of two bi-nuclear species $[Pr_2(NO_3)_4(dppeO_2)_5][NO_3]_2$ and $[Dy_2(NO_3)_6(dppeO_2)_3]$. These, alongside a lutetium species, $[Lu_2(NO_3)_6(dppeO_2)_3]$, produced in a solvothermal reaction as described above, were the only molecular compounds obtained in the study. The formation of the binuclear species were especially surprising for the earlier lanthanides, as the flexible $dppeO_2$ ligand is shown to form the polymeric $[Ln(NO)_3(dppeO_2)_{1.5}]_n$ (Ln = Pr, Dy) under higher ligand concentrations, after which it becomes insoluble. The author suggests the lanthanide contraction is a likely explanation for the unsuccessful preparation of a polymeric lutetium complex, as the $dppeO_2$ ligand is possibly too short to hold the small nodes apart. While this explanation is plausible, it is important to remember that binuclear species were also produced for both praseodymium and neodymium salts. It is, therefore, suggested that crystallisation of a species is affected by a number of factors and the reaction conditions are extremely important in determining the solid product obtained. Curiously, the binuclear

praseodymium structure shows two NO_3^- ligands being displaced from the metal centre, leading to an ionic salt, which is uncommon due to the strong coordinating nature of the nitrate ligands. The formation of an ionic salt is also observed for the $dppmO_2$ species described above, $[Ln(NO_3)_2(dppmO_2)_2(H_2O)][NO_3]$ (Ln = Nd, Gd, Ho), and so bidentate phosphine oxides are clearly quite strongly coordinating ligands.

2.1.3 Aims

This chapter aims to study the coordination chemistry and structures of three phosphine oxides; $dppmO_2$ ($Ph_2POCH_2POPh_2$), $dppeO_2$ ($Ph_2PO\{CH_2\}_2POPh_2$) and PPO_2 (*o*-$C_6H_4\{POPh_2\}_2$) with a range of trivalent lanthanides. The emphasis will be on lanthanum and lutetium salts, owing to their positions at the start and end of the series. This will allow the exploration of the effect of various metal centres, counter-ions and ligand architectures. Literature data shows that, individually, these are some of the major factors in the outcome of these types of reactions, for the few lanthanide(III) salts known. Here a focus is placed on studying how varying each of these factors affects the outcome specifically.

2.2 Results and Discussion

Initial reactions of hydrated lanthanide halides with phosphine oxides were performed with $dppmO_2$, as bidentate chelation would lead to a favourable six membered coordination ring, such as the example shown in Scheme 2.1. Reactions were performed in ethanol, whereas with the more moisture sensitive LaI_3 and LuI_3, reactions performed in rigorously dried ethanol.

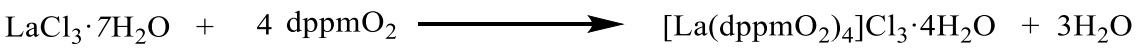

Scheme 2.1. A scheme showing a representative example of the reaction between a hydrated lanthanide halide and $dppmO_2$.

In order to study the effect of anions with different coordinating strengths on the lanthanide speciation, a range of counter ions was selected, Cl^-, I^-, PF_6^-. Reactions of $LaCl_3{\cdot}7H_2O$, LaI_3 and $LaCl_3{\cdot}7H_2O$ with three molar equivalents of $[NH_4][PF_6]$ and four molar equivalents of $dppmO_2$ in ethanol solutions were performed in order to provide an excess of ligand to allow each lanthanide to accommodate its optimal number of phosphine oxide ligands. These reactions led to the formation of the complexes, $[La(dppmO_2)_4]Cl_3{\cdot}4H_2O$, $[La(dppmO_2)_4]I_3{\cdot}2H_2O$, and $[La(dppmO_2)_4][PF_6]_3$, respectively. The large La^{3+} ion readily achieves the same eight-coordinate cation as seen above for the lanthanum triflate salt, $[La(dppmO_2)_4][OTf]_3{\cdot}1.5H_2O$,[20] even in the presence of potentially competing coordination anions Cl^- and I^-. The presence of $[PF_6]^-$ anions is confirmed by $^{31}P\{^1H\}$ NMR spectroscopy, however due to the insolubility of these compounds integration of the resonances is difficult due to noise. As such the use of elemental analysis to confirm the molecular formulae is necessary.

The presence of the same $[La(dppmO_2)_4]^{3+}$ cation in all three salts is confirmed by the $^{31}P\{^1H\}$ NMR spectra in CD_2Cl_2 solution which show a singlet with nearly identical chemical shifts for the Cl^-, PF_6^- and I^- salts at 33.1, 33.5 and 33.8 ppm, respectively. The solubility in CH_2Cl_2 is rather poor (but adequate). Using MeOD, where solubility was much better, the spectra exhibited very similar chemical shifts, suggesting the presence of the same cation. The $^{31}P\{^1H\}$ NMR chemical shifts of free $dppmO_2$ are $\delta(^{31}P) = 25.3$ (CH_2Cl_2) and 29.9 (MeOH) and there is no evidence that methanol displaces the $dppmO_2$ from the lanthanum (III) ion. The ^1H NMR spectra are also identical between the three complexes, except for resonances

relating to the presence of EtOH or water lattice solvent. The residual proton signals in CD_3OD are almost coincident with the $\delta(CH_2)$ resonance in the $dppmO_2$, (3.30 ppm) in the ^1H NMR spectra. Therefore, by using both NMR solvents, the resonance of the CH_2 protons was unambiguously identified. The IR spectra also show two ν(P=O) vibrations for each of the three salts, at identical energies (1160, 1100 cm^{-1}), consistent with the presence of the same cation, which appear not to be influenced by the specific anion present.

Unambiguous confirmation of the presence of the $[La(dppmO_2)_4]^{3+}$ cation was provided by the X-ray crystal structures of $[La(dppmO_2)_4][PF_6]_3$ and $[La(dppmO_2)_4][I_3][I]_2$. Colourless crystals of $[La(dppmO_2)_4][PF_6]_3$ were grown by layering ethanolic solutions of $dppmO_2$, $LaCl_3.7H_2O$ and $[NH_4][PF_6]$, Figure 2.4. The solid state data both show an eight coordinate distorted square antiprismatic cation formed by the four bidentate chelating $dppmO_2$ ligands forming a six-membered coordination ring. Pale yellow-brown single crystals grown from ethanolic solutions of $[La(dppmO_2)_4]I_3 \cdot 2H_2O$ were found to be $[La(dppmO_2)_4][I_3][I]_2$. The crystal quality was modest, but the data confirm the presence of the $[La(dppmO_2)_4]^{3+}$ cation. It is expected that adventitious oxygen lead to the oxidation of the iodide anion to form $[I_3]^-$, an effect observed in similar iodide systems.[24] The LaO_8 coordination environment provided by the four chelating $dppmO_2$ ligands is thus found with Cl^-, I^-, PF_6^- and $CF_3SO_3^-$ anions. Only the more strongly coordinating nitrate ions can compete for binding to the lanthanum as in $[La(dppmO_2)_2(NO_3)_3]$.[18]

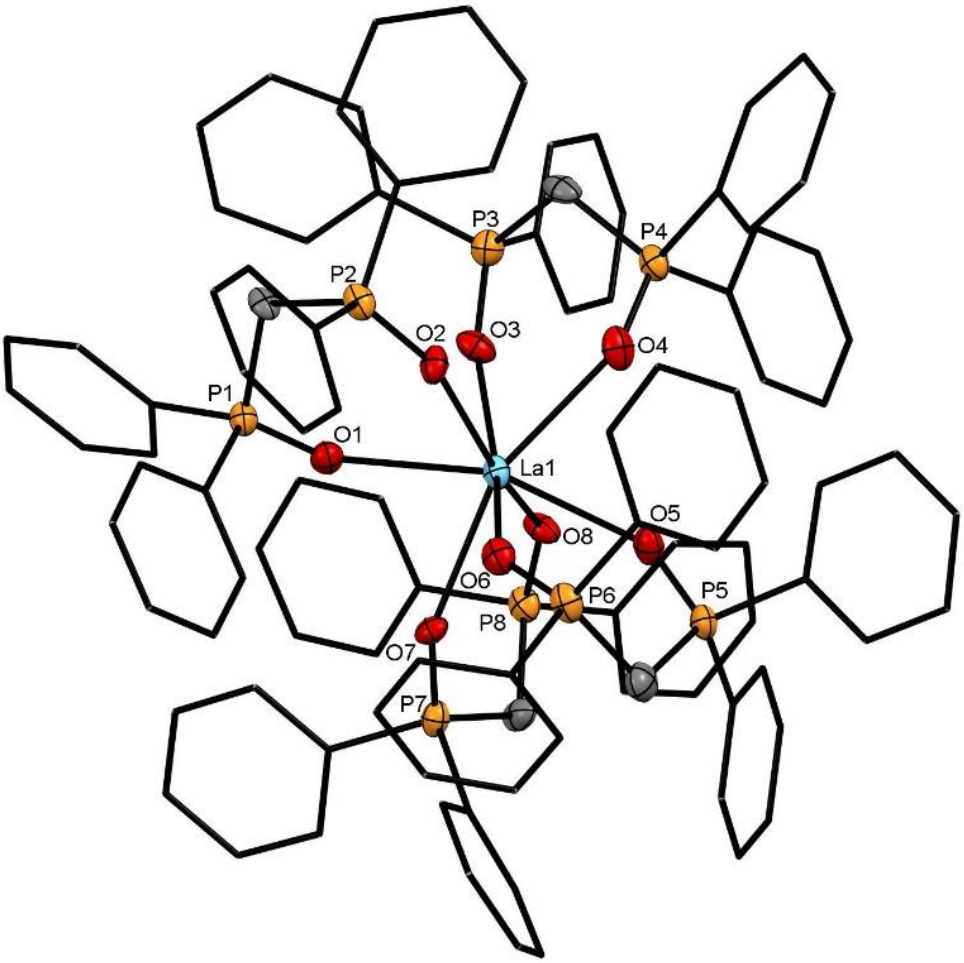

Figure 2.4. The core geometry of the cation in $[La(dppmO_2)_4][PF_6]_3$·(EtOH) with atom numbering scheme. H atoms are omitted, and the phenyl rings are depicted as a wire frame for clarity. Thermal ellipsoids are drawn with a 50% probability level. Cation is isostructural to the species in $[La(dppmO_2)_4][I_3][I]_2$. Selected bond lengths (Å) and angles (°): La1-O1 = 2.502(7), La1-O2 = 2.487(7), La1-O3 = 2.518(7), La1-O4 = 2.566(7), La1-O5 = 2.467(7), La1-O6 = 2.556(8), La1-O7 = 2.506(7), La1-O8 = 2.514(7), O1-La1-O2 = 71.1(2), O1-La1-O3 = 74.4(2), O1-La1-O6 = 100.2(2), P1-O1-La1 = 140.8(4), P2-O2-La1 = 148.8(4), P3-O3-La1 = 148.2(4), P4-O4-La1 = 139.4(4).

The bidentate $dppmO_2$ forms a six-membered chelate ring upon coordination to the lanthanide ion and this is conformationally favourable. In contrast, the reaction of $LaCl_3·7H_2O$ with $dppeO_2$ leads to a polymeric structure of a similar form to those described in Section 2.2.1. Attempts were made to synthesise a mononuclear trivalent lanthanide species with $dppeO_2$, however, irrespective of the ratio of metal salt to ligand attempted (1:1.5, 1:3, 1:4), reactions

produced the polymer $[LaCl_3(dppeO_2)_{1.5}]\cdot n$EtOH, as confirmed by elemental analysis. The same complex was obtained even in the presence of excess $[NH_4][PF_6]$, which was used in an attempt to replace Cl^- with the non-coordinating PF_6^- anion. This might have been expected to lead to the formation of a mononuclear complex, e.g. $[LaCl(dppeO_2)_3][PF_6]_2$. The formation of the polymeric complex is clearly driven by precipitation of the product.

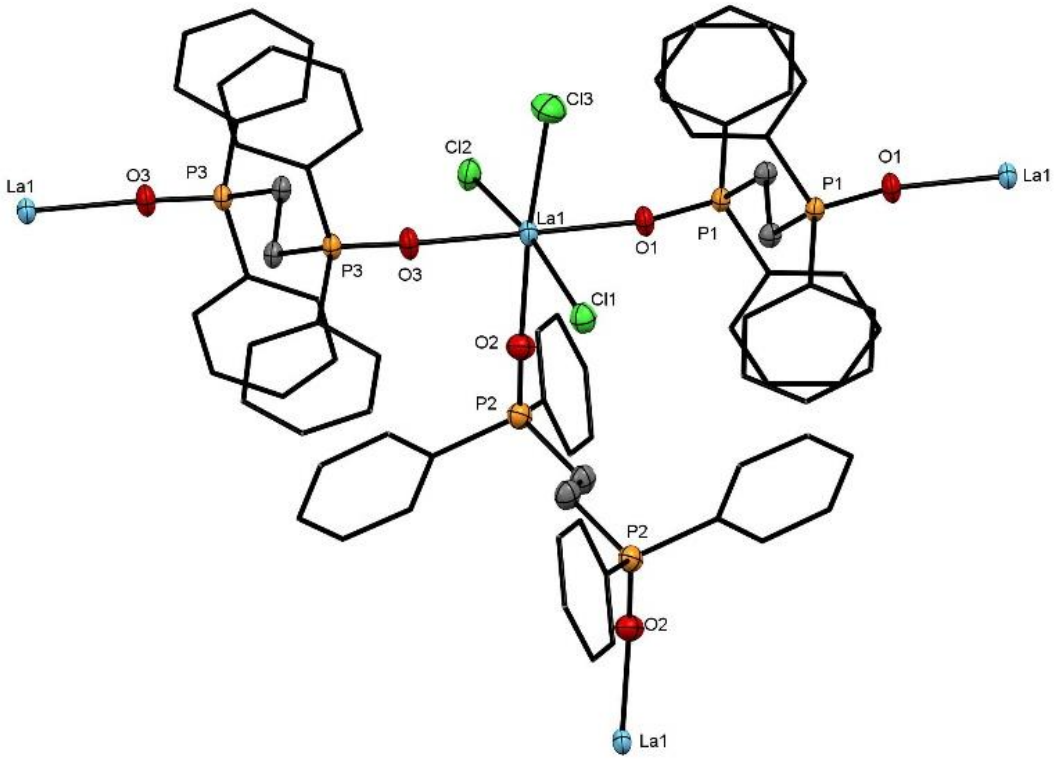

Figure 2.5. The lanthanum coordination environment present in the polymer $[LaCl_3(dppeO_2)_{1.5}]_n$ *with atom numbering scheme. H atoms are omitted and phenyl rings are displayed as wire frames for clarity. Thermal ellipsoids are drawn with a 50% probability level. Selected bond lengths (Å) and angles (°) are: La1-O1 = 2.375(3), La1-O3 = 2.382(3), La1-O2 = 2.414(3), La1-Cl3 = 2.7170(16), La1-Cl2 = 2.7892(14), La1-Cl1 = 2.8005(14), O1-La1-O2 = 86.97(11), O3-La1-O2 = 92.12(11), O1-La1-Cl3 = 89.38(8), O3-La1-Cl3 = 91.71(8), O1-La1-Cl2 = 89.59(8), O3-La1-Cl2 87.07(8), O2-La1-Cl2 = 85.89(8), Cl3-La1-Cl2 = 97.44(4), O1-La1-Cl1 = 90.78(8), O3-La1-Cl1 = 92.36(8), O2-La1-Cl1 = 82.88(8), Cl3-La1-Cl1 = 93.82(4).*

The lanthanum ion lies in a distorted octahedral environment composed of three chlorides and three phosphine oxide groups from different $dppeO_2$ ligands, giving a *mer*-geometry, and therefore a 'brick' architecture. The polymer assembles via the bridging $dppeO_2$ units and is isomorphous to those reported by Spichal *et. al*.[23]

It was proposed that *bis*(diphenylphosphino)benzene dioxide, PPO_2, may preferably form a seven membered chelate ring, due to its more rigid backbone being pre-organised for chelation. It is also bulkier, and these different steric effects would likely lead to different geometries or coordination numbers, even on a large metal ion like La^{3+}. The reaction of $LaCl_3 \cdot 7H_2O$ with four molar equivalents of PPO_2, (to allow for the possibility of a tetrakis centre), in ethanol produced a white powder upon work-up, which was found to be $[LaCl_2(PPO_2)_2(H_2O)_2]Cl$. In the presence of $[NH_4][PF_6]$, the complex $[LaCl_2(PPO_2)_2(H_2O)_2][PF_6]$ was formed instead. In both cases the formulation is suggested by the microanalytical data. The IR spectra of the two complexes also show the presence of the same cation, with ν(P=O) stretches at 1158 and 1095 cm^{-1} for the chloride salt and 1156 and 1095 cm^{-1} for the PF_6 salt. The only difference between the two IR spectra being the presence of the PF_6^- in the latter. The $^{31}P\{^1H\}$ NMR spectra of $[LaCl_2(PPO_2)_2(H_2O)_2]Cl$ were different in CD_2Cl_2 and CD_3OD solutions, with singlets observed at δ = 40.1 (CD_3OD) and δ = 35.5 (CD_2Cl_2). In both cases the resonance has shifted from that seen for free ligand (PPO_2) which lie at δ = 31.4 (CH_2Cl_2) and δ = 37.5 (MeOH), respectively. A single crystal suitable for X-ray diffraction studies, grown from an EtOH solution of the compound stored at -18 ˚C, showed the formation of $[LaCl_2(PPO_2)_2(H_2O)(EtOH)]Cl$. This strongly suggests that the differing $^{31}P\{^1H\}$ NMR chemical shifts can be explained by changes in speciation, with $[LaCl_2(PPO_2)_2(H_2O)_2]Cl$ present in the non-coordinating CH_2Cl_2 and $[LaCl_2(PPO_2)_2(H_2O)_{2-x}(ROH)_x]Cl$ in CD_3OD. The alcohol competes with the water for the lanthanum centre, there is no evidence that alcohols displace the PPO_2 from lanthanum.

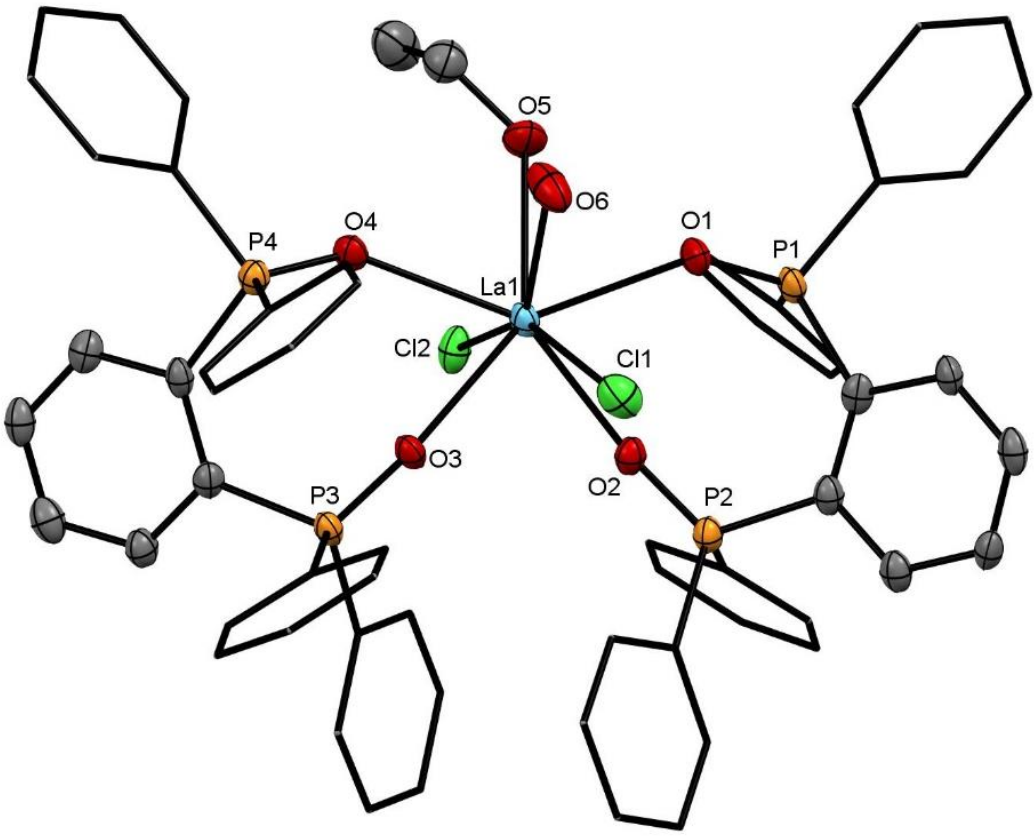

Figure 2.6. The structure of the cation in [$LaCl_2(PPO_2)_2(H_2O)(EtOH)$]Cl.3.5EtOH with atom numbering scheme. H atoms are omitted, and pendant phenyl rings are depicted as a wire frame for clarity. Thermal ellipsoids are drawn with a 50% probability level. Selected bond lengths (Å) and angles (˚) are: *La1-O3 = 2.448(3), La1-O1 = 2.458(3), La1-O2 = 2.493(3), La1-O4 = 2.523(4), La1-O5 = 2.607(4), La1-O6 = 2.637(4), La1-Cl2 = 2.8261(14), La1-Cl1 = 2.9073(15), Cl2-La1-Cl1 = 150.01(4), O3-La1-O2 = 86.32(11), O1-La1-O2 = 71.15(11), O3-La1-O4 = 68.65(11), O1-La1-O5 = 68.61(12), O4-La1-O5 = 74.15(11), O1-La1-O6 = 74.85(12), O4-La1-O6 = 76.76(12), O5-La1-O6 = 69.25(13), O3-La1-Cl2 = 87.91(8), O2-La1-Cl2 = 74.67(8), O4-La1-Cl2 = 83.20(8), O5-La1-Cl2 77.75(10), O3-La1-Cl1 = 77.15(8), O1-La1-Cl1 = 79.02(9), O2-La1-Cl1 = 78.51(8), O6-La1-Cl1 = 65.05(11).*

In a separate experiment a few crystals were grown from the slow evaporation of an EtOH solution of $[LaCl_2(PPO_2)_2(H_2O)_2][PF_6]$. These proved, upon structure solution, to be $[LaCl(PPO_2)_3][PF_6]_2$, Figure 2.7, with three chelating PPO_2 ligands on a seven-coordinate, distorted capped octahedral lanthanum centre. The capping chloride ligand was disordered over two sites, but this was satisfactorily modelled. The crystallisation of different complexes from

solution is a common observation in lanthanide coordination chemistry, for example $[Ln(Ph_3PO)_3(NO_3)_3]$ or $[Ln(Ph_3PO)_2(EtOH)(NO_3)_3]$ crystallise from ethanol solutions of $Ln(NO_3)_3$ and Ph_3PO under very similar conditions.

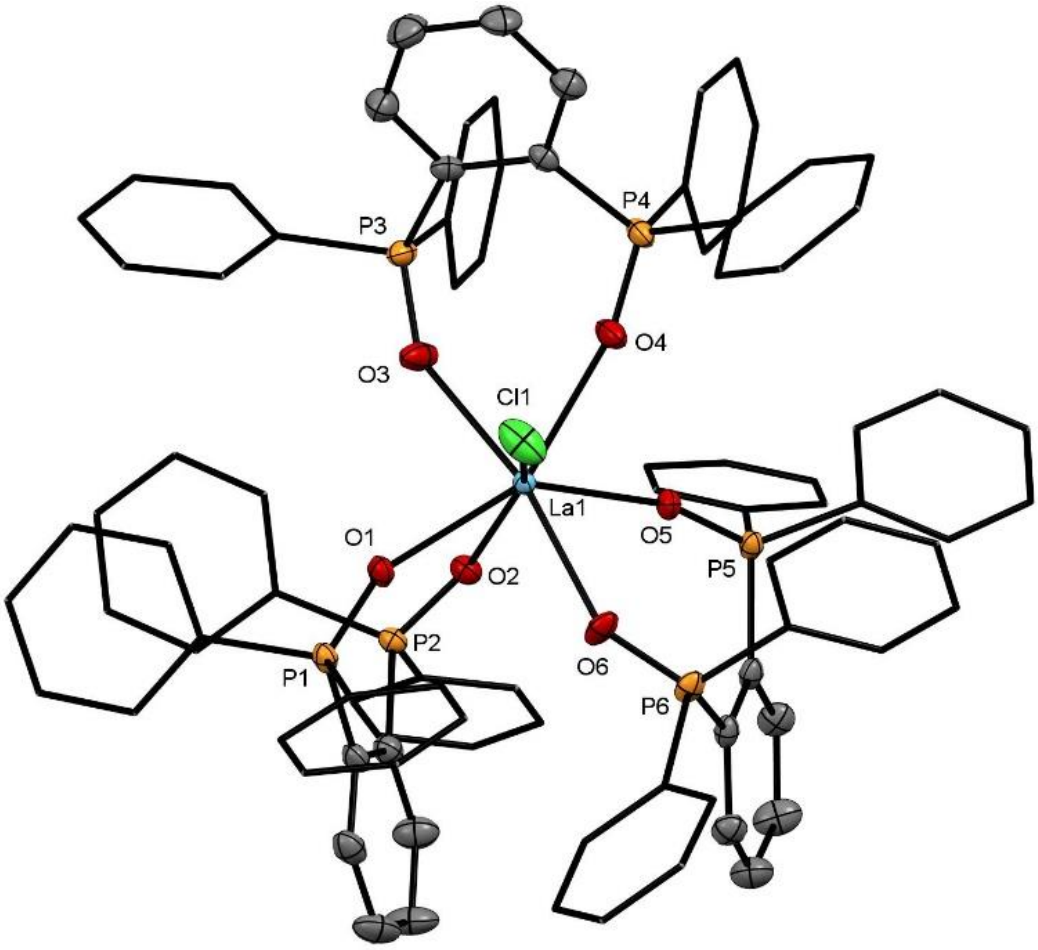

Figure 2.7. The structure of the cation in $[LaCl(PPO_2)_3][PF_6]_2$ with atom numbering scheme. H atoms are omitted, and pendant phenyl rings are displayed as wire frames for clarity. Thermal ellipsoids are drawn with a 50% probability level. The chloride was disordered over two sites in the ratio 9:1 and only the major form one is shown. Selected bond lengths and angles are: La1-O3 = 2.413(4), La1-O6 = 2.413(4), La1-O4 = 2.436(4), La1-O5 = 2.450(3), La1-O2 = 2.453(3), La1-O1 = 2.454(3), La1-Cl1A = 2.747(15), O3-La1-O4 = 70.52(14), O6-La1-O5 = 70.53(12), O4-La1-O5 = 71.16(12), O3-La1-O2 = 87.22(13), O6-La1-O2 = 86.64(13), O5-La1-O2 = 77.50(12), O3-La1-O1 = 86.09(14), O6-La1-O1 = 82.71(13), O2-La1-O1 = 70.49(11), O3-La1-Cl1A = 61.9(6), O6-La1-Cl1A = 116.3(6), O4-La1-Cl1A = 79.8(5).

The formation of a *tris*-PPO_2 complex, as opposed to a *tetrakis*-$dppmO_2$ cation similar to that described above, is likely to be a consequence of the greater steric demands of PPO_2. In the cations $[LaCl_2(PPO_2)_2(H_2O)_2]^+$ and $[LaCl_2(PPO_2)_2(H_2O)(EtOH)]^+$, two chelating PPO_2 ligands are present and the large lanthanum centre achieves eight-coordination by binding four less sterically demanding ligands. A seven-coordination La complex with three PPO_2 ligands and one chloride is shown, Figure 2.7, though an eight-coordination species via a *tetrakis*-PPO_2 cation is likely ruled out on steric grounds.

It is well known that the lanthanides often display a stepwise reduction of coordination numbers as you go across the series, (La → Lu). However, historically, it was common to use two representative metal ions (typically La and Lu) and extrapolate across the series. Instead, in this work, several lanthanide chlorides were reacted with the less sterically demanding ligand, $dppmO_2$ to attempt to observe the trend along the series.

The reaction of $CeCl_3.7H_2O$ with 4 molar equivalents of $dppmO_2$ in ethanol resulted in the growth of colourless crystals of $[Ce(dppmO_2)_4]Cl_3.4H_2O$ with a cation *iso*-structural to that of the previously discussed $[La(dppmO_2)_4]^{3+}$, Figure 2.4. A $^{31}P\{^1H\}$ NMR study (CD_2Cl_2) of $[Ce(dppmO_2)_4]Cl_3$ showed a shift in the $^{31}P\{^1H\}$ NMR spectrum from free ligand (δ = 24.9) to δ = 48.6 and ν(P=O) stretches are seen at 1157 and 1099 cm^{-1}. A ^1H NMR study showed that the methylene peaks are extremely broad and difficult to identify, likely owing to some lability of the protons in solution. Reactions were also attempted on a 1:2 and 1:3 (metal halide : ligand) ratio however these produced identical $^{31}P\{^1H\}$ NMR and infrared spectra and single crystal x-ray diffraction determined they were also the *tetrakis*- species.

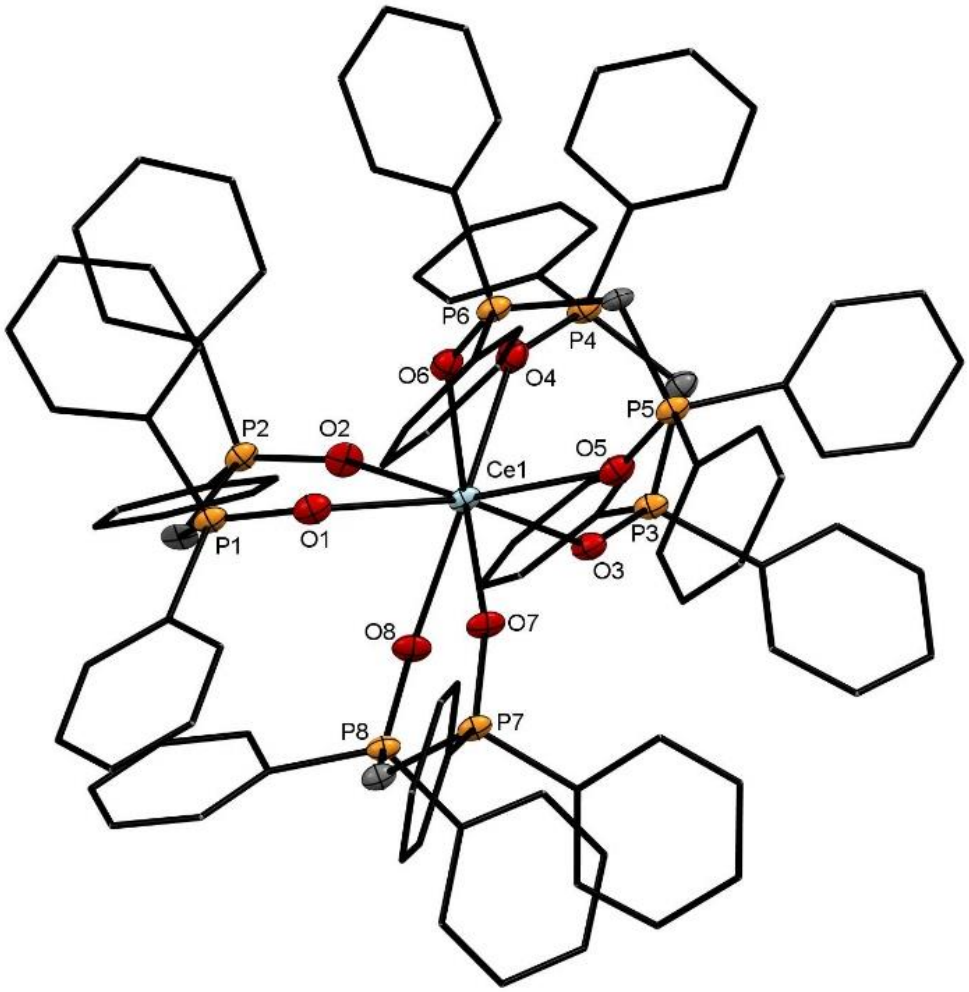

Figure 2.8. The structure of the cation in $[Ce(dppmO_2)_4]Cl_3 \cdot 4H_2O$ with atom numbering scheme. H atoms are omitted for clarity and phenyl rings are depicted as wireframes. Thermal ellipsoids are drawn with a 50% probability level. Selected bond lengths (Å) and angles (°): Ce1-O1 = 2.479(7), Ce1-O2 = 2.482(6), Ce1-O3 = 2.498(8), Ce1-O4 = 2.494(7), Ce1-O5 = 2.495(7), Ce1-O6 = 2.474(8), Ce1-O7 = 2.484(7), Ce1-O8 = 2.487(8), P1-O1-Ce1 = 144.7(4), P2-O2-Ce1 = 141.8(4), P3-O3-Ce1 = 146.0(5), P4-O4-Ce1 = 142.9(4), P5-O5-Ce1 = 141.0(4), P6-O6-Ce1 = 146.8(5), P7-O7-Ce1 = 147.5(4), P8-O8-Ce1 = 144.1(4), O1-Ce1-O2 = 73.0, O1-Ce1-O5 = 156.2(2), O1-Ce1-O8 = 70.4(2).

Following this, to study the trend of Ln(III) chloride complexes with $dppmO_2$ along the series, a series of reactions of lanthanide chloride hydrates (Sm, Eu, Gd, Tb, Dy, Er, Yb) and anhydrous holmium trichloride, with three molar equivalents of $dppmO_2$ were performed in ethanol. The NMR and key infrared spectroscopic data are tabulated below, Table 2.1. These cannot be compared across the series, but each complex shows evidence of coordinated

$dppmO_2$ and a rapidly exchanging system in solution. The presence of Ln-Cl infrared bands are assigned where observed (between 205 – 215 cm^{-1}), in Section 2.4.2, however this range is approaching the limits of the spectrometer (200 cm^{-1}) and as such assignments are made tentatively Each of the products was rigorously dried and then stored in a vacuum desiccator to remove any residual solvent and elemental analysis confirms the products to have the empirical formulation $LnCl_3(dppmO_2)_3$. Crystals obtained of $[EuCl(dppmO_2)_3]Cl_2$ and $[YbCl(dppmO_2)_3]Cl_2$, Figure 2.9, suggest that this is a likely speciation for all of these later lanthanides, and provide unambiguous evidence for the formation of *tris*-$dppmO_2$ cations.

Table 2.1. Selected data from $^{31}P\{^1H\}$ NMR and infrared spectra for a range of tris complexes of the form $[LnCl(dppmO_2)_3]Cl_2$.

Suggested Species	$^{31}P\{^1H\}$ NMR (ppm)	P=O Stretch (cm^{-1})
$[SmCl(dppmO_2)_3]Cl_2$	38.15	1153, 1097
$[EuCl(dppmO_2)_3]Cl_2$	-14.85	1153, 1098
$[GdCl(dppmO_2)_3]Cl_2$	-32.10	1153, 1097
$[TbCl(dppmO_2)_3]Cl_2$	-28.74	1153, 1097
$[HoCl(dppmO_2)_3]Cl_2$	-14.15	1152, 1096
$[YbCl(dppmO_2)_3]Cl_2$	9.19	1154, 1097

The reaction of $SmCl_3{\cdot}6H_2O$ with three molar equivalents of $dppmO_2$ led to precipitation of a white solid via concentration of the reaction mixture and the addition of 1 mL of n-hexane. Elemental analysis of this powder suggests the sample to have empirical formula $SmCl_3(dppmO_2)_3$, although it is very difficult to determine whether this adopts a seven or eight coordinate species. An ethanolic solution of the product was left to evaporate, yielding colourless crystals of $[Sm(dppmO_2)_4]Cl_3$, presumably a minor product formed by rearrangement of the *tris*-$dppmO_2$ complex.

The remaining lanthanides all formed complexes of the form $[LnCl(dppmO_2)_3]Cl_2$ (Ln = Eu, Gd, Tb, Ho, Yb). As displayed above, Table 2.1, there is no particular trend in the $^{31}P\{^1H\}$ NMR data. In each case, the single resonance is often displayed as a broad singlet, suggesting either a single cation or a dynamic rapidly exchanging process on the NMR timescale. The infrared spectra show a clear shift from free ligand for the ν(P=O) stretch, however, there is no observable trend that can be identified in the two ν(P=O) stretches as the metal centre gets smaller. The formulation of each of the compounds were confirmed by elemental analysis,

including the samarium complex. The coordination environment was unequivocally determined in the case of $[YbCl(dppmO_2)_3]Cl_2$ by single crystal X-ray analysis. The coordination environment was unequivocally determined in the case of $[YbCl(dppmO_2)_3]Cl_2$ by single crystal X-ray analysis. The structure of $[YbCl(dppmO_2)_3]Cl_2$, shown in Figure 2.9, shows a distorted pentagonal bipyramidal geometry around the metal centre, with the metal centre sitting just 0.078 Å out of the plane of the equatorial oxygen atoms. This seven-coordinate geometry was also displayed in the europium complex, $[EuCl(dppmO_2)_3]Cl_2$. Although the single crystal data of the latter was of poorer quality, it was sufficient to confirm the geometry around the europium centre.

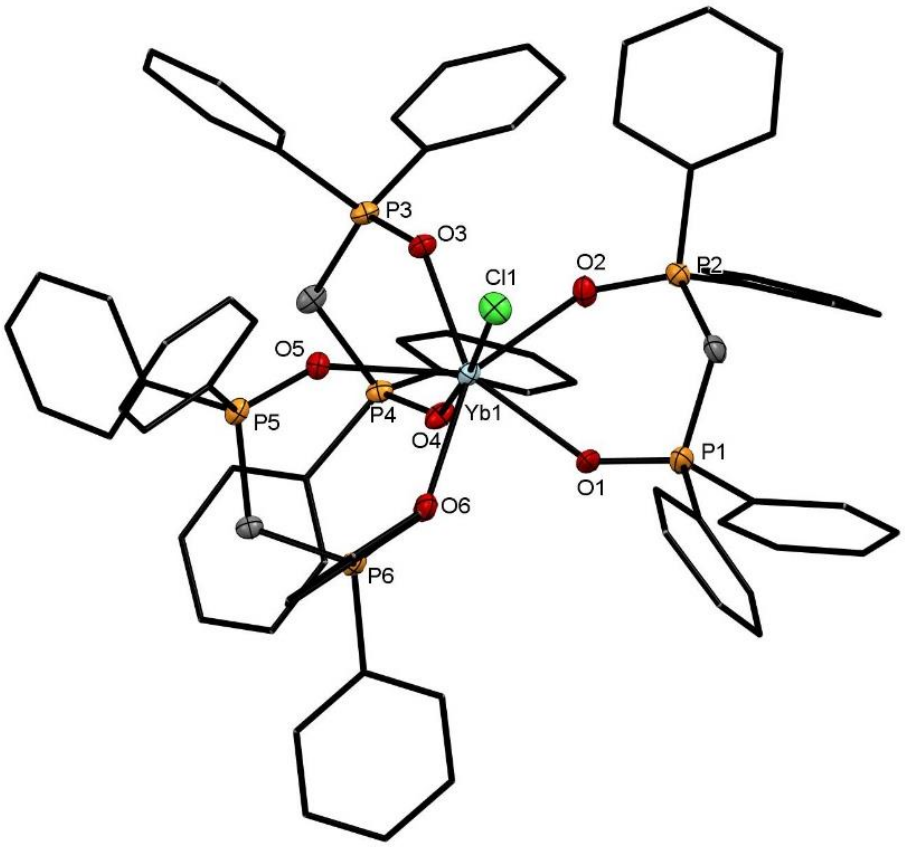

Figure 2.9. The structure of the cation in $[YbCl(dppmO_2)_3]Cl_2 \cdot 4EtOH$ with atom numbering scheme. H atoms are omitted and phenyl rings are drawn as wire frames for clarity. Thermal ellipsoids are drawn at a 50% probability level. Selected bond lengths (Å) and angles (°) are: Yb1-Cl1 = 2.5851 (19), Yb1-O1 = 2.286(6), Yb1-O2 = 2.284(5), Yb1-O3 = 2.263(5), Yb1-O4 = 2.254(6), Yb1-O5 = 2.346(6), Yb1-O6 = 2.260(6), P1-O1-Yb1 = 141.5(4), P2-O2-Yb1 = 140.6(3), P3-O3-Yb1 = 139.4(3), P4-O4-Yb1 = 138.8(3), P5-O5-Yb1 = 146.5(4), P6-O6-Yb1 = 147.7(3), O1-Yb1-O2 = 74.0(2), O1-Yb1-Cl1 = 91.78(18), O1-Yb1-O6 = 71.2.

Attempts to make complexes with the smaller, later lanthanides coordinated by four $dppmO_2$ ligands were unsuccessful and all led to similar spectroscopic and solid state data which were indicative of the tris-complexes. However, a crystal obtained from a cooled ethanolic solution of $YbCl_3 \cdot 6H_2O$ with 4 equivalents of $dppmO_2$ led to a structure of $[Yb(dppmO_2)_3(H_2O)]Cl_3 \cdot (dppmO_2)(H_2O)_{12}$. The structure of the cation and excess ligand is shown below, Figure 2.1. The H_2O molecules are all hydrogen bonded to each other and are holding each of the Cl^- counter ions in place. The structure shows the heptadentate molecule with the expected three $dppmO_2$ ligands coordinated to the metal centre. A coordinated water takes the place of the chloride from the previously discussed structure and holds the excess ligand in place with hydrogen bonding. Rather than the pentagonal bipyramidal structure displayed above, the geometry is a distorted capped octahedral geometry. Given the ease with which the larger lanthanides form a *tetra*-coordination complex, this structure is quite compelling evidence that, owing to the lanthanide contraction, *tris*-coordination complexes are heavily preferred for the smaller lanthanides with the *tetra*-coordination complexes being much more difficult to achieve.

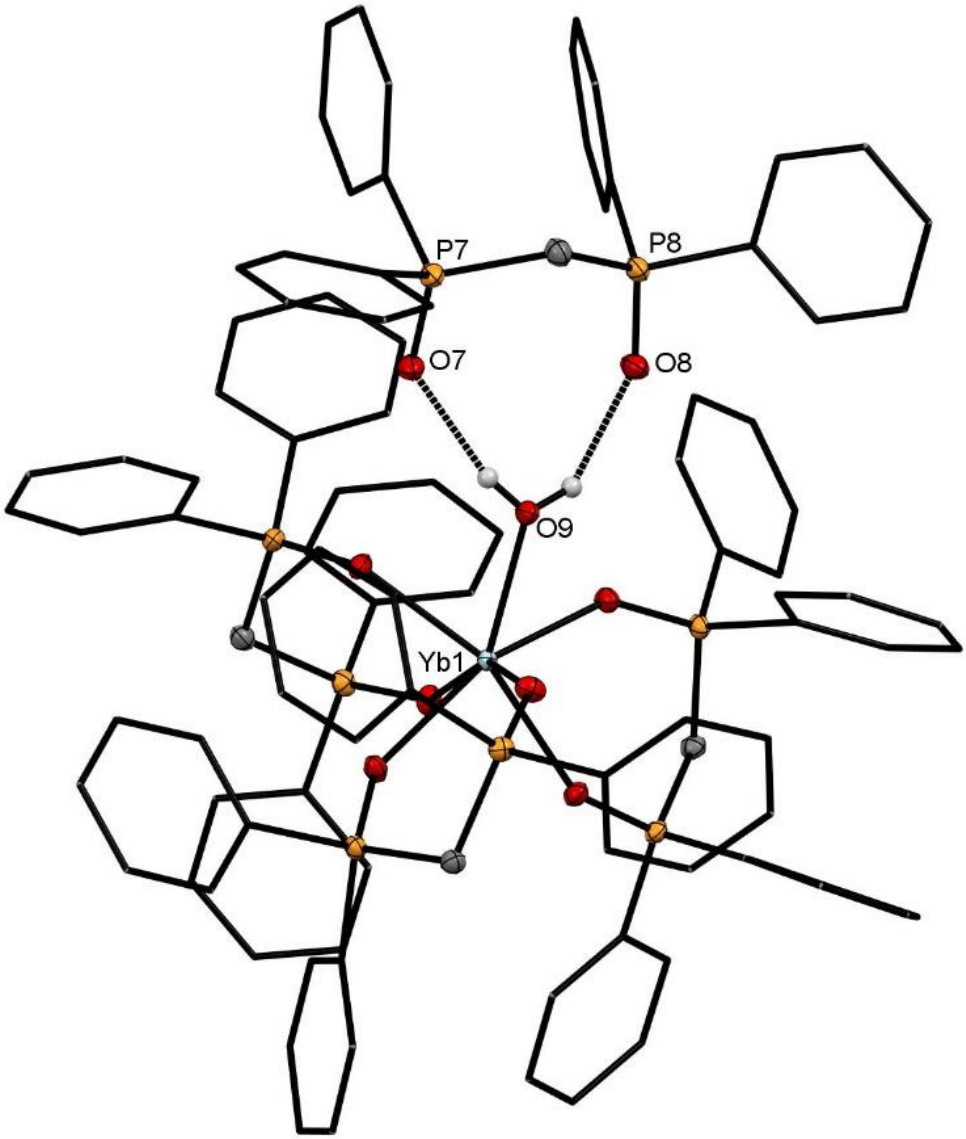

Figure 2.10. A crystal structure depicting the cation $[Yb(dppmO_2)_3(H_2O)]^{3+}$ *and a free dppmO2 ligand hydrogen bonding to the coordinated water. Ellipsoids are drawn at a 50% probability level. Hydrogen atoms have been omitted, phenyl rings have been displayed as wire frames and only relevant labels have been displayed for clarity. Selected bond lengths (Å): Yb1-O1 = 2.2346(16), Yb1-O2 = 2.2912(16), Yb1-O3 = 2.2346(16), Yb1-O4 = 2.2706(16), Yb1-O5 = 2.2220(16), Yb1-O6 = 2.2702(16), Yb1-O9 = 2.3302(17), H9A-O8 = 1.938, H9B-O7 = 1.903.*

The reaction of $LuCl_3 \cdot 6H_2O$ with three molar equivalents of $dppmO_2$ in ethanol gave a *bis*-$dppmO_2$ complex formulated on the basis of microanalytical data as $[LuCl_2(dppmO_2)_2]Cl$, containing six-coordinate lutetium. Repeating the reaction with lutetium iodide yielded $[LuI_2(dppmO_2)_2]I$. The IR spectra of each complex showed two ν(P=O) stretches at slightly

different frequencies, 1158 and 1098 cm^{-1} and 1147 and 1094 cm^{-1} respectively, reflecting the different halides present. The $^{31}P\{^{1}H\}$ NMR spectrum of the $[LuCl_2(dppmO_2)_2]Cl$ in CH_2Cl_2, in which it was poorly soluble, contained a singlet at δ = 36.3, whilst in MeOH solution the resonance was observed at δ = 39.1 ppm. The reaction of $LuCl_3{\cdot}6H_2O$ with three equivalents of $dppmO_2$ in the presence of $[NH_4][PF_6]$ gave a complex of microanalytical composition $LuCl(dppmO_2)_2(PF_6)_2{\cdot}3H_2O$. The presence of a six-coordinate cation, $[LuCl(dppmO_2)_2(H_2O)]^+$ seems highly likely, due to the preference for a six-coordinate metal centre, for example Figure 2.11. A 4 ppm shift in the $^{31}P\{^{1}H\}$ NMR spectra between the cation resonances in CD_2Cl_2 and CD_3OD is observed, this is attributed to changes ins speciation *via* the partial displacement of the chloride or water in CD_3OD. The $^{31}P\{^{1}H\}$ NMR spectrum of $[LuI_2(dppmO_2)_2]I$ in CD_2Cl_2 shows four sharp resonances, at 41.4, 40.6, 39.1 and 36.0 ppm, suggesting a mixture of species present in solution, likely due to reactions with the solvent. None of the resonances corresponded to that of free $dppmO_2$. In CD_3OD only a single sharp resonance is observed. This is likely due to a displacement of the iodides from the coordination sphere by methanol.

The lutetium–PPO_2 complexes isolated were $[LuCl_2(PPO_2)_2]Cl$, $[Lu(PPO_2)_2(H_2O)_2][PF_6]_3$ and $[LuI_2(PPO_2)_2]I$, all based upon six-coordinate lutetium. The solution $^{31}P\{^{1}H\}$ NMR, CD_2Cl_2 spectra show a single resonance for $[LuCl_2(PPO_2)_2]Cl$ and $[Lu(PPO_2)_2(H_2O)_2][PF_6]_3$, at 42.1 and 41.1 ppm respectively, consistent with the presence of one significant species in each with equivalent phosphine oxide groups. The $^{31}P\{^{1}H\}$ NMR, CD_2Cl_2, of $[LuI_2(PPO_2)_2]I$ shows three peaks likely owing to some decomposition of the product and displacement of the iodide ligands from the coordination sphere caused by the solvent, as seen for $[LuI_2(dppmO_2)_2]I$. A single resonance is seen for all three species in CD_3OD as expected. A single crystal structure of a lutetium species, $[LuCl_2(PPO_2)_2]Cl$ was obtained, Figure 2.11. The crystal was of modest quality and although the cation appears to be well resolved, the anion was disordered and therefore this data should only be used to determine the geometry around lutetium centre, with little other structural information being reliable.

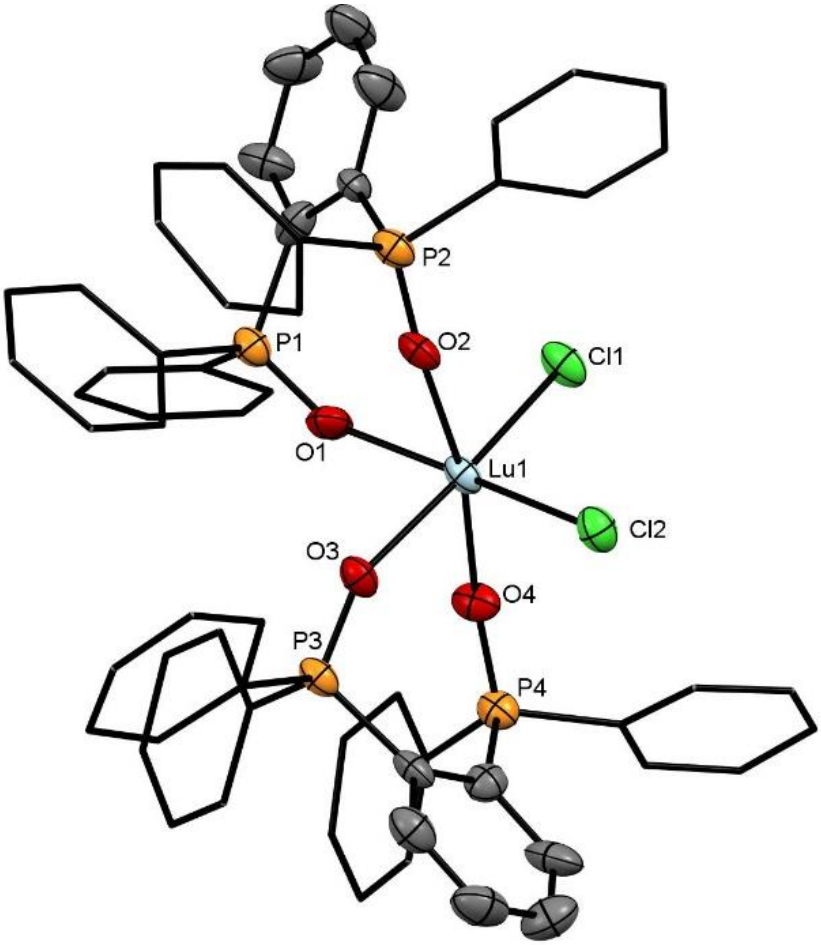

Figure 2.11. The structure of the cation in $[LuCl_2(PPO_2)_2]Cl$ with atom numbering scheme. H atoms are omitted, and pendant phenyl rings are displayed as wire frames for clarity. Thermal ellipsoids are drawn with a 50% probability level.

2.3 Conclusions

The successful synthesis of the lanthanum complexes; $[La(dppmO_2)_4]Cl_3$, $[La(dppmO_2)_4][PF_6]_3$, $[La(dppmO_2)_4]I_3$, $[LaCl_3(dppeO_2)_{1.5}]_n$, $[LaCl_2(PPO_2)_2(H_2O)_2]Cl$ and $[LaCl_2(PPO_2)_2(H_2O)_2][PF_6]$ have been described. The products have been analysed with infrared spectroscopy, ^1H NMR and $^{31}P\{^1H\}$ NMR spectroscopy, elemental analysis and single crystal X-ray diffraction where possible. It is clear that the large La^{3+} cation is readily able to accommodate eight-coordination with four $dppmO_2$ ligands, forming six-membered chelate rings even in the presence of Cl^- or I^-. However, the extra CH_2 unit in the ethylene backbone of $dppeO_2$ led to only polymeric compounds. Attempts to form mononuclear species with the ligand were ultimately unsuccessful. It was possible to achieve seven-membered chelate rings through the use of the bulkier and more rigid PPO_2 ligand, which also formed eight-coordinate species. Due to the size and steric bulk of the ligand, the eight-coordinate geometry is instead achieved with the small monodentate ligands, Cl^- and water. It is likely that the steric bulk three PPO_2 ligands are the most this metal centre would be able to accommodate, as displayed in a crystal structure of $[LaCl(PPO_2)][PF_6]_2$. It is often much easier to analyse lanthanide complexes in the solid state, as solutions often consist of an equilibrium of rapidly exchanging species and spectra often show only an average of these. These rapidly exchanging solutions precipitate the least soluble product and so it is often not the case that the solution data is describing only the product seen in the solid state.

Also described are $[Ce(dppmO_2)_4]Cl_3$ and complexes of the form $[LnCl(dppmO_2)_3]Cl_2$ (Ln = Sm, Eu, Gd, Tb, Ho, Yb). The large cerium metal centre, much like lanthanum, readily adopts four $dppmO_2$ ligands, with crystals of the *tetrakis*-complex grown regardless as to the M:L ratio in the reaction mixture. The samarium metal centre, though smaller than cerium, is also large enough to accommodate four $dppmO_2$ ligands as shown by the crystal structure of $[Sm(dppmO_2)_4]Cl_3$. However, elemental analysis of the bulk product suggested a 1:3 ratio of metal to ligand. This is likely due to the size of the samarium metal centre, and given different solvent conditions, different products are able to precipitate out. The formulation $[SmCl(dppmO_2)_3]Cl_2$ is given tentatively based on the other complexes described here, however it is acknowledged that given the larger size of samarium it is possible it is able to accommodate more than one chloride in the coordination sphere. Crystals of $[EuCl(dppmO_2)_3]Cl_2$ and $[YbCl(dppmO_2)_3]Cl_2$ were grown, with the europium structure being of modest quality but good enough to confirm the geometry around the metal centre. The formulation of these *tris*-complexes were also confirmed by elemental analysis. A series of

$^{31}P\{^{1}H\}$ NMR studies of the complexes in CD_2Cl_2, showed a single resonance for each complex, all these were significantly shifted from free ligand. Addition of excess ligand to a solution of $[YbCl(dppmO_2)_3]Cl_2$ afforded a crystal, which on structure solution was determined to be solvated $[Yb(dppmO_2)_3(H_2O)]Cl_3 \cdot (dppmO_2)$, with the free $dppmO_2$ ligand held in place by hydrogen bonding to the coordinated water molecule. This is strong evidence that the metal centre is likely not large enough to accommodate a fourth $dppmO_2$ ligand.

Finally, the successful synthesis of the lutetium complexes; $[LuCl_2(dppmO_2)]Cl$, $[LuI_2(dppmO_2)]I$, $[LuCl(dppmO_2)_2(H_2O)][PF_6]_2$, $[LuCl_2(PPO_2)_2]Cl$, $[LuI_2(PPO_2)_2]I$ and $[Lu(PPO_2)_2(H_2O)_2][PF_6]_3$ have been described. The small lutetium metal centre is six-coordinate in all of the reported complexes. While the anion was disordered, the six-coordinate geometry of $[LuCl_2(PPO_2)_2]^+$ is clearly visible in the only structural data obtained. The $^{31}P\{^{1}H\}$ NMR studies showed that the counter-ions and water are readily displaced by methanol, however there is no evidence of methanol displacing the ligand. The iodide complexes are more readily decomposed in dichloromethane, compared to the chloride and PF_6^- salts, however, all solutions are likely showing an exchanging system. The infrared data show coordinated ligand, via a shift in the P=O band from free ligand, and also changes in coordinated counter-ions.

2.4 Experimental

2.4.1 General Experimental

Lanthanide salts and other reagents were obtained from Sigma–Aldrich and used as received. The diphosphine dioxides ($dppmO_2$, $dppeO_2$ and PPO_2) were obtained by air-oxidation of the corresponding diphosphines in anhydrous CH_2Cl_2 solution catalysed by SnI_4.[25] Syntheses involving lanthanide iodides were carried out under a dinitrogen atmosphere, which is essential in the case of the iodide complexes to prevent polyiodide formation.[24]

2.4.2 Lanthanide Phosphine Oxides

$[La(dppmO_2)_4]Cl_3{\cdot}4H_2O$ - $LaCl_3{\cdot}7H_2O$ (0.025 g, 0.067 mmol) was dissolved in ethanol (10 mL). $DppmO_2$ (0.11 g, 0.264 mmol) dissolved in ethanol (15 mL) was then added to the reaction mixture and stirred for 16 h. The solution was concentrated, cooled at −4 °C overnight and then filtered. The resulting white solid was washed with n-hexane (5 mL) then ice-cold ethanol (10 mL) and dried *in vacuo*. Yield: 0.045 g, 34 %. Required for $C_{100}H_{96}LaO_{12}P_8$ (1982.9): C, 60.57; H, 4.88 %. Found: C, 60.41; H, 4.56 %. ^{1}H NMR (CD_2Cl_2): δ = 1.56 (s, H_2O), 3.36 (br m, [2H], PC***H*****$_2$**P), 7.15 (s, [8H], Ph), 7.37 (br m, [4H], Ph), 7.84 (br m, [8H], Ph). $^{31}P\{^1H\}$ NMR (CD_2Cl_2): δ = 33.1 (s). IR spectrum (Nujol mull)/cm^{-1}: 3500 vbr, 1623 m (H_2O), 1159 s, 1100 m (P=O).

$[La(dppmO_2)_4][PF_6]_3$ – $LaCl_3{\cdot}7H_2O$ (0.025 g, 0.067 mmol) and $[NH_4][PF_6]$ (0.033 g, 0.202 mmol) were dissolved in ethanol (10 mL). $DppmO_2$ (0.11 g, 0.264 mmol) dissolved in ethanol (15 mL) was then added to the reaction mixture, which immediately became cloudy. The resulting mixture was stirred for 16 h. The solvent was removed *in vacuo* and the residual white solid was washed with n-hexane (5 mL) then cold ethanol (10 mL), the solid separated and dried *in vacuo*. Yield: 0.097 g, 65 %. Crystals were grown by layering a solution of $dppmO_2$ in ethanol on top of a solution of $LaCl_3{\cdot}7H_2O$ and $[NH_4][PF_6]$ (4:1:3 M ratio) in ethanol. Required for $C_{100}H_{88}F_{18}LaO_8P_{11}$ (2239.3): C, 53.64; H, 3.96 %. Found: C, 53.50; H, 3.79 %. ^{1}H NMR (CD_2Cl_2): δ = 3.30 (t, [2H], PC***H*****$_2$**P), 7.13 (br, [8H], Ph), 7.50 (m, [4H], Ph), 7.74 (m, [8H], Ph). $^{31}P\{^1H\}$ NMR (CD_2Cl_2): δ = 33.5 (s, [8P], ***P***=O), −143.6 (m, [3P], ***P***F_6). IR spectrum (Nujol mull)/cm^{-1}: 1157 s, 1098 m (P=O), 836 s (PF_6), 557 s (PF_6).

$[La(dppmO_2)_4]I_3{\cdot}2H_2O$ - $DppmO_2$ (0.16 g, 0.385 mmol) was dissolved in dry ethanol (15 mL). LaI_3 (0.05 g, 0.096 mmol) dissolved in dry ethanol (10 mL), under nitrogen, was then

added to the ligand solution and stirred for 16 h. The solvent was removed *in vacuo*, and the residual bright yellow solid was washed with dry dichloromethane (5 mL) and dried *in vacuo*. Yield: 0.151 g, 71 %. Crystals were grown by layering a solution of $dppmO_2$ in ethanol on top of a solution of LaI_3 (4:1 M ratio) in ethanol. Required for $C_{100}H_{92}I_3LaO_{10}P_8$ (2185.2): C, 54.07; H, 4.17 %. Found: C, 52.20; H, 4.21 %. ^{1}H NMR (CD_2Cl_2): δ = 1.56 (s, H_2O), 3.47 (m, [2H], PC***H*****$_2$**P), 7.12 (s, [4H], Ph), 7.35 (m, [8H], Ph), 7.71 (m, [4H]), 7.95 (m, [4H], Ph). ^{31}P{^{1}H} NMR (CD_3OD): δ = 33.8 (s). IR spectrum (Nujol mull)/cm^{-1}: 3500 vbr, 1623 m (H_2O), 1161 s, 1098 s (P=O).

[Ce(dppmO$_2$)$_4$]Cl$_3$ - To a solution of $CeCl_3.7H_2O$ (0.025 g, 0.067 mmol) in ethanol (5 mL) was added a solution of $dppmO_2$ (0.112 g, 0.268 mmol) in ethanol (10 mL) and the mixture was stirred for 20 min. The solution was then concentrated and colourless crystals were formed through layering with n-hexane (1 mL). Yield: 0.095 g, 74 %. Required for $C_{100}H_{88}CeCl_3O_8P_8$ (1910.91): C, 62.80; H, 4.64 %. Found: C, 63.56; H, 4.75 %. ^{1}H NMR (CD_2Cl_2): δ = 3.60 (vbr, [2H] PC***H*****$_2$**P), 7.10 (s, [8H], Ph), 7.35 (m, [4H], Ph), 7.70 (m, [8H], Ph). ^{31}P NMR (CD_2Cl_2): δ = 48.55 ppm (s). IR (Nujol mull)/cm^{-1}: 1157 s, 1099 s (P=O).

[SmCl(dppmO$_2$)$_3$]Cl$_2$ - To a solution of $SmCl_3.6H_2O$ (0.025 g, 0.069 mmol) in ethanol (5 mL) was added a solution of $dppmO_2$ (0.086 g, 0.206 mmol) in ethanol (10 mL) and the mixture was stirred for 20 min. The solution was concentrated and a white solid was precipitated with n-hexane (1 mL), which was filtered and dried. Colourless crystals were obtained via slow evaporation of an ethanolic solution of the product. Yield: 0.065 g, 63 %. Required for $C_{75}H_{66}Cl_3O_6P_6Sm$ (1505.05): C, 59.80; H, 4.42 %. Found: C, 59.62; H, 4.55 %. ^{1}H NMR (CD_2Cl_2): δ = 3.67 (br m, [2H], PC***H*****$_2$**P), 7.15 (br, [8H], Ph), 7.35 (m, [4H], Ph), 8.05 (m, [8H], Ph). ^{31}P NMR (CD_2Cl_2): δ = 38.15 ppm (s). IR (Nujol mull)/cm^{-1}: 1153 s, 1097 s (P=O).

[EuCl(dppmO$_2$)$_3$]Cl$_2$ - To a solution of $EuCl_3.6H_2O$ (0.025 g, 0.068 mmol) in ethanol (5 mL) was added a solution of $dppmO_2$ (0.085 g, 0.205 mmol) in ethanol (10 mL) and the mixture was stirred for 20 min. The solution was then concentrated and a white solid was precipitated with n-hexane (1 mL), which was filtered and dried. Yield: 0.058 g, 56 %. Required for $C_{75}H_{66}Cl_3EuO_6P_6$ (1506.65): C, 59.74; H, 4.41 %. Found: C, 59.71; H, 4.56 %. ^{1}H NMR ($CDCl_3$): δ = 3.66 (br, [2H], PC***H***$_2$P), 7.03 (br m, [12H], Ph), 7.87 (br, [8H], Ph). ^{31}P NMR ($CDCl_3$): δ = -14.84 ppm (s). IR (Nujol mull)/cm^{-1}: 1153 s, 1098 s (P=O), 209 w (Eu-Cl).

[TbCl(dppmO$_2$)$_3$]Cl$_2$ - To a solution of $TbCl_3.6H_2O$ (0.025 g, 0.067 mmol) in ethanol (5 mL) was added a solution of $dppmO_2$ (0.084 g, 0.201 mmol) in ethanol (10 cm^3) and the mixture was stirred for 20 min. The solution was concentrated and a white solid was precipitated with n-hexane (1 mL) which was filtered and dried. Yield: 0.056 g, 55%. Required for $C_{75}H_{66}Cl_3O_6P_6Tb$ (1513.61): C, 59.46; H, 4.39 %. Found: C, 59.41; H, 4.54 %. ^{1}H NMR (CD_2Cl_2): δ = 3.50 (br m, [2H], PC***H$_2$***P), 5.89 (br, [12H], Ph), 7.46 (br, [8H], Ph). ^{31}P NMR (CD_2Cl_2): δ = -28.74 ppm (s). IR (Nujol mull)/cm^{-1}: 1153 s, 1097 s (P=O), 206 w (Tb-Cl).

[HoCl(dppmO$_2$)$_3$]Cl$_2$ - To a solution of $HoCl_3$ (0.050g, 0.184 mmol) in ethanol (5 mL) was added a solution of $dppmO_2$ (0.230 g, 0.55 mmol) in ethanol (10 mL), giving pink solution, which was stirred for 20 min. The solution was concentrated and a very pale pink solid was precipitated with n-hexane (1 mL) which was filtered and dried. Yield: 0.211 g, 75%. Required for $C_{75}H_{66}Cl_3HoO_6P_6$ (1519.62): C, 59.23; H, 4.38 %. Found: C, 59.41; H, 4.52 %.^{1}H NMR (CD_2Cl_2): δ = 3.72 (br s, [2H], PC***H$_2$***P), 6.78 (br, [12H], Ph), 7.68 (br, [8H], Ph)]. ^{31}P NMR (CD_2Cl_2): δ = (s). IR (Nujol mull)/cm^{-1}: 1154 s, 1097 s (P=O), 206 w (Ho-Cl).

[YbCl(dppmO$_2$)$_3$]Cl$_2$ - To a solution of $YbCl_3.6H_2O$ (0.025 g, 0.065 mmol) in ethanol (5 mL) was added a solution of $dppmO_2$ (0.080 g, 0.194 mmol) in ethanol (10 mL) and the mixture was stirred for 20 min. The solvent was removed *in vacuo* and the resulting white powder was washed with ice cold ethanol then dried *in vacuo*. Yield: 0.062 g, 63 %. Required for $C_{75}H_{66}Cl_3YbO_6P_6$ (1527.73): C, 58.91; H, 4.35 %. Found: C, 58.73; H, 4.45 %. ^{1}H NMR (CD_2Cl_2): δ = 3.50 (m, [2H], PC***H$_2$***P), 6.64 (br, [8H], Ph), 7.15 (br, [12H], Ph). ^{31}P{^{1}H} NMR (CD_2Cl_2): δ = 9.19 ppm (s). IR (Nujol mull)/cm^{-1}: 1154 s, 1097 s (P=O), 209 w (Yb-Cl).

[LuCl$_2$(dppmO$_2$)$_2$]Cl - $LuCl_3 \cdot 6H_2O$ (0.05 g, 0.13 mmol) was dissolved in ethanol (10 mL). $DppmO_2$ (0.16 g, 0.39 mmol) dissolved in ethanol (15 mL) was then added to the reaction mixture and stirred for 16 h. The solvent was removed *in vacuo* and the residual fawn solid was washed with cold ethanol (5 mL) and dried *in vacuo*. Yield: 0.08 g, 55 %. Required for $C_{52}H_{50}Cl_3LuO_5P_4$ (1160.16): C, 53.84; H, 4.34 %. Found: C, 53.55; H, 3.65%. ^{1}H NMR (CD_2Cl_2): δ = 3.72 (br s, [2H], PC***H$_2$***P), 7.25 (br s, [8H], Ph), 7.42 (m, [4H], Ph), 7.91 (br s, [8H], Ph). ^{31}P{^{1}H} NMR (CD_2Cl_2): δ = 36.4 (s); (CD_3OD): δ = 40.1 (s). IR spectrum (Nujol mull)/cm^{-1}: 1158 s, 1098 s (P=O).

[LuCl(dppmO$_2$)$_2$(H$_2$O)][PF$_6$]$_2$·2H$_2$O - $LuCl_3·6H_2O$ (0.05 g, 0.13 mmol) and $[NH_4][PF_6]$ (0.063 g, 0.39 mmol) were dissolved in ethanol (10 mL). $DppmO_2$ (0.16 g, 0.38 mmol) dissolved in ethanol (15 mL) was then added to the reaction mixture which immediately turned cloudy. The resulting mixture was stirred for 16 h. The solvent was removed *in vacuo* and the residual fawn solid was washed with cold ethanol (5 mL) and dried *in vacuo*. Yield: 0.15 g, 85 %. Required for $C_{50}H_{50}ClF_{12}LuO_7P_6$ (1386.60): C, 43.27; H, 3.63 %. Found: C, 43.37; H 3.64%. ^{1}H NMR (CD_2Cl_2): δ = 2.38 (br, H_2O), 3.84 (br, [2H], PC***H$_2$***P), 7.25 (s, [8H], Ph), 7.46 (m, [4H], Ph), 7.66 (m, [8H], Ph). ^{31}P{^{1}H} NMR (CD_2Cl_2): δ = 35.8 (s, ***P***=O), −143.2 (m, ***P***F$_6$); (CD_3OD): δ = 40.1 (s, ***P***=O), −143.2 (m, ***P***F$_6$). IR spectrum (Nujol mull)/cm^{-1}: 3200 br, 1620 m (H_2O), 1152 s, 1096 s (P=O), 839 s, 557 s (PF_6).

[LuI$_2$(dppmO$_2$)$_2$]I - LuI_3 (0.022 g, 0.04 mmol) was dissolved in dry ethanol (10 mL). $DppmO_2$ (0.05 g, 0.12 mmol) dissolved in ethanol (15 mL) was then added to the reaction mixture, which was stirred for 16 h. The solvent was removed *in vacuo* and the resulting product washed with *n*-pentane (5 mL) and ethanol (5 mL) and dried *in vacuo*. Yield: 0.046 g, 82 %. Required for $C_{50}H_{44}I_3LuO_4P_4$ (1387.90): C, 43.25; H, 3.19 %. Found: C, 43.64; H, 3.09%. ^{1}H NMR (CD_2Cl_2): δ = 4.49 (br s, [2H], PC***H$_2$***P), 7.21 (br s, [8H], Ph), 7.47 (br s, [4H], Ph), δ 7.94 (m, [8H], Ph). ^{31}P{^{1}H} NMR (CD_2Cl_2): δ 41.4 (s), 40.6 (s), 39.1 (s), 36.0 (s). IR spectrum (Nujol mull)/cm^{-1}: 1147 br s, 1094 s (P=O).

[LaCl$_3$(dppeO$_2$)$_{1.5}$]$_n$ - $LaCl_3·7H_2O$ (0.05 g, 0.135 mmol) was dissolved in ethanol (10 mL). $DppeO_2$ (0.09 g, 0.21 mmol) dissolved in ethanol (15 mL) was then added to the reaction mixture. Solid immediately precipitated out and the mixture was stirred for 16 h. The mixture was filtered and the white solid was washed with n-hexane (5 mL) and dried *in vacuo*. Yield: 0.081 g, 67 %. Crystals were grown by layering a solution of $dppeO_2$ in ethanol on top of a solution of $LaCl_3·7H_2O$ (2:1 M ratio) in ethanol. Required for $C_{78}H_{72}Cl_6La_2O_6P_6$ (1781.76): C, 52.58; H, 4.07 %. Found: C, 52.68; H, 3.89%. ^{1}H NMR (CD_3OD): δ = 2.80 (m [4H], PC***H$_2$***C***H$_2$***P), 7.46 (m, [8H], Ph), 7.62 (m, [4H], Ph), 7.79 (m, [8H], Ph). ^{31}P{^{1}H} NMR (CD_3OD): δ = 43.2 (s). IR spectrum (Nujol mull)/cm^{-1}: 1144 s, 1091 s (P=O).

[LaCl$_2$(PPO$_2$)$_2$(H$_2$O)$_2$]Cl - $LaCl_3·7H_2O$ (0.01 g, 0.0269 mmol) was dissolved in ethanol (10 mL). PPO_2 (0.05 g, 0.11 mmol) dissolved in ethanol (15 mL) was then added to the reaction mixture and stirred for 16 h. The solvent was removed *in vacuo*, and the residual white solid was washed with n-hexane (5 mL) and ice cold ethanol (10 mL) and dried *in vacuo*. Yield:

0.028 g, 84 %. Crystals were grown by dissolving the product in ethanol and cooling the solution in a freezer. These were identified as $[LaCl_2(PPO_2)_2(H_2O)(EtOH)]Cl$ by X-ray crystallography. Required for $C_{60}H_{52}Cl_3LaO_6P_4$ (1238.19): C, 58.20; H, 4.23 %. Found: C, 57.35; H, 3.98%. ^{1}H NMR (CD_2Cl_2): δ = 1.67 (s, H_2O), 7.15 (m), 7.32 (m), 7.50 (m). $^{31}P\{^1H\}$ NMR (CD_3OD): δ = 40.1 (s); (CD_2Cl_2): δ = 35.5 (s). IR spectrum (Nujol mull)/cm^{-1}: 1158 s, 1095 s (P=O), 208 m (La-Cl).

$[LaCl_2(PPO_2)_2(H_2O)_2][PF_6]$ - $LaCl_3{\cdot}7H_2O$ (0.010 g, 0.027 mmol) and $[NH_4][PF_6]$ (0.012 g, 0.081 mmol) were dissolved in ethanol (10 mL). PPO_2 (0.050 g, 0.11 mmol) dissolved in ethanol (15 mL) was then added to the reaction mixture and stirred for 16 h, the solution remained clear in this time. The solvent was removed *in vacuo*, and the residual white solid was washed with n-hexane (5 mL) then cold ethanol (10 mL) and dried *in vacuo*. Yield: 0.020 g, 65 %. A small number of crystals grown from this complex in ethanol were solved giving a structure of $[LaCl(PPO_2)_3][PF_6]_2$. Required for $C_{60}H_{52}Cl_2F_6LaO_6P_5$ (1347.05): C, 53.45; H, 3.89 %. Found: C, 53.36; H, 3.72%. ^{1}H NMR (CD_2Cl_2): δ = 1.56 (s, H_2O), 7.04 (br m), 7.26 (br m), 7.41 (br m), 7.72 (br m). $^{31}P\{^1H\}$ NMR (CD_3OD): 40.0 (s, PPO_2), −143.2 (m, PF_6); (CD_2Cl_2): δ = 35.4 (PPO_2), −143.2 (m, PF_6). IR spectrum (Nujol mull/cm^{-1}) 3200 br, 1620 m (H_2O), 1156 s, 1095 s (P=O), 841 s, 559 m (PF_6).

$[LuCl_2(PPO_2)_2]Cl$ - $LuCl_3{\cdot}6H_2O$ (0.014 g, 0.035 mmol) was dissolved in ethanol (10 mL). PPO_2 (0.05 g, 0.10 mmol) dissolved in ethanol (15 mL) was then added to the reaction mixture, which was then stirred for 16 h. The solvent was removed *in vacuo*, and the residual white solid was washed with n–hexane (5 mL) then cold ethanol (10 mL) and dried *in vacuo*. Yield: 0.022 g, 83 %. Required for $C_{60}H_{48}Cl_3LuO_4P_4$ (1238.23): C, 58.20; H, 3.91 %. Found: C, 57.95; H, 4.08%. ^{1}H NMR (CD_2Cl_2): δ = 7.25 (br, [8H]), 7.47 (br [16H]). $^{31}P\{^1H\}$ NMR (CD_2Cl_2): δ = 42.1 (s), (CD_3OD): δ = 40.7 (s). IR spectrum (Nujol mull)/cm^{-1}: 1156 br s, 1094 s (P=O).

$[Lu(PPO_2)_2(H_2O)_2][PF_6]_3$ - $LuCl_3{\cdot}6H_2O$ (0.014 g, 0.035 mmol) and $[NH_4][PF_6]$ (0.017 g, 0.105 mmol) were dissolved in ethanol (10 mL). PPO_2 (0.05 g, 0.104 mmol) dissolved in ethanol (15 mL) was then added to the reaction mixture, which was then stirred for 16 h. The solvent was removed *in vacuo*, and the residual white solid was washed with n-hexane (5 mL), then cold ethanol (10 mL) and dried *in vacuo*. Yield: 0.05 g, 90 %. Required for $C_{60}H_{52}F_{18}LuO_6P_7$ (1584.78): C, 44.96; H, 3.27 %. Found: C, 45.61; H, 3.57%. ^{1}H NMR

(CD_2Cl_2): δ = 1.26 (s, H_2O), 7.26 (br [8H]), 7.42 (br [16H]). $^{31}P\{^1H\}$ NMR (CD_2Cl_2): δ = 41.1 (br, PPO_2), −143.2 (sept, PF_6). IR spectrum (Nujol mull)/cm^{-1}: 1155 br, 1094 m (P=O), 839 s, 560 s (PF_6).

[Lu(PPO_2)$_2$$I_2$]I - LuI_3 (0.05 g, 0.088 mmol) was dissolved in dry ethanol (10 mL). PPO_2 (0.182 g, 0.38 mmol) dissolved in ethanol (15 mL). The solution was stirred for 20 min. and then taken to dryness *in vacuo*. The white product was dissolved in acetonitrile and the solution cooled to −4 °C overnight, resulting in a white powder. This was filtered off and dried *in vacuo*. The solid was finally recrystallised by layering a solution in dichloromethane with n-hexane. Yield: 0.055 g, 41 %. Required for $C_{60}H_{48}I_3LuO_4P_4$ (1511.93): C, 47.62; H, 3.20 %. Found: C, 47.84; H, 3.31%. ^1H NMR (CD_2Cl_2): δ 7.00–7.42 (br m). $^{31}P\{^1H\}$ NMR (CD_2Cl_2): δ = 42.5 (br). IR spectrum (Nujol mull)/cm^{-1}: 1142 s, 1094 s (P=O).

Table 2.2. Crystallographic data[a]

Compound	**$[La(dppmO_2)_4][PF_6]_3\cdot 2EtOH$**	**$[LaCl_3(dppeO_2)_{1.5}]_n\cdot EtOH$**	**$[LaCl(PPO_2)_3][PF_6]_2\cdot 3.5EtOH\cdot 2.8H_2O$**
Formula	$C_{104}H_{98}F_{18}LaO_{10}P_{11}$	$C_{41}H_{42}Cl_3LaO_4P_3$	$C_{97}H_{98.6}ClF_{12}LaO_{12.3}P_8$
M	2329.40	936.92	2111.28
Crystal system	monoclinic	triclinic	triclinic
Space group (no.)	*Cc* (9)	P-1 (2)	P-1 (2)
a (Å)	19.551(3)	13.049(5)	13.3783(10)
b (Å)	19.565(4)	13.779(5)	14.6431(10)
c (Å)	28.384(5)	14.880(6)	26.1970(10)
α (°)	90	106.674(4)	91.251(2)
β (°)	102.974(5)	97.070(2)	90.9680(10)
γ (°)	90	116.987(3)	99.7980(10)
U ($Å^3$)	10580(3)	2180.9(14)	5054.8(5)
Z	4	2	2
μ(Mo Kα) (mm^{-1})	0.659	1.311	0.655
F(0 0 0)	4744	946	2162
Total number reflections	29 447	18 685	82 915
R_{int}	0.082	0.061	0.055
Unique reflections	16 131	8545	19 883
No. of parameters, restraints	1191, 187	496, 4	1254, 206
R_1, $wR_2[I > 2\sigma(I)]$[b]	0.078, 0.171	0.044, 0.136	0.063, 0.168
R_1, wR_2 (all data)	0.115, 0.196	0.050, 0.143	0.083, 0.188

Table 2.2 Continued

Compound	**$[LaCl_2(PPO_2)_2(H_2O)(EtOH)]Cl \cdot 3.5EtOH$**	**$[Ce(dppmO_2)_4]Cl_3 \cdot 4H_2O$**	**$[YbCl(dppmO_2)_3]Cl_2$**
Formula	$C_{69}H_{77}Cl_3LaO_{9.50}P_4$	$C_{100}H_{96}CeCl_3O_{12}P_8$	$C_{83}H_{88}Cl_3O_{10}P_6Yb$
M	1427.45	1983.99	1710.74
Crystal system	triclinic	monoclinic	monoclinic
Space group (no.)	P-1 (2)	C2 (5)	Pc (7)
a (Å)	11.463(3)	54.1331(11)	14.2041(2)
b (Å)	11.583(3)	14.1385(3)	12.9655(2)
c (Å)	26.786(4)	14.1470(2)	24.0255(3)
α (°)	79.027(4)	90	90
β (°)	85.736(4)	93.501(2)	95.8800(13)
γ (°)	75.822(5)	90	90
U (Å^3)	3384.0(13)	10807.4(4)	4401.32(11)
Z	2	4	2
μ (Mo Kα) (mm^{-1})	0.900	0.667	1.315
F(0 0 0)	1470	4084.0	1754.0
Total number reflections	54 018	81502	55153
R_{int}	0.102	0.0826	0.0322
Unique reflections	13 311	21158	16681
No. of parameters, restraints	836, 35	1134, 13	931, 2
R_1,wR_2 [$I > 2\sigma(I)$][b]	0.062, 0.159	0.0807, 0.2232	0.0433, 0.1199
R_1, wR_2 (all data)	0.079, 0.178	0.0845, 0.2277	0.0461, 0.1219

Table 2.2 Continued

Compound	**[Yb(dppmO$_2$)$_3$(H$_2$O)]Cl$_3$·dppmO$_2$**	**[LuCl$_2$(PPO$_2$)$_2$]Cl**
Formula	$C_{100}H_{114}Cl_3O_{21}P_8Yb$	$C_{60}H_{48}Cl_3LuO_4P_4$
M	2179.06	1190.30
Crystal system	orthorhombic	Triclinic
Space group (no.)	Pbca (61)	P-1 (2)
a (Å)	26.1159(2)	13.3111(8)
b (Å)	27.7086(2)	14.1509(9)
c (Å)	29.1373(2)	15.7520(8)
α (°)	90	91.639(5)
β (°)	90	101.386(5)
γ (°)	90	95.132(5)
U (Å^3)	21084.8(3)	2893.8(3)
Z	8	2
μ(Mo Kα) (mm^{-1})	1.150	1.997
F(0 0 0)	8984.0	1149.0
Total number reflections	351992	44639
R_{int}	0.0285	0.0967
Unique reflections	20719	11367
No. of parameters, restraints	1235, 0	658, 0
R_1, $wR_2[I > 2\sigma(I)]$[b]	0.0279, 0.0758	0.1197, 0.3366
R_1, wR_2 (all data)	0.0312, 0.0779	0.1352, 0.3513

[a] Common data: $T = 293$ K; wavelength (Mo Kα) = 0.71073 Å; θ(max) = 27.5°.
[b] $R_1 = \Sigma||Fo| - |Fc||/\Sigma|Fo|$; $wR_2 = [\Sigma w(Fo^2 - Fc^2)^2/\Sigma wFo^4]^{1/2}$.

2.5 References

1 M. Szostak, N. J. Fazakerley, D. Parmar and D. J. Procter, *Chem. Rev.*, 2014, **114**, 5959–6038.

2 K. C. Nicolaou, S. P. Ellery and J. S. Chen, *Angew. Chemie Int. Ed.*, 2009, **48**, 7140–7165.

3 H. Wang, B.-W. Wang, Y. Bian, S. Gao and J. Jiang, *Coord. Chem. Rev.*, 2016, **306**, 195–216.

4 P. Zhang, L. Zhang and J. Tang, *Dalton Trans.*, 2015, **44**, 3923–3929.

5 S. Aime, D. D. Castelli, S. G. Crich, E. Gianolio and E. Terreno, *Acc. Chem. Res.*, 2009, **42**, 822–831.

6 S. Zhang, P. Winter, K. Wu and A. D. Sherry, *J. Am. Chem. Soc.*, 2001, **123**, 1517–1518.

7 M. Bottrill, L. Kwok and N. J. Long, *Chem. Soc. Rev.*, 2006, **35**, 557–571.

8 S. A. Cotton, *Lanthanide and Actinide Chemistry*, John Wiley & Sons, Ltd., Chichester, 2006.

9 S. A. Cotton and P. R. Raithby, *Coord. Chem. Rev.*, 2017, **340**, 220–231.

10 S. A. Cotton, in *Comprehensive Coordination Chemistry II - 3.2.2 Yttrium and the Lanthanides*, eds. J. A. McCleverty and T. J. Meyer, Elsevier Pergamon, Oxford, 2004, pp. 108–171.

11 N. J. Hill, L.-S. Leung, W. Levason and M. Webster, *Acta Cryst.*, 2002, **C58**, m295–m296.

12 N. J. Hill, L.-S. Leung, W. Levason and M. Webster, *Inorg. Chim. Acta*, 2003, **343**, 169–174.

13 M. J. Glazier, W. Levason, M. L. Matthews, P. L. Thornton and M. Webster, *Inorg. Chim. Acta*, 2004, **357**, 1083–1091.

14 W. Levason, E. H. Newman and M. Webster, *Polyhedron*, 2000, **19**, 2697–2705.

15 A. Bowden, A. W. G. Platt, K. Singh and R. Townsend, *Inorg. Chim. Acta*, 2010, **363**, 243–249.

16 J.-C. Berthet, M. Nierlich and M. Ephritikhine, *Polyhedron*, 2003, **22**, 3475–3482.

17 A. W. G. Platt, *Coord. Chem. Rev.*, 2017, **340**, 62–78.

18 A. M. J. Lees and A. W. G. Platt, *Inorg. Chem.*, 2003, **42**, 4673–4679.

19 L. Huang, B.-Q. Ma, C. H. Huang, T. C. W. Mak, G. Q. Yao and G. X. Xu, *J. Coord. Chem.*, 2001, **54**, 95–103.

20 J. Fawcett and A. W. G. Platt, *Polyhedron*, 2003, **22**, 967–973.

21 W. Hewertson, B. T. Kilbourn and R. H. B. Mais, *Chem. Commun.*, 1970, 952–953.

22 K. Nakamura, Y. Hasegawa, H. Kawai, N. Yasuda, Y. Wada and S. Yanagida, *J. Alloys Compd.*, 2006, **408-412**, 771–775.

23 Z. Spichal, M. Necas and J. Pinkas, *Inorg. Chem.*, 2005, **44**, 2074–2080.

24 N. J. Hill, W. Levason, M. C. Popham, G. Reid and M. Webster, *Polyhedron*, 2002, **21**, 445–455.

25 W. Levason, R. Patel and G. Reid, *J. Organomet. Chem.*, 2003, **688**, 280–282.

Chapter 3 Divalent Lanthanide Complexes

3.1 Introduction

As discussed in Chapter 2, the overwhelming majority of lanthanide coordination chemistry focusses on the Ln(III) oxidation state, due to the inherent instability of most Ln(II) ions. This chapter explores the coordination chemistry of divalent lanthanide halides (SmI_2, $EuBr_2$, EuI_2 and YbI_2) with neutral hard monodentate phosphine oxides ($OPMe_3$ and $OPPh_3$). As such the first examples of divalent lanthanide halide complexes bearing phosphine oxide ligands are isolated and characterised. In addition, a series of macrocyclic lanthanide complexes, including mixed donor macrocycles with hard O donor ether groups combined with soft thioether or selenoether functions, are described.

3.1.1 Trivalent lanthanide complexes with monodentate phosphine oxide ligands

A recent review of lanthanide phosphine oxide systems acknowledged the majority of the complexes studied are for trivalent metals and that divalent lanthanide phosphine oxide complexes further investigation.[1] Examples of group (II) metals demonstrate they can coordinate both monodentate and bidentate phosphine oxides[2] and it is reasonable to expect that the divalent lanthanides may behave similarly. Owing to the lack of divalent lanthanide phosphine oxide systems, this review will look primarily at trivalent lanthanide phosphine oxide systems, bearing OPR_3 ligands.

Trivalent lanthanide complexes with monodentate phosphine oxides have been widely studied and examples of these systems with a range of counter-ions are known. By far the most prevalent ligand system is $OPPh_3$, while common counter-ions include nitrate, thiocyanate, triflate and, more recently, halides.[1,3–7] While the lability of these systems is noted and discussed in Chapter 2, monodentate phosphine oxide lanthanide complexes show a broader range of species owing to the lack of a chelate effect. As such, many lanthanide species can be obtained from a single ligand system, depending on the size of the metal centre and the reaction conditions.[1,5,8] For example, a range of lanthanide nitrates, (Ln = La → Lu; Ln ≠ Pm), when reacted with three equivalents of $OPPh_3$, form the complexes $[Ln(NO)_3(OPPh_3)_3]$, as 9-coordinate species (with bidentate nitrates).[9,10] However, the addition of excess $OPPh_3$ (≥ 6 equiv.) can lead to the formation of the complexes $Ln(NO)_3(OPPh_3)_4$ (Ln = La → Nd; Tb → Lu). The larger, lighter lanthanides form crystals of $[Ln(\kappa^2\text{-}NO_3)_2(\kappa^1\text{-}NO_3)(OPPh_3)_4]\cdot Me_2CO$ (Ln = La, Ce, Pr or Nd) from acetone solutions.

The $^{31}P\{^{1}H\}$ NMR spectroscopic studies of these nine-coordinate complexes show they rapidly decompose to $[Ln(NO)_3(OPPh_3)_3]$ and excess free ligand. A crystal structure of $[La(\kappa^2\text{-}NO_3)_2(\kappa^1\text{-}NO_3)(OPPh_3)_4]\cdot Me_2CO$ was determined, whilst PXRD and elemental analysis was used to confirm the structures of the $[Ln(\kappa^2\text{-}NO_3)_2(\kappa^1\text{-}NO_3)(OPPh_3)_4]$ (Ln = Ce, Pr or Nd) complexes. The smaller, heavier lanthanides can form $[Ln(\kappa^2\text{-}NO_3)_2(OPPh_3)_4]NO_3$ (Ln = Tb - Lu) as 8-coordinate ionic species, but only from cold ethanol solutions, as demonstrated by a crystal structure of $[Lu(\kappa^2\text{-}NO_3)_2(OPPh_3)_4]NO_3$, Figure 3.1. Reactions performed in acetone led to the formation of the $[Ln(OPPh_3)_3(NO_3)_3]$ complex. In the presence of excess $OPPh_3$, in acetone or ethanol, lanthanides in the middle of the series (Ln = Sm, Eu or Gd) afforded only the $[Ln(OPPh_3)_3(NO_3)_3]$ species.[4] A rare example of a Ce(IV) structure has also been described in the literature, $[Ce(NO_3)_4(OPPh_3)_2]$, synthesised from the addition of $OPPh_3$ to $(NH_4)_2[Ce(NO_3)_6]$ in acetone.[11] The structure shows the two *trans*-$OPPh_3$ ligands in an axial position and the four bidentate nitrate ligands in equatorial positions. These complexes further demonstrate the need for careful control of reactants and reaction conditions in the synthesis of lanthanide phosphine oxides. Also, due to the rapid exchange of ligands on the lanthanide ions, solution state data does not always reflect the species observed in the solid state. As such it is important to pair infrared spectroscopy, elemental analysis and single crystal X-ray diffraction with $^{31}P\{^{1}H\}$ and ^{1}H NMR spectroscopy where possible in order to get a more complete picture of the behaviour of the systems both in solution and in the solid state.

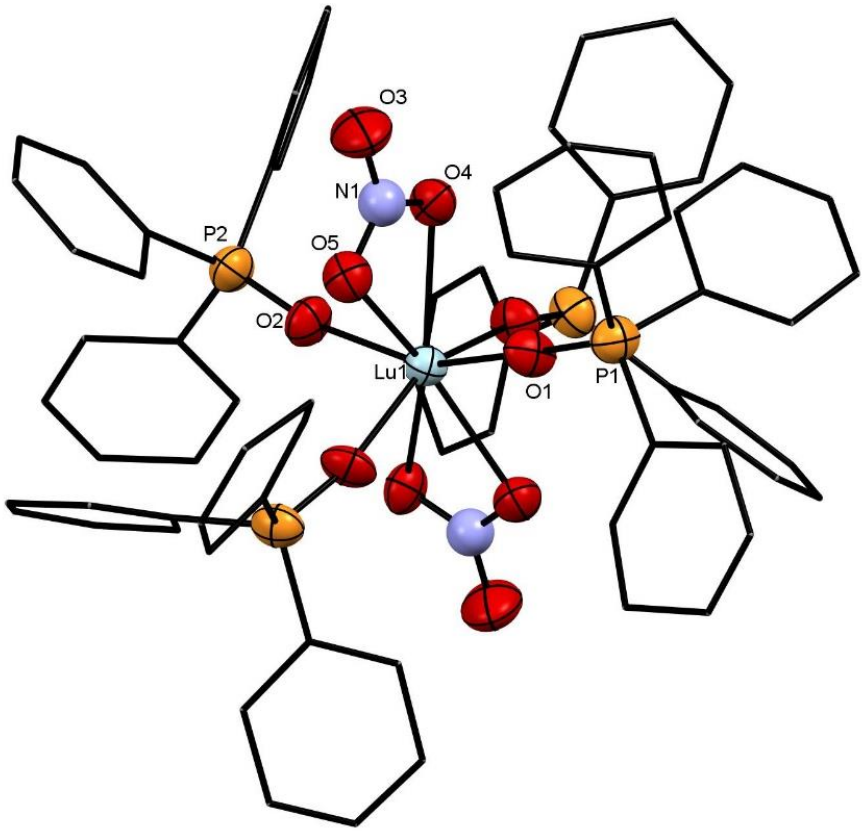

Figure 3.1. A crystal structure of the cation $[Lu(NO_3)_2(OPPh_3)_4]^+$ with hydrogen atoms omitted and phenyl rings presented as wire frames for clarity. The 8-coordinate metal centre coordinates four $OPPh_3$ ligands in a distorted equatorial plane and two bidentate NO_3^- ligands in axial positions.[4]

Whilst reaction conditions clearly play an important role in the product of a reaction, the lanthanide counter ion is also an important consideration, as discussed in Chapter 2. The ability of a ligand to coordinate to the metal centre, relative to the counter ion and solvent used, can affect the final products generated. In the examples above, the earlier lanthanides (Ln = La → Nd) appear to show a much greater affinity for nitrate over $OPPh_3$, coordinating $OPPh_3$ only where unoccupied coordination sites are available. Whereas the presence of $[Ln(NO_3)_2(OPPh_3)_4]NO_3$, even in solution suggests a higher affinity for $OPPh_3$ over nitrate increases down the series.[4] It is pertinent, therefore, to study the behaviour of these metal ions, not only with differing ligand systems, but sometimes also in various solvent systems and with a range of counter ions.

Examples of aryl phosphine oxides, particularly $OPPh_3$, with trivalent lanthanides are abundant, while examples of trialkyl phosphine oxides are relatively sparser.[12–14] Only a single example of a lanthanide nitrate coordinating $OPMe_3$ exists in the literature,

$[Nd(NO_3)_3(OPMe_3)_3]$, characterised by infrared spectroscopy, elemental analysis and conductivity studies.[10] The complex is determined to be 9-coordinate on the basis of the infrared spectroscopy. A crystal structure of $[Y(NO_3)_3(OPMe_3)_3]$ shows a similar coordination of bidentate nitrate ligands. Considering the NO_3^- as a pseudo-monodentate ligand, the structure shows a *facial* octahedral geometry.[15] The $^{31}P\{^1H\}$ NMR spectrum of $[Y(NO_3)_3(OPMe_3)_3]$ shows only a single resonance at 48.3 ppm, due to the equivalent phosphine environment. However, it should be noted that $[Y(NO_3)_3(OPPh_2Me)_3]$ produced crystals of a *meridional* geometry structure which would have two different phosphorus environments in the $^{31}P\{^1H\}$ NMR spectrum, yet the $^{31}P\{^1H\}$ NMR spectrum showed only a single resonance even upon cooling to 200K. It is, therefore, likely that both of these systems show fast exchange between the two isomers, and only the *meridional* structure crystallizes out of solution.[16] These reported yttrium complexes are the most similar crystallographically confirmed structures to the neodymium complex, $[Nd(NO_3)_3(OPMe_3)_3]$. Comparing the *fac*-$[Y(NO_3)_3(OPMe_3)_3]$ to a similar series of lanthanide complexes coordinating $OPEt_3$ shows a marked difference in the structural data afforded. Whilst the products, $[Ln(NO_3)_3(OPEt_3)_3]$, also show bidentate nitrate ligands, the ligands are of a *meridional* arrangement, when treating the nitrate ligands as a pseudo monodentate, Figure 3.2. The authors attribute this difference between *fac* and *mer* geometries, for the $OPMe_3$ and $OPEt_3$ complexes respectively, as being due to the increased steric bulk of $OPEt_3$ compared to $OPMe_3$.

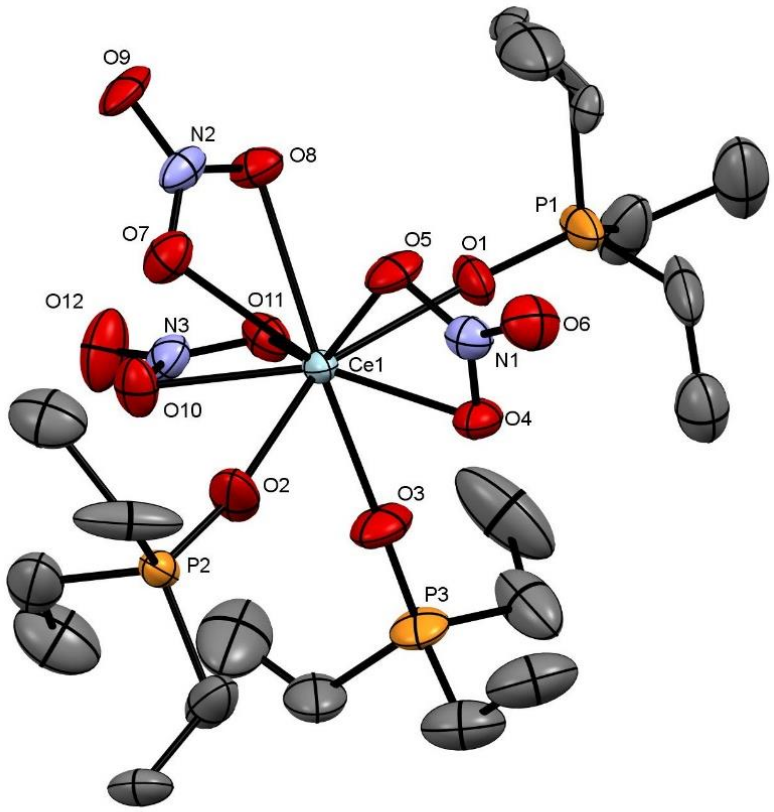

Figure 3.2. A crystal structure of [Ce(NO$_3$)$_3$(OPEt$_3$)$_3$] showing a pseudo-octahedral geometry with the nitrate ligands in meridional positions when considered as monodentate ligands.[17]

The $^{31}P\{^{1}H\}$ spectrum of [La(NO$_3$)$_3$(OPEt$_3$)$_3$] shows a single resonance at 63.4 ppm which did not split on cooling to -60 ℃. This was nearly identical to the chemical shift of the lanthanum complex in the solid state (63.1 ppm) suggesting the solid state structure is retained in solution. The $^{31}P\{^{1}H\}$ NMR spectra of the smaller, heavier lanthanide complexes (Yb and Lu) showed a single sharp resonance and a broad resonance which separated on cooling. This was attributed to the presence of [Ln(NO$_3$)$_3$(OPEt)$_2$] (sharp singlet) and both *fac*- and *mer*-[Ln(NO$_3$)$_3$(OPEt$_3$)$_3$] (broad resonance) in solution. It is interesting that the smaller, heavier lanthanide systems show evidence of the more sterically crowded *fac*-isomer. More interesting is evidence of [Ln(NO$_3$)$_3$(OPEt$_3$)$_2$] in solution, whereas the more sterically bulky ^{i}Bu$_3$PO and Cy$_3$PO (Cy = cyclohexyl) analogues show exclusively [Ln(NO$_3$)$_3$(OPR$_3$)$_3$]. While generally the lanthanide ion size and the steric bulk of the ligand are the determining factors in structure geometry, in this case the donor ability of the ligand is also a key consideration.

Lanthanide triflates ($LnOTf_3$) illustrate how changing the counter-ion can affect the most commonly precipitated complexes. Whilst trifluoromethanesulfonate ($CF_3SO_3^-$, triflate) is a weakly coordinating anion with a low donating capacity, it has the ability to coordinate to a metal centre as a mono- bi- or tridentate ligand, or as a bridge.[18] This allows for flexibility in the coordination sphere, not afforded by the strongly coordinating nitrate. As such, structures of $[Ln(OTf)_2(OPPh_3)_4]OTf$ have been obtained for lanthanides across the series (Ln = La, Ce, Nd, Er, Lu).[19,20] Unlike for the lanthanide nitrate complexes, where the heavier lanthanides begin to show a preferential coordination of $OPPh_3$, the coordination of $OPPh_3$ is similar across the series. Whilst crystallisation of the lanthanum product produces $[La(^2\eta\text{-}OTf)(^1\eta\text{-}OTf)(OPPh_3)_4]OTf$, whose structure has been determined, further along the series, as the metal centre gets smaller, the bidentate triflate ligand coordinates in a monodentate fashion due to steric clashes. As such, the erbium and lutetium analogues afforded most likely $[Ln(^1\eta\text{-}OTf)_2(OPPh_3)_4]OTf$ (Ln = Er, Lu), which have also been structurally characterised.[19]

Complexes of both $[LnCl_3(OPPh_3)_3]$ and $[LnCl_2(OPPh_3)_4]Cl$, have been published for all lanthanides (Ln = La → Lu ≠ Pm).[8] The $[LnCl_3(OPPh_3)_3]$ complexes are formed from the addition of $OPPh_3$ with the hydrated lanthanide in acetone in a 3.5:1 ratio. While the chloride salts, $[LnCl_2(OPPh_3)_4]Cl$, are formed from a 6:1 ligand to metal ratio in ethanol. These species interconvert in solution and the earlier, lighter lanthanides (e.g. La, Ce, Pr or Nd) show a preference for the neutral species, while the later, heavier lanthanides (e.g. Er, Tm, Yb or Lu) favour the ionic *tetrakis* species. Crystal structures of $[LnCl_3(OPPh_3)_3]\cdot 0.5Me_2CO$ (Ln = La or Ce) show the complex has a *meridional* geometry and structures of $[LnCl_2(OPPh_3)_4]Cl\cdot nEtOH$ (Ln = Tb or Yb) show the ligands in an equatorial position with the chloride ligands in a *trans* position, Figure 3.3.

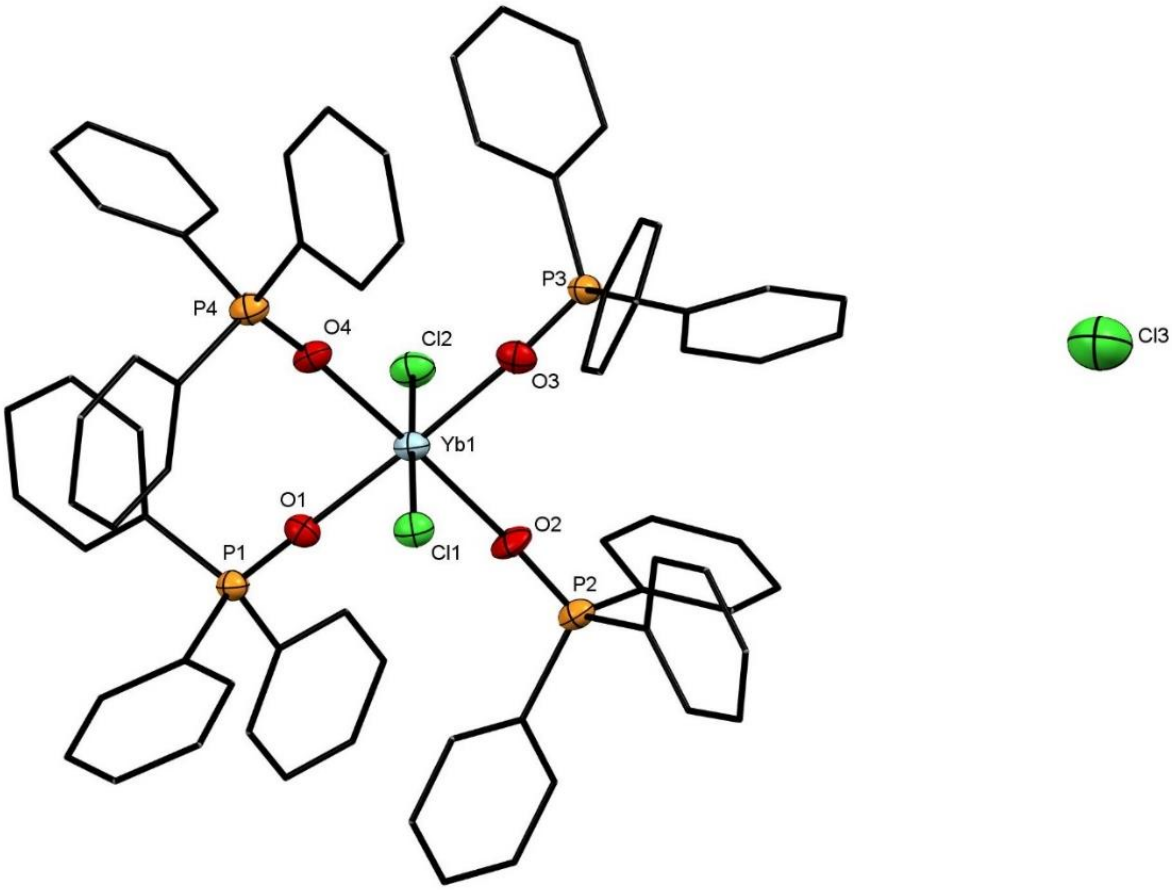

Figure 3.3. A crystal structure of [YbCl$_2$(OPPh$_3$)$_4$]Cl·3(EtOH), with the phenyl rings displayed as wire frames and disordered solvent has been omitted for clarity. The trans-isomer and six-coordinate geometry are clearly displayed.[8]

Both series, [LnCl$_3$(OPPh$_3$)$_3$] and [LnCl$_2$(OPPh$_3$)$_4$]Cl, are characterised by infrared spectroscopy, $^{31}P\{^1H\}$ NMR spectroscopy and elemental analysis. A similar series of complexes of the form [LnCl$_2$(OPPh$_3$)$_4$][PF$_6$] were synthesised and characterised similarly, and did not show the same interconversion of *tris*- and *tetrakis* species, due to PF_6^- being so poorly coordinating. A discussion of the importance of $^{31}P\{^1H\}$ NMR spectroscopy in these systems is included in Section 1.6.2. It explains how, despite the large impact of the paramagnetic metal centre on the chemical shift, $^{31}P\{^1H\}$ NMR studies can be used to identify specific cations, and, despite the paramagnetic effect of the lanthanide metal centre, separate species can still be observed in the NMR spectra. In this study the $^{31}P\{^1H\}$ NMR spectra of the [LnCl$_2$(OPPh$_3$)$_4$]Cl complexes (Ln = Ce → Lu; Ln ≠ Pm) show resonances for [LnCl$_3$(OPPh$_3$)$_3$] and free OPPh$_3$. Also,$^{31}P\{^1H\}$ NMR studies of the complexes of [LnCl$_3$(OPPh$_3$)$_3$] (Ln = Tb → Lu) also show resonances attributed to the *tetrakis* ionic species, Table 3.1. The exchanging systems can be easily observed in the solution state, despite only single products being obtained in the precipitate. It also helps to determine the

observed trend, i.e. the preference for the neutral species displayed by the early lanthanides and for the ionic by the later lanthanides.

Table 3.1. A table of the infrared and $^{31}P\{^{1}H\}$ NMR spectroscopic data of a few representative examples of $[LnCl_3(OPPh_3)]$, $[LnCl_2(OPPh_3)_4][PF_6]$ and $[LnCl_2(OPPh_3)_4]$.[8]

Complex	ν(P=O) cm^{-1}	$\delta(^{31}P)$
$[CeCl_3(OPPh_3)_3]$	1146, 1172	78
$[PrCl_3(OPPh_3)_3]$	1145, 1175	130
$[TbCl_3(OPPh_3)_3]$	1153, 1184	-95 (-129)
$[HoCl_3(OPPh_3)_3]$	1153, 1188	49 (-6)
$[YbCl_3(OPPh_3)_3]$	1155, 1187	21 (33)
$[CeCl_2(OPPh_3)_4][PF_6]$	1141	80
$[PrCl_2(OPPh_3)_4][PF_6]$	1140	131
$[TbCl_2(OPPh_3)_4][PF_6]$	1146	-130
$[HoCl_2(OPPh_3)_4][PF_6]$	1148	-6
$[YbCl_2(OPPh_3)_4][PF_6]$	1150	33
$[CeCl_2(OPPh_3)_4]Cl$	1141	80 (78)
$[PrCl_2(OPPh_3)_4]Cl$	1141	131 (129)
$[TbCl_2(OPPh_3)_4]Cl$	1146	-130 (-94)
$[HoCl_2(OPPh_3)_4]Cl$	1147	-6 (49)
$[YbCl_2(OPPh_3)_4]Cl$	1150	33 (21)

The data show that despite a large change in chemical shift from that of the "free" ligand (δ29 ppm), caused by the paramagnetic metal centre, the presence of more than one cation can be readily observed, slowly exchanging in solution, while the addition of $[PF_6]^-$ salts can be used to identify the resonances attributed to the *tetrakis* species. In addition to the elemental analysis and crystal structures obtained, the infrared spectra also show a clear difference in the solid-state structure between the *tris* and *tetrakis* products, with a slight shift in the major feature (νP=O) (from 1145 to 1155 cm^{-1}) and a shoulder at 1170 – 1190 cm^{-1} present for the *tetrakis* complexes, absent in the *tris*. The addition of excess $OPPh_3$ to the lanthanide chloride complexes leads to $[LnCl_2(OPPh_3)_4]Cl$, however examples of

$[LaCl(OPPh_3)_5]^{2+}$ are only formed following halide abstraction with a strong Lewis acid (e.g. $FeCl_3$ or $CuCl_2$).[21] The addition of excess $OPMe_3$ to $LnCl_3{\cdot}7H_2O$ (Ln = La or Ce) in methanol forms $[LnCl_3(OPMe_3)_4]{\cdot}nH_2O$. The addition of three equivalents of $[NH_4][PF_6]$ led to the formation of $[Ln(OPMe_3)_6][PF_6]_3$ (Ln = La → Lu; Ln ≠ Pm), with $[Ln(OPMe_3)_6][PF_6]_3$ (Ln = Pr, Gd or Dy) being structurally characterised using single crystal X-ray diffraction.[22]

Much of the work on lanthanide halide phosphine oxides has focussed on $LnCl_3$, but there are also examples of both bromide and iodide complexes.[5,23,24] The octahedral complexes *trans*-$[LnBr_2(OPPh_3)_4]Br$ (Ln = Pr, Nd, Gd, Tb, Er, Yb and Lu) were prepared as a direct comparison to the corresponding lanthanide chlorides. The complexes were formed by addition of the ligand to the hydrated lanthanide bromide in 4:1 (phosphine oxide to metal) ratios in ethanol. Attempts to synthesise $[LnBr_3(OPPh_3)_3]$, using a 3:1 ratio, instead led exclusively to the *tetrakis* complexes in an apparent contrast to the lanthanide chlorides, whereby only the later lanthanides preferentially formed the ionic species.[23] The complexes $[LnI_2(OPPh_3)_4]I$ (Ln = La, Ce or Nd) have also been synthesised via the addition of $OPPh_3$ to LnI_3 in a 4:1 ratio. These complexes have all been structurally characterised by single crystal X-ray diffraction. No attempts were made to prepare any compounds of $[LnI_3(OPPh_3)_3]$ via reaction in a 3:1 ligand to metal ratio.

Platt *et. al.* demonstrated that complexes of hydrated lanthanide bromides with tricyclohexylphosphine oxide ($OPCy_3$) form two distinct species, $[LnBr_3(OPCy_3)_3]$ (Ln = La, Pr, Nd, Gd and Ho), and the ionic $[Ln(OPCy_3)_n(H_2O)_5]^{3+}$ (n = 2 or 3, Ln = Lu; n = 4; Ln = La, Dy, Er or Yb).[5] The neutral $[LnBr_3(OPCy_3)_3]$ complexes demonstrate the same octahedral *meridional* geometry (confirmed by the solid state structure of $[LaBr_3(OPCy_3)_3]$) observed for the other neutral lanthanide halide species described above, and appear to only form for the lighter, larger lanthanides.[5] On standing, ethanolic solutions of $LnBr_3$ with three equivalents of $OPCy_3$ led to crystals of the ionic compounds $[Ln(OPCy_3)_n(H_2O)_5]^{3+}$. The crystal structures show a pentagonal bipyramidal geometry around the metal centre, with two ligands in axial positions and five water ligands in the equatorial plane. While the cation, $[Ln(OPCy_3)_n(H_2O)_5]^{3+}$, is consistent throughout all of the metal complexes, and is analogous to a series of lanthanide chloride complexes also made by Platt *et. al.* (Figure 3.4), the outer sphere differs depending on the size of the metal centre and cation.[5,25] For example, $[Er(OPCy_3)_2(H_2O)_5]Br_3{\cdot}(OPCy_3)_2$ shows the three bromide ions and two ligand molecules held in the outer sphere by hydrogen bonding. The similar erbium structure shown below, Figure 3.4, shows one ligand held in the outer coordination sphere by hydrogen bonding, with the other sites occupied by the three chloride anions and a water molecule. Finally the structural data of $[Lu(OPCy_3)_2(H_2O)_5]Br_3{\cdot}EtOH$ shows the molecules are more tightly

packed than in the larger lanthanide examples and only the bromide anions and an ethanol molecule are held by hydrogen bonding.

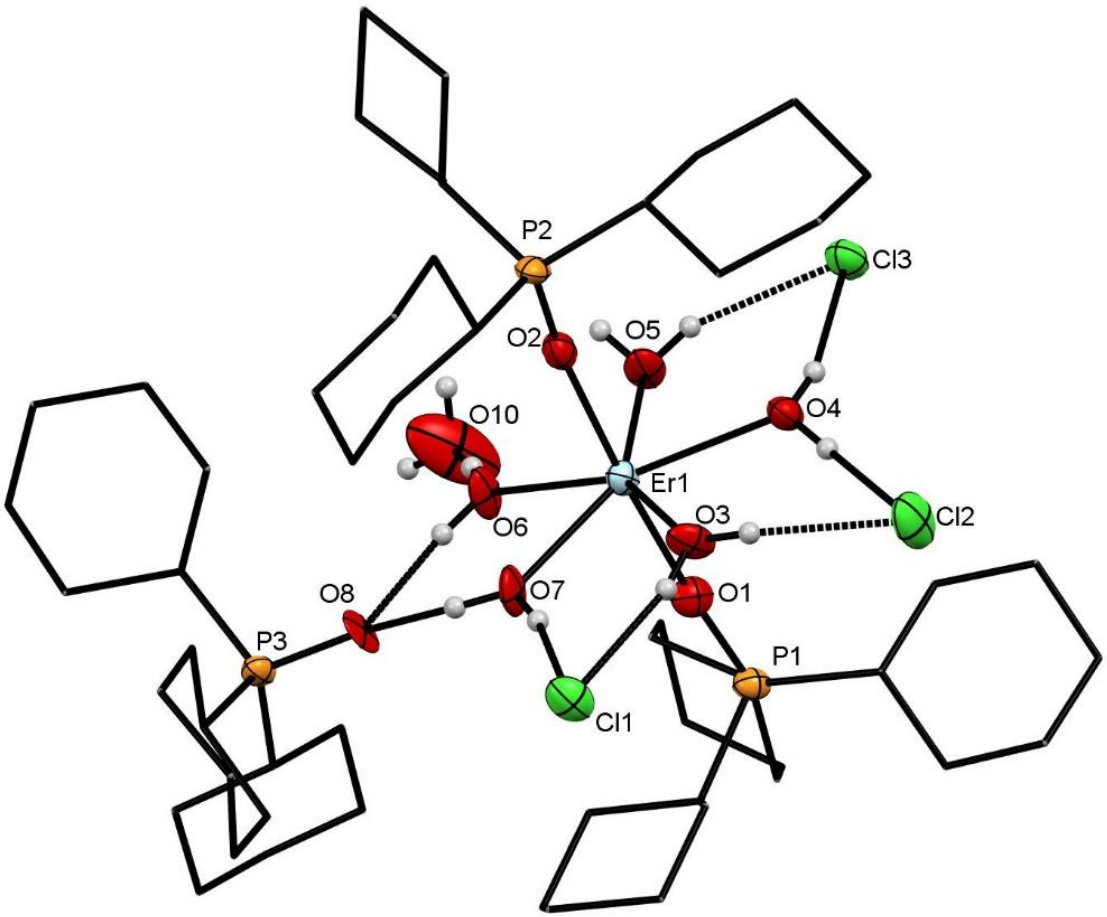

Figure 3.4. A crystal structure of $[Er(Cy_3PO)_2(H_2O)_5]\cdot OPCy_3\cdot Cl_3$ *showing the chloride anions bound in place by hydrogen bonding to the coordinated water. The uncoordinated* $OPCy_3$ *also displays hydrogen bonding between O8 and the hydrogen atoms on O6 and O7.*[25]

3.1.2 Macrocycles

The coordination chemistry of the trivalant lanthanide ions is mostly driven by electrostatic interactions involving ionic bonding, with a heavy preference towards hard donor ligands such as H_2O, oxo-anions or halides.[26,27] Due to their extremely oxophilic nature, the affinity of these f-block ions for neutral soft donor ligands, e.g. phosphines, thioethers or selenoethers is very low. The use of mixed O/S, O/Se donor macrocycles helps to combat this by utilizing the oxophilic nature of the metal centre, in addition to the macrocyclic effect, to form additional bonds to soft donors such as thioether or selenoether functions, Section 1.4.3.[28–33] Previous work from the Reid group explored the possibility of using the enhanced coordinating ability of macrocyclic ligands to promote bonding of soft S and Se functions to the trivalent lanthanides.[34] The work focussed primarily on the lanthanide triiodides due to their lower lattice enthalpies (when compared to the chlorides), hence allowing for greater solubility in low-polarity solvents such as MeCN. This approach led to the successful isolation of several very unusual complexes of the form $[LnI_3([18]aneO_4X_2)]$ (Ln = La, Lu; X = N, S, Se) involving thioether and selenoether ligands coordinated to the f-block metal ion.

Figure 3.5 shows the nine-coordinate complex, $[LaI_3([18]aneO_4Se_2)]$, featuring involving a hexadentate mixed donor macrocycle.[34] Both the La-Se (~3.09 Å), and La-O bond lengths (~2.60 Å) are noted as being much larger than the Lu-Se (~2.89 Å) and Lu-O bond lengths (~2.35 Å) in the analogous Lu(III) system, consistent with the trends expected due to the lanthanide contraction. The macrocycle coordinated to the lutetium atom shown in Figure 3.5 below appears much more constrained and distorted in order to accommodate the favourable metal oxygen bonding. As a result, the lutetium atom sits ca. 1.30 Å out of the plane of the oxygen donor atoms. This contrasts with the La(III) atom sitting only 0.77 Å out of plane of the oxygen atoms in the corresponding species, Figure 3.6. This, alongside the fact that the lanthanum system is able to accommodate an extra iodide ligand, further illustrates difference in the ionic radii caused by the lanthanide contraction. It also demonstrates the effect that choice of macrocycle, and specifically the macrocycle hole size vs. cation radius, has on the overall stability of the complex.

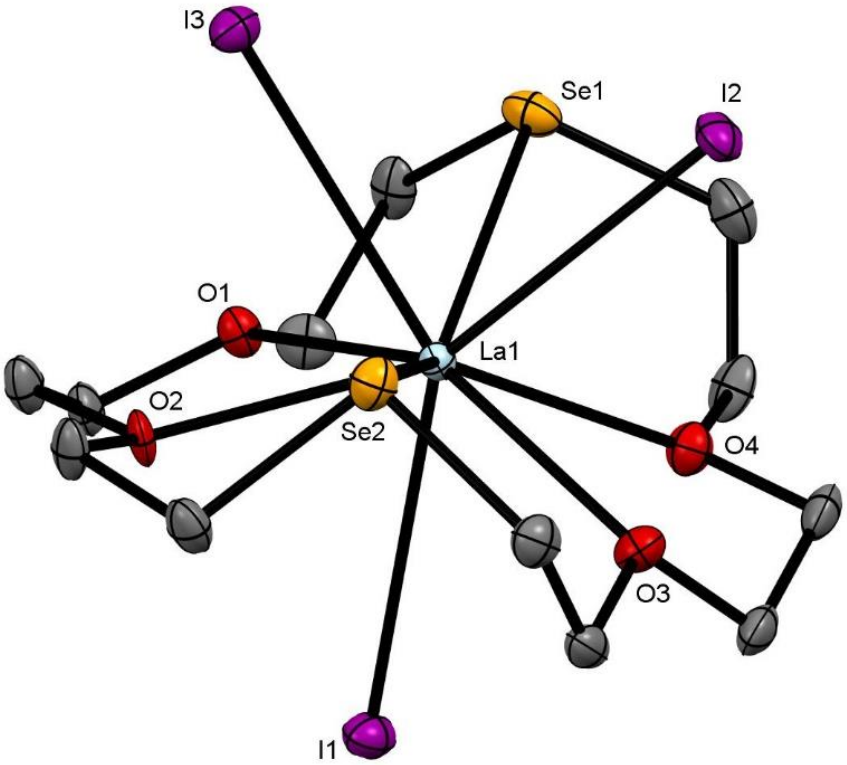

Figure 3.5. A crystal structure of [LaI_3([18]aneO_4Se_2)] with hydrogen atoms removed for clarity.[34]

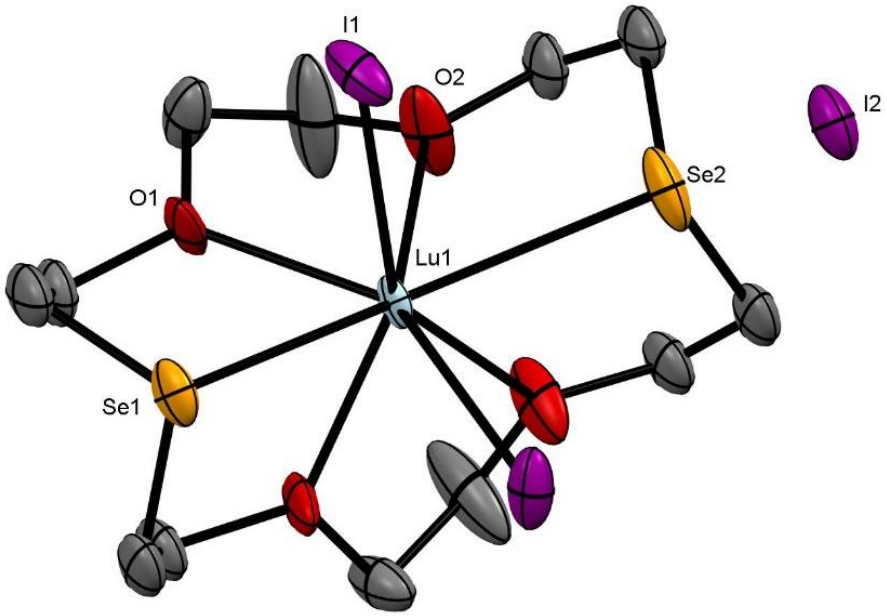

Figure 3.6. A crystal structure showing the structure of [LuI_2([18]aneO_4Se_2)]I.[34]

While ligand exchange is commonly observed in lanthanide complexes, once the macrocycles are bound, they are moderately stable, with any exchange in solution apparently more likely to involve a substitution of iodide for water. This is due to the inherent kinetic stability of macrocyclic complexes. Proton NMR spectra of the complexes above show broadening of the macrocyclic resonances, evidence of a dynamic process. One possibility given for this broadening include the reversible dissociation of one or two coordination sites (likely the sulfur or selenium donor atom).[34]

Following this work on trivalent complexes, ytterbium(II) diiodide was reacted with a range of mixed donor macrocycles, [18]aneO_4X_2 (X = O, NH, S or Se).[35] Ytterbium diiodide was selected because it is isoelectric with Lu^{3+} (f^{14}) and it is diamagnetic, allowing for the use of ^{1}H NMR as a spectroscopic probe. The family of ytterbium diiodide macrocyclic compounds was analysed by elemental analysis, infrared spectroscopy, conductivity studies, ^{1}H NMR spectroscopy and a single crystal X-ray diffraction study of [YbI_2([18]aneO_4Se_2)]. This complex represents the first example of a selenoether coordinated to a divalent ytterbium centre. The structure appears similar to the cation of [LuI_2([18]aneO_4Se_2)]I shown above, but the Yb^{2+}-Se bond lengths are significantly longer than the Lu^{3+}-Se bond lengths (by 0.1 – 0.15 Å), corresponding to the larger ionic radius of the 2+ metal lanthanide ions than the 3+. The ionic radius of Yb^{2+} (1.16 Å) is much more similar to Ca^{2+} (1.14 Å) than to Lu^{2+} (1.00 Å). As such, a more similar comparison of this structure would be to the known structure [CaI_2([18]aneO_4Se_2)].[36] The Ca^{2+}-Se bond lengths (3.106(1) Å) are much more comparable to the Yb^{2+}-Se bond lengths (3.1036(7) Å). The structure of [LaI_3([18]aneO_4Se_2-)] also showed La^{3+}-Se bond lengths of 3.0971(7) and 3.0885(7) Å which are significantly shorter than the Yb^{2+}-Se bond lengths, despite the larger ionic radius of La^{3+} (1.22 Å).

3.1.3 Divalent Lanthanide Chemistry

Whilst this review of the literature has primarily focussed on examples of trivalent lanthanide phosphine oxides, it is pertinent to discuss divalent lanthanide chemistry. The coordinative chemistry of Ln(II) ions is directed primarily by organometallic chemistry, with much of this being lanthanide Cp (cyclopentadienyl) complexes.[37,38] Evans *et. al* have pioneered this area of chemistry and shown the accessibility of non-classical divalent lanthanide complexes (i.e. Ln ≠ Sm, Eu, Yb) for all lanthanides except radioactive promethium.[39–42] Although ligands containing Ln-C bonds are not the focus of this work, no examples of divalent lanthanide phosphine oxides, prior to this work, are known in the literature. Other coordination complexes of divalent lanthanides predominantly contain the ligands THF, DME (1,2-dimethoxyethane), or macrocyclic ligands, such as 18-crown-6.[35,43,44] Given the

relative scarcity of even oxygen donor ligands on divalent lanthanide species, it is important to at least take note of these organometallic divalent lanthanide complexes. This is, therefore, not a comprehensive review of divalent lanthanide organometallic chemistry. It does, however, look at how the chemistry developed and the challenges faced with working with extremely reactive compounds.

The vast majority of Ln(II) organometallic complexes utilise Cp^R (Cp = C_5R_5; R = H, alkyl, silyl or aryl groups) rings. This class of compounds was first reported by Evans *et. al.*, with the complex [$Sm(Cp^*)_2(THF)_2$] ($Cp^* = C_5Me_5$) synthesised by a vaporising the metal into a hexane solution of the cyclopentadiene ligand, and extracting the resulting product in THF.[45] It was later shown that high vacuum sublimation of this product led to [$Sm(Cp^*)_2$], and [$Eu(Cp^*)_2$] could be made similarly, via the [$Eu(Cp^*)_2(THF)$] analogue.[46] Interestingly, despite not being coordinatively saturated, the Cp*-Ln-Cp* angle (using the centre of the ring as a point) are 140.1 and 140.3 ˚ respectively. This complex, [$Sm(Cp^*)_2$] is very reductive and has been shown to be useful in a range of small molecule activation experiments, however these are beyond the scope of this work.[47–50]

For non-classical Ln(II) metal centres, bulky R groups are used for kinetic stabilisation of the divalent lanthanide ion. Following the synthesis of [$TmI_2(DME)_3$],[51] which provided a route to the divalent metal in solution, the first organothulium(II), [$Tm(Cp'')_2(THF)$] ($Cp'' = C_5H_3(SiMe_3)_2$), was produced. Evans notes that organothulium(II) complexes are difficult to isolate due to activating N_2, as such experiments were performed under atmospheres of argon. Also attempts to form [$Tm(Cp^*)_2(THF)_n$], under argon in diethyl ether, led to decomposition of the solvent.[52] No non-classical examples of [$Ln(Cp^*)_2(THF)_n$] are currently known, likely due to this reactivity with coordinated solvent.[37] The [$Tm(Cp'')_2(THF)$] forms in both diethyl ether or THF, but does require the atmosphere of argon. The purple solid is stable, in diethyl ether, for several hours at 25 ˚C and several weeks at -30 ˚C.[52]

Other organometallic divalent lanthanide systems include the use of phospholyl ligands, e.g. [$Ln(\eta^5\text{-}PC_4Me_4)_2(THF)_2$] (Ln = Sm or Yb),[53] alkyl ligands, e.g. [$Ln(C\{SiMe_3\}_2)$] (Ln = Sm, Eu or Yb),[54–56] and aryl ligands, e.g. [$Yb(C_6F_5)_2(THF)_4$].[57,58] While examples of cyclopentadienyl complexes are known for all divalent lanthanides, besides Pm, no examples of the less stable, alkyl or aryl non-classical divalent lanthanides exist to date.[37] These unusual bulky ligands impart stability, both sterically and electronically, and have been used initially to coordinate to classical divalent lanthanides, before being translated to the non-classical Ln(II) ions. For example, [$Tm(Dtp)_2$] (Dtp = $P\{C(^tBu)C(Me)\}_2$) which shows one of very few examples of an organothulium complex with phospholyl ligands.[59,60] This fascinating area of chemistry is rapidly expanding and with a greater

commercial availability of both classical divalent lanthanide starting materials (e.g. SmI_2, EuI_2 and YbI_2) and also non-classical divalent lanthanides (TmI_2, DyI_2 and NdI_2).

3.1.4 Synthesis and spectroscopy

Divalent lanthanide systems are extremely air and moisture sensitive. Whilst Sm(II), Eu(II) and Yb(II) are the most stable systems, they are still readily oxidised.[61] As such great care must be taken to eliminate all traces of air and moisture. Both divalent samarium and europium are paramagnetic. A discussion of paramagnetic NMR is presented in Section 1.6.2, and the effects of this on lanthanide systems are shown above, in Section 3.2.1. As such ^{1}H NMR often provides little information. Where possible $^{31}P\{^{1}H\}$ NMR analysis has been utilized, however there are relatively few spectroscopic probes for the macrocyclic complexes.

3.1.5 Aims

This chapter aims to explore the coordination chemistry of the first divalent lanthanide phosphine oxide complexes, utilizing two monodentate phosphine oxides ($OPPh_3$ and $OPMe_3$) and a range of divalent lanthanide halides (SmI_2, EuI_2, $EuBr_2$ and YbI_2). The divalent metal iodides mentioned will also be reacted with a range of mixed donor macrocycles, [18]aneO_4X_2 (X = O, NH, S, Se) and Me_6[18]aneN_6 (Section 1.4.3, Figure 1.4), as comparisons to the [YbI_2([18]aneO_4X_2)] species described above.[35]

3.2 Results and discussion

3.2.1 Lanthanide(II) Halide Phosphine Oxide Complexes

The reactions of LnI_2 (Ln = Eu or Yb) with four equivalents of OPR_3 (R = Me or Ph), in anhydrous MeCN under an inert (N_2) atmosphere, produced pale yellow powders of $[EuI_2(OPR_3)_4]$ and yellow powders of $[YbI_2(OPR_3)_4]$, respectively. The powders were isolated by concentration of the respective solutions until a precipitate formed. This was filtered off and washed with deoxygenated hexane. The yellow powdered $[EuBr_2(OPR_3)_4]$ complexes were obtained in a similar manner, although the reactions required a longer reaction time (16 hours), due to the poorer solubility of $EuBr_2$ in MeCN. Attempts to synthesise $[EuCl_2(OPR_3)_4]$ were unsuccessful. Analogous reactions with SmI_2 were performed in THF, due to SmI_2 reacting readily with acetonitrile,[62] and the dark blue powdered products $[SmI_2(OPPh_3)_4]$ were isolated, Scheme 3.1. Attempts to form similar products with TmI_2, NdI_2 and DyI_2 were ultimately unsuccessful, with the THF solutions rapidly decolourising upon addition of OPR_3. The isolated $[LnX_2(OPR_3)_4]$ complexes are highly air and moisture sensitive and so the samples were manipulated and stored under nitrogen. Even in the glove box, solid samples deteriorated and discoloured over a matter of days, indicating product degradation, and as such, spectroscopic measurements were made on freshly prepared samples. Samples were analysed by using elemental analysis, infrared spectroscopy, $^{31}P\{^1H\}$ NMR spectroscopy, UV-vis spectroscopy and single crystal X-ray analysis where possible.

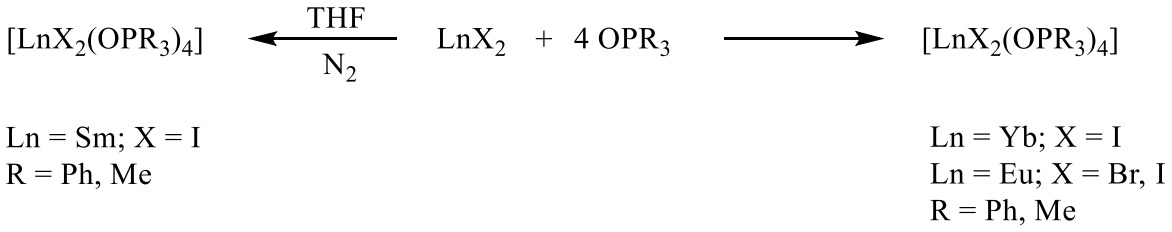

Scheme 3.1. Synthetic routes used for the preparation of the new LnX_2 phosphine oxide complexes.[63]

The experiments for both europium diiodide and ytterbium diiodide phosphine oxides were performed in acetonitrile, and as there was no evidence of exchange between solvent and OPR_3, deuterated acetonitrile was used for the $^{31}P\{^1H\}$ NMR experiments. Complexes of ytterbium (II) are diamagnetic, and as such do not show the same large changes in chemical shift or broadening of the peaks upon coordination to the metal centre. The $^{31}P\{^1H\}$ NMR

spectrum of $[YbI_2(OPPh_3)_4]$ showed a single sharp resonance at +36.1 ppm while $[YbI_2(OPMe_3)_4]$ showed a single sharp resonance at +50.9 ppm. These values shifted significantly from free ligand at +29 for $OPPh_3$ and +36 for $OPMe_3$.[8,64] In contrast $[EuX_2(OPR_3)_4]$ (X = Br or I; R = Me or Ph) showed no ^{31}P resonance in the observed window. Similar $^{31}P\{^1H\}$ NMR studies of the $[LnCl_3(OPPh_3)_3]$ and $[LnCl_2(OPPh_3)_4]Cl$ systems described above showed that the gadolinium (III) complexes, also f^7, displayed no ^{31}P resonance.[8] During a prolonged $^{31}P\{^1H\}$ NMR experiment of $[EuI_2(OPPh_3)]$ the MeCN solution turned slowly from yellow to colourless on standing, and a resonance at -125.0 ppm appeared, relating to the oxidation product $[EuI_2(OPPh_3)_4][I_3]$. Similar exposure of $[EuBr_2(OPPh_3)_4]$ to dry air produced a resonance in the $^{31}P\{^1H\}$ spectrum at -97.0 ppm. Following this, an NMR experiment was undertaken on each complex before and after the sample was exposed to dry O_2. For the lanthanide iodides, a further sample had an excess of I_2 added to the spectroscopic solution and subsequent $^{31}P\{^1H\}$ NMR experiments were performed in order to show the air oxidation did lead to the $[LnI_2(OPR_3)_4][I_3]$ product. This deliberate oxidation of the product was beneficial because it not only for showed the presence of coordinated ligand in the europium (II) samples which displayed no resonance, but it also demonstrated the product in the original solution was in fact the 2+ oxidation state product. These systems proved to be extremely sensitive and challenging to work with, decomposing over a short period of time (ca. 30 mins) upon standing in solution, and demonstrating that the samples were in fact the divalent species (especially for samarium and europium where both divalent and trivalent species are paramagnetic) would be difficult without these experiments. Upon oxidation, either via the addition of dry oxygen or I_2 to an acetonitrile solution of the lanthanide complex, the ^{31}P resonances displayed by the divalent $[YbI_2(OPPh_3)_4]$ showed a large shift from 36.1 to -39.0 ppm. The $[YbI_2(OPMe_3)_4]$ shifted from 50.9 to show two resonances at -13.9 and -25.0 ppm. Only a single resonance would be expected for $[YbI_2(OPMe_3)_4][I_3]$ and so there are likely at least two degredation products forming, however identifying these was beyond the scope of this work, and was used primarily to show a shift from the diamagnetic divalent ytterbium species upon being exposed to an oxidising agent. Upon exposure to air, $[EuBr_2(OPMe_3)_4]$ went from having no observed resonance to showing a singlet at -7.7 ppm and $[EuI_2(OPMe_3)_4]$ displayed a singlet at -8.0 ppm after exposure to dry oxygen. It is possible this is indicative of a consistent cation, however no further analysis was performed on these samples. The blue solution of $[SmI_2(OPPh_3)_4]$ in d_8-thf showed a single broad resonance at +18.8 ppm which, upon addition of excess I_2, shifted to +35.6 ppm. Unfortunately, $[SmI_2(OPMe_3)]$ was not sufficiently soluble in d_8-thf or CD_2Cl_2, and decomposes in CD_3CN so no solution state data was able to be obtained. The solution state data is displayed alongside the infrared

spectroscopy data in Table 3.2. Attempts to form $[EuCl_2(OPPh_3)_4]$ were abandoned due to the poor solubility of $EuCl_2$.

Poor solubility of these divalent lanthanide phosphine oxide complexes and their low stability meant crystallisation attempts were particularly difficult. Many attempts to obtain crystals resulted in decomposition of the sample or powdered products. Orange crystals of $[EuBr_2(OPPh_3)_4]$ were grown by slow evaporation of an acetonitrile solution of the product in the glovebox. The structure, Figure 3.7, shows the six-coordinate octahedral metal centre in a *trans*-geometry. The d(Eu-Br) bond distances, 3.0463(8) and 3.0173(8) Å, are significantly longer than in the structure of $[GdBr_2(OPPh_3)_4]Br$, described in Section 3.2.1, 2.8099(12) and 2.8088(13) Å. This is owing to the much larger size of the divalent metal centre. The Eu-O-P bond angles, between 157.1 and 162.7˚ are actually much closer to the values of Ln-O-P displayed in $[YbBr_2(OPPh_3)_4]Br$ (≈ 161.0 ˚) than $[GdBr_2(OPPh_3)_4]Br$ (≈171.5 ˚). There is a small amount of residual density around the europium metal centre, probably attributed to an absorption correction issue, common in heavy metal systems. In the trivalent lanthanide bromide examples described, a decrease in lanthanide ion size is the cause of the bending of the Ln-O-P bond, however that is clearly not the case here.

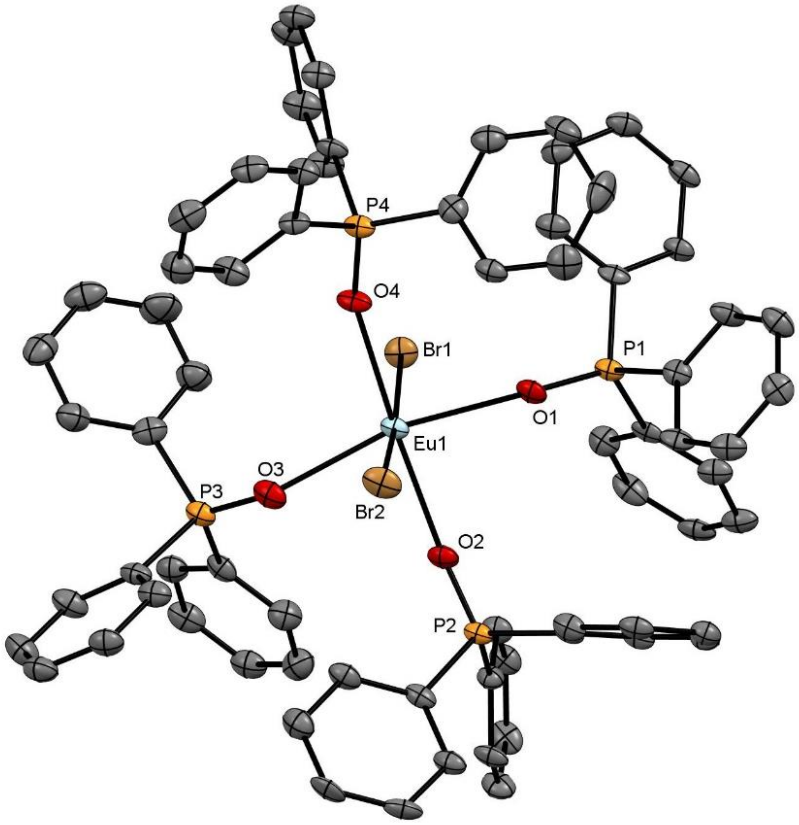

Figure 3.7. A crystal structure of trans-[EuBr$_2$(OPPh$_3$)$_4$] with atom numbering scheme. The crystal displays the six-coordinate octahedral geometry of the metal centre. Thermal ellipsoids are drawn at a 50% probability level and hydrogen atoms are omitted for clarity. Selected bond lengths (Å) and angles (˚): Eu1 – Br1 = 3.0463(8), Eu1 – Br2 = 3.0173(8), Eu1 – O1 = 2.487(5), Eu1 – O2 = 2.477(5), Eu1 – O3 = 2.540(5), Eu1 – O4 = 2.494(5), O1 – P1 = 1.489(5), O2 – P2 = 1.486(5), O3 – P3 = 1.484(6), O4 – P4 = 1.495(5), Eu1 – O1 – P1 = 162.7(3), Eu1 – O2 – P2 = 160.7(3), Eu1 – O3 – P3 = 157.1(3), Eu1 – O4 – P4 = 158.8(3), Br1 – Eu1 – Br2 = 172.65(2), O1 – Eu1 – O2 = 84.31(16), O1 – Eu1 – O3 = 162.32(17).

Yellow crystals of [EuI$_2$(OPPh$_3$)$_4$] were grown from an acetonitrile solution of the product cooled to – 8˚C and left to stand, Figure 3.8. The crystal shows the six-coordinate metal centre with a *cis*-geometry. The formation of the *cis*-geometry was unexpected as all previously known examples of the trivalent lanthanide halides, [LnX$_2$(OPPh$_3$)$_4$]X (X = Cl, Br or I), and the above [EuBr$_2$(OPPh$_3$)$_4$] complex show a *trans*- geometry, likely due to the steric bulk of the OPPh$_3$ ligand. The energy differences between the two geometries are likely to be small, and production of one over the other is most likely to be due to solid state packing. Solution state NMR data for lanthanides generally show separate resonances for different complexes, e.g. the lanthanide chloride systems ([LnCl$_3$(OPPh$_3$)$_3$] and

[$LnCl_2(OPPh_3)_4$]) discussed above, however separate environments within one complex are not commonly observed due to the systems being fluxional. As such, two separate resonances would not be expected for *cis*-[$LnX_2(OPPh_3)_4$]. The Eu-O-P bond angles are between 165.3(4) and 173.9(5)˚ and as such are much closer to linear than in the analogous [$EuBr_2(OPPh_3)_4$]. This does suggest that the divalent metal centre still has quite a strong repulsion effect on the phosphorus atom and while this alone is not the reason for the more bent angle in the bromide structure above steric effects and solid-state packing are also factors. The Eu-O bond lengths for the two systems are very similar, despite the differing geometries.

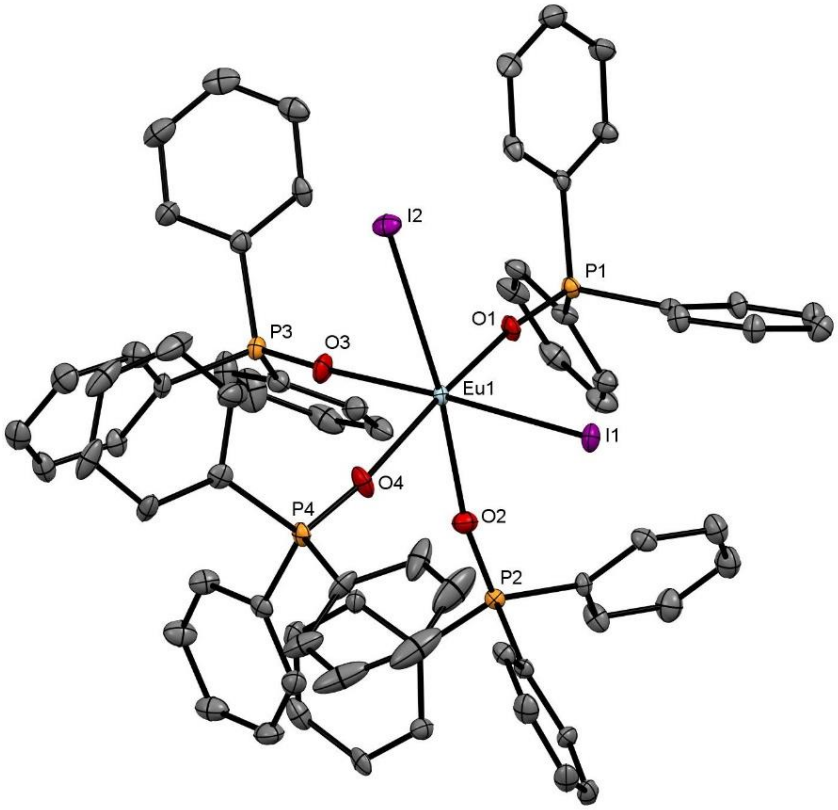

Figure 3.8. The structure of cis-[$EuI_2(OPPh_3)_4$]·MeCN with atom numbering scheme. Thermal ellipsoids are drawn at a 50% probability level and H atoms and solvent molecules are omitted for clarity. Selected bond lengths (Å) and angles (˚): Eu1 – I1 = 3.3250(6), Eu1 – I2 = 3.3787(6), Eu1 – O1 = 2.475(6), Eu1 – O2 = 2.476(6), Eu1 – O3 = 2.451(6), Eu1 – O4 = 2.445(7), O1 – P1 = 1.503(6), I1 – Eu1 – I2 = 95.970(17), I1 – Eu1 – O1 = 101.30(14), O1 – Eu1 – O2 = 87.8(2), Eu1 – O1 – P1 = 165.3(4), Eu1 – O2 – P2 = 168.2(4), Eu1 – O3 – P3 = 173.9(5), Eu1 – O4 – P4 = 166.4(4).

Crystals of the oxidised Eu(III) product, $[EuI_2(OPPh_3)_4]I_3 \cdot MeCN$, were obtained by exposing an MeCN solution of the divalent complex to air, followed by cooling the solution in a freezer to -20 ˚C for several days. The resulting crystal structure shows the octahedral Eu(III) cation with a *trans*-geometry, Figure 3.9. The Eu–I bond distances in the divalent $[EuI_2(OPPh_3)_4]$ complex (3.3250(6), 3.3787(6) Å) are significantly longer than in the trivalent $[EuI_2(OPPh_3)_4]^+$ cation (3.0305(6) - 3.0866(6) Å), which is a consequence of the larger ionic radius of Eu(II). Similarly, the Eu–O bond lengths (Eu(II): 2.451(6)–2.476(6) Å) are all *ca*. 0.2 Å longer than in the Eu(III) complex. The Ln-O-P bond angles are between 166.1 and 171.5˚, which are much closer to the values from *cis*-$[EuI_2(OPPh_3)_4]$ structure than the *trans*-$[EuBr_2(OPPh_3)_4]$ structure.

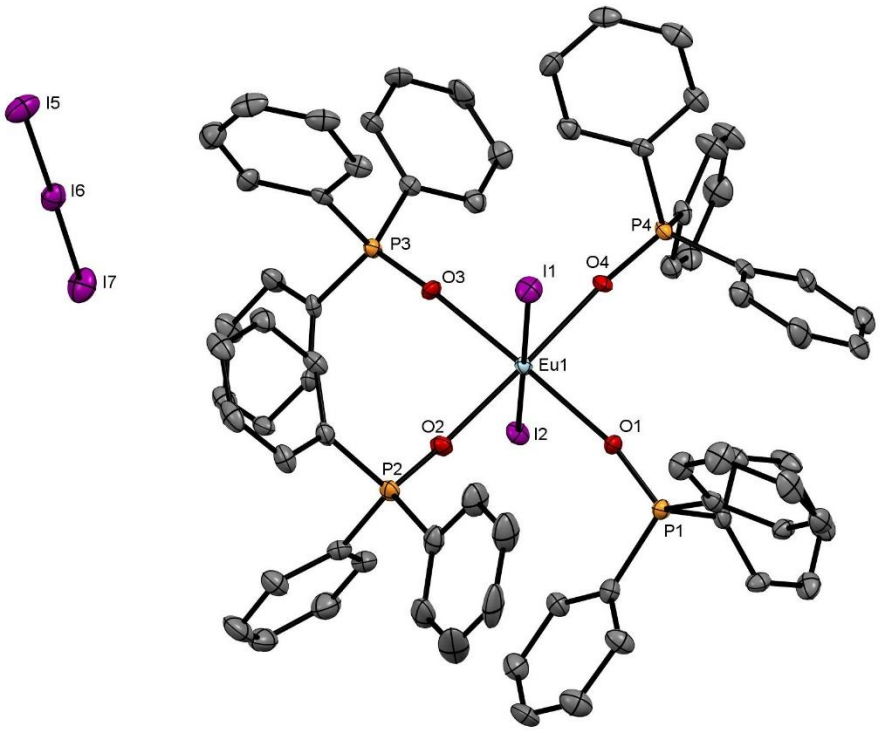

Figure 3.9. View of the crystal structure of $[EuI_2(OPPh_3)_4][I_3]$ with atom numbering scheme. Note that the asymmetric unit contains a second, crystallographically independent cation and $[I_3]^-$ anion and 3 acetonitrile molecules. H atoms are omitted for clarity and ellipsoids are shown at the 50% probability level. Selected bond lengths (Å) and angles (°): Eu1 – I1 = 3.0866(6), Eu1 – I2 = 3.0481(6), Eu1 – O1 = 2.254(5), Eu1 – O2 = 2.253(5), Eu1 – O3 = 2.273(5), Eu1 – O4 = 2.254(5), O1 – P1 = 1.498(5), I1 – Eu1 – I2 = 177.024(18), I1 – Eu1 – O1 = 93.55(13), O1 – Eu1 – O2 = 89.39(18), Eu1 – O1 – P1 = 166.1(3), Eu1 – O2 – P2 = 166.5(3), Eu1 – O3 – P3 = 166.3(3), Eu1 – O4 – P4 = 163.3(3), I5 – I6 – I7 = 179.24(3).

The infrared spectra of the $[LnX_2(OPPh_3)_4]$ systems show two bands in the ranges 1140-1170 cm^{-1} and 1070-1085 cm^{-1}, assigned as the ν(P=O) stretches. These are shifted from the value of 1196 cm^{-1} in "free" $OPPh_3$. The two bands are indicative of a *cis*-geometry, suggesting that the bulk $OPPh_3$ complexes are all *cis* isomers. This would suggest that the crystal obtained of *trans*-$[EuBr_2(OPPh_3)_4]$ was a consequence of the crystallisation conditions and is not representative of the bulk solid isolated from the original reaction. The $[LnX_2(OPMe_3)_4]$ complexes all show a single band in their IR spectra, 1100-1115 cm^{-1}, which is shifted from free $OPMe_3$ (1141 cm^{-1}) and indicative of a *trans* isomer. Unfortunately, despite numerous attempts, no crystals suitable for X-ray diffraction were obtained of $[LnX_2(OPMe_3)_4]$.

Table 3.2. Selected infrared, $^{31}P\{^1H\}$ NMR and UV-Vis spectroscopic data for the two series of divalent lanthanide phosphine oxides.

Compound	ν(P=O) cm^{-1}	$^{31}P\{^1H\}$ NMR Shift[a]	UV-Vis (diffuse reflectance/ cm^{-1})
$[SmI_2(OPPh_3)_4]$	1167, 1071	18.5 (35.6)	26730, 17300
$[EuBr_2(OPPh_3)_4]$	1141, 1084	N.o.[b] (-97.0)	26040
$[EuI_2(OPPh_3)_4]$	1135, 1082	N.o.[b] (-125.0)	26900
$[YbI_2(OPPh_3)_4]$	1140, 1085	36.1 (-39.0)	27320
$[SmI_2(OPMe_3)_4]$	1103	— [c]	— [d]
$[EuBr_2(OPMe_3)_4]$	1108	— [b] (-7.7)	25840
$[EuI_2(OPMe_3)_4]$	1104	N.o.[b] (-8.0)	27470, 26460
$[YbI_2(OPMe_3)_4]$	1112	50.9 (-13.9, -25.0)	— [d]

[a] *NMR experiments run at 298 K in CD_3CN for $EuBr_2$, EuI_2 and YbI_2 products and d_8-thf for SmI_2. Resonance observed due to oxidation product after addition of dry O_2 or excess I_2 displayed in brackets.*[b] *Resonance not observed due to rapid relaxation and paramagnetic centre.*[8,22] [c] *Insoluble in d8-thf and CD_2Cl_2, decomposes in CD_3CN.* [d] *Insufficient pure sample.*

UV-vis data were also collected on the solid samples. A brief description of UV-vis spectroscopy and its use on divalent lanthanide systems can be found in Section 1.6.5. The UV-Vis spectra of LnI_2 display $4f^n \rightarrow 4f^{n-1}\ 5d^1$ transitions, which are not present in Ln^{3+} systems.[65–67] The near UV region of the spectra were dominated by the $\pi \rightarrow \pi^*$ transitions of

P=O (and for $OPPh_3$ the $\pi \rightarrow \pi^*$ transitions of the aryl groups).[68] At lower energy a weak feature is observed for the Ln(II) transitions. The values are quoted in Table 3.2, and the presence of an f-d transition is further evidence to support the assignment of these complexes as divalent systems.

3.2.2 Lanthanide(II) Halide Macrocyclic Complexes

One of the aims of this work was to probe divalent metal centres with both hard and soft donor ligand coordination. One of the previously used methods used to coordinate lanthanides with soft donors is using mixed donor macrocycles.[34] An initial study undertaken previously within the Reid group described the synthesis of a series of YbI_2 complexes: $[YbI_2(18\text{-crown-6})]$, $[YbI_2([18]aneO_4S_2)]$, $[YbI_2([18]aneO_4Se_2)]$ and $[YbI_2([18]aneN_2O_4)]$.[35] In the present work other LnI_2 (Ln = Sm, Eu) and $EuBr_2$ mixed donor macrocyclic complexes are synthesised, Scheme 3.2, and analysed by infrared spectroscopy, elemental analysis and UV-vis spectroscopy. The ytterbium macrocyclic complexes were also reproduced as a comparison and attempts to make $[LnI_2([18]aneS_4O_2)]$ (Ln = Eu or Yb) and $[EuI_2(Me_6[18]aneN_6)]$ were undertaken. Unlike the ytterbium macrocyclic complexes, divalent europium and samarium are paramagnetic, and ^1H NMR spectra are often poorly defined if resonances are observed at all. As such, NMR spectroscopy is not a useful tool for these systems, and hence, without structural data, analytical tools are relatively limited.

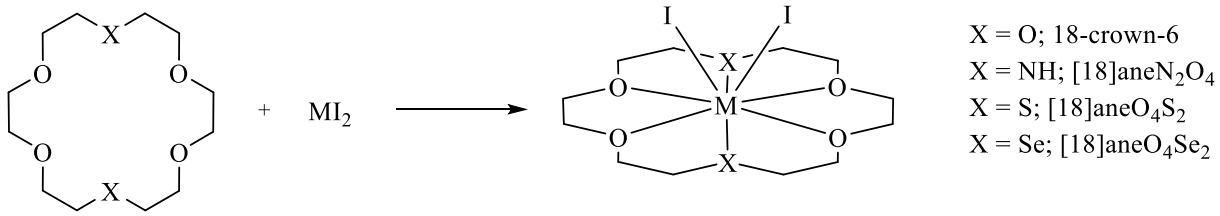

Scheme 3.2. Reaction between a divalent lanthanide iodide and $[18]aneO_4X_2$ where M = Yb, Eu, Sm and X = O, S, Se, NH.

Yellow powders of $[EuI_2([18]aneO_4S_2)]$, $[EuI_2([18]aneN_2O_4]$, $[EuI_2([18]aneO_4Se_2)]$, $[EuI_2(18\text{-crown-6})]$ and $[EuI_2(Me_6[18]aneN_6)]$ have been synthesized in low to moderate yield, via the addition of the appropriate macrocycle to a stirring solution of EuI_2 in anhydrous MeCN, under an inert (N_2) atmosphere. The resulting yellow solution was stirred for *ca*. 10 minutes and then concentrated *in vacuo*, precipitating a yellow solid which was

collected by filtration. Microanalytical data are consistent with the stated formulae, and IR spectroscopic studies on each of the products confirms the presence of the macrocyclic ligand, with no evidence for either water or MeCN solvent. The growth of single crystals suitable for single crystal X-ray diffraction proved unsuccessful. Initial reactions of SmI_2 with [18]aneO_4X_2 (X = NH, O, S, Se) were performed in acetonitrile. Under these conditions, the reaction mixture would turn from dark green to colourless over a short period of time, indicating the degradation of the product as the samarium diiodide reacted with the acetonitrile. The rapid degradation of SmI_2 in acetonitrile has been observed in the literature.[62] The reactions were, therefore, performed using THF as a solvent instead, forming a dark blue solution, to which the macrocycle was then added and the solution was stirred for *ca*. 10 minutes, then concentrated *in vacuo*, precipitating dark blue solids in moderate to high yield. Formulation of the products were ultimately established by elemental analysis, while infrared spectroscopy showed no retained solvent or water. It was therefore confirmed that this family, of mixed donor macrocycles coordinated to divalent metal centres, can be extended to both the larger samarium and europium diiodides. UV-vis spectra were recorded for the solids [EuI_2([18]aneO_4S_2)], [SmI_2([18]aneO_4S_2)] and [SmI_2([18]aneN_2O_4]. Experiments required large amounts of product which could often not be recovered as discolouration was observed whilst running the experiments suggesting the decomposition of samples during the experiment. Bands attributed to the f-d transitions typical for divalent lanthanide systems were present and confirmed the assignment of these systems as divalent.[65–67] The observed bands are shown in Table 3.3 below.

Attempts to coordinate EuI_2 and YbI_2 to [18]aneO_2S_4, incorporating a 1:2 O:S ratio, were unsuccessful, typically leading to re-isolation of the uncomplexed macrocycle. It is unclear whether this is a result of the poor solubility of the macrocycle in MeCN, or that there may be a minimum number of hard O-donor atoms required to stabilize the complex, as in the case of the complexes with [18]aneO_4S_2. The complex [EuI_2(Me_6[18]aneN_6)] was successfully synthesised and its formulation was confirmed by elemental analysis. Infrared spectroscopy showed an absence of both H_2O and MeCN in the bulk product.

Table 3.3. UV-Vis spectroscopic data for three mixed donor macrocyclic complexes of divalent lanthanides.

Compound	UV-Vis (diffuse reflectance/ cm^{-1})
EuI_2	24300 (s)
$[EuI_2([18]aneO_4S_2)]$	28200 (s), 18000 (vw)
SmI_2	24300 (m, br), 16600 (s, br),
$[SmI_2([18]aneO_4S_2)]$	27100 (m), 18500 (w), 15900 (s)
$[SmI_2([18]aneN_2O_4]$	26700 (m), 17600 (s), 15000 (s)

Given the limited information available on these complexes from the spectroscopic methods described, attempts were made to match the simulated PXRD pattern for the bulk Yb(II) powders, and $[EuI_2([18]aneO_4S_2)]$, against the pattern simulated from the published $[YbI_2([18]aneO_4Se_2)]$. This showed a good match for $[YbI_2([18]aneO_4Se_2)]$ and also for the two $[LnI_2([18]aneO_4S_2)]$ (Ln = Eu or Yb), however the signal : noise ratio was relatively poor, due to poor crystallinity of the powders, and therefore unambiguous assignment was not possible.

A few crystals of a hydrolysis product, $[Eu(Me_6[18]aneN_6)(MeCONH_2)]I_2{\cdot}2MeCN$, were obtained from an attempt to crystallise $[EuI_2(Me_6[18]aneN_6)]$ in an acetonitrile solution. These were likely formed by the reaction of MeCN with adventitious H_2O to form acetamide, Figure 3.10. The structure shows the macrocycle coordinated by all six nitrogen atoms. The methyl groups on N2 and N3 are pointed towards the acetamide ligand and those on N1 and N4 are directed away. There is a hydrogen bond between the acetamide ligand and one molecule of acetonitrile. Of particular interest is the linear nature of the Eu1 – O1 – C1 bond, which has a bond angle of 178.8(4)˚. It has been observed that, much like Ln-O-P bond angles in lanthanide phosphine oxide complexes, the M-O-C bond angles for lanthanide acetamide complexes are notably larger than for similar transition metals, with near linear bond angles commonly observed.[69,70] The d(O1 – C1) bond length of 1.238 Å is typical of the C=O bond length in similar structures and the d(C1 – N1) bond length of 1.350(8) Å is typical of the C-N bond lengths. The d(Eu1-O1) bond length of 2.426(3) Å is significantly longer than the Eu-O bonds in the trivalent $[Eu(CH_3CONH_2)_4(H_2O)_4]I_3$ (2.337 – 2.349 Å), indicative of a Eu^{2+} metal centre.[70]

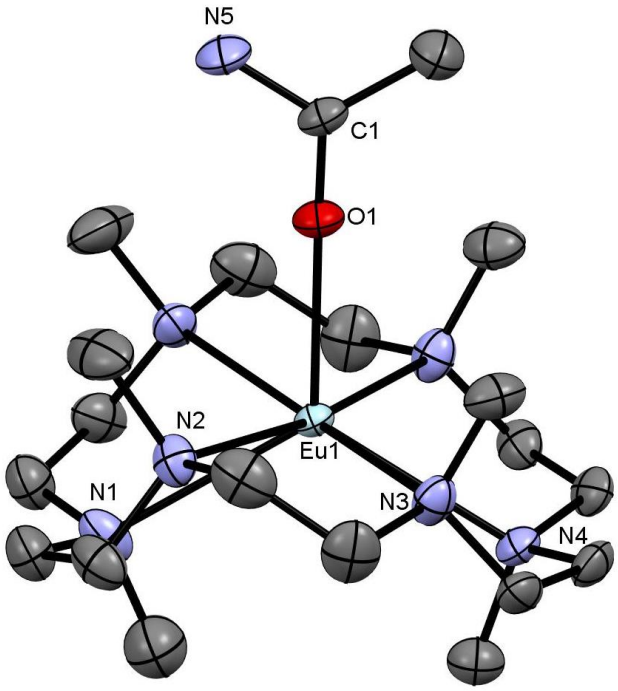

Figure 3.10. The structure of the cation [Eu(Me$_6$[18]aneN$_6$)(MeCONH$_2$)]$^{2+}$ with atom numbering scheme. H atoms, anions and three acetonitrile molecules are omitted for clarity. Thermal ellipsoids are drawn with a 50% probability level. Selected bond lengths (Å) and angles (°) are: Eu1 – O1 = 2.426(3), Eu1 – N1 = 2.743(5), Eu1 – N2 = 2.771(3), Eu1 – N3 = 2.771(3), Eu1 – N4 = 2.769(5), O1 – C1 = 1.238(6), C1 – N5 = 1.350(8), N1 – Eu1 – N2 = 64.50(9), N1 – Eu1 – N4 = 116.08(15), Eu1 – O1 – C1 = 178.8(4), O1 – C1 – N1 = 121.0(6).

Coordination of acetamide to macrocyclic complexes, from acetonitrile solutions, has been observed in the literature.[71] Based upon the absence of a *v*(C=O) stretch, which would show the presence of acetamide, in the infrared spectrum of bulk [EuI$_2$(Me$_6$[18]aneN$_6$)] and the microanalytical data that are consistent with this formula, it is likely that this decomposition occurs via adventitious water during recrystallization and is not representative of the bulk powder.

Attempts were made to form macrocyclic complexes of EuBr$_2$ and EuCl$_2$. Due to the poor solubility of EuCl$_2$ this metal halide was quickly abandoned. Infrared spectroscopy of [EuBr$_2$(18-crown-6)], [EuBr$_2$([18]aneN$_2$O$_4$] and [EuBr$_2$([18]aneO$_4$S$_2$] all show the retention of ligand, after isolating the product, and an absence of acetonitrile or water in the infrared spectra. Only [EuBr$_2$(18-crown-6)] led to satisfactory elemental analysis, likely due to problems with the purification step due to impurities with similar solubilities. Further reactions were not pursued due to time restrictions.

Whilst there is sufficient data to conclude that the family of mixed donor macrocycles coordinated to divalent lanthanide halides can be extended to include the larger iodides, EuI_2 and SmI_2, the lack of NMR spectroscopy, due to the paramagnetic metal centres, does mean this work is heavily reliant on structural data and due to the rapid decomposition of the products and poor compatibility with many solvents, single crystals suitable for X-ray crystallography were not obtained despite many attempts.

3.3 Conclusion

The successful synthesis of the complexes $[LnI_2(OPR_3)_4]$ (Ln = Sm, Eu or Yb; R = Me or Ph) and $[EuBr_2(OPR_3)_4]$ (R = Me or Ph) have been described. The products have been analysed by infrared spectroscopy, elemental analysis, $^{31}P\{^1H\}$ NMR spectroscopy, UV-Vis spectroscopy and single crystal X-ray crystallography where possible. Infrared spectroscopy suggests that the $[LnX_2(OPPh_3)_4]$ products are six-coordinate octahedral *cis*-geometry structures, while the $[LnX_2(OPMe_3)_4]$ products are *trans*- structures. Crystal structures of *cis*-$[EuI_2(OPPh_3)_4]$ and *trans*-$[EuBr_2(OPPh_3)_4]$ suggest that these may be dynamic in solution and the energy barrier between the two is small. Unfortunately, no crystal structures were obtained for any $OPMe_3$ structures. UV-vis analysis of the solid powdered products confirmed the presence of f-d transitions typically observed in divalent lanthanide systems and all of the formulae were confirmed by elemental analysis. The $^{31}P\{^1H\}$ NMR studies showed coordination of the free ligand for $[SmI_2(OPPh_3)_4]$, $[YbI_2(OPPh_3)_4]$ and $[YbI_2(OPMe_3)_4]$. The resonances displayed by the divalent ytterbium complexes show small shifts from free ligand owing to the diamagnetic metal centre. While $^{31}P\{^1H\}$ NMR data for the divalent europium complexes initially showed no resonance, oxidation of the sample by addition of dry O_2 or I_2 led to resonances caused by the phosphine oxide coordinated to the Eu^{3+} metal centre. Similar experiments on the ytterbium and samarium complexes confirmed an initial 2+ oxidation state in solution, which is oxidised to 3+ on addition of dry O_2 or I_2 with the phosphine oxide remaining coordinated to the metal centre. A crystal structure of $[EuI_2(OPPh_3)_4][I_3]$ suggests this is the likely decomposition route for the iodide complexes. A range of mixed donor macrocycles were coordinated to europium diiodide and samarium diiodide to form the complexes $[LnI_2([18]aneO_4X_2)]$ (Ln = Sm or Eu; X = NH, O, S or Se), to expand a family of mixed donor macrocycles coordinated to ytterbium diiodide.[35] The europium complexes were synthesised by the addition of the macrocycle to the metal iodide in acetonitrile, whilst the samarium complexes were synthesised in THF. The complex $[EuI_2(Me_6[18]aneN_6)]$ was synthesised similarly by the addition of the macrocycle to the metal halide in dry acetonitrile. Infrared spectroscopy was used to confirm the absence of H_2O and acetonitrile and the continued presence of ligand and all formulae were confirmed by elemental analysis. UV-vis spectroscopy was used to confirm the presence of a divalent metal centre for the powdered products $[EuI_2([18]aneO_4S_2)]$, $[SmI_2([18]aneO_4S_2)]$ and $[SmI_2([18]aneN_2O_4)]$, showing the presence of f-d transitions typical of these divalent lanthanide metal centres. Crystals of $[Eu(Me_6[18]aneN_6)(MeCONH_2)][I]_2{\cdot}3MeCN$ were grown from a solution of $[EuI_2(Me_6[18]aneN_6)]$ in an acetonitrile solution cooled in the freezer, with the acetamide likely formed by adventitious water.

3.4 Experimental

3.4.1 General Experimental

Lanthanide dihalides, triphenylphosphine oxide, trimethylphosphine oxide, Me_6[18]aneN_6, [18]aneN_2O_4 and 18-crown-6 were obtained from Sigma–Aldrich and used as received. 18-Crown-6 was dried by dissolution in anhydrous CH_2Cl_2 followed by addition of thionyl chloride and then stirred for 1 h. when the solvent and excess thionyl chloride were removed *in vacuo*. [18]aneO_4S_2 and [18]aneO_4Se_2 were prepared according to literature procedures.[31] Trimethylphosphine oxide was dried by sublimation *in vacuo* and triphenylphosphine oxide melted under vacuum prior to use. Syntheses were routinely carried out under a dry dinitrogen atmosphere, and all solids and spectroscopic samples were handled in a dry dinitrogen filled glove box. Since the complexes have limited stability in dilute solution, NMR samples were freshly prepared immediately before recording data. For further details regarding the instrumentation see Appendix A.

3.4.2 Preparation of divalent lanthanide phosphine oxides

$[YbI_2(OPPh_3)_4]$ - YbI_2 (0.05 g, 0.12 mmol) was dissolved in anhydrous MeCN (10 mL), a solution of $OPPh_3$ (0.13 g, 0.47 mmol) in MeCN (5 mL) was added, and the mixture was stirred for 20 min. during which the orange colour of the solution deepened. The solution was concentrated to a small volume when a bright yellow precipitate formed. The solid was filtered and dried *in vacuo* to yield a bright yellow powder. Yield 0.14 g, 79 %. Required for $C_{72}H_{60}I_2O_4P_4Yb$ (1539.2): C, 56.13; H, 3.93 %. Found: C, 55.89; H, 3.77%. $^{31}P\{^1H\}$ NMR (CD_3CN): $\delta = +36.1$. IR spectrum (Nujol mull)/cm^{-1}: 1140 br s, 1085 m (P=O). UV–Vis (diffuse reflectance/cm^{-1}): 27 320.

The MeCN solution of $[YbI_2(OPPh_3)_4]$ exposed to air or O_2 resulted in rapid diminution of the $^{31}P\{^1H\}$ NMR resonance and development of a new resonance at $\delta = -39.0$, assigned as a Yb(III) species, often with a weak feature at +29.6 ppm ($OPPh_3$). The same species was generated by addition of I_2 to a MeCN solution of the divalent complex.

$[YbI_2(OPMe_3)_4]$ - Was made similarly from YbI_2 (0.05 g, 0.12 mmol) and $OPMe_3$ (0.043 g, 0.47 mmol) in MeCN. The product was a pale yellow powder. Yield 0.02 g, 21 %. Required for $C_{12}H_{36}I_2O_4P_4Yb$ (795.0): C, 18.11; H, 4.56 %. Found: C, 18.05; H, 4.56%. $^{31}P\{^1H\}$ NMR (CD_3CN): $\delta = +50.9$. Treatment of the CD_3CN solution with I_2 produced an orange-brown solution, $\delta(^{31}P\{^1H\}) = -13.9$ and -25.0. IR spectrum (Nujol mull)/cm^{-1}: 1112 br s (P=O).

[$EuI_2(OPPh_3)_4$] - EuI_2 (0.05 g, 0.12 mmol) was dissolved in anhydrous MeCN (10 mL), a solution of $OPPh_3$ (0.14 g, 0.49 mmol) in MeCN (5 mL) was added, and the pale yellow solution was stirred for 20 min. The solution was concentrated to small volume when a yellow precipitate formed. This was filtered off and dried *in vacuo* to yield a yellow powder. Yield 0.12 g, 64 %. Crystals were obtained from cooling a MeCN solution of the complex. Required for $C_{72}H_{60}EuI_2O_4P_4$ (1598.1): C, 56.91; H, 3.98 %. Found: C, 56.63; H, 4.11%. $^{31}P\{^1H\}$ NMR (CD_3CN): not observed. $^{31}P\{^1H\}$ NMR after exposure to air / I_2 (CD_3CN): $\delta = -125.0$. IR spectrum (Nujol mull)/cm^{-1}: 1135 br s, 1082 m (P=O). UV–Vis (diffuse reflectance/cm^{-1}): 26 900.

[$EuI_2(OPMe_3)_4$] - Was made similarly from EuI_2 (0.05 g, 0.12 mmol) and $OPMe_3$ (0.045 g, 0.49 mmol) in MeCN. The product was a pale yellow powder. Yield 0.06 g, 66 %. Required for $C_{12}H_{36}EuI_2O_4P_4$ (773.9): C, 18.61; H, 4.69. Found: C, 18.41; H, 4.53%. $^{31}P\{^1H\}$ NMR (CD_3CN): $\delta =$ not observed. $^{31}P\{^1H\}$ NMR after exposure to air (CD_3CN): $\delta = -8.0$. IR spectrum (Nujol mull)/cm^{-1}: 1142 m, 1104 br s, (P=O). UV–Vis (diffuse reflectance/cm^{-1}): 27 470(sh), 26 455.

[$EuBr_2(OPPh_3)_4$] - $EuBr_2$ (0.05 g, 0.16 mmol) was dissolved in MeCN (10 mL) and a solution of $OPPh_3$ (0.18 g, 0.64 mmol) in MeCN (10 mL) was added, and the mixture was stirred overnight. On standing a yellow precipitate formed, and the solution was concentrated to small volume, and the precipitate filtered off and dried *in vacuo*. Yield 0.14 g, 62 %. Crystals of [$EuBr_2(OPPh_3)_4$] were obtained from a cooled MeCN solution of the product. Required for $C_{72}H_{60}Br_2EuO_4P_4$ (1424.1): C, 60.67; H, 4.25 %. Found: C, 60.55; H, 4.43%. $^{31}P\{^1H\}$ NMR (CD_3CN): not observed. $^{31}P\{^1H\}$ NMR after exposure to air (CD_3CN): $\delta = -97.0$. IR spectrum (Nujol mull)/cm^{-1}: 1141 br s, 1084 m (P=O). UV–Vis (diffuse reflectance/cm^{-1}): 26 040.

[$EuBr_2(OPMe_3)_4$] - Was made similarly from $EuBr_2$ (0.05 g, 0.16 mmol) and $OPMe_3$ (0.059 g, 0.64 mmol). The product was a pale yellow powder. Yield 0.07 g, 64 %. Required for $C_{12}H_{36}Br_2EuO_4P_4$ (680.1): C, 21.19; H, 5.34 %. Found: C, 21.31; H, 5.45%. $^{31}P\{^1H\}$ NMR (CD_3CN): not observed. $^{31}P\{^1H\}$ NMR after addition of Br_2 (CD_3CN, 298 K): −7.7. IR spectrum (Nujol mull)/cm^{-1}: 1108 br s (P=O). UV–Vis (diffuse reflectance/cm^{-1}): 25 840.

[$SmI_2(OPPh_3)_4$] - SmI_2 (0.05 g, 0.12 mmol) was dissolved in THF (10 mL) to form a dark blue solution. A solution of $OPPh_3$ (0.14 g, 0.49 mmol) in THF (5 mL) was then added. On stirring, the solution became dark purple and on concentration a dark blue solid was deposited, which was filtered off and dried *in vacuo*. Yield: 0.13 g, 71 %. Required for $C_{72}H_{60}I_2O_4P_4Sm$ (1516.5): C, 56.97; H, 3.99 %. Found: C, 56.59; H, 4.24%.. $^{31}P\{^1H\}$ NMR (d8-THF): $\delta = +18.5$. Treatment of the d_8-THF solution with I_2 produced a red brown solution with new resonances at $\delta = +35.6$, +25.7 (Ph_3PO), together with a red-brown precipitate. IR spectrum (Nujol mull)/cm^{-1}: 1167 br s, 1071 s (P=O). UV–Vis (diffuse reflectance/cm^{-1}): 26 730, 17 300.

[$SmI_2(OPMe_3)_4$] - Was made similarly from SmI_2 (0.05 g, 0.12 mmol) and $OPMe_3$ (0.046 g, 0.49 mmol) in THF. The product was a pale blue powder. Yield 0.08 g, 84 %. Required for $C_{12}H_{36}I_2O_4P_4Sm$ (772.3): C, 18.64; H, 4.70. Found: C, 18.53; H, 4.70 %. $^{31}P\{^1H\}$ NMR: insoluble in d_8-THF and CD_2Cl_2, decomposed by CD_3CN. IR spectrum (Nujol mull)/cm^{-1}: 1103 br s, (P=O).

3.4.3 Preparation of divalent lanthanide macrocyclic complexes

[YbI_2([18]aneO_4S_2)][35] **–** Prepared as reported in the literature. YbI_2 (0.05 g, 0.117 mmol) was dissolved in in dry acetonitrile (10 mL) to give a yellow solution. A solution of [18]aneO_4S_2 (0.035 g, 0.117 mmol) in dry acetonitrile (10 mL) was added dropwise. The solution was stirred for 30 minutes and then the solution concentrated to 3 mL. The solution was filtered and the pale yellow powdered precipitate was washed with n-hexane (5 mL). Yield: 0.044 g, 52 %. ^1H NMR (CD_3CN): δ = 3.63 (br s, [8H], OCH_2), 3.35 (br s, [8H], SCH_2CH_2O), 2.80 (br s, [8H], SCH_2CH_2O).

[EuI_2([18]aneO_4S_2)] - EuI_2 (0.05 g, 0.123 mmol) was dissolved in in dry acetonitrile (10 mL) to give an orange solution. A solution of [18]aneO_4S_2 (0.037 g, 0.123 mmol) in dry acetonitrile (10 mL) was added dropwise. The solution was stirred for 30 minutes and then the solution concentrated to ca. 3 mL. The solution was filtered and the dark yellow powdered precipitate was washed with n-hexane (5 mL). Yield 0.035 g, 40 %. Required for $C_{12}H_{24}EuI_2O_4S_2$ (702.02): C, 20.52; H, 3.45. Found C, 20.65; H, 3.39 %. IR spectrum (Nujol mull)/cm^{-1}: 1104, 1070, 1037, 1010 . It also shows an absence of both water and acetonitrile. UV–Vis (diffuse reflectance/cm^{-1}): 28200, 18000.

[EuI_2([18]aneSe_2O_4)] - To an orange solution of EuI_2 (0.05 g, 0.123 mmol) in dry acetonitrile (10 mL) was added one mole equivalent of macrocycle [18]aneO_4Se_2 (0.048 g, 0.123 mmol) in dry acetonitrile (10 mL) dropwise. The solution was stirred for 15 minutes and then the solution concentrated to ca. 3 mL. The solution was filtered and the dark yellow powdered precipitate was washed with n-hexane (5 mL). Yield 0.026 g, 26 %. Required for $C_{12}H_{24}EuI_2O_4Se_2$ (795.99): C, 18.11; H, 3.04. Found C, 18.01; H, 3.13 %. IR spectrum (Nujol mull)/cm^{-1}: 1100, 1072, 1017. It also shows an absence of both water and acetonitrile.

[EuI_2([18]aneN_2O_4)] - To an orange solution of EuI_2 (0.05 g, 0.123 mmol) in dry acetonitrile (10 mL) was added one mole equivalent of macrocycle [18]aneN_2O_4 (0.032 g, 0.123 mmol) in dry acetonitrile (10 mL) dropwise. The solution was stirred for 15 minutes and then the solution concentrated to ca. 3 mL. The solution was filtered and the light orange powdered precipitate was washed with n-hexane (5 mL). Yield: 0.038 g, 46 %. Required for $C_{12}H_{26}EuI_2N_2O_4$ (668.09): C, 21.57; H, 3.93 %; N, 4.19. Found C, 21.45; H, 4.11; N, 4.12 %. IR spectrum (Nujol mull)/cm^{-1}: 3171 m, 1087 s, br. It also shows an absence of both water and acetonitrile.

[EuI_2(18-crown-6)] - To an orange solution of EuI_2 (0.05 g, 0.123 mmol) in dry acetonitrile (10 mL) was added one mole equivalent of macrocycle 18-crown-6 (0.033 g, 0.123 mmol) in dry acetonitrile (10 mL) dropwise. The solution was stirred for 15 minutes and then the solution concentrated to ca. 3 mL. The solution was filtered and the beige powdered precipitate was washed with n-hexane (5 mL). Yield 0.038 g, 46 %. Required for $C_{12}H_{24}EuI_2O_6$ (670.06): C, 21.51; H, 3.61 %. Found C, 21.61; H, 3.53%. IR spectrum (Nujol mull)/cm^{-1}: 1104, 1070, 1037, 1010. It also shows an absence of both water and acetonitrile.

[EuI_2(Me_6[18]aneN_6)] – To an orange solution of EuI_2 (0.05 g, 0.123 mmol) in dry acetonitrile (10 mL) was added one mole equivalent of macrocycle Me_6[18]aneN_6 (mass, moles) in dry acetonitrile (10 mL) dropwise. The solution was stirred for 15 minutes and then the solution concentrated to ca. 3 mL. The solution was filtered and the dark yellow powdered precipitate was washed with n-hexane (5 mL). Orange crystals of [Eu(Me_6[18]aneN_6)($MeCONH_2$)]I_2·3MeCN were grown from storing the filtrate in the freezer. Yield 0.036 g, 39 %. Required for $C_{18}H_{42}EuI_2N_6$ (748.12): C, 28.87; H, 5.66; N, 11.23 %. Found: C, 29.04; H, 5.76; N, 11.35 %. IR spectrum (Nujol mull)/cm^{-1}: 1102 m, 1055 w, 1018 w.

[SmI_2([18]aneO_4S_2)] - To a solution of SmI_2 (0.05 g, 0.124 mmol) in dry THF (10 mL) was added one equivalent of [18]aneO_4S_2 (0.037, 0.124 mmol) in dry THF (10 mL), dropwise, resulting in a dark blue solution. The solution was stirred for 15 minutes during which the solution turned blue-green. The solvent removed *in vacuo*. The resulting dark green powder was washed with n-hexane (5 mL). Yield 0.071 g, 81 %. Required for $C_{12}H_{24}I_2S_2SmO_4$ (700.41): C, 20.58; H, 3.45 %. Found C, 20.71; H, 3.50 %. IR spectrum (Nujol mull)/cm^{-1}: 1087, 1047, 1019. It also shows an absence of water. UV–Vis (diffuse reflectance/cm^{-1}): 27100, 18500.

[SmI_2([18]aneSe_2O_4)] - To a solution of SmI_2 (0.05 g, 0.124 mmol) in dry THF (10 mL) was added one equivalent of [18]aneO_4Se_2 (0.048 g, 0.124 mmol) in dry THF (10 mL), dropwise, resulting in a dark blue solution. The solution was stirred for 10 minutes and then the solvent removed *in vacuo*. The resulting solid dark blue solid was washed with n-hexane (5 mL). Yield 0.072 g, 73 %. Required for $C_{12}H_{24}I_2Se_2SmO_4$ (794.39): C, 18.14; H, 3.04 %. Found C, 18.01; H, 2.97%. IR spectrum (Nujol mull)/cm^{-1}: 1108, 1039. It also shows an absence of water.

[SmI_2([18]aneN_2O_4)] - To a solution of SmI_2 (0.05 g, 0.124 mmol) in dry acetonitrile (10 mL) was added one equivalent of [18]aneN_2O_4 (0.032 g, 0.124 mmol) in dry acetonitrile (10 mL), dropwise, resulting in a dark green solution. The solution was stirred for 10 minutes and then the solvent removed *in vacuo*. The resulting dark green solid was washed with n-hexane (5 mL). Yield 0.050 g, 61 %. Required for $C_{12}H_{26}I_2N_2O_4Sm$ (666.49): C, 21.63; H, 3.93; N, 4.20 %. Found C, 21.75; H, 4.04; N, 4.25%. IR spectrum (Nujol mull)/cm^{-1}: 3173 m, 1093 s. It also shows an absence of water. UV–Vis (diffuse reflectance/cm^{-1}): 26700, 17600.

[SmI_2(18-crown-6)] - To a solution of SmI_2 (0.05 g, 0.124 mmol) in dry THF (10 mL) was added one equivalent of 18-crown-6 (0.033 g, 0.124 mmol) in dry THF (10 mL), dropwise, resulting in a dark blue solution. The solution was stirred for 15 minutes whereby a dark blue precipitate formed. This was filtered and the resulting dark blue solid was washed with n-hexane (5 mL). Yield 0.065 g, 79 %. Required for $C_{12}H_{24}I_2O_6Sm$ (668.46): C, 21.56; H, 3.62 %. Found C, 21.68; H, 3.72%. IR spectrum (Nujol mull)/cm^{-1}: 1086 br, 1025 w. It also shows an absence of water.

Table 3.4. Crystallographic data[a]

Compound	**$[EuBr_2(OPPh_3)_4]$**	**$[EuI_2(OPPh_3)_4]\cdot MeCN$**	**$[EuI_2(OPPh_3)_4][I_3]$**
Formula	$C_{72}H_{60}Br_2EuO_4P_4$	$C_{74}H_{63}EuI_2NO_4P_4$	$C_{150}H_{129}Eu_2I_{10}N_3O_8P_8$
M	1424.86	1559.89	3922.23
Crystal system	triclinic	monoclinic	triclinic
Space group (no.)	P-1 (2)	Pn (7)	P-1 (2)
a (Å)	12.5310(5)	13.6401(4)	13.6846(3)
b (Å)	12.9745(6)	17.5450(4	20.1433(4)
c (Å)	21.3736(10)	14.0307(4)	28.4990(4)
α (°)	78.464(4)	90	91.6050(10)
β (°)	88.971(4)	95.185(3)	91.58(2)
γ (°)	66.695(4)	90	109.605(2)
U (Å^3)	3119.8(3)	3344.03(16)	7391.9(3)
Z	2	2	2
μ(Mo Kα) (mm^{-1})	2.438	2.006	3.071
F(0 0 0)	1434	1550	3780
Total number reflections	38412	63559	94005
R_{int}	0.060	0.125	0.040
Unique reflections	12249	13995	28933
No. of parameters, restraints	748, 0	776, 710	1609, 0
R_1, $wR_2[I > 2\sigma(I)]$[b]	0.067, 0.174	0.045, 0.100	0.050, 0.112
R_1, wR_2 (all data)	0.084, 0.183	0.053, 0.103	0.063, 0.116

Table 3.4 Continued

Compound	**[Eu(Me$_6$[18]aneN$_6$)(MeCONH$_2$)] 3I·3MeCN**
Formula	$C_{28}H_{65}EuI_2N_{11}O$
M	977.67
Crystal system	monoclinic
Space group (no.)	C2/m (12)
a (Å)	16.3121(4)
b (Å)	13.7147(3)
c (Å)	18.0647(4)
α (°)	90
β (°)	94.842(2)
γ (°)	90
U (Å^3)	4026.93(16)
Z	4
μ(Mo Kα) (mm^{-1})	3.126
F(0 0 0)	1948.0
Total number reflections	11003
R_{int}	0.022
Unique reflections	5227
No. of parameters, restraints	231, 0
R_1, $wR_2[I > 2\sigma(I)]$[b]	0.036, 0.093
R_1, wR_2 (all data)	0.046, 0.097

[a] Common data: $T = 293$ K; wavelength (Mo Kα) = 0.71073 Å; θ(max) = 27.5°.
[b] $R_1 = \Sigma||Fo| - |Fc||/\Sigma|Fo|$; $wR_2 = [\Sigma w(Fo^2 - Fc^2)^2/\Sigma wFo^4]^{1/2}$.

3.5 References

1 A. W. G. Platt, *Coord. Chem. Rev.*, 2017, **340**, 62–78.

2 M. B. Hursthouse, W. Levason, R. Ratnani, G. Reid, H. Stainer and M. Webster, *Polyhedron*, 2005, **24**, 121–128.

3 S. J. Coles, S. J. Fieldhouse, W. T. Klooster and A. W. G. Platt, *Polyhedron*, 2019, **161**, 346–351.

4 W. Levason, E. H. Newman and M. Webster, *Polyhedron*, 2000, **19**, 2697–2705.

5 A. Bowden, A. M. J. Lees and A. W. G. Platt, *Polyhedron*, 2015, **91**, 110–119.

6 R. P. Feazell, J. B. Gary, J. A. Kautz and K. K. Klausmeyer, *Acta Crystallogr. Sect. E*, 2004, **E60**, m532–m534.

7 L. Troxler, A. Dedieu, F. Hutschka and G. Wipff, *J. Mol. Struct.*, 1998, **431**, 151 – 163.

8 M. J. Glazier, W. Levason, M. L. Matthews, P. L. Thornton and M. Webster, *Inorg. Chim. Acta*, 2004, **357**, 1083–1091.

9 D. R. Cousins and F. A. Hart, *J. inorg. nucl. Chem*, 1967, **29**, 1745–1757.

10 A. G. M. Massabni, M. L. R. Gibran and O. A. Serra, *Inorg. Nucl. Chem. Lett.*, 1978, **14**, 419–427.

11 M. Ul-Haque, C. N. Caughlan, F. A. Hart and R. Vannice, *Inorg. Chem.*, 1971, **10**, 115–122.

12 A. Bowden, P. N. Horton and A. W. G. Platt, *Inorg. Chem.*, 2011, **50**, 2553–2561.

13 A. Bowden, S. J. Coles, M. B. Pitak and A. W. G. Platt, *Inorg. Chem.*, 2012, **51**, 4379–4389.

14 A. Bowden, S. J. Coles, M. B. Pitak and A. W. G. Platt, *Polyhedron*, 2014, **68**, 258–264.

15 M. Bosson, W. Levason, T. Patel, M. C. Popham and M. Webster, *Polyhedron*, 2001, **20**, 2055–2062.

16 L. Deakin, W. Levason, M. C. Popham, G. Reid and M. Webster, *J. Chem. Soc., Dalton Trans.*, 2000, **1**, 2439–2447.

17 A. Bowden, K. Singh and A. W. G. Platt, *Polyhedron*, 2012, **42**, 30–35.

18 F. L. Alencar, L. B. Zinner, K. Zinner and J. E. X. Matos, *J. Coord. Chem.*, 1999, **46**, 471–478.

19 J. Fawcett, A. W. G. Platt and D. R. Russell, *Polyhedron*, 2002, **21**, 287–293.

20 J.-C. Berthet, M. Nierlich and M. Ephritikhine, *Polyhedron*, 2003, **22**, 3475–3482.

21 R. Wang, H.-G. Wang, H.-K. Wang, M.-J. Zhang, X.-Y. Jing and J.-T. Wang, *Inorg. Chim. Acta*, 1989, **163**, 19–23.

22 N. J. Hill, L.-S. Leung, W. Levason and M. Webster, *Inorg. Chim. Acta*, 2003, **343**, 169–174.

23 A. Bowden, A. W. G. Platt, K. Singh and R. Townsend, *Inorg. Chim. Acta*, 2010, **363**, 243–249.

24 J. C. Berthet, M. Nierlich and M. Ephritikhine, *Polyhedron*, 2003, **22**, 3475–3482.

25 A. M. J. Lees and A. W. G. Platt, *Polyhedron*, 2014, **67**, 368–372.

26 S. A. Cotton, *Lanthanide and Actinide Chemistry*, John Wiley, Chichester, 2006.

27 S. A. Cotton, in *Comprehensive Coordination Chemistry II - 3.2.2 Yttrium and the Lanthanides*, eds. J. A. McCleverty and T. J. Meyer, Elsevier Pergamon, Oxford, 2004, pp. 108–171.

28 M. J. Hesford, W. Levason, M. L. Matthews and G. Reid, *Dalton Trans.*, 2003, **14**, 2852–2858.

29 W. Levason and G. Reid, in *Comprehensive Coordination Chemistry II - 1.18 Macrocyclic Thio-Seleno-, and Telluroether Ligands*, eds. J. McCleverty and T. Meyer, Elsevier Pergamon, Oxford, 2003, pp. 399–410.

30 M. J. D. Champion, W. Levason, D. Pugh and G. Reid, *Dalton Trans.*, 2015, **44**, 18748–18759.

31 P. Farina, T. Latter, W. Levason and G. Reid, *Dalton Trans.*, 2013, **42**, 4714–24.

32 W. Levason and G. Reid, *J. Chem. Res.*, 2002, **2**, 467–472.

33 P. Farina, W. Levason and G. Reid, *Dalton Trans.*, 2013, **42**, 89–99.

34 M. J. D. Champion, P. Farina, W. Levason and G. Reid, *Dalton Trans.*, 2013, **42**, 13179–13189.

35 P. N. Bartlett, M. J. D. Champion, M. E. Light, W. Levason, G. Reid and P. W. Richardson, *Dalton Trans.*, 2015, **44**, 2953–2955.

36 W. Levason, D. Pugh, J. M. Purkis and G. Reid, *Dalton Trans.*, 2016, **45**, 7900–7911.

37 H. M. Nicholas and D. P. Mills, in *Encyclopedia of Inorganic and Bioinorganic Chemistry*, American Cancer Society, 2017, pp. 1–10.

38 F. Nief, *Dalton Trans.*, 2010, **39**, 6589 – 6598.

39 M. R. Macdonald, E. Bates, J. W. Ziller, F. Furche and W. J. Evans, *J. Am. Chem. Soc.*, 2013, **135**, 9857 – 9868.

40 M. A. Angadol, D. H. Woen, C. J. Windorff, J. W. Ziller and W. J. Evans, *Organometallics*, 2019, **38**, 1151 – 1158.

41 M. R. Macdonald, E. Bates, M. E. Fieser, J. W. Ziller, F. Furche and W. J. Evans, *J. Am. Chem. Soc.*, 2012, **134**, 8420 – 8423.

42 M. R. Macdonald, J. W. Ziller and W. J. Evans, *J. Am. Chem. Soc.*, 2011, **133**, 15914–15917.

43 W. J. Evans, 2000, **207**, 263–283.

44 M. N. Bochkarev, *Coord. Chem. Rev.*, 2004, **248**, 835–851.

45 W. J. Evans, I. Bloom, W. E. Hunter and J. L. Atwood, *J. Am. Chem. Soc.*, 1981, **103**, 6507–6508.

46 W. J. Evans, A. Hughes and T. P. Hanusa, *Organometallics*, 1986, **5**, 1285 – 1291.

47 W. J. Evans, T. A. Ulibarri and J. W. Ziller, *J. Am. Chem. Soc.*, 1988, **110**, 6877–6879.

48 W. J. Evans, J. W. Grate and L. A. Hughes, *J. Am. Chem. Soc.*, 1985, **107**, 3728–3730.

49 W. J. Evans, C. A. Seibel and J. W. Ziller, *Inorg. Chem.*, 1998, **37**, 770 – 776.

50 W. J. Evans, J. W. Grate, I. Bloom, W. E. Hunter and J. L. Atwood, *J. Am. Chem. Soc.*, 1985, **107**, 405–409.

51 M. N. Bochkarev, I. L. Fedushkin, A. A. Fagin, T. V Petrovskaya, J. W. Ziller, R. N. R. Broomhall-Dillard and W. J. Evans, *Angew. Chemie Int. Ed.*, 1997, **36**, 133–135.

52 W. J. Evans, N. T. Allen and J. W. Ziller, *Angew. Chemie Int. Ed.*, 2002, **41**, 359–361.

53 F. Nief and F. Mathey, *Synlett*, 1991, 745–746.

54 C. Eabom, P. B. Hitchcock, K. Izod and J. D. Smith, *J. Am. Chem. Soc.*, 1994, **116**, 12071–12072.

55 C. Eaborn, P. B. Hitchcock, K. Izod, Z. Lu and J. D. Smith, *Organometallics*, 1996, **15**, 4783–4790.

56 G. Qi, Y. Nitto, A. Saiki, T. Tomohiro, Y. Nakayama and H. Yasuda, *Tetrahedron*, 2003, **59**, 10409–10418.

57 G. B. Deacon, W. D. Raverty and D. G. Vince, *J. Organomet. Chem.*, 1977, **135**, 103 – 114.

58 G. B. Deacon and V. D. G., *J. Organomet. Chem.*, 1976, **112**, C1 – C2.

59 D. Turcitu and L. Ricard, *Chem. Commun.*, 2002, 1646–1647.

60 D. Turcitu, F. Nief and L. Ricard, *Chem. Eur. J.*, 2003, **9**, 4916–4923.

61 C. J. Weiss and T. J. Marks, *Dalton Trans.*, 2010, **39**, 6576–6588.

62 T. Maisano, K. E. Tempest, D. V. Sadasivam and R. A. Flowers, *Org. Biomol. Chem.*, 2011, **9**, 1714–1716.

63 R. D. Bannister, W. Levason, M. E. Light and G. Reid, *Polyhedron*, 2018, **154**, 259–262.

64 N. J. Hill, W. Levason, M. C. Popham, G. Reid and M. Webster, *Polyhedron*, 2002, **21**, 445–455.

65 N. B. Mikheev, S. A. Kulyukhin, A. N. Kamenskaya, I. A. Rumer and N. A. Konovalova, *Radiochemistry*, 2004, **46**, 521–535.

66 E. Rogers, P. Dorenbos, J. T. M. De Haas and E. Van Der Kolk, *J. Phys. Condens. Matter*, 2012, **24**, 275502 (5pp).

67 O. Yoshihiro and I. Toshiyuki, *Inorg. Chim. Acta*, 1988, **144**, 143–146.

68 H. Schindlbauer, *Monatshefte für Chemie*, 1963, **94**, 99–105.

69 E. V. Savinkina, D. V. Golubev and M. S. Grigoriev, *J. Coord. Chem.*, 2011, **64**, 3758–3766.

70 D. V. Golubev, D. V. Al'bov, V. V. Kravchenko, L. Y. Alikberova and N. S. Rukk, *Koord. Khim. (Russ.) (Coord. Chem.)*, 2010, **36**, 831.

71 M. P. Suh, K. Y. Oh, J. W. Lee and Y. Y. Bae, *J. Am. Chem. Soc.*, 1996, **118**, 777–783.

Chapter 4 Complexes of $TaOCl_3$ and $TaSCl_3$ with Neutral N- and O- Donor Ligands

4.1 Introduction

Owing to the similarity of niobium and tantalum chemistry, comparisons between analogous complexes are often discussed in the literature. Unlike their niobium analogues, reported complexes of $TaOCl_3$ and $TaSCl_3$ are scarce due to the inherent instability of the $TaOCl_3$ or $TaSCl_3$ fragment. The work in this Chapter details the synthesis and characterisation of a series of novel tantalum oxide trichloride compounds with hard phosphine oxide and diimine ligands, of the general form $[TaOCl_3(L\text{-}L)]$, and their tantalum sulfide trichloride analogues, $[TaSCl_3(L\text{-}L)]$.

4.1.1 Niobium(V) and Tantalum(V) Coordination Chemistry

Many standard texts and reviews discuss niobium(V) and tantalum(V) coordination chemistry together due to their similar chemistry, see Chapter 1. Although they can be easily compared, such as in the case for niobium and tantalum pentahalides, in the case of $TaOCl_3$ and $NbOCl_3$, the chemistry of $TaOCl_3$ is much less well developed. However, owing to the lack of research on $TaOCl_3$ reported in the literature, we must instead look to the coordination chemistry of other Ta(V) species, such as the pentahalides, and similar niobium compounds for comparison, and then compare the compounds described within this chapter with their niobium oxychloride analogues.

Niobium and tantalum pentahalides, MX_5, are known for all halides, with bromide, chloride and iodide forming the dimeric M_2X_{10} shown in Scheme 4.1, and fluoride forming a tetramer.[1,2] Typically, these dimeric structures are broken up by the introduction of an oxygen-, nitrogen- or sulfur-containing compound, such as a ligand or a reagent such as $O(SiMe_3)_2$, leading to mononuclear species. However, this also means they are readily hydrolysed in the presence of even trace amounts of water. They are rarely soluble in non-coordinating solvents and reactions using these solvents can require heating, for example in dichloromethane or long reaction times. The chemistry of niobium and tantalum pentahalides with a range of O-donor ligands has been studied at length by Marchetti *et. al.* There are extensive reports focussing on both the coordination chemistry and exploring the bond activation of O-donor ligands. The work in this chapter, however, will focus primarily on developing a wider coordination chemistry of these systems, with occasional acknowledgement of bond activation or catalytic properties.

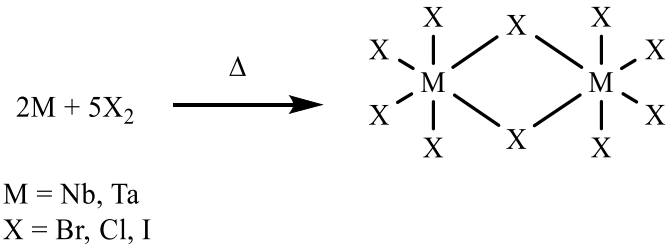

Scheme 4.1. The reaction of elemental niobium and tantalum with the respective halogen while heating leads to the formation of the dinuclear M_2X_{10} species. Similar reactions with fluorine produces M_4X_{20}.[1,2]

4.1.2 Synthesis of MX_5L

Reactions of oxygen-donor ligands with niobium and tantalum pentahalides can be separated into three main categories, the formation of mononuclear MX_5L, the formation of ionic species and bond activation catalysis. The synthesis of MX_5L *via* the addition of a neutral ligand, such as an alcohol, ester, thioether, phosphine oxide, *etc*., to $[MX_5]_n$ in a 1:1 M:L ratio (2:1 for bidentate ligands), breaking up the dimer/tetramer and resulting in a six coordinate octahedral species, is well documented.[3–8] Until 2007, fully characterised species were very limited and even to-date there are very few examples in the literature of crystal structures of the form $[MF_5L]$, with many of the fluorides instead forming ionic species, such as $[MX_6]^-L^+$, $[MX_4L_4]^+[MX_6]^-$ or $[MX_4(L\text{-}L)_2]^+[MX_6]^-$ Section 4.1.3.[9–13] As shown in Scheme 4.2, these six-coordinate species are known for both niobium and tantalum with fluoride, chloride and bromide co-ligands. Bidentate ligands often form ligand-bridged structures between two tantalum metal centres. The ligand systems vary quite drastically and include thioethers and selenoethers, nitriles, and ethers to name a few.[9,14–16]

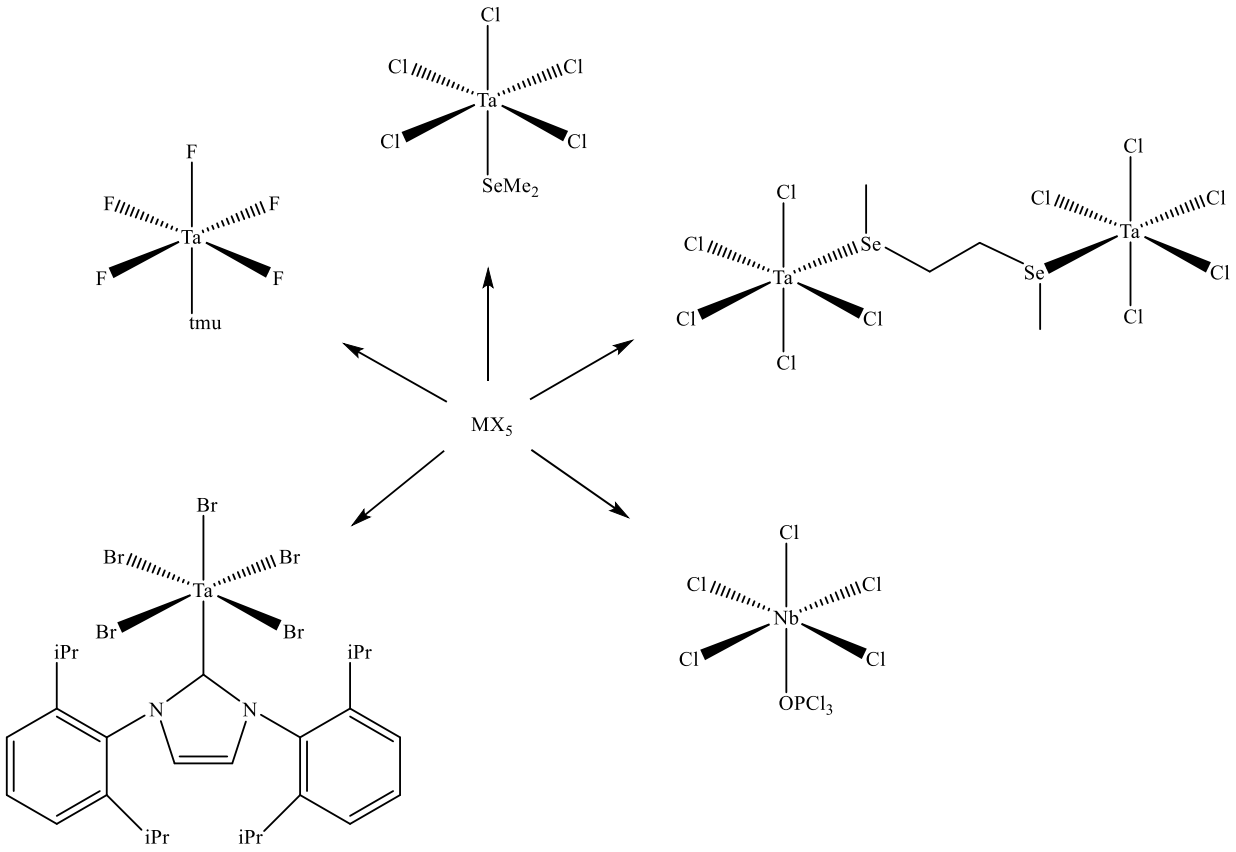

Scheme 4.2. Some examples of [MX_5L] from the literature.[9,17–20] *All except [TaF_5(tmu)], (tmu = N,N,N',N'-tetramethylurea), have been structurally characterised by single crystal X-ray diffraction and [$Cl_5Ta(\mu_2$-$MeSeCH_2CH_2SeMe)TaCl_5$] provides an example of a bidentate ligand coordinating two Ta metal centres.*

Kinetic studies by Merbach et. al. demonstrated that ligand exchange on these metal complexes from MX_5L to MX_5L*, (L/L* = Me_2O, Me_2S, Me_2Se, Me_2Te) can occur *via* an associative or dissociative mechanism.[21] First order dissociative mechanisms are reported for ethers and second order associative mechanisms for the chalcogenoethers. Although less common, there is precedent for associative ligand substitution on an octahedral d-block metal. With Nb(V) and Ta(V) being d^0 ions, there is an empty t_{2g} orbital, which allows for the formation of a seventh bond.[21] In all of the chemistry described within this chapter, factors such as the metal centre, the halide, the steric bulk of the ligand, the solvent system and the stoichiometry of the reaction are significant in directing the products formed and their stabilities. Interestingly, it was noted that the stability of [$MX_5(ER_2)$] (X = Cl, Br; E = O, S, Se, Te) increases as the halide gets lighter, but also as the chalcogen gets heavier. At the time it was suggested that this was evidence for an apparent soft character of the Nb(V) and Ta(V) metal centres according to HSAB theory. [1,21–25] However, soft donor – hard acceptor complexes are now well established and it is important to take into account a

number of factors in these systems when analysing stability.[26–28] These systems are especially sensitive to the solvent system, halide, steric requirements of the ligand, amongst a number of other factors.

4.1.3 Formation of ionic species $[MX_4L_n][MX_6]$ and $[MX_4(L\text{-}L)_n][MX_6]$

Niobium and tantalum pentahalides, when reacted with monodentate ligands, also have a tendency to produce complexes of the form $[MX_6][MX_4L_n]$ such as $[TaBr_6][TaBr_4(PH_2cy)_4]$[29] and $[MCl_6][MCl_4(IMes)_2]$ (M = Nb, Ta; IMes = 1,3-bis(2,4,6-trimethylphenyl)-imidazol-2-ylidene)[30]. When reacted with bidentate ligands they often produce complexes of the form $[MX_6][MX_4(L\text{-}L)_n]$ (M = Nb, Ta; X = F, Cl, Br) such as $[TaF_6][TaF_4(dithiahexane)_2]$[9], $[MBr_6][MBr_4\{(2,6\text{-}C_6H_3{}^iPr_2)NCHCHN(2,6\text{-}C_6H_3{}^iPr_2)\}]$ (M = Ta, Nb)[31], and $[NbCl_6][NbCl_4(Me_2S_2)_2]$[32]. Formation of these salts over the neutral monomers described above is determined by the ligand system, reaction conditions, stoichiometry and halide amongst other factors. For example, $[TaCl_6][TaCl_4(IMes)_2]$ is produced from the addition of a solution $TaCl_5$ in toluene to a solution of IMes in toluene at -60 ˚C in a 1:1 ratio, the solution is then warmed to -5 ˚C. However the analogous reaction of $TaCl_5$ with IPr (1,3-bis(2,6-diisopropylphenyl)imidazol-2-ylidene), forms the mononuclear $[TaCl_5(IPr)]$.[30] Similarly in the reaction of TaX_5 with N,N,N',N'-tetramethylurea, (tmu). The reaction of one equivalent of TaX_5 (X = F, Cl) with one equivalent of tmu in an acetonitrile/benzene solution or a dichloromethane solution leads to a mononuclear $[TaX_5(tmu)]$ (X = F, Cl).[18,20] However the reaction of one equivalent of $TaBr_5$ with one equivalent of tmu in dichloromethane leads to $[TaBr_4(tmu_2)][TaBr_6]$, Scheme 4.3.[20]

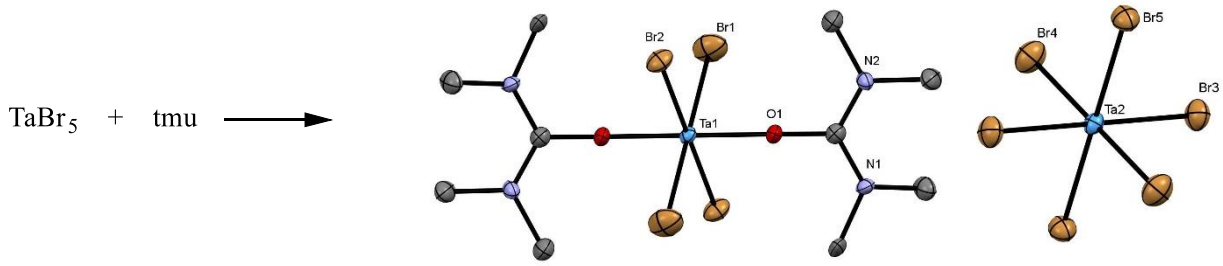

Scheme 4.3. The reaction of one equivalent of $TaBr_5$ with one equivalent of N,N,N',N'-trimethylurea in dichloromethane to produce the ionic species $[TaBr_4(tmu)_2][TaBr_6]$.[20]

This illustrates how specific reaction conditions can lead to two distinct products and the need for careful control of all factors when attempting to synthesise specific tantalum complexes of this type. Another example demonstrating the influence of stoichiometric

control, is the reaction of TaF_5 and Me_2S in dichloromethane. The 1:1 reaction of Me_2S with TaF_5 leads to the formation of $[TaF_5(Me_2S)]$. However, the addition of more than three equivalents gives $[TaF_4(Me_2S)_4][TaF_6]$. Interestingly, $^{19}F\{^1H\}$ NMR spectra of solutions of TaF_5 with large excesses of Et_2S at 185 K showed two species, $[TaF_6]^-$ and $[TaF_4(Et_2S)_4]^+$, however, at 220 K these merged into one peak and $[TaF_5(Et_2S)]$ was isolated from the solution.[9]

4.1.4 Niobium and tantalum oxychloride and tantalum thiochloride

Niobium(V) oxide trichloride forms readily by the hydrolysis of $NbCl_5$ when exposed to trace moisture. It can also be formed in a more controlled manner by heating niobium in a Cl_2/O_2 mixture, by heating $NbCl_5$ with non-metal oxides, and by Cl/O exchange of $NbCl_5$ with siloxanes, such as $O(SiMe_3)_2$.[33] Solid $NbOCl_3$ contains dimeric $[Cl_2Nb(O)(\mu\text{-}Cl)_2Nb(O)Cl_2]$ units linked into chains *via* unsymmetrical oxide bridges, giving six-coordinate niobium.[34] It vaporises upon heating to give $NbOCl_3$ monomers.[35] In contrast, the less stable $TaOCl_3$ is formed through the reaction of $TaCl_5$ with Cl_2O in CCl_4 or by pyrolysis of $[TaCl_5(Et_2O)]$.[33,36–38] $TaOCl_3$ is also a product of the hydrolysis of $TaCl_5$ in air, however, degradation of the sample continues until a highly insoluble Ta_2O_5 species is formed. Structural information in the literature is limited to an early powder X-ray pattern, which indicated that its structure was similar to that of $NbOCl_3$,[34,39]

Recent work within the Reid group described a series of niobium oxychloride complexes with a range of O- and N-donor ligands, including phosphine oxides ($aOPPh_3$, $OPMe_3$, $dppmO_2$, $dppeO_2$), diimines (2,2'-bipy, 1,10-phen) and others ($OAsPh_3$, tmeda, dmso).[40] Alongside these was a novel series of niobium(V) oxide trifluoride complexes. Most of these complexes form as neutral six-coordinate species, $[NbOX_3(L)_2]$ (L = monodentate ligands) and $[NbOX_3(L\text{-}L)]$ (L-L = bidentate ligands) for X = Cl or F. The chlorides were formed by the combination of $NbCl_5$ and $O(SiMe_3)_2$ in MeCN to give $[NbOCl_3(MeCN)_2]$, followed by the addition of the neutral ligand L or L-L.

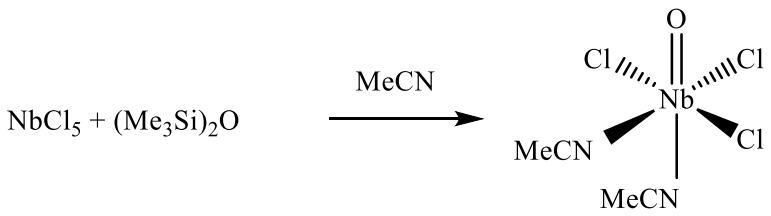

Scheme 4.4. The reaction of $NbCl_5$ with $O(SiMe_3)_2$ in acetonitrile to produce $[NbOCl_3(MeCN)_2]$.[40]

Interestingly, when the diimines (2,2'-bipy and 1,10-phen), are reacted with NbF_5 in 1:1 reactions in dichloromethane, they produce the $[NbF_4(diimine)_2][NbF_6]$ species with the cation forming an eight-coordinate distorted dodecahedron. Complexes featuring a $TaOCl_3$ unit in the older literature mostly result from the hydrolysis of $TaCl_5$ coordination complexes or by oxygen abstraction from ligands. Crystallographically authenticated examples are rare and in contrast to the Nb species described above, and crystal structures often show dinuclear complexes with oxide bridges. Examples of the dinuclear species include $[(MeO(CH_2)_2OMe)Cl_3Ta(\mu\text{-}O)TaCl_5]$,[1] $[LCl_4Ta(\mu\text{-}O)TaCl_4L]$ (L= trimethylphosphate),[20] $[Cl_5Ta(\mu\text{-}O)TaCl_3(^iPrS(CH_2)_2S^iPr)]$,[41] $[Cl_4Ta((\mu\text{-}O)(\mu\text{-}Me_2Se_2)TaCl_4]$,[41] the latter two are shown in Figure 4.1.

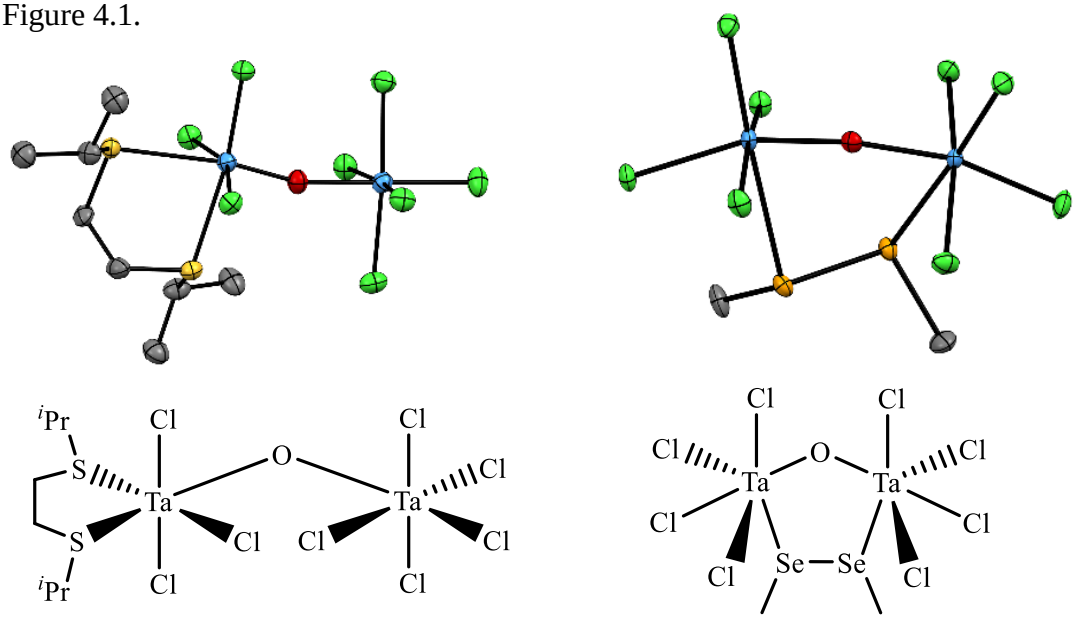

Figure 4.1. Showing two representative examples of Ta-O-Ta bridged species from the literature and their crystal structures.[41]

Unlike for the tantalum oxychloride complexes, where the only examples of structural data feature bridged Ta-O-Ta units, there is crystallographic evidence for a mononuclear tantalum thiochloride complexes, $[TaSCl_3(PhSCH_2CH_2SPh)]$.[42] Rice *et. al.* reported a series of $TaSCl_3$ and $TaSBr_3$ compounds of the form $[TaSX_3(L)_2]$ and $[TaSX_3(L\text{-}L)]$, (X = Cl, Br; L = Me_2S, tetrahydrothiophene, MeCN; L-L = 1,2-bis(phenylthio)ethane).[42] The sulfur-containing ligands are further discussed in Chapter 5. The protracted preparation of $[TaSCl_3(MeCN)]$, obtained as a yellow powder by precipitation from the reaction of $TaCl_5$ with Sb_2S_3 in a 3:1 molar ratio in MeCN at 70 °C after stirring for 17 days. The compound was analysed by infrared spectroscopy, ^1H NMR spectroscopy and elemental analysis, although no crystal structure was obtained for the species.

4.1.5 Aims

The aim of this chapter was to develop the first series of tantalum oxytrichloride and thiotrichloride coordination complexes of the form $[TaECl_3(L\text{-}L)]$ or $[TaECl_3(L)_2]$ (E = O or S) and to explore their properties. The ligands used include O-donor ligands ($dppmO_2$, $dppeO_2$, PPO_2 and $OPPh_3$) and the diimines, 1,10-phen and 2,2'-bipy. Comparisons are made between these species and their niobium analogues.

4.2 Results and Discussion

4.2.1 Complexes of $TaOCl_3$ and comparisons to analogous $NbOCl_3$ species

The complexes $[TaOCl_3(L\text{-}L)]$ (L-L = 2,2'-bipy, 1,10-phen, $dppmO_2$, $dppeO_2$, PPO_2 and $[TaOCl_3(OPPh_3)_2]$ were obtained as moisture sensitive white powders in moderate to good yields (40-70%). The direct reaction of $TaOCl_3$ with the neutral ligands is not a viable route to the desired coordination complexes, and in this work the reaction of $TaCl_5$ with $O(SiMe_3)_2$ and the appropriate ligand in MeCN or CH_2Cl_2 solution was used, Scheme 4.5.

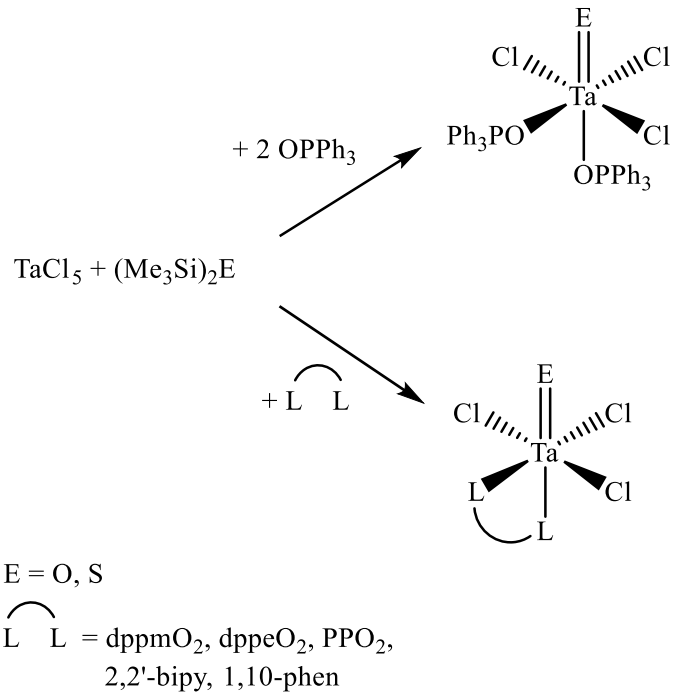

Scheme 4.5. A reaction scheme showing the synthesis of $[TaECl_3(L\text{-}L)]$ and $[TaECl_3(L)_2]$, (E = O, S; L-L = 1,10-phen, 2,2'-bipy, $dppmO_2$, $dppeO_2$, PPO_2; L = $OPPh_3$).[43]

Care over the (1:1) tantalum chloride to diimine molar ratio and the use of rigorously dried solvent is imperative for the successful formation of these compounds. The diimine complexes are readily hydrolysed in solution with formation of protonated diimine, which was commonly observed as a minor species during NMR analysis.

Colourless crystals of [$TaOCl_3$(1,10-phen)] were grown by slow evaporation of a CH_2Cl_2 solution of the complex in the dry box. The structure shows the 1,10-phen ligand *trans* to O/Cl in a six coordinate distorted octahedral geometry, Figure 4.2. In contrast to many other transition metal complexes containing oxide and chloride ligands, the structure is free of O/Cl disorder. The tantalum coordination sphere is distorted by the short chelate bite of the rigid 1,10-phenanthroline, and the axial Cl-Ta-Cl unit is bent away from the Ta=O group (Cl3–Ta1–Cl1 = 161.7°). The d(Ta1-Cl2) = 2.3449(4) is shorter than the d(Ta1-Cl1) = 2.3729(4) owing to the effect of the ligand *trans* Cl. The d(Ta=O) is 1.7268(13) Å which is within the expected range for this type of bond. As indicated in Section 4.1.4, although a range of complexes of $TaOCl_3$ has been reported, this [$TaOCl_3$(1,10-phen)] structure is the first crystallographically authenticated example of a mononuclear complex of this type.

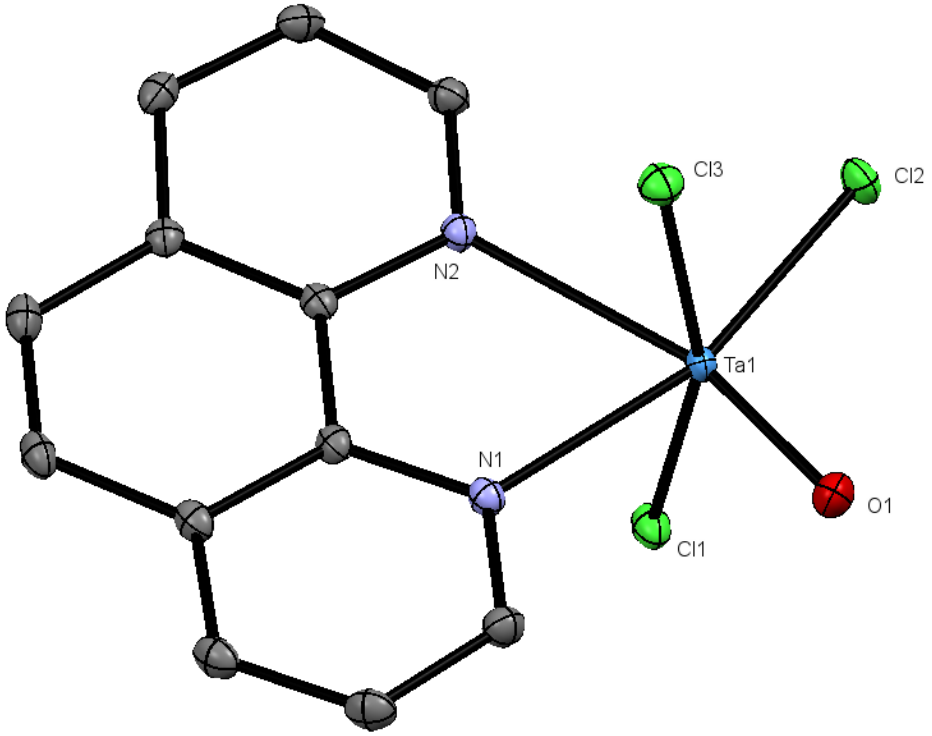

Figure 4.2. The structure of [$TaOCl_3$(1,10-phen)] showing the atom numbering scheme. Ellipsoids drawn at the 50% probability level and H atoms are omitted for clarity. Selected bond lengths (Å) and angles (°): Ta1—Cl2 = 2.3449(4), Ta1—Cl1 = 2.3729(4), Ta1—Cl3 = 2.3807(4), Ta1—O1 = 1.7268(13), Ta1—N2 = 2.3849(14), Ta1—N1 = 2.2374(15), Cl2—Ta1— Cl1 = 92.315(15), Cl2—Ta1—Cl3 = 94.463(15), Cl2—Ta1—N2 = 91.15(4), Cl1—Ta1—N2 = 82.35(4), Cl3—Ta1—N2 = 80.51(4), O1—Ta1—Cl2 = 106.40(4), O1—Ta1—Cl1 = 97.14(5), O1—Ta1— Cl3 = 97.24(5), O1—Ta1—N1 = 91.60(6), N1—Ta1—Cl1 = 83.32(4), N1—Ta1—Cl3 = 84.98(4), N1—Ta1—N2 = 70.88(5).

Infrared spectroscopy of the bulk complex shows a single stretching vibration at 941 cm^{-1}, indicative of a terminal Ta=O bond, and two *v*(Ta-Cl) bands at 322 and 350 cm^{-1}. The ^{1}H NMR spectrum obtained for [$TaOCl_3$(1,10-phen)] is shown in Figure 4.3. The spectrum is consistent with the 1,10-phen ligand occupying the coordination sites trans to O and Cl, hence doubling the number of resonances relative for the ligand itself, due to the inequivalence of the N environments in the coordinated form. As expected, the ^{1}H resonances are also significantly shifted to high frequency upon coordination. Both the ^{1}H NMR data and the infrared data are in good agreement with the analogous [$NbOCl_3$(1,10-phen)],[44] suggesting the ligand is *trans* O/Cl, and in the same geometry exhibiting a terminal Nb=O stretching vibration at 944 cm^{-1}.

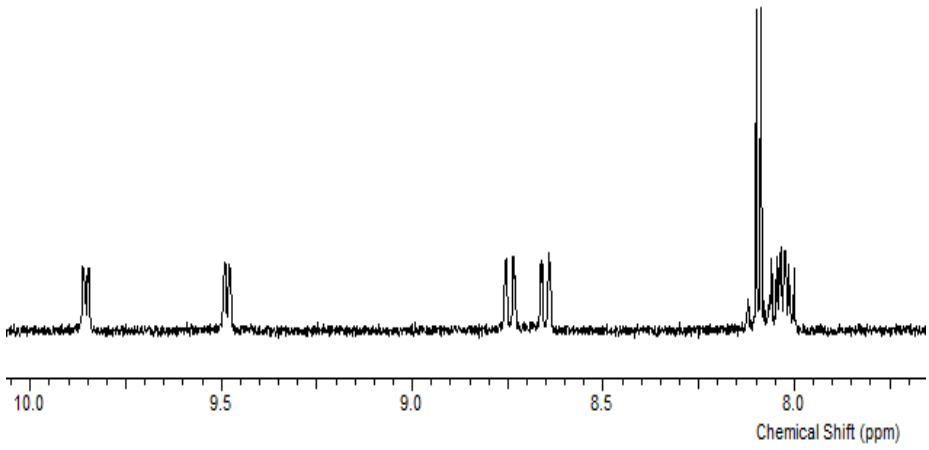

Figure 4.3. The ^{1}H NMR spectrum of [$TaOCl_3$(1,10-phen)] in CD_2Cl_2, showing the distinct proton environments of the 1,10-phen resulting from the reduction in symmetry caused by the different trans ligands (O and Cl).

The formation of [$TaOCl_3$(2,2'-bipy)], by a similar method, was confirmed by elemental analysis and the complex exhibits a similar terminal Ta=O band in the IR spectrum at 938 cm^{-1}. The ^{1}H NMR spectrum is in close agreement with the analogous [$NbOCl_3$(2,2'-bipy)], and consistent with the structure of [$TaOCl_3$(1,10-phen)]. Although the ^{1}H NMR spectrum also shows evidence of some protonated 2,2'-bipy, this is almost certainly a result of trace hydrolysis in the NMR solvent, since the solid state data (elemental analysis and IR spectroscopy) are fully consistent with [$TaOCl_3$(2,2'-bipy)].

Four phosphine oxide complexes were obtained as white moisture sensitive powders, [$TaOCl_3(OPPh_3)_2$], [$TaOCl_3(dppmO_2)$], [$TaOCl_3(dppeO_2)$] and [$TaOCl_3(PPO_2)$]. The compounds were made using the same 'one pot' method, via the addition of $(Me_3Si)_2O$ to a suspension of one equivalent of $TaCl_5$ in dry CH_2Cl_2, followed by the addition of one

equivalent of bidentate phosphine oxide or two equivalents of $OPPh_3$. The compounds were analysed by infrared spectroscopy, ^1H and $^{31}P\{^1H\}$ NMR spectroscopy, elemental analysis and, where possible, by single crystal X-ray analysis. Due to their poor solubility in low polarity solvents, $[TaOCl_3(dppmO_2)]$, $[TaOCl_3(dppeO_2)]$ and $[TaOCl_3(PPO_2)]$ precipitate readily from solution in dichloromethane upon addition of the ligand. $[TaOCl_3(OPPh_3)]$, however, was soluble in dichloromethane so required precipitation by the addition of hexane.

Crystals of $[TaOCl_3(PPO_2)]$ were grown from the slow evaporation from a solution of the complex in dichloromethane. Several sets of diffraction data were collected from different crystals and all produced the same structure refinement. This was well defined, with two exceptions, disorder in the phenyl ring backbone, and one of the pendant phenyl rings. The disorder problem is discussed in Section 4.4.2. Because of this disorder, the metrical data needs to be viewed with care, but it is certainly good enough to identify the structure as shown in Figure 4.4, which reveals the second example of a discrete $TaOCl_3$ monomer. While the poor data quality and disorder preclude detailed analysis of the bond lengths and angles, the data are sufficient to establish the coordination environment, confirming that the PPO_2 ligand lies *trans* to O and Cl, similar to the $[TaOCl_3(1,10\text{-phen})]$ described above, and with *meridional* chlorides.

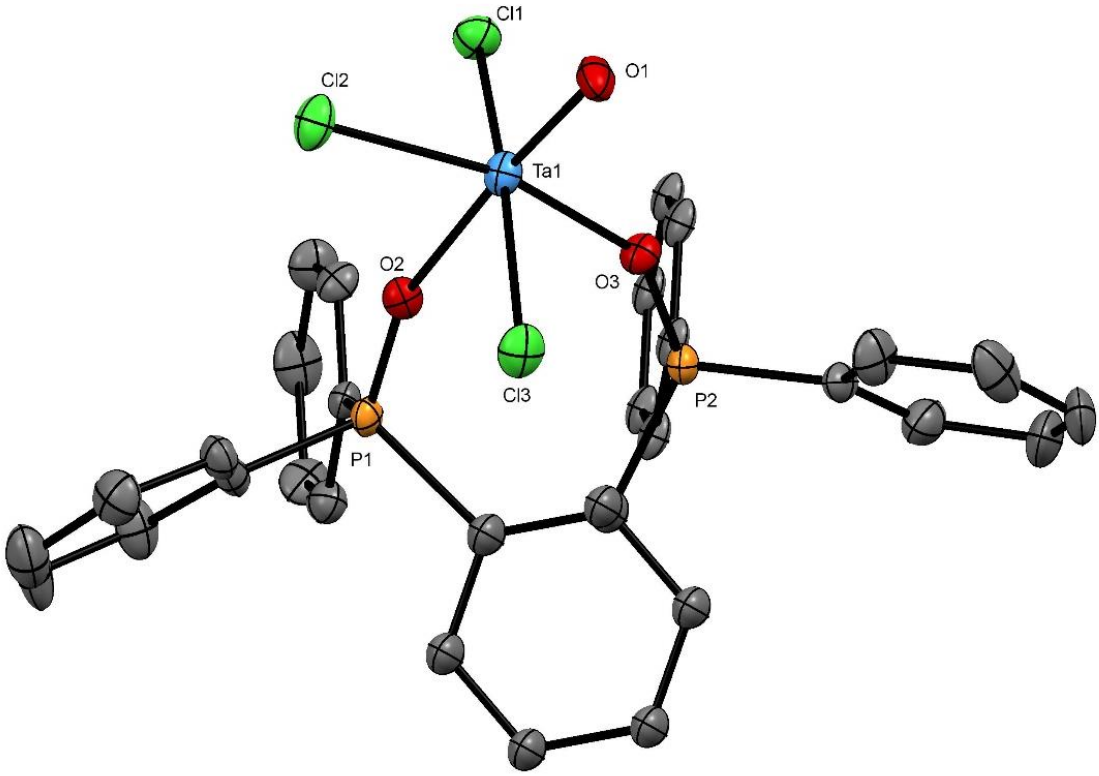

Figure 4.4. The structure of [TaOCl$_3$(PPO$_2$)$_2$] showing the atom numbering scheme. Thermal ellipsoids are drawn at the 50% probability level and H atoms are omitted for clarity. Due to serious disorder in two of the aromatic rings (not shown) the data should be viewed with care. Selected bond lengths (Å) and angles (°) are: Ta1–Cl1 = 2.381(4), Ta1–Cl2 = 2.353(3), Ta1–Cl3 = 2.414(4), Ta1–O1 =1.760(10), Ta1–O2 = 2.230(10), Ta1–O3 = 2.047(9), Cl(2) –Ta1–Cl1 = 93.14(13), Cl2–Ta1–Cl3 = 91.68(13), O1–Ta1–Cl1 = 97.3(4), O1–Ta1–Cl2 = 98.1(4), O1–Ta1–Cl3 = 96.0(4), O1–Ta1–O3 = 96.7(4), O2–Ta1–Cl1 – 81.5(3), O2–Ta1–Cl2 = 87.7(3), O2–Ta1–Cl3 = 84.5(3), O3–Ta1–Cl1 = 87.8(3), O3–Ta1–Cl3 = 84.0(3), O3–Ta1–O2 = 77.5(4).

Other than confirming the presence of the PPO_2 ligand, the ^1H NMR spectrum is rather uninformative. However, the $^{31}P\{^1H\}$ NMR spectrum shows two singlets at 42.4 ppm and 52.5 ppm, representative of the two different phosphorus environments and shifted significantly to high frequency compared to 'free' PPO_2 (31.7 ppm). Infrared spectroscopy shows Ta-Cl stretches at 306 and 324 cm^{-1}, a terminal Ta=O band at 935 and two P=O stretches 1068 and 1162 cm^{-1}, the latter are shifted to low frequency from 'free' PPO_2, (νP=O = 1195 cm^{-1}).[45] Elemental analysis was also consistent with the expected formula.

Although no crystals were obtained, [TaOCl$_3$(dppmO$_2$)] and [TaOCl$_3$(dppeO$_2$)] were made similarly and the spectroscopic data are consistent with analogous structures being present.

Free $dppmO_2$ displays a resonance in the $^{31}P\{^1H\}$ NMR spectrum at 25.1 ppm, which shifts and splits into two separate singlets at 38.3 and 49.9 ppm in $[TaOCl_3(dppmO_2)]$. Uncoordinated $dppeO_2$ displays a $^{31}P\{^1H\}$ NMR resonance at 33.1 ppm, which also shifts and splits into two separate singlets at 47.3 and 59.0 ppm in the $TaOCl_3$ complex, consistent with the P=O functions occupying different environments. The infrared spectrum for $[TaOCl_3(dppmO_2)]$ shows the following key absorptions: Ta-Cl (312, 334 cm^{-1}), Ta=O (1095 cm^{-1}) and P=O (1095, 1154 cm^{-1}). The P=O stretches are shifted to low frequency from 'free' ligand (P=O = 1187 cm^{-1}). Finally, the infrared spectrum for $[TaOCl_3(dppeO_2)]$ also shows the following bands: Ta-Cl (297, 337 cm^{-1}), Ta=O (934 cm^{-1}), P=O (1075, 1173 cm^{-1}); again the P=O stretches are shifted to low frequency from 'free' ligand (P=O = 1187 cm^{-1}). The results are consistent with a six-coordinate tantalum centre with the phosphine oxide groups *trans* to O/Cl, and containing terminal Ta=O groups.

Crystals of $[TaOCl_3(OPPh_3)_2]$ were grown by evaporation of a CH_2Cl_2 solution, Figure 4.5, and the X-ray crystal structure confirms the distorted octahedral geometry which is analogous to that of $[NbOCl_3(OPPh_3)_2]$ and $[NbOF_3(OPPh_3)_2]$.[44] There are some issues with this Ta(V) structure and it is suspected the structure is of lower symmetry, however, at this time it has not been possible to resolve this and therefore the structure is presented as orthorhombic, as is the structure reported for the analogous Nb compound. This space-group imposes disorder on one of the O/Cl sites and this has been modelled with split atom occupancies. The large difference peaks (both positive and negative) are indicative of the unresolved crystallographic issues and are left unexplained. Therefore, while this confirms the coordination geometry present, comparisons of the structural parameters require extreme caution.

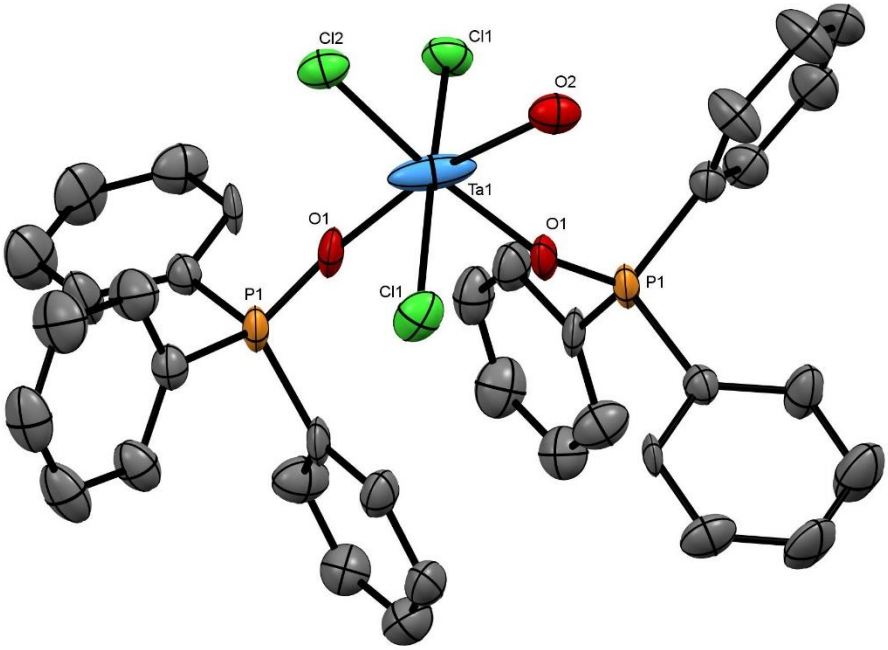

Figure 4.5. A crystal structure of [TaOCl$_3$(OPPh$_3$)$_2$] with atom numbering scheme. Thermal ellipsoids are drawn at the 50% probability level and H atoms are omitted for clarity. The data quality were poor, hence the structure is poorly defined and comparisons of geometric parameters are not justified.

The $^{31}P\{^{1}H\}$ NMR (298 K, CD_2Cl_2) spectrum shows two singlets at 53.4 and 42.5 ppm, however, there are a number of minor impurities evident, which are not observed in any of the bidentate species. Elemental analysis of the bulk microcrystalline solid suggests the formula [TaOCl$_3$(OPPh$_3$)$_2$]·2CH$_2$Cl$_2$, the residual solvent could not be removed *in vacuo*. Infrared spectroscopy of the solid does show the expected Ta-Cl, Ta=O and P=O bands, these are listed in Table 4.1.

Table 4.1. Selected IR spectroscopic data for [$MOCl_3(L)_2$] and [$MOCl_3$(L-L)] (M = Nb,[40] Ta).

Metal Complex	ν(M-Cl) cm^{-1}	ν(M=O) cm^{-1}	ν(P=O) cm^{-1}
[$NbOCl_3$(2,2'-bipy)]	338, 349	943	-
[$NbOCl_3$(1,10-phen)]	338 (br)	944	-
[$NbOCl_3(OPPh_3)_2$]	294, 325	936	1074, 1159
[$NbOCl_3(dppmO_2)$]	294, 327	928	1095, 1157
[$NbOCl_3(dppeO_2)$]	293, 320	943	1066, 1172
[$TaOCl_3$(2,2'-bipy)]	319, 350	938	-
[$TaOCl_3$(1,10-phen)]	322, 350	952	-
[$TaOCl_3(OPPh_3)_2$]	302, 325	930	1076, 1160
[$TaOCl_3(dppmO_2)$]	312, 334	919	1095, 1154
[$TaOCl_3(dppeO_2)$]	297, 337	934	1075, 1173
[$TaOCl_3(PPO_2)$]	306, 324	935	1068, 1162

With these being the first crystallographically confirmed mononuclear tantalum oxychloride complexes, we were able to compare the data to a similar series of niobium species.[44] Table 4.1 compares some of the available data between analogous species – showing good agreement between the infrared spectra and lending weight to the suggested formulae.

4.2.2 Complexes of $TaSCl_3$

Previous syntheses of $TaSCl_3$ complexes have used pre-isolated $TaSCl_3$, which was subsequently reacted with the neutral ligand in a non-coordinating solvent. Attempts to synthesise the compounds described in this Chapter were initially attempted by first synthesising and isolating the known complex [$TaSCl_3(MeCN)_2$].[42] However, drying this complex under gentle vacuum resulted in the partial removal of the weakly coordinating MeCN ligand and was therefore not satisfactory. Consequently, attempts were made to synthesise [$TaSCl_3(MeCN)_2$] *in situ* and then replace the coordinated MeCN with the neutral ligand. However, the excess MeCN solvent competed with the phosphine oxide or diimine ligand and coordinated MeCN could be seen in both the infrared spectra and ^{1}H NMR spectra of the isolated products, hence, this route was not pursued. During these studies, crystals of [$TaSCl_3(MeCN)_2$] were formed, allowing determination of its crystal structure, Figure 4.6. S/Cl disorder is a common problem in thiochloride complexes due to the similar scattering power of S and Cl.[46] It is often difficult to determine the extent of the disorder, and it is not possible to say for certain that at least some disorder is not present in samples. Disorder in selenochlorides or oxychlorides is much easier to observe by simply examining the thermal parameters. If disorder is absent or only small amounts present, expected bond lengths of

Ta-Cl and Ta=S would differ by ~ 0.10 – 0.15 Å and the d(Ta-N) should also differ due to the different *trans* influence of S and Cl. Here, d(Ta1=S1) = 2.2332(14) Å and d(Ta1-Cl2) = 2.2989(14) Å. Also, d(Ta1–N2) = 2.280(5) Å and d(Ta1–N1) = 2.356(5) Å, so although the Ta=S and Ta-Cl distances are slightly closer than expected, there is a significant difference in the ligands *trans* to them, suggesting the S/Cl disorder is either absent or relatively minor. Analysis of a solution of the crystals by ^{1}H NMR and infrared spectroscopy were in close agreement with the literature data. The infrared spectrum shows Ta-Cl bands, (329 and 349 cm^{-1}), a Ta=S band (515 cm^{-1}) and C≡N (2283, 2314 cm^{-1}) and the ^{1}H NMR (298 K, CD_2Cl_2) shows a single resonance at 2.02 ppm for coordinated ligand.

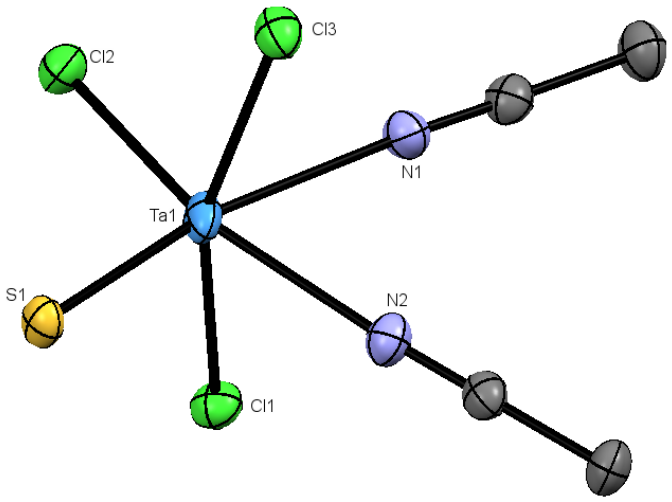

Figure 4.6. A crystal structure of [TaSCl$_3$(MeCN)$_2$] with atom numbering scheme. Thermal ellipsoids are drawn at the 50% probability level and H atoms are omitted for clarity. Selected bond lengths (Å) and angles (°): Ta1–Cl1 = 2.3704(13), Ta1–Cl3 = 2.3823(13), Ta1–S1 = 2.2332(14), Ta1–Cl2 = 2.2989(14), Ta1–N2 = 2.280(5), Ta1–N1 = 2.356(5), Cl3–Ta1–N2 = 81.12(13), S1–Ta1–Cl1 = 97.40(5), S1–Ta1–Cl3 = 97.12(5), S1–Ta1–Cl2 = 103.26(5), S1–Ta1–N1 = 91.65(13), Cl2–Ta1–Cl1 = 94.97(5), Cl2–Ta1–Cl3 = 95.32(5), Cl2–Ta1–N1 = 88.41(13), N1–Ta1–Cl1 = 81.81(13), N2–Ta1–Cl1 = 83.26(13), N1–Ta1–Cl3 = 82.32(13), N1–Ta1–N2 = 76.68(17).

In order to eliminate competition for coordination to the Ta(V) centre from the donor solvent, the procedure was modified such that in the present work, $TaSCl_3$ was generated *in situ* by reaction of $TaCl_5$ and $S(SiMe_3)_2$ in CH_2Cl_2, followed by addition of the appropriate ligand. The complexes [$TaSCl_3$(L-L)] (L-L = 2,2'-bipy, 1,10-phen, $dppmO_2$, $dppeO_2$, PPO_2) and

[$TaSCl_3(OPPh_3)_2$] were obtained successfully, as moisture sensitive yellow powders in 50 – 80% yield, using this method.

The X-ray structure of [$TaSCl_3$(1,10-phen)], Figure 4.7, is isostructural to that of [$TaOCl_3$(1,10-phen)], although in the thiochloride structure the S/Cl atoms lying *trans* to the 1,10-phen ligand are disordered. The structure displays a pseudo-octahedral geometry, distorted by the bite angle of the ligand leading to a N1-Ta1-N2 bond angle of 71.64(8)°. Also, similarly to [$TaOCl_3$(1,10-phen)], the axial Cl1-Ta1-Cl3 chlorides are bent away from the terminal Ta=S group. The d(Ta1=S1) is 2.2347(7) Å and d(Ta1-Cl2) is 2.2548(7) Å, also d(Ta1–N1) = 2.294(2) Å, d(Ta1–N2) = 2.309(2) Å – indicative of close to 50/50 disorder. Unlike the acetonitrile complex above, both the Ta1=S1 and Ta1-Cl2 have nearly identical bond lengths and there is seemingly no effect on the *trans* Ta-N bond lengths. Attempts to model the disorder by splitting the S and Cl atom occupancies, made little difference to the distances or overall refinement of the structure.

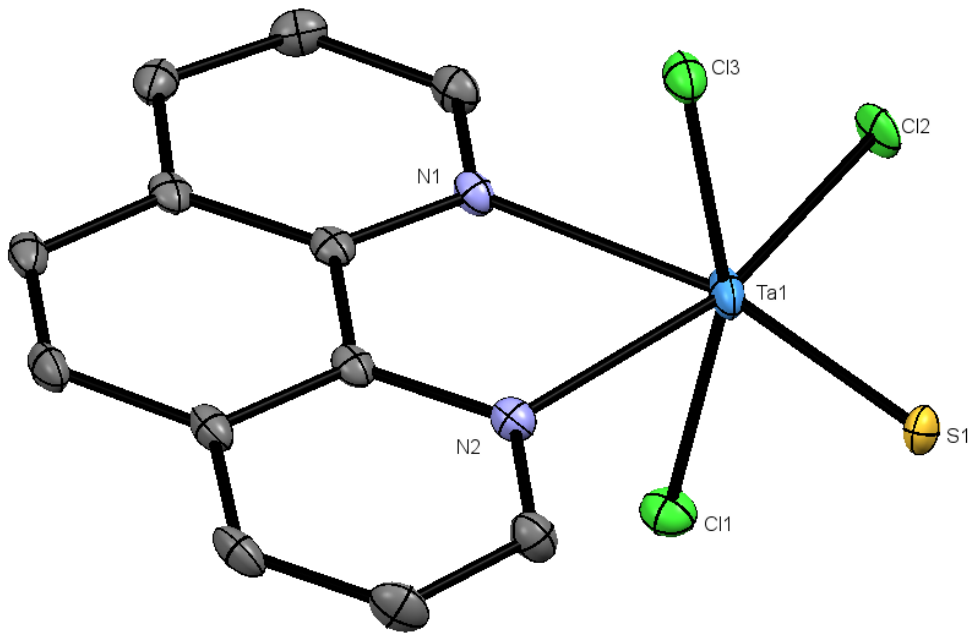

Figure 4.7. The structure of [$TaSCl_3$(1,10-phen)] showing the atom numbering scheme. Thermal ellipsoids are drawn at the 50% probability level and H atoms are omitted for clarity. Note that S1/Cl2 are disordered and only the major component is shown (see Section 4.4.2). Selected bond lengths (Å) and angles (°) are: Ta1–S1 = 2.2347(7), Ta1–Cl2 = 2.2548(7), Ta1–N1 = 2.294(2), Ta1–N2 = 2.309(2), Ta1–Cl1 = 2.3692(7), Ta1–Cl3 = 2.3733(7), Cl2–Ta1–N1 = 93.40(6), S1–Ta1–N2 = 91.23(6), N1–Ta1–N2 = 71.64(8), S1–Ta1–Cl1 = 96.69(3), Cl2–Ta1–Cl1 = 97.10(3), N1–Ta1–Cl1 = 82.14(6), N2–Ta1–Cl1 = 82.58(6), S1–Ta1–Cl3 = 95.22(3), Cl2–Ta1–Cl3 = 94.90(3), N1–Ta1–Cl3 = 81.97(6), N2–Ta1–Cl3 = 81.88(6), S1–Ta1–Cl2 = 103.71(3).

The spectroscopic properties of [$TaSCl_3$(1,10–phen)] and [$TaSCl_3$(2,2'–bipy)] are similar with ν(Ta=S) in the range 500–505 cm^{-1} and ν(Ta–Cl) 315–345 cm^{-1}. As in the case of the oxido-chloride analogue, the ^1H NMR spectra show inequivalent rings, consistent with the structures proposed. There is also evidence for a small amount of hydrolysis in solution, with resonances attributed to protonated ligand present at 9.71 and 9.30 ppm and a very weak signal at 10.12 ppm attributed to N-H. A separate attempt to grow crystals of the 1,10-phenanthroline complex afforded only a few colourless crystals which proved, on structure solution, to be the hydrolysis product, [Cl_3(1,10–phen)Ta(μ-O)Ta(1,10–phen)Cl_3], shown in Figure 4.8, almost certainly caused by adventitious water. The complex contains a linear Ta–O–Ta bridge, with the ligand occupying the expected *trans* O/Cl position. The $d(Ta–Cl)_{transO}$ is ~ 0.15 Å longer than $d(Ta–Cl)_{transCl}$ and the d(Ta-O) is ~ 0.15 Å longer than the d(Ta=O) in [$TaOCl_3$(1,10-phen)]. It is similar in appearance to some of the hydrolysis products mentioned in Section 4.1.4 and also seen in niobium systems.[47–49]

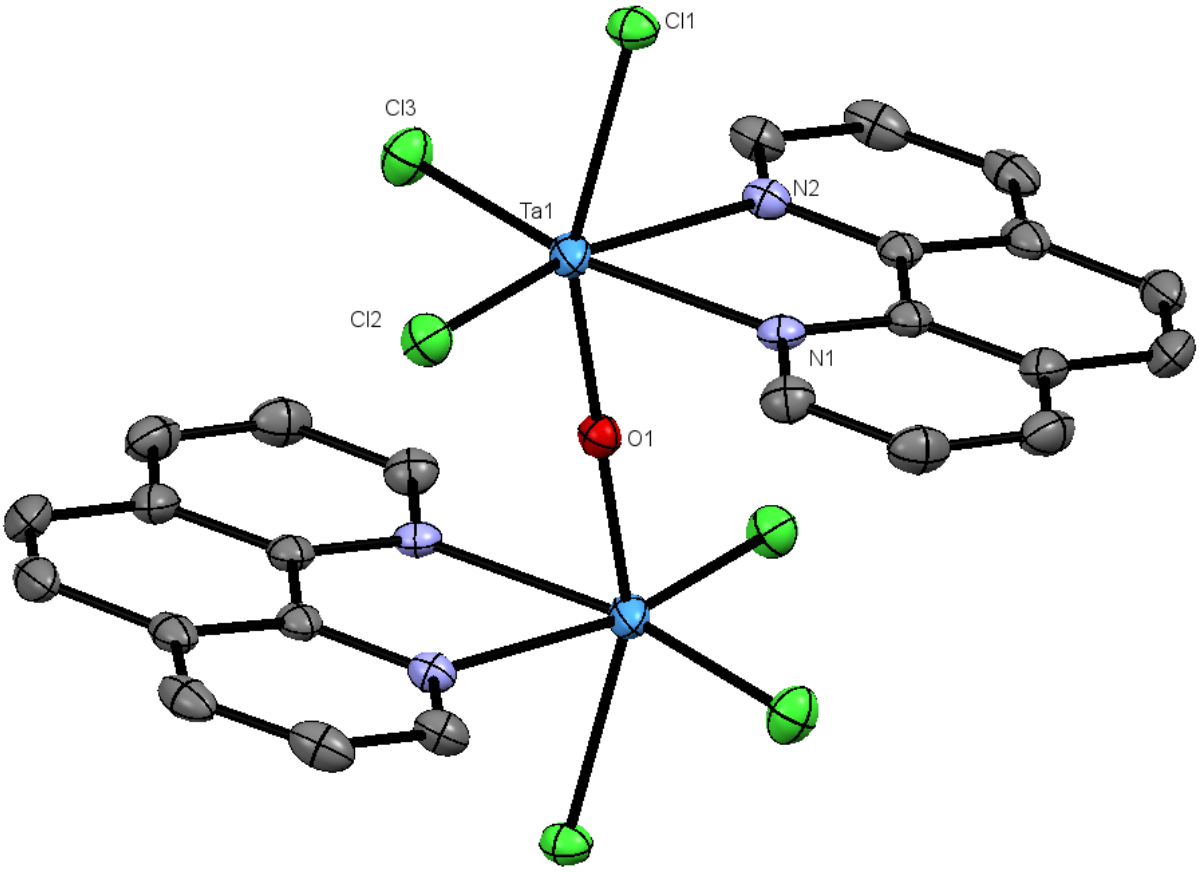

Figure 4.8. The structure of [Cl_3(1,10-phen)Ta(μ-O)Ta(1,10-phen)Cl_3].2CH_2Cl_2 showing the atom numbering scheme. Thermal ellipsoids are drawn at the 50% probability level and H atoms are omitted for clarity. Selected bond lengths (Å) and angles (°) are: Ta1–O1 = 1.88306(14), Ta1–Cl2 = 2.2689(7), Ta1–Cl3 = 2.2710(8), Ta1–N2 = 2.313(2), Ta1–N1 = 2.316(3), Ta1–Cl1 = 2.4274(8), O1–Ta1–Cl2 = 97.10(2), O1–Ta1–Cl3 = 98.58(2), Cl2–Ta1–Cl3 = 103.31(3), O1–Ta1–N2 = 79.33(6), Cl3–Ta1–N2 = 92.75(6), O1–Ta1–N1 79.79(6), Cl2–Ta1–N1 = 92.24(6), N2–Ta1–N1 = 71.72(9), Cl2–Ta1–Cl1 = 95.16(3), Cl3–Ta1–Cl1 = 96.17(3), N2–Ta1–Cl1 = 83.88(6), N1–Ta1–Cl1 = 81.65(6), Ta1–O1–Ta1' = 180.0.

Four phosphine oxide complexes, [$TaSCl_3(OPPh_3)_2$], [$TaSCl_3(dppmO_2)$], [$TaSCl_3(dppeO_2)$] and [$TaSCl_3(PPO_2)$], were obtained as yellow powders from the reaction of $TaCl_5$, $S(SiMe_3)_2$ and the phosphine oxide in anhydrous CH_2Cl_2.

Crystals of [$TaSCl_3(dppeO_2)$], Figure 4.9, were grown by layering a dichloromethane solution of the product with hexane. The crystal shows the expected pseudo-octahedral geometry with the P=O groups *trans* to S/Cl. For the chelating diphosphine dioxides the presence of the interdonor linkage leads to a rather acute O1-Ta1-O2 angle of 80.09 °. The

different ligands lying *trans* to the P=O groups put the two phosphorus atoms in different environments, which is clearly observable in the $^{31}P\{^{1}H\}$ NMR spectrum, whilst the chemical shifts and the ^{1}H NMR spectra lie to high frequency of the dppeO2 itself. The d(Ta1=S1), 2.2025(11) Å and the d(Ta1-Cl2), 2.3175(11) Å, are within an expected range for bonds of these types. Also d(Ta1-O1) and d(Ta1-O2) vary by ca. 0.12 Å, in accordance with the different *trans* influences of the sulfide and chloride ligands as discussed. These data suggest that there is minimal Cl/S disorder present in the crystal structure of this complex.

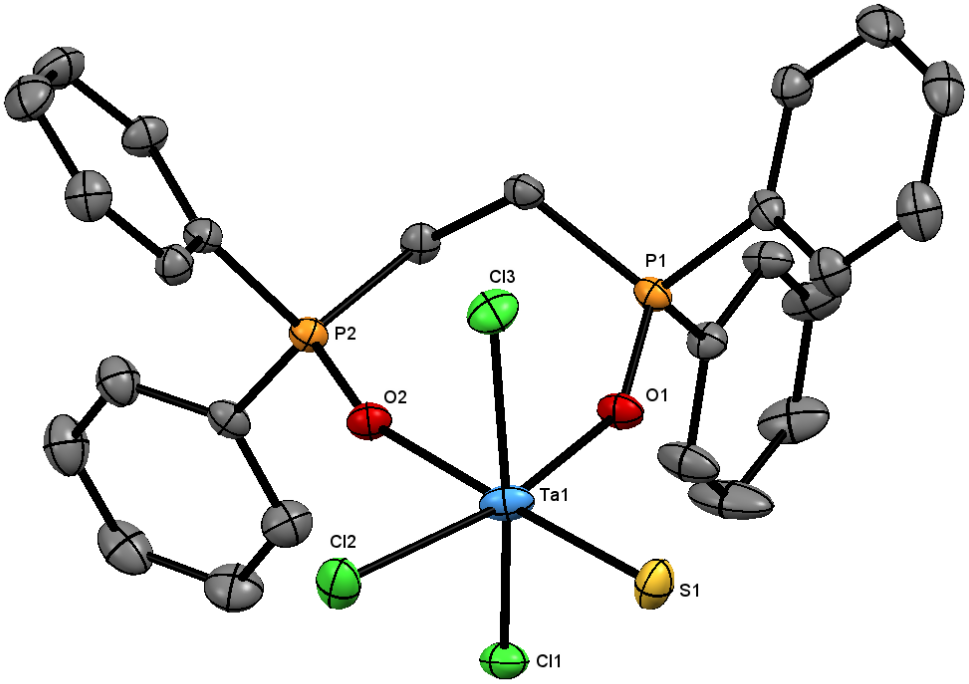

Figure 4.9. The structure of [TaSCl3(dppeO2)] showing the atom numbering scheme. Thermal ellipsoids are drawn at the 50% probability level and H atoms are omitted for clarity. Selected bond lengths (Å) and angles (°) are: Ta1–O1 = 2.061(3), Ta1–O2 = 2.184(3), Ta1–S1 = 2.2025(11), Ta1–Cl2 = 2.3175(11), Ta1–Cl1 = 2.3826(10), Ta1–Cl3 = 2.3849(11), O1–Ta1–O2 = 80.09(11), O1–Ta1–S1 = 96.55(9), O2–Ta1–Cl2 = 84.67(8) , S1–Ta1–Cl2 = 98.70(4), O1–Ta1–Cl1 = 84.93(8), O2–Ta1–Cl1= 82.10(8), S1–Ta1–Cl1 = 96.37(4), Cl2–Ta1–Cl1 = 93.37(4), O1–Ta1–Cl3 = 85.83(8), O2–Ta1–Cl3 = 84.10(8), S1–Ta1–Cl3 = 97.00(4), Cl2–Ta1–Cl3 = 92.28(4).

The IR spectra of all these species show a strong ν(Ta=S) vibration at ~ 500 cm^{-1}, ν(Ta-Cl) in the range 290–330 cm^{-1}, and two well separated ν(P=O) vibrations, indicative of six-coordinate tantalum, with *mer*-chlorides and the P=O groups *trans* S/Cl, i.e. with retention of the structure observed in the solid state. The key IR data are tabulated below, alongside

the analogous [$TaOCl_3$(L-L)] species, Table 4.2. The $^{31}P\{^1H\}$ NMR spectra show two separate phosphorus environments in each complex, owing to the P=O groups lying *trans* to S and *trans* to Cl, Figure 4.10.

Table 4.2. Selected IR spectroscopic data comparing the tantalum oxychloride complexes and the tantalum thiochloride complexes.

Metal Complex	*v(Ta-Cl) cm^{-1}*	*v(Ta=E) cm^{-1}*	*v(P=O) cm^{-1}*
[$TaOCl_3(OPPh_3)_2$]	302, 325	930	1076, 1160
[$TaOCl_3(dppmO_2)$]	312, 334	919	1095, 1154
[$TaOCl_3(dppeO_2)$]	297, 337	934	1075, 1173
[$TaOCl_3(PPO_2)$]	306, 324	935	1068, 1162
[$TaSCl_3(OPPh_3)_2$]	294, 320	495	1064, 1152
[$TaSCl_3(dppmO_2)$]	293, 322	503	1093, 1145
[$TaSCl_3(dppeO_2)$]	300, 323	497	1066 (sh), 1168
[$TaSCl_3(PPO_2)$]	304, 322	494	1066, 1156

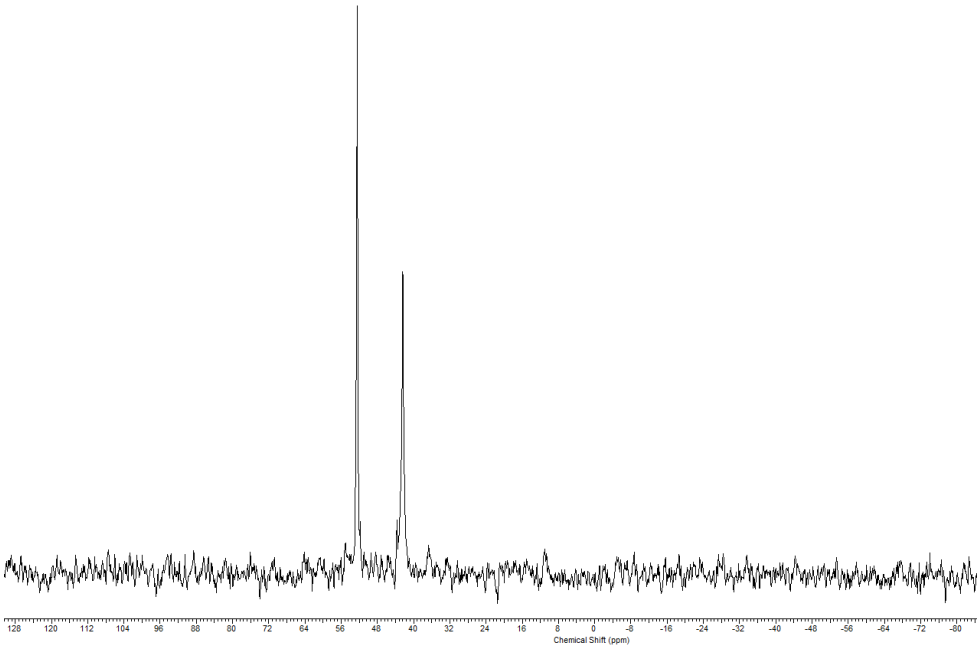

Figure 4.10. $^{31}P\{^1H\}$ NMR spectrum of [$TaSCl_3(PPO_2)$] (CD_2Cl_2), showing the two different phosphorus environments at 42.4 and 52.4 ppm. The resonance at 42.4 ppm is broader than the resonance at 52.4 ppm likely due to some exchange, but these resonances integrate to a 1:1 ratio.

Crystals of $[TaSCl_3(OPPh_3)_2]$ suitable for crystallographic analysis, Figure 4.11, were grown by layering a dichloromethane solution of the product with hexane. As in $[TaSCl_3(1,10\text{-phen})]$, d(Ta1=S1) = 2.275(3) Å and d(Ta1-Cl2) = 2.271(2) Å are nearly identical due to the S/Cl disorder. This also impacts the Ta-O bond lengths, d(Ta1-O1) = 2.108(7) Å and d(Ta1-O2) = 2.089(6) Å, hence close comparisons of the bond lengths are not justified. An attempt has also been made to model this disorder in a similar fashion to in $[TaSCl_3(1,10\text{-phen})]$ and is discussed in Section 4.4.2.

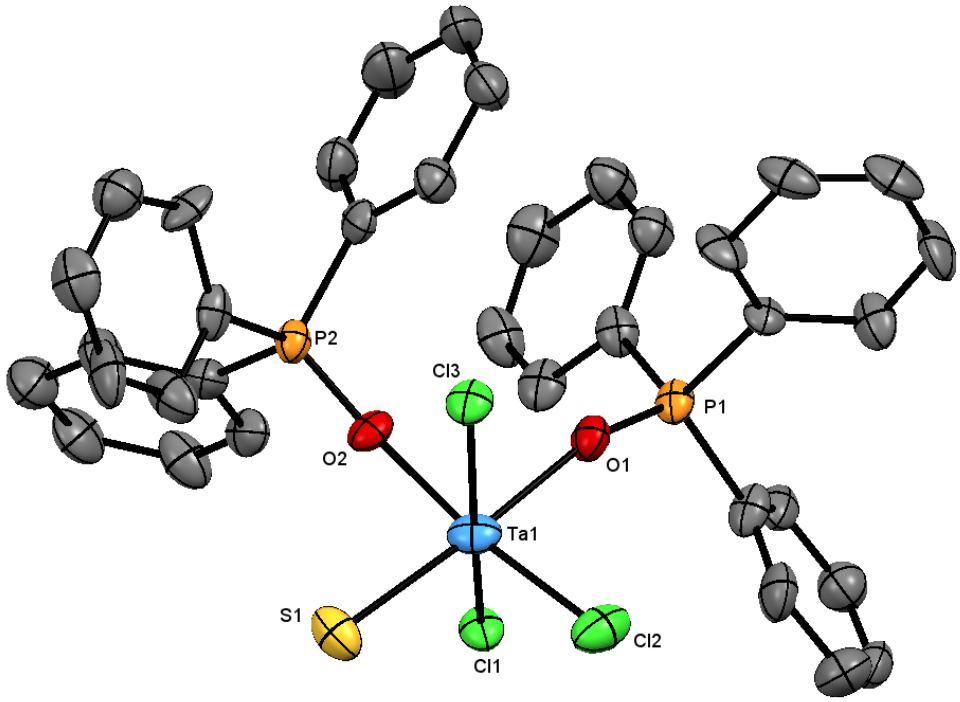

Figure 4.11. The structure of $[TaSCl_3(OPPh_3)_2]$ showing the atom numbering scheme. Thermal ellipsoids are drawn at the 50% probability level and H atoms are omitted for clarity. Note that Cl2 and S1 are disordered (see experimental). Selected bond lengths (Å) and angles (°) are: Ta1–O2 = 2.089(6), Ta1–O1 = 2.108(7), Ta1–Cl2 = 2.271(3), Ta1–S1 = 2.275(3), Ta1–Cl1 = 2.386(2), Ta1–Cl3 = 2.388(2), O2–Ta1–O1 = 83.09(13), O1–Ta1–Cl2 = 90.84(19), O2–Ta1–S1 = 91.3(2), Cl2–Ta1–S1 = 95.01(6), O2–Ta1–Cl1 = 85.67(17), O1–Ta1–Cl1 = 84.00(17), Cl2–Ta1–Cl1 = 97.04(9), S1–Ta1–Cl1 = 92.01(8), O2–Ta1–Cl3 = 83.93(16), O1–Ta– Cl3 = 85.76(17), Cl2–Ta1–Cl3 = 92.34(9), S1–Ta1–Cl3 = 97.25(9).

4.3 Conclusions

The successful synthesis of a series of under explored tantalum complexes, derived from $TaOCl_3$, with neutral phosphine oxides and diimine ligands are described, alongside a series of analogous $TaSCl_3$ complexes. The reaction of $TaCl_5$ with $O(SiMe_3)_2$ or $S(SiMe_3)_2$ and a neutral phosphine oxide ($OPPh_3$, $dppmO_2$, $dppeO_2$ or PPO_2) or diimine (1,10-phen or 2,2;-bipy) in CH_2Cl_2 led to the complexes $[TaECl_3(OPPh_3)_2]$, $[TaECl_3(L\text{-}L)]$ (E = O, S; L-L = 1,10- phen, 2,2'-bipy, $dppmO_2$, $dppeO_2$ and PPO_2).

The complexes derived from $TaOCl_3$ exhibit a rare octahedral monomeric structure, as demonstrated by the structurally characterised $[TaOCl_3(1,10\text{-phen})]$, $[TaOCl_3(PPO_2)]$ and $[TaOCl_3(OPPh_3)_2]$. Whilst the data set on the latter was modest it was enough to confirm the coordination environment of the ligands on the metal centre. The other two crystal structures were free from any O/Cl disorder. The products are characterised by infrared spectroscopy, ^1H and $^{31}P\{^1H\}$ NMR and elemental analysis. The monomeric geometry of the complexes derived from $TaSCl_3$ were confirmed by the structurally characterised $[TaSCl_3(1,10\text{-phen})]$, $[TaSCl_3(dppeO_2)]$ and $[TaSCl_3(OPPh_3)_2]$.

The tantalum complexes appear significantly less stable than their niobium analogues, and crystallographically authenticated examples of monomeric $TaOCl_3$ structures are incredibly rare. Often structures are dinuclear with oxide bridges, as demonstrated here by the structure of $[Cl_3(1,10\text{-phen})Ta(\mu\text{-}O)Ta(1,10\text{-phen})Cl_3].2CH_2Cl_2$. Comparisons of the spectroscopic data on the $TaOCl_3$ and $TaSCl_3$ phosphine oxide complexes, specifically $\nu(P{=}O)$ and $\delta(^{31}P)$, reveal only small and irregular differences between comparable complexes and the spectroscopic studies of the oxychloride complexes are in good agreement with their niobium analogues.

4.4 Experimental

4.4.1 General Experimental

Syntheses were performed by using standard Schlenk and glove-box techniques under a dry N_2 atmosphere. $TaCl_5$, $O(SiMe_3)_2$ and $S(SiMe_3)_2$ were obtained from Sigma-Aldrich and used as received. Ligands (2,2'-bipy, 1,10-phen, Ph_3PO) were obtained from Sigma-Aldrich and dried by heating *in vacuo*. The diphosphine dioxides $dppmO_2$, $dppeO_2$ and PPO_2 were made by dry air oxidation of the corresponding diphosphines in CH_2Cl_2 solution, catalysed by SnI_4,[50] and were checked for purity by $^{31}P\{^1H\}$ NMR spectroscopy (25.1, 33.1 and 31.8 ppm respectively). For further details regarding the instrumentation see Appendix A.

4.4.2 Modelling of Disordered Structures

$[TaSCl_3(PPO_2)]$ - With two exceptions, the molecule refines very nicely. The two exceptions are one of the terminal phenyl rings and the *o*-phenylene ring between the P=O functions. These both exhibit disorder, which requires severe restraints and constraints to fit to a geometrically sensible result. This suggests that there may be an underlying crystallographic issue which we have been unable to identify. Lower symmetry settings (all primitive and centred monoclinic options) and appropriate twin laws also resulted in worse refinements. Another possibility is a modulated structure in which the disordered parts are modulated, however, examination of the diffraction pattern does not reveal the characteristic satellite reflections. The structure presented here has problematical parts of the structure modelled as disordered, but care should be taken in any detailed interpretation of the refined model.

There are large residuals < 1 angstrom from the Ta atom which is probably a result of poorly modelled absorption (analytical), other residuals (positive and negative) are in the vicinity of the disorder. Full details of the refinement are in the cif file.

4.4.3 Tantalum Oxychloride Complexes

$[TaOCl_3(1,10\text{-phen})]$ - $TaCl_5$ (0.300 g, 0.837 mmol) was dissolved in acetonitrile (10 mL) at 70 °C. To the clear solution was added $O(SiMe_3)_2$ (0.136 g, 0.837 mmol), dissolved in acetonitrile, dropwise and the clear solution was stirred for 1 hour. A solution of 1,10-phen (0.151 g, 0.837 mmol) in acetonitrile (5 mL) was added dropwise to the solution and after stirring for 1 h the resulting clear solution was allowed to cool to room temperature. The reaction solution slowly precipitated a white solid, which was filtered off and dried *in vacuo*. Yield: 0.236 g, 58%. Clear crystals were obtained by slow evaporation of a dichloromethane

solution of the product. Required for $C_{12}H_8Cl_3N_2OTa$ (483.37): C, 29.79; H, 1.67; N, 5.79 %. Found: C, 29.77; H, 1.75; N, 5.71 %. ^{1}H NMR (CD_2Cl_2): δ = 8.12 (m, [2H]), 8.20 (m, [2H]), 8.73 (m, [H]), 8.82 (m, [H]) 9.57 (d, [H]) 9.93 (d, [H]). IR spectrum (Nujol mull)/cm^{-1}: 941 s (Ta=O), 350 s, 322 s (Ta-Cl).

[$TaOCl_3$(2,2'-bipy)] - $TaCl_5$ (0.300 g, 0.837 mmol) was dissolved in dichloromethane (10 mL) at 70 °C. To the clear solution was added $O(SiMe_3)_2$ (0.136 g, 0.837 mmol), dissolved in dichloromethane (5 mL), dropwise and the clear solution was stirred for 30 min. A solution of 2,2'-bipy (0.151 g, 0.837 mmol) in dichloromethane (5 mL) was added dropwise to the solution and after stirring for 1 h the resulting clear solution was allowed to cool to room temperature. The reaction mixture was then filtered to remove particulates, leaving a clear solution. The solvent was removed from the filtrate *in vacuo*, yielding a white powder, which was washed with n-hexane (2 mL), and dried *in vacuo*. Yield: 0.197 g, 51%. Required for $C_{10}H_8Cl_3N_2OTa$ (459.37): C, 26.12; H, 1.76; N, 6.10 %. Found: C, 26.11; H, 1.84; N, 6.03 %. ^{1}H NMR (CD_2Cl_2): δ = 7.75 (m, [H]), 7.85 (m, [H]), 8.21 (m, [2H]), 8.35 (m, [2H]), 8.92 (m, [H]), 8.97 (m, [H]). IR spectrum (Nujol mull)/cm^{-1}: 938 s (Ta=O), 350 m, 319 s (Ta-Cl).

[$TaOCl_3(OPPh_3)_2$]·$2CH_2Cl_2$ - $TaCl_5$ (0.300 g, 0.837 mmol) was dissolved in dichloromethane (10 mL) at 70 °C. To the clear solution was added $O(SiMe_3)_2$ (0.136 g, 0.837 mmol), dissolved in dichloromethane (5 mL), and the solution was stirred for 30 min. A solution of $OPPh_3$ (0.466 g, 1.68 mmol) in dichloromethane (5 mL) was then added dropwise and the reaction mixture was allowed to cool to room temperature. The solution was filtered to remove particulates, the filtrate concentrated *in vacuo*, and a white precipitate was formed with the addition of n-hexane (2 mL). This was then filtered off and dried *in vacuo*. Yield: 0.368 g, 43 %. Crystals were grown from a solution of the complex in CH_2Cl_2 by slow evaporation in the glove box. Required for $C_{38}H_{34}Cl_7O_3P_2Ta$ (1029.32): C, 44.32; H, 3.33 %. Found: C, 44.51; H, 3.21 %. ^{1}H NMR (CD_2Cl_2): δ = 7.34-7.94 (m). ^{31}P{^{1}H} NMR (CD_2Cl_2): δ = 53.4 (s, [P]), 42.5 (s, [P]). IR spectrum (Nujol mull)/cm^{-1}: 1160 s, 1076 s (P=O), 930 s (Ta=O), 325 s, 302 s(Ta-Cl).

[$TaOCl_3(dppmO_2)$] - $TaCl_5$ (0.100 g, 0.279 mmol) was dissolved in dichloromethane (10 mL) at 70 °C. $O(SiMe_3)_2$ (0.045 g, 0.279 mmol) dissolved in dichloromethane was added dropwise and the solution was stirred for 30 min. A solution of $dppmO_2$ (0.116 g, 0.279 mmol) in dichloromethane (5 mL) was added dropwise to the solution and the reaction mixture was allowed to cool to room temperature. The solution was filtered to remove a

small amount of solid and the filtrate was concentrated *in vacuo*. Addition of n-hexane (2 mL) afforded a white precipitate that was collected by filtration and dried *in vacuo*. Yield: 0.080 g, 40 %. Required for $C_{25}H_{22}Cl_3O_3P_2Ta$ (719.41): C, 41.70; H, 3.08 %. Found: C, 41.85; H, 3.19 %. ^{1}H NMR (CD_2Cl_2): δ = 3.87 (t, [2H], PC***H***$_2$P), 7.37 (m, [8H], Ph), 7.55 (m, [4H], Ph), 7.66 (m, [8H], Ph). ^{31}P{^{1}H} NMR (CD_2Cl_2): δ = 38.3 (s, [P]), 49.9 (s, [P]). IR spectrum (Nujol mull)/cm^{-1}: 1154 s, 1095 m (P=O), 919 s (Ta=O), 334 m, 312 s (Ta-Cl).

[TaOCl$_3$(dppeO$_2$)] - $TaCl_5$ (0.150 g, 0.419 mmol) was dissolved in acetonitrile (10 mL) at 70 °C. To the clear solution was added $O(SiMe_3)_2$ (0.068 g, 0.419 mmol) dissolved in acetonitrile (5mL), and the solution was stirred for 30 min.. A solution of dppeO_2 (0.180 g, 0.419 mmol) in acetonitrile (5 mL) was then added dropwise and the reaction mixture was allowed to cool to room temperature over ~30 min. The solution was filtered and the filtrate was concentrated *in vacuo*, yielding a white precipitate, which was filtered off and dried *in vacuo*. Yield: 0.237 g, 77 %. Anal: Required for $C_{26}H_{24}Cl_3O_3P_2Ta$ (733.43): C, 42.54; H, 3.30. Found: C, 42.31; H, 3.16 %. ^{1}H NMR (CD_2Cl_2, 298 K): δ = 2.78 (m, [2H] CH_2CH_2), 2.83 (m, [2H], CH_2CH_2), 7.46-7.65 (m, [12H]), 7.91 (m, [8H]). ^{31}P{^{1}H} NMR (CD_2Cl_2 298 K): δ = 47.3 (s, [P]), 59.0 (s, [P]). IR spectrum (Nujol mull)/cm^{-1}: 1173 s, 1075 s (P=O), 934 s (Ta=O), 337 s, 297 s (Ta-Cl).

[TaOCl$_3$(PPO$_2$)] - $TaCl_5$ (0.150 g, 0.419 mmol) was dissolved in acetonitrile (10 mL) at 70 ^{0}C. To the solution was added dropwise $O(SiMe_3)_2$ (0.068 g, 0.419 mmol), dissolved in acetonitrile (5 mL) and the clear solution was stirred for 30 min. A solution of PPO_2 (0.200 g, 0.419 mmol) in acetonitrile (5 mL) was added dropwise and the reaction mixture was allowed to cool to room temperature. The solution was filtered and the filtrate concentrated, yielding a white precipitate. This was filtered off and dried *in vacuo*. Yield: 0.212 g, 65 %. Crystals were grown from a solution of the complex in CH_2Cl_2 by slow evaporation. Required for $C_{30}H_{24}Cl_3O_3P_2Ta$ (781.43): C, 46.07; H, 3.10 %. Found: C, 46.19; H, 3.27 %. ^{31}P{^{1}H} NMR (CD_2Cl_2): δ = 42.4 (s, [P]), 52.5 (s, [P]). IR spectrum (Nujol mull)/cm^{-1}: 1162 s, 1068 s (P=O), 935 s (Ta=O), 324 w, 306 br s (Ta-Cl).

4.4.4 Tantalum thiochloride species

[$TaSCl_3$(1,10-phen)] - $TaCl_5$ (0.300 g, 0.837 mmol) was dissolved in dichloromethane (20 mL) at 50 °C and the solution cooled to room temperature. To the clear solution was added $S(SiMe_3)_2$ (0.149 g, 0.837 mmol) in dichloromethane (5 mL). The solution immediately turned bright yellow and then a precipitate formed and the solution turned light brown. The reaction mixture was stirred for 1 h. A solution of 1,10-phen (0.151 g, 0.837 mmol) in dichloromethane (5 mL) was added dropwise and the reaction mixture was stirred for a further 2 h. No visible change was observed. The solution was filtered giving a light brown filtrate, which was concentrated *in vacuo* causing precipitation of a light brown solid, which was collected by filtration and dried *in vacuo*. Yield: 0.251 g, 60%. Yellow crystals were obtained by layering a dichloromethane solution of the product with n-hexane. Required for $C_{12}H_8Cl_3N_2STa$ (499.35): C, 28.84; H, 1.61; N, 5.61 %. Found: C, 28.76; H, 1.59; N, 5.51 %. ^{1}H NMR (CD_2Cl_2): δ = 7.77─7.80 (m, [2H]), 8.32─8.34 (m, [2H]), 8.77 (m, [H]), 8.79 (m, [H]), 8.92 (m, [H]), 8.9 (m, [H]). IR spectrum (Nujol mull)/cm^{-1}: 502 s (Ta=S), 317 br, s (Ta-Cl).

[$TaSCl_3$(2,2'-bipy)] - $TaCl_5$ (0.300 g, 0.837 mmol) was dissolved in dichloromethane (10 mL) at 50 °C and the solution cooled to room temperature. To the clear solution was added $S(SiMe_3)_2$ (0.149 mg, 0.837 mmol) in dichloromethane (5 mL). The solution immediately turned bright yellow and then some precipitate formed and the solution turned light brown. A solution of 2,2'-bipy (0.130 g, 0.837 mmol) in dichloromethane (5 mL) was added dropwise and stirred for 1 h. The reaction mixture was then filtered, leaving a clear yellow solution. This was concentrated to 5 mL and a yellow precipitate was formed through the addition of n-hexane (3 mL), which was collected by filtration and dried *in vacuo*. Yield: 0.267 g, 67 %. Required for $C_{10}H_8Cl_3N_2STa$ (475.35): C, 25.24; H, 1.70; N, 5.89 %. Found: C, 25.43; H, 1.85; N, 5.86 %. ^{1}H NMR (CD_2Cl_2): δ = 7.77 (m, [H]), 7.78 (m, [H]), 8.30-8.34 (m, [2H]), 8.77 (m, [H]), 8.79 (m, [H]), 8.92 (m, [H]), 8.93 (m, [H]). IR spectrum (Nujol mull)/cm^{-1}: 504 s (Ta=S), 345 s, 322 s (Ta-Cl).

[$TaSCl_3(OPPh_3)_2$]·0.5CH_2Cl_2 - $TaCl_5$ (0.300 g, 0.837 mmol) was dissolved in dichloromethane (10 mL) at 50 °C and the solution cooled to room temperature. To the clear solution was added $S(SiMe_3)_2$ (0.149 g, 0.837 mmol) in dichloromethane (3 mL), when the solution immediately turned bright yellow and then a precipitate formed. A solution of $OPPh_3$ (0.466 g, 1.68 mmol) in dichloromethane (5 mL) was added and the precipitate immediately dissolved. The solution was stirred for 1 h, then filtered, giving a dark orange

solution. This was concentrated *in vacuo* and a small amount of orange precipitate formed. Filtration gave a yellow solution and the solvent was removed *in vacuo* to give a yellow powder. Yield: 0.415 g, 54% Required for $C_{36}H_{30}Cl_3O_2P_2STa \cdot 0.5CH_2Cl_2$ (918.41): C, 49.35; H, 3.45 %. Found: C, 47.72; H, 3.40 %. $^{31}P\{^1H\}$ NMR (CD_2Cl_2): 43.9 (s, [P]), 54.4 (s, [P]). IR spectrum (Nujol mull)/cm^{-1}: 1152 s, 1064 s (P=O), 495 m (Ta=S), 320 s, 294 s (Ta-Cl).

[$TaSCl_3(dppmO_2)$] - $TaCl_5$ (0.100 g, 0.279 mmol) was dissolved in dichloromethane (10 mL) at 50 °C and then cooled to room temperature. To the clear solution was added $S(SiMe_3)_2$ (0.050 g, 0.279 mmol) in dichloromethane (3 mL). The solution immediately turned bright yellow and then a precipitate formed and the solution turned light brown. A solution of $dppmO_2$ (0.116 g, 0.279 mmol) in dichloromethane (5 mL) was added dropwise. After 30 min. the reaction mixture was filtered to remove some suspended solid and from the resulting yellow filtrate, yellow crystals immediately began to form. The solution was concentrated *in vacuo* and then the crystals were collected by filtration and dried *in vacuo*. Yield: 0.125 g, 61 %. Required for $C_{25}H_{22}Cl_3O_2P_2STa$ (735.39): C, 40.79; H, 3.02 %. Found: C, 40.93; H, 3.16%. ^1H NMR (CD_2Cl_2): δ = 3.89 (m, [2H], PC***H***$_2$P), 7.40 (m, [8H], Ph), 7.64-7.74 (m, [12H], Ph). $^{31}P\{^1H\}$ NMR (CD_2Cl_2): 38.1 (s, [P]), 48.7 (s, [P]). IR spectrum (Nujol mull)/cm^{-1}: 1145 s, 1093 s (P=O), 503 m (Ta=S), 322 s, 293 s (Ta-Cl).

[$TaSCl_3(dppeO_2)$] - $TaCl_5$ (0.150 g, 0.419 mmol) was dissolved in dichloromethane (10 mL) at 50 °C and then cooled to room temperature. To the clear solution was added $S(SiMe_3)_2$ (0.075 g, 0.419 mmol) in dichloromethane. A solution of $dppeO_2$ (0.180 g 0.419 mmol) in dichloromethane (5 mL) was added dropwise. The reaction mixture was filtered to remove some suspended solids, giving a bright yellow solution. The solution was concentrated and a yellow precipitate was formed through the addition of n-hexane (2 mL), which was filtered off and dried *in vacuo*. Yield: 0.240 g, 76 %. Required for $C_{26}H_{24}Cl_3O_2P_2STa$ (749.40): C, 41.63; H, 3.23 %. Found: C, 41.44; H, 3.33 %. ^1H NMR (CD_2Cl_2): δ = 2.81 (m, [2H], CH_2C***H***$_2$), 2.95 (m, [2H], C***H***$_2CH_2$), 7.48-7.73 (m, [12H]), 7.90 (m, [8H], Ph). $^{31}P\{^1H\}$ NMR (CD_2Cl_2): 46.71 (s, [P]), 57.15 (s, [P]). IR spectrum (Nujol mull)/cm^{-1}: 1168 s, 1057 s br (P=O), 497 (Ta=S), 323 s, 300 s (Ta-Cl).

[$TaSCl_3(PPO_2)$] - $TaCl_5$ (0.150 g, 0.419 mmol) was dissolved in dichloromethane (10 mL) at 50 °C and then cooled to room temperature. To the solution was added $S(SiMe_3)_2$ (0.075 g, 0.419 mmol) in dichloromethane (3 mL) forming a brown precipitate. A solution of PPO_2 (0.200 g, 0.419 mmol) in dichloromethane (5 mL) was added dropwise and the precipitate immediately dissolved. After 10 min. a straw coloured precipitate formed. The reaction was

stirred for 1 h, then filtered to give a dark yellow solution. This was concentrated and a yellow precipitate formed, which was filtered off and dried *in vacuo*. Yield: 0.220 g, 66 %. Required for $C_{30}H_{24}Cl_3O_2P_2STa$ (797.40): C, 45.15; H, 3.03 %. Found: C, 44.91; H, 3.06 %. $^{31}P\{^1H\}$ NMR (CD_2Cl_2): δ = 42.4 (s, [P]), 52.4 (s, [P]). IR spectrum (Nujol mull)/cm^{-1}: 1156 s, 1066 s (P=O), 494 s (Ta=S), 322 s, 304 s (Ta-Cl).

$[TaSCl_3(MeCN)_2]$[42] -$TaCl_5$ (0.30 g, 0.837 mmol) was stirred in acetonitrile (5 mL) and then $S(Me_3Si)_2$ (0.149 g, 0.837 mmol) in acetonitrile was added and the mixture was stirred for 16 h, when it turned from yellow to orange to a very dark brown. The solution was concentrated, and n-hexane (1 mL) was added, forming some yellow crystals suitable for X-ray structure determination. ^1H NMR (CD_2Cl_2): 2.02 (s). IR spectrum (Nujol mull/cm^{-1}): 515 s (Ta=S), 349 w, 329 s (Ta-Cl). Lit. ^1H NMR (CD_2Cl_2, 298 K): 2.02(s). IR spectrum (Nujol mull)/cm^{-1}: 510 (Ta=S).[42]

Table 4.3. Crystallographic data[a]

Compound	**[$TaOCl_3$(1,10-phen)]**	**[$TaOCl_3(PPO_2)$]**	**[$TaOCl_3(OPPh_3)_2$]**
Formula	$C_{12}H_8Cl_3N_2OTa$	$C_{30}H_{24}Cl_3O_3P_2Ta$	$C_{36}H_{30}Cl_3O_3P_2Ta$
M	483.50	781.73	859.84
Crystal system	monoclinic	orthorhombic	Monoclinic
Space group (no.)	$P2_1/c$ (14)	$C222_1$ (20)	$C2/_c$ (15)
a /Å	7.75820(12)	10.86425(9)	13.9027(2)
b /Å	17.6961(2)	17.33118(17)	12.95380(10)
c /Å	10.24375(14)	30.4143(2)	19.0339(2)
α/°	90	90	90
β/°	106.3180(15)	90	95.0740(10)
γ/°	90	90	90
U /Å^3	1349.71(3)	5726.71(9)	3414.44(7)
Z	4	8	4
μ(Mo-K_α) /mm^{-1}	8.727	4.262	3.583
F(000)	904	356	1696.0
Total no. reflns	34031	158344	68582
R_{int}	0.0204	0.042	0.0247
Unique reflns	3487	9605	4355
No. of params, restraints	172, 0	238, 0	207, 204
R_1, wR_2 [$I > 2\sigma(I)$][b]	0.0119, 0.0283	0.064, 0.181	0.1124, 0.2618
R_1, wR_2 (all data)	0.0126, 0.0285	0.065, 0.181	0.1135, 0.2622

Table 4.3 continued.

Compound	**$[TaSCl_3(MeCN)_2]$**	**$[TaSCl_3$ (1,10-phen)]**
Formula	$C_8H_{12}Cl_6N_4S_2Ta_2$	$C_{12}H_8Cl_3N_2STa$
M	401.47	499.56
Crystal system	triclinic	monoclinic
Space group (no.)	P-1 (2)	$P2_1/c$ (14)
a /Å	6.0617(3)	7.3598(2)
b /Å	7.1013(3)	19.3732(4)
c /Å	12.7630(9)	10.4977(2)
α/°	80.152(5)	90
β/°	85.422(5)	107.787(2)
γ/°	80.847(4)	90
U /Å^3	533.63(5)	1425.24(6)
Z	2	4
μ(Mo-K$_\alpha$) /mm^{-1}	11.189	8.405
F(000)	368	936
Total number reflns	11003	15172
R_{int}	0.0367	0.0223
Unique reflns	2756	2796
No. of params, restraints	102, 0	172, 1
R_1, wR_2 [$I > 2\sigma(I)$] [b]	0.0302, 0.0817	0.0151, 0.0322
R_1, wR_2 (all data)	0.0341, 0.0842	0.0168, 0.0327

Table 4.3 continued.

Compound	**$[Ta_2O(1,10\text{-phen})_2Cl_6]\cdot 2CH_2Cl_2$**	**$[TaSCl_3(dppeO_2)]$**
Formula	$C_{26}H_{20}Cl_{10}N_4OTa_2$	$C_{26}H_{24}Cl_3O_2P_2STa$
M	1120.86	749.75
Crystal system	triclinic	monoclinic
Space group (no.)	P-1 (2)	$P2_1/c$ (14)
a /Å	8.6177(3)	15.7268(3)
b /Å	10.3709(3)	9.63510(10)
c /Å	11.3478(4)	18.0202(3)
α/°	101.753(3)	90
β/°	109.543(3)	97.254(2)
γ/°	111.146(3)	90
U /Å^3	828.48(5)	2708.73(7)
Z	1	4
μ(Mo-K$_\alpha$) /mm^{-1}	7.436	4.573
F(000)	528	1464
Total number reflns	17672	30650
R_{int}	0.0422	0.0225
Unique reflns	3265	5325
No. of params, restraints	196, 0	316, 1
R_1, wR_2 [$I > 2\sigma(I)$] [b]	0.0183, 0.0459	0.0300, 0.0634
R_1, wR_2 (all data)	0.0197 , 0.0464	0.0351, 0.0653

Table 4.3 continued.

Compound	**$[TaSCl_3(OPPh_3)_2]$**
Formula	$C_{36}H_{30}Cl_3O_2P_2STa$
M	875.90
Crystal system	monoclinic
Space group (no.)	$P2_1/n$ (14)
a /Å	13.7854(3)
b /Å	13.0247(5)
c /Å	19.3056(6)
α/°	90
β/°	95.087(2)
γ/°	90
U /Å^3	3452.68(19)
Z	4
μ(Mo-K$_\alpha$) /mm^{-1}	3.601
F(000)	1728
Total number reflns	68989
R_{int}	0.0553
Unique reflns	9623
No. of params, restraints	408, 22
R_1, wR_2 [$I > 2\sigma(I)$] [b]	0.0436, 0.1087
R_1, wR_2 (all data)	0.0971, 0.1378

[a] Common data: $T = 293$ K; wavelength (Mo Kα) = 0.71073 Å; θ(max) = 27.5°.

[b] $R_1 = \Sigma||Fo| - |Fc||/\Sigma|Fo|$; $wR_2 = [\Sigma w(Fo^2 - Fc^2)^2/\Sigma wFo^4]^{1/2}$.

4.5 References

1 F. Marchetti and G. Pampaloni, *Chem. Commun.*, 2012, **48**, 635–653.

2 L. G. Hubert-Pfalzgraf, in *Encyclopedia of Inorganic Chemistry*, eds. R. B. King, R. H. Crabtree, C. M. Lukehart, D. A. Atwood and R. A. Scott, American Cancer Society, 2006, p. 3.

3 M. Jura, W. Levason, R. Ratnani and M. Webster, *Dalton Trans.*, 2010, **2**, 883–891.

4 G. R. Willey, T. Woodman and M. Drew, *Polyhedron*, 1997, **16**, 351–353.

5 K. H. Grundy, A. Thompson and F. Fairbrother, *J. Chem. Soc.*, 1965, 765–770.

6 D. Brown, J. Hill and C. E. F. Rickard, *J. Chem. Soc.*, 1970, 476–480.

7 M. Aresta, A. Dibenedetto, P. Stufano, B. M. Aresta, S. Maggi, P. Imre, T. A. Rokob and B. Gabriele, *Dalton Trans.*, 2010, **39**, 6985–6992.

8 K. Stumpf, R. Blachnik and G. Roth, *Z. Krist. NCS*, 1999, **214**, 397–398.

9 S. L. Benjamin, A. Hyslop, W. Levason and G. Reid, *J. Fluor. Chem.*, 2012, **137**, 76–83.

10 R. Bini, C. Chiappe, F. Marchetti, G. Pampaloni, S. Zacchini, V. Lastruccia, I.-S. Fiorentino, D. Chimica, V. Risorgimento, I.- Pisa, C. Industriale, V. Risorgimento and C. Fisica, *Inorg. Chem.*, 2010, **5**, 339–351.

11 R. Haiges, P. Deokar and K. O. Christe, *Zeitschrift für Anorg. und Allg. Chemie*, 2014, **640**, 1568–1575.

12 W. Levason, M. E. Light, G. Reid and W. Zhang, *Dalton Trans.*, 2014, **43**, 9557–9566.

13 F. Marchetti, G. Pampaloni and S. Zacchini, *Polyhedron*, 2016, **115**, 99–104.

14 F. Marchetti, G. Pampaloni and S. Zacchini, *Eur. J. Inorg. Chem.*, 2010, 767–774.

15 S. L. Benjamin, Y.-P. Chang, C. Gurnani, A. L. Hector, M. Huggon, W. Levason and G. Reid, *Dalton Trans.*, 2014, **43**, 16640–16648.

16 K. Stumpf, R. Blachnik and H. Reuter, *Z. Krist. NCS*, 1999, **214**, 281–282.

17 M. Bortoluzzi, E. Ferretti, F. Marchetti, G. Pampaloni and S. Zacchini, *Dalton Trans.*, 2016, **45**, 6939–6948.

18 A. O. Baghlaf, K. Behzadi and A. Thompson, *J. Less Common Met.*, 1978, **61**, 31–37.

19 C. I. Branden and I. Lindqvist, *Acta Chem. Scand.*, 1963, **17**, 353–361.

20 F. Marchetti, G. Pampaloni and S. Zacchini, *Eur. J. Inorg. Chem.*, 2008, 453–462.

21 R. Good and A. E. Merbach, *Inorg. Chem.*, 1975, **14**, 1030–1034.

22 H. Vanni and A. E. Merbach, *Inorg. Chem.*, 1979, **18**, 2758–2762.

23 A. E. Merbach, *J. Chem. Soc., Chem. Commun.*, 1974, 163–164.

24 C. M. P. Favez, H. Rollier and A. E. Merbach, *Helv. Chim. Acta*, 1976, **59**, 2383–2392.

25 R. G. Pearson, *J. Am. Chem. Soc.*, 1963, **85**, 3533–3539.

26 E. G. Hope and W. Levason, *Coord. Chem. Rev.*, 1993, **122**, 109–170.

27 W. Levason and G. Reid, *J. Chem. Res.*, 2002, **2**, 467–472.

28 Y.-P. Chang, W. Levason and G. Reid, *Dalton Trans.*, 2016, **15**, 18393–18416.

29 M. J. Heeg, J. Scheper and C. H. Winter, *CCDC 781504 Exp. Cryst. Struct. Determ.*, 2011.

30 Z. Wei, W. Zhang, G. Luo, F. Xu and Y. Mei, *New J. Chem.*, 2016, **40**, 6270–6275.

31 N. Bartalucci, M. Bortoluzzi, G. Pampaloni, C. Pinzino, S. Zacchini and F. Marchetti, *Dalton Trans.*, 2018, **47**, 3346–3355.

32 P. J. McKarns, M. J. Heeg and C. H. Winter, *Inorg. Chem.*, 2002, **37**, 4743–4747.

33 F. Fairbrother, in *Halogen Chemistry*, ed. V. Gutmann, Academic Press, N.Y., 1967, p. 123.

34 M. Ströbele and H. Meyer, *Z. Anorg. Allg. Chem.*, 2002, **628**, 488–491.

35 I. N. Belova, N. I. Giricheva, G. V Girichev, V. N. Petrova and S. A. Shlykov, *J. Struct. Chem.*, 1996, **37**, 257–264.

36 F. Fairbrother, A. H. Cowley and N. Scott, *J. Less Common Met.*, 1959, **1**, 206–216.

37 F. Preuss, G. Lambing and S. Müller-Becker, *Zeitschrift für Anorg. und Allg. Chemie*, 1994, **620**, 1812–1817.

38 K. Dehnicke, *Naturwiss*, 1965, **52**, 58.

39 D. V. Drobot and E. A. Pisarev, *Russ. J. Inorg. Chem.*, 1984, **29**, 2723.

40 W. Levason, G. Reid, J. Trayer and W. Zhang, *Dalton Trans.*, 2014, **43**, 3649–3659.

41 S. L. Benjamin, A. Hyslop, W. Levason and M. Webster, *Acta Crystallogr. Sect. C*, 2011, **67**, m221–m223.

42 M. G. B. Drew, D. A. Rice and D. M. Williams, *Dalton Trans.*, 1984, 845–848.

43 R. D. Bannister, W. Levason, M. E. Light, G. Reid and W. Zhang, *Polyhedron*, 2019, **167**.

44 W. Levason, G. Reid, J. Trayer and W. Zhang, 2014, **2**, 3649–3659.

45 M. Stankevič and A. Włodarczyk, *Tetrahedron*, 2013, **69**, 73–81.

46 Y.-P. Chang, A. L. Hector, W. Levason and G. Reid, *Dalton Trans.*, 2017, **46**, 9824–9832.

47 A. M. Andreu, F. A. Jalon, A. Otero, P. Roy, A. M. Manotti and A. Tiripicchio, *J. Chem. Soc., Dalton Trans.*, 1987, 953–956.

48 F. Marchetti and S. Zacchini, *Dalton Trans.*, 2009, 6759–6772.

49 H. W. Roesky, J. Liebermann, M. Noltemeyer and H. Schmidt, *Chem. Ber.*, 1989, **122**, 1641–1643.

50 W. Levason, R. Patel and G. Reid, *J. Organomet. Chem.*, 2003, **688**, 280–282.

Chapter 5 Complexes of $TaSCl_3$ with Neutral Soft Donor Ligands

5.1 Introduction

With an increasing interest in thin films of early transition metal chalcogenides, ME_2 (E = S, Se or Te), new methods of synthesis are becoming ever more important. Chemical vapour deposition (CVD) is a versatile, scalable and cheap method of synthesis for accessing these thin films. The primary focus of this chapter is to produce an unusual series of chalcogenoether complexes of tantalum thio-chloride to study the interactions between the soft thioether ligands with the hard tantalum metal centre. Complexes with longer chain chalcogenoethers will then be tested by low pressure chemical vapour deposition experiments, to determine their viability as single source precursors for the deposition of thin films of TaS_2. In addition, a similar synthetic route is used in an attempt to synthesise the tantalum(V) phosphine complex,$[TaSCl_3(dppe)]$, in an attempt to probe the tantalum(V)-phosphine interactions.

5.1.1 Niobium and tantalum halide chalcogenoethers

Examples of soft donor coordination complexes with Ta(V) are less ubiquitous than the hard donor counterparts.[1] The properties of early transition metal halides with soft, neutral donor ligands (such as phosphines, thio- seleno- or telluro-ethers), often differs quite drastically from complexes formed with hard donor ligands,[2,3] and as such it is pertinent to compare the tantalum species with a range of niobium compounds as they are more prevalent in the literature. These soft donor systems are prone to oxidation and hydrolysis with adventitious water or air,[3,4] as such, the use of rigorously dried solvents and an inert atmosphere are imperative.

Initial interest, within the Reid group, in niobium and tantalum chalcogenoethers was developed from an interest in soft donor interactions with a range of other hard early transition metal halides. Examples include TiX_4 (X = Cl, Br, I),[5,6] MX_4 (M = Zr, Hf; X = Cl, Br),[7] MO_2X_2 (M = Mo, W; X = Cl, Br).[8,9] Of particular interest was the difference between these metal halide complexes and those of the metal fluorides. It was noted that the fluoride analogues of these species are particularly difficult to form, due to their instability, and attempts to make complexes often led to fluorination of the donor heteroatom.[10,2,11] Some of the metal chloride complexes, particularly those with terminal butyl substituents, were identified as potential single-source precursors for CVD growth of metal dichalcogenide

films, due to their relatively high volatility and the availability of a low energy decomposition mechanism through β-hydride elimination.[6,12]

The first chalcogenoether complexes of MF_5 (M = Nb, Ta) were described by Fairbrother *et al.* who reported the synthesis of $[MX_5(R_2S)]$ (M = Nb, Ta; X = F, Cl, Br; R = Me, Et) by direct reaction of MX_5 with R_2S in the absence of a solvent.[13] Limited characterisation, including vapour pressure measurements and microanalysis, were reported. This work was followed by Merbach *et al.* who performed detailed kinetic studies on ligand exchange reactions of niobium and tantalum pentahalides with dimethyl sulfide, selenide and telluride.[14–16] Through detailed ^1H NMR studies it was determined that the species are formed by an associative mechanism, contrary to the ether analogues, $[MX_5(Me_2O)]$, which are formed by a dissociative mechanism. Although, as discussed previously in Section 4.1.2, understanding of HSAB theory was quite different at the time and both understanding and chemical practice have advanced significantly.

Over two studies by the Reid group, a series of six and eight coordinate thio- and seleno-ether complexes of MX_5 (M = Nb[10] or Ta[2], X = F, Cl or Br) were synthesised. The reaction of three equivalents of Et_2S or one equivalent of Me_2Se with one equivalent of MF_5 in dichloromethane led to the formation of a 1:1 complex of $[MF_5(R_2E)]$. The complex, $[MF_5(R_2E)]$, was also obtained by the addition of neat R_2S (R = Me, Et) to MF_5, Scheme 5.1. The resulting products are extremely moisture sensitive and decompose readily, even in the solid state, via fluorination of the neutral ligand. The reaction of neat Me_2S with MF_5, led to the formation of the ionic $[NbF_4(Me_2S)_4][NbF_6]$. In all cases, the infrared spectra of $[MF_5(R_2E)]$ showed three bands, as expected for the C_{4v} geometry. This is confirmed by the $^{19}F\{^1H\}$ NMR spectra, which all (with one notable exception) show a broad single peak at room temperature which splits into two singlets in a 1:4 ratio, at low temperature, again indicative of the C_{4v} geometry, Table 5.1. The notable exception is $[NbF_5(Me_2Se)]$, which shows a singlet both at 295 K and 200 K. Although the presence of a singlet even at low temperature, could be explained by the weaker donor character of the selenoether ligand. The analogous tantalum complex also shows a singlet at room temperature, however upon cooling to 185 K, this complex does show a splitting of the resonances into two singlets in a 1:4 ratio, as expected. Alternatively, $[MF_4(Me_2S)_4][MF_6]$ each show a single broad $^{19}F\{^1H\}$ NMR resonance at room temperature, which separate, when cooled, into two resonances with a 2:3 integral. Upon further cooling to 200 K, $[NbF_4(Me_2S)][NbF_6]$ shows a ten-line pattern characteristic of $[NbF_6]^-$ and this was not observed for any of the other reported monodentate species.

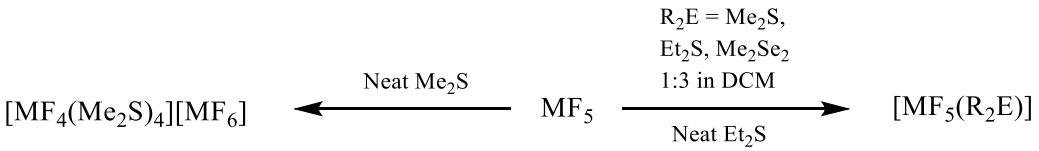

Scheme 5.1. Synthesis of $[MF_4(Me_2S)_4][MF_6]$, $[MF_5(Me_2S)]$, $[MF_5(Et_2S)]$ and $[MF_5(Me_2Se)]$ (M = Nb,[10] Ta [2]).

Table 5.1. A table of M-F IR bands and $^{19}F\{^1H\}$ NMR shifts for a series of niobium and tantalum thio- and seleno-ether species.[10,2]

Compound	Infrared ν(M-F) cm^{-1} (Nujol)	$\delta(^{19}F\{^1H\})$ (CD_2Cl_2)
$[NbF_5(Me_2S)]$	662s, 641m, 600s	150.5 (br) (295 K) 146.0 [F], 134.4 [4F] (253 K)
$[NbF_5(Me_2Se)]$	662s, 641m, 600s	143.2 (295 K) 144.2 (200 K)
$[NbF_5(Et_2S)]$	640sh, 614vs (br), 594s	141.6 (br) (295 K) 144.4 [F], 119.4 [4F] (253 K)
$[NbF_4(Me_2S)_4][NbF_6]$	678sh, 610s, 552m	136.3 (br) (295 K) 119.5 (s) [4F], 102.5 (s) [6F] (223 K) 119.5 (s) [4F], 102.5 (10 lines) [6F] (200 K)
$[TaF_5(Me_2S)]$	630s, 614s, 593s	79 (br) (295 K) 71.0 [F], 59.6 [4F] (190 K)
$[TaF_5(Me_2Se)]$	630sh, 612vs, 576vs	84.6 (br) (295 K) 71.0 [F], 61.0 [4F] (185 K)
$[TaF_5(Et_2S)]$	665sh, 630s, 576sh	82.8 (br) (295 K) 80.1 [F], 70.6 [4F] (190 K)
$[TaF_4(Me_2S)_4][TaF_6]$	606s, 576s	71.6 (br) (295 K) 63.1 [4F], 42.0 [6F] (220 K)

Colourless crystal of $[NbF_4(Me_2S)_4][NbF_6]$ grown from a refrigerated solution of the reaction mixture, provided confirmation of the formation of the 8-coordinate dodecacahedral cation, $[NbF_4(Me_2S)_4]^+$, Figure 5.1. The eight-coordinate geometry around the metal centre is not entirely unexpected for niobium or tantalum complexes.[3,17–19] Small yellow crystals of $[NbBr_5(Me_2S)]$ were also obtained in the same manner and show the expected octahedral geometry around the niobium, Figure 5.1.

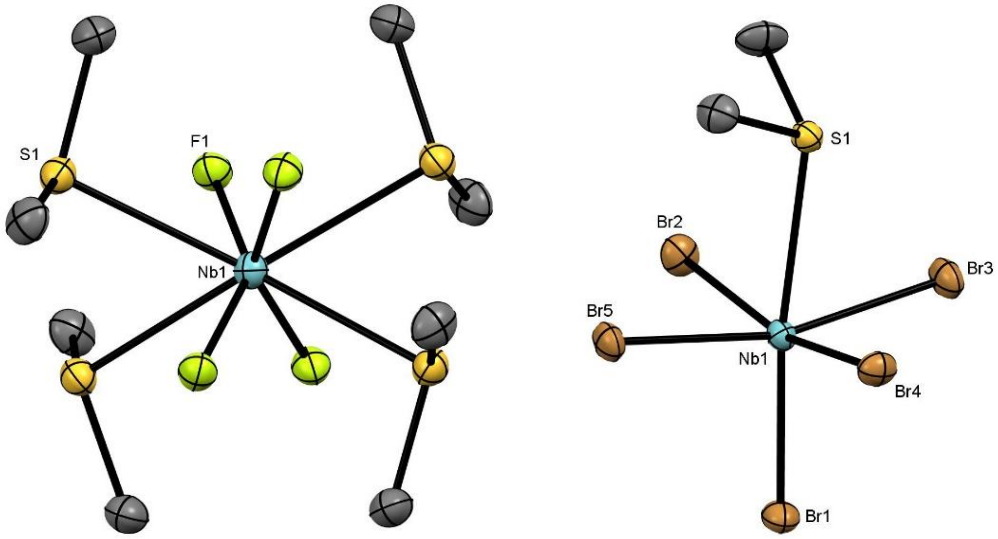

Figure 5.1. Crystal structures depicting the cation $[NbF_4(Me_2S)_4]^+$ (left) and $[NbBr_5(Me_2S)]$ (right). Hydrogen atoms are omitted for clarity. The cation in the crystal structure of $[NbF_4(Me_2S)][NbF_6]$ requires only a single Nb-F and Nb-S with the rest generated by symmetry.[10]

The formation of the metal chloride and metal bromide species, MX_5 (M = Nb or Ta; X = Cl, Br) are much more straightforward, and the resulting complexes are more stable than their metal fluoride analogues. They form the 1:1 $[MX_5(R_2E)]$ complexes, seemingly irrespective of the metal, halide, chalcogenoether or stoichiometry employed. They are synthesised via the addition of a solution of ligand to a stirring solution of the metal halide in dichloromethane and the synthesis can be performed at room temperature. Crystal structures have been described for $[NbBr_5(Me_2S)]$, $[NbCl_5(Me_2Se)]$ and $[TaCl_5(Me_2Se)]$.
The reactions of MX_5 (M = Nb[10] or Ta[2]; X = F, Cl or Br) with series of bidentate thio- and seleno-ethers of these metal halides have also been reported. A series of ionic species, $[MX_4\{RS(CH_2)_2SR\}][MX_6]$ (M = Nb, Ta; X = F; R = Me, Et, ^{i}Pr or M = Nb, Ta; X = Cl, Br; R = Me), were synthesised by the 1:1 reaction of the metal halide with the appropriate thioether. Crystal structures were obtained for $[MF_4\{MeS(CH_2)_2SMe\}][MF_6]$ (M = Nb, Ta), Figure 5.2, and $[NbF_4\{^iPrS(CH_2)_2S^iPr\}][NbF_6]$, providing evidence for the ionic speciation. The crystal structure of $[NbF_4\{MeS(CH_2)_2SMe\}][NbF_6]$ displays the cation, $[NbF_4\{MeS(CH_2)_2SMe\}]^+$, with the niobium in a dodecahedral geometry with the fluorides surrounding the metal centre in a flattened tetrahedral structure and the NbS_4 unit displayed an elongated tetrahedral structure. Evidence of the $[MF_6]^-$ ion could be easily identified by low temperature $^{19}F\{^1H\}$ NMR experiments, which show a distinct 10 line pattern at around 39 ppm. Due to the lack of suitable spectroscopic probes for the Cl and Br salts, the use of

infrared and Raman spectroscopy, alongside $^{93}Nb\{^{1}H\}$ NMR spectroscopy (where appropriate) were used to identify the ionic species.

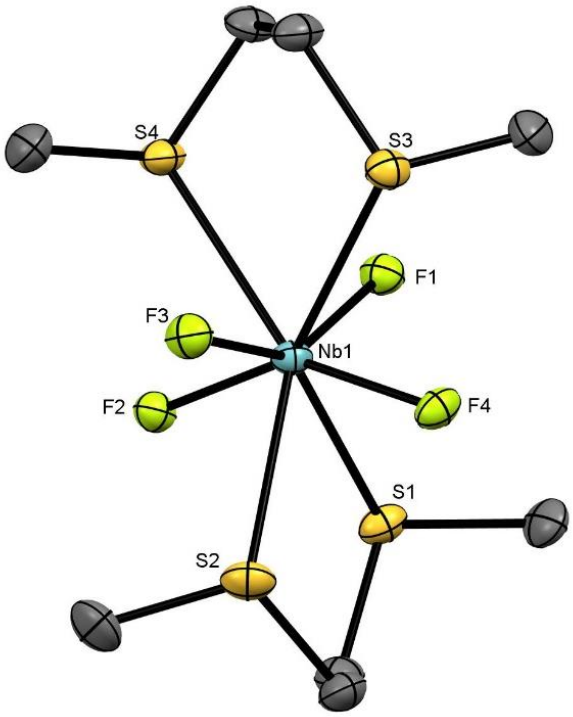

Figure 5.2. A crystal structure depicting the cation $[NbF_4\{MeS(CH_2)_2SMe\}]^+$ with the hydrogen atoms omitted for clarity.[10]

Table 5.2. A table showing M-X bands in the infrared (t_1u) and Raman spectra (a_1g) and the shift (where applicable) in the $^{93}Nb\{^{1}H\}$ NMR spectrum.[10,2]

Compound	*ν*(M-X)/ cm^{-1} (IR/Nujol)	*ν*(M-X)/ cm^{-1} (Raman)	$^{93}Nb\{^{1}H\}$ NMR (CD_2Cl_2, 295 K)
$[NbCl_4\{MeS(CH_2)_2SMe\}][NbCl_6]$	333	360	+3, +150[a]
$[NbBr_4\{MeS(CH_2)_2SMe\}][NbBr_6]$	232	214	+722
$[TaCl_4\{MeS(CH_2)_2SMe\}][TaCl_6]$	316	n/a	n/a
$[TaBr_4\{MeS(CH_2)_2SMe\}][TaBr_6]$	213	n/a	n/a

[a] *+150 tentatively ascribed to the dodecahedral cation but no corresponding resonance was found in the bromide complex.*

In contrast to the ionic species described above, reactions of the metal fluorides, chlorides and bromides all form bridged species of the form $[(MX_5)_2\{RSe(CH_2)_2SeR\}]$, when reacted with selenoethers, as confirmed by the crystal structure of $[(NbCl_5)_2\{MeSe(CH_2)_2SeMe\}]$, Figure 5.3. The metal halides, MX_5 (M = Nb or Ta, X = F, Cl or Br), can also be reacted with thio- and seleno-ethers with *o*-xylyl backbones, e.g. $[(NbCl_5)_2\{o\text{-}C_6H_4(CH_2SMe)_2\}]$ demonstrating that the donor atom is not the only factor in determining whether these species form ionic or bridging complexes, as steric demands contribute largely to this. These

complexes were all extremely air and moisture sensitive, with the chlorides and bromides proving to be more robust than their fluoride counterparts, which decompose readily via fluorination of the neutral ligand.

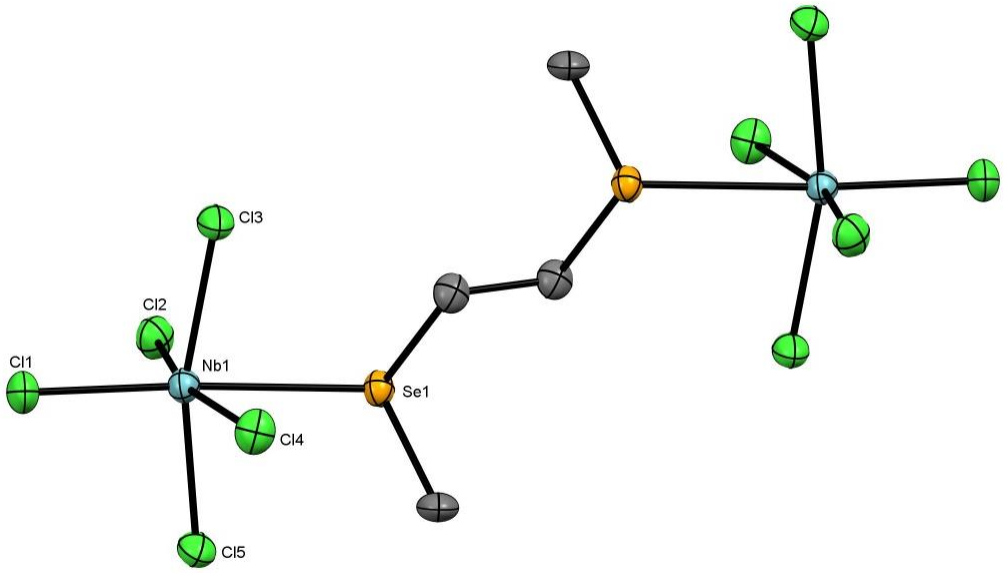

Figure 5.3. A crystal structure of the bridging species, [(NbCl$_5$)$_2${MeSe(CH$_2$)$_2$SeMe}].[10]

From the direct reaction of the metal halide with the ligand in dichloromethane, a further series of metal halide chalcogenoethers, [MCl$_5$(^{n}Bu$_2$E)] (M = Nb or Ta, E = S or Se; M = Ta, E = Te) and [(MCl$_5$)$_2${*o*-C$_6$H$_4$(CH$_2$SEt)$_2$}] has been reported.[20] These complexes were synthesised as candidates for single source precursors to ME$_2$ thin films. The development of single source precursors and the uses of these ME$_2$ thin films are discussed in Section 1.5. Chemical vapour deposition experiments were performed at a range of temperatures from 600 – 750 ˚C. The experiments using the tantalum analogues led to no deposition (except for some crystalline tellurium from [TaCl$_5$(^{n}Bu$_2$Te)]), while [(NbCl$_5$)$_2${*o*-C$_6$H$_4$(CH$_2$SEt)$_2$}] also did not deposit NbS$_2$. The mononuclear niobium species, [NbCl$_5$(^{n}Bu$_2$E)] (E = S or Se), on the other hand, have been demonstrated as suitable single source CVD precursors, and LPCVD experiments showed the successful growth of NbS$_2$ and NbSe$_2$ from their respective precursor. The formation of ME$_2$ films from these complexes is interesting as the M:E ratio in the precursor is only 1:1, and the deposition is also accompanied by a change in oxidation state from +5 to +4.

TaE_2 was not formed from similar LPCVD experiments and this may be explained by the higher molecular weights associated with tantalum complexes, hence their lower volatilities, and/or the increased stability of the +5 oxidation state for the 5d metal ion. The paper also describes the synthesis of $[TaX_5(Me_2Te)]$ (X = F, Cl or Br), the first evidence of a soft telluroether ligand coordinated to Ta(V), and confirmed by the crystal structure of $[TaCl_5(Me_2Te)]$. These telluroether complexes were made in a similar manner to $[MCl_5(^nBu_2E)]$ (E = S or Se), but at a lower temperature, and represent the highest oxidation state transition metal complexes with telluroether coordination structurally authenticated in the literature.[20]

A range of ionic tantalum(V) and niobium(V) halide complexes with phosphine co-ligands have been synthesised by the direct reaction of the niobium or tantalum halides with bidentate phosphines in MeCN solutions.[21] For example, reaction of MF_5 (M = Nb or Ta) with *o*-$C_6H_4(PMe_2)_2$, *o*-$C_6H_4(PPh_2)_2$ or $R_2P(CH_2)_2PR$ (R = Me or Et) all produced species of the form $[MF_4(L\text{-}L)_2][MF_6]$. While the corresponding reactions with MCl_5 produced the $[TaCl_4\{o\text{-}C_6H_4(PMe_2)_2\}_2][TaCl_6]$, $[NbCl_4\{o\text{-}C_6H_4(PMe_2)_2\}_2]Cl$ and $[NbCl_4\{Me_2P(CH_2)_2PMe_2\}_2][NbCl_6]$.[21] The salt formation was unambiguously identified by the crystal structures of $[MF_4\{o\text{-}C_6H_4(PMe_2)_2\}_2][MF_6]$ (M = Nb or Ta). The presence of the $[MF_6]^-$ ions were also identified in each case by the characteristic 10 line pattern in the $^{19}F\{^1H\}$ NMR spectra, at 103 ppm for $[NbF_6]^-$ and 39 ppm for $[TaF_6]^-$, as well as a 3:2 integral of this 10 line pattern to the other observed resonance. These complexes are contrasting to a series of niobium and tantalum halide phosphines described in 1978 by Jamieson and Lindsell.[22] The synthesis of mononuclear species with bidentate ligands of the form $[MCl_5(L\text{-}L)]$ (M = Nb or Ta; L-L = $PhP(CH_2)_2PPh$ or $MeP(CH_2)_2PMe$) were described and characterised by elemental analysis, ^1H NMR spectroscopy and $^{31}P\{^1H\}$ NMR spectroscopy. The authors did acknowledge that ionic species of the form $[MCl_4(L\text{-}L)][MCl_6]$ were possible, as a 7-coordinate species with five Cl ligands might be unstable due to the Cl···Cl repulsion. However, they concluded that the 8-coordinate cation may be too sterically crowded, especially with the bulkier ligands, such as dppe.[22] Given the formation of the crystallographically characterised complex $[NbCl_4\{Me_2P(CH_2)_2PMe_2\}_2][NbCl_6]$ described above, it is likely the steric clash of the 8-coordinate geometry of the cation is not large enough to be disfavoured over the increased Cl···Cl repulsion caused by the $[MX_5(L\text{-}L)]$ speciation proposed.

5.1.2 Complexes of [$NbSCl_3(L)_{1-3}$] and [$NbSCl_3(L\text{-}L)$]

Niobium sulfide halides are modest Lewis acids, readily forming complexes with neutral ligands from groups 15 and 16, although they have received much less study than the corresponding oxide halides.[3,23,24] Prior to recent developments, structurally characterised species were extremely limited, including [$NbSBr_3$(tht)] (tht = tetrahydrothiophene),[25] [$NbSCl_3(SPPh_3)$],[26,27] [$NbSCl_3(PMe_3)_3$][28] and [$NbSCl_3${$MeS(CH_2)_2SMe$}].[29]

Following the work within the Reid group investigating single source precursors for ME_2 (M = Nb or Ta, E = S or Se) thin films, a series of complexes, [$NbSCl_3$(L-L)] (L-L = $MeS(CH_2)_2SMe$, $^{i}PrS(CH_2)_2S^{i}Pr$, $MeS(CH_2)_3SMe$, $MeSe(CH_2)_3SeMe$ or $^{n}BuS(CH_2)_3S^{n}Bu$) were synthesised, alongside the complexes [$NbSCl_3(R_2E)$] (E = S or R = Me or ^{n}Bu, E = Se, R = ^{n}Bu).[29] The *n*-butyl ligands were targeted as potential CVD precursors. Reid and co-workers obtained the thio- and seleno-ether complexes by either the direct addition of $NbCl_5$ with $S(SiMe_3)_2$ and the appropriate thioether in dichloromethane, or by the addition of the thioether to a solution of [$NbSCl_3(MeCN)_2$].[30,31]While the addition of $S(SiMe_3)_2$ and Me_2S to $NbCl_5$ produced a yellow-green solid, the use of $^{n}Bu_2S$ led to a dark oil. Studies of an analogous tantalum species suggest a mononuclear speciation [$TaSCl_3(Me_2S)_2$] based on elemental analysis.[32] However, a structure showing the binuclear niobium complex, [$Nb_2S_2Cl_6(SMe_2)_2$], Figure 5.4, shows each metal centre occupied by a single Me_2S ligand, *trans* to a chloride ligand, and bridged by two Cl ligands. This speciation is also confirmed by the ^{1}H NMR spectrum, which shows a single resonance consistent with the single proton environment. The spectroscopic data for the [$NbSCl_3(^{n}Bu_2S)$] complex suggests an analogous structure. The relevant IR bands for these niobium species are shown in Table 5.3.

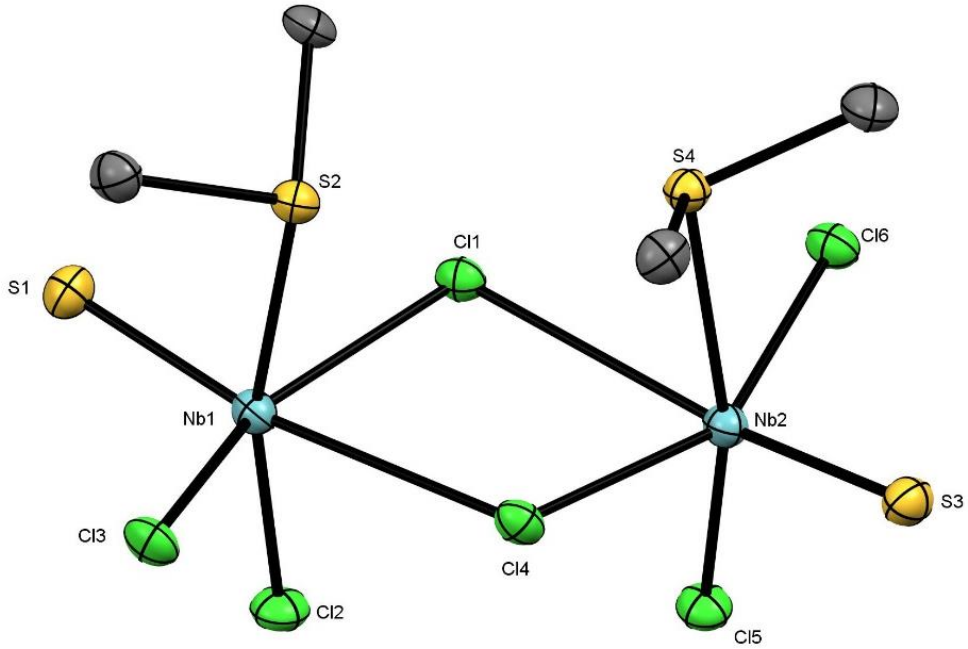

Figure 5.4. A crystal structure depicting the binuclear [$Nb_2S_2Cl_6(Me_2S)_2$]. Hydrogen atoms are omitted for clarity. The bridging Cl ligands are highly asymmetric. Selected bond lengths (Å): Nb1-Cl1 = 2.420(2), Nb1-Cl4 = 2.921(2).[29]

The acetonitrile adduct, [$NbSCl_3(MeCN)_2$], is used in the synthesis of the bidentate species, [$NbSCl_3$(L-L)] (L-L = $MeS(CH_2)_2SMe$, $^{i}PrS(CH_2)_2S^{i}Pr$, $MeS(CH_2)_3SMe$ or $MeSe(CH_2)_3SeMe$), owing to the entropically favoured coordination of a chelating bidentate ligand. These reactions form powdered solids ranging from green to brown, likely due to trace impurities of $Nb_2S_3Cl_4$, whereas the synthesis using $^{n}BuS(CH_2)_3S^{n}Bu$ resulted in a green oil. The key infrared bands, *ν*(Nb=S) and *ν*(Nb-Cl), for each of the complexes are shown in Table 5.3. Crystal structures of [$NbSCl_3${$MeSe(CH_2)_3SeMe$}], [$NbSCl_3${$MeS(CH_2)_2SMe$}] and [$NbSCl_3${$^{i}PrS(CH_2)_2S^{i}Pr$}] were obtained and all show a mononuclear pseudo-octahedral niobium complex. There is some S/Cl disorder in the selenoether structure, which is quite common in these species, however, the other two crystals show no evidence of such disorder. The ^{1}H NMR spectrum of [$NbSCl_3${$MeS(CH_2)_2SMe$}] in CD_2Cl_2 at 295 K shows two very broad MeS resonances, and two CH_2 resonances, consistent with the two distinct environments formed by the ligand being *trans* S/Cl. The complex [$NbSeCl_3(MeCN)_2$] was synthesised from $NbCl_5$ and $Se(SiMe_3)_2$ in MeCN to form a brown solid. Attempts were made to prepare dithio- or diseleno-ether complexes from [$NbSeCl_3(MeCN)_2$], however these were ultimately unsuccessful. It is unclear if this is due to the relatively low Lewis-acidity of the $NbSeCl_3$ unit, or competition of the soft-donor ligands with the acetonitrile ligands, although it is likely to be a combination of these factors.[29]

Table 5.3. A table of v(Nb=S) and v(Nb-Cl) bands for a series of niobium thio-chlorides.[29]

Compound	*v*(Nb=S)/ cm^{-1} (IR/Nujol)	*v*(Nb-Cl)/ cm^{-1} (IR/Nujol)
$[NbSCl_3(MeCN)_2]$	530	355, 343, 319
$[NbSeCl_3(MeCN)_2]$	397[a]	377, 344
$[NbSCl_3(Me_2S)]$	530	369, 356, 322
$[NbSCl_3(^nBu_2S)]$	544	387, 374, 359
$[NbSCl_3(^nBu_2Se)]$	530	380, 366, 355
$[NbSCl_3\{MeS(CH_2)_2SMe\}]$	526	361, 349, 319
$[NbSCl_3\{MeS(CH_2)_3SMe\}]$	524	369, 345, 323
$[NbSCl_3\{MeSe(CH_2)_3SeMe\}]$	521	342, 320
$[NbSCl_3\{^iPrS(CH_2)_2S^iPr\}]$	527	365, 348, 318
$[NbSCl_3\{^nBuS(CH_2)_2S^nBu\}]$	529	349, 322

[a] *Tentatively assigned Ta=Se terminal bond stretch for the only niobium seleno-chloride described.*

5.1.3 Tantalum sulfide and selenide halides

The complexes $TaECl_3$ (E = S, Se) were first obtained some 50 years ago by reaction of $TaCl_5$ with Sb_2E_3 or Bi_2E_3 in CS_2,[24,32] but in marked contrast to $NbECl_3$,[27,29,30,33] only a very small number of $TaECl_3$ complexes have been described. These include $[TaSCl_3(MeCN)_2]$,[30,32] $[TaSCl_3(SMe_2)_2]$, $[TaSCl_3(tht)_2]$ (tht = tetrahydrothiophene) and $[TaSCl_3\{PhS(CH_2)_2SPh\}]$,[32] the last of which was structurally characterized by single crystal X-ray diffraction. The tantalum thiohalides, $TaSX_3$ (X = Cl or Br) were first synthesised through the addition of Sb_2S_3 to three mol. equivalents of TaX_5 in CS_2. The resulting $TaSX_3$ was then reacted with the appropriate ligand, such as $PhS(CH_2)_2SPh$, and left stirring with heating for several days. Green crystals of $[TaSCl_3\{PhS(CH_2)_2SPh\}]$ were obtained by recrystallization of the product from a CS_2 solution. The structure displays a mononuclear pseudo-octahedral geometry with a terminal Ta=S bond. There is also mention of likely S/Cl disorder in the molecule due to the shorter than expected Ta-Cl bond *trans* to the ligand. The terminal Ta=S bond was identified in each case by the characteristic IR band at 505 cm^{-1}. This band is significantly shifted from starting materials at 463 cm^{-1} ($TaSCl_3$) and 448 cm^{-1} ($TaSBr_3$), allowing quick confirmation of successful coordination in the solid state. The lower frequency evident in the $TaSX_3$ species are attributed to $TaSX_3$ consisting of bridging sulfide ligands which are cleaved upon coordination. This behaviour is in direct contrast to the niobium analogues which have similar Nb=S stretches with or without a coordinated thioether. The mononuclear six-coordinate geometries were assigned based on

comparisons to similar $NbOCl_3$ species. The ^1H NMR spectra were obtained at room temperature, and based upon the structure of $[NbSCl_3(Me_2S)]$, Figure 5.4, it is possible this tantalum species also adopts a chloride bridge with a single ligand attributed to each metal centre. This could possibly be determined from low temperature ^1H NMR spectroscopy as splitting of the broad S-C$\boldsymbol{H}_3$ resonance would confirm two separate Me_2S environments.

Table 5.4. A table of v(Ta=S) bands for a series of tantalum thio-chlorides, v(Ta-Cl) bands were not given.[32]

Compound	ν(Ta=S)/ cm^{-1} (IR/Nujol)
$[TaSCl_3]$	463
$[TaSBr_3]$	448
$[TaSCl_3(Me_2S)_2]$	510
$[TaSBr_3(Me_2S)_2]$	506
$[TaSCl_3(tht)_2]$	505
$[TaSBr_3(tht)_2]$	504
$[TaSCl_3(MeCN)_2]$	510
$[TaSBr_3(MeCN)_2]$	508
$[TaSCl_3\{PhS(CH_2)_2SPh\}]$	516, 510
$[TaSBr_3\{PhS(CH_2)_2SPh\}]$	512, 508

5.1.4 Aims

This chapter aims to develop an underexplored series of tantalum thiochloride complexes with a range of chalcogenoethers. Long chain chalcogenoethers, such as $^nBuS(CH_2)_3S^nBu$, will be used to synthesise possible candidates for single source precursors for LPCVD of TaS_2. Once a synthetic method is established, it will be used in an attempt to make $[TaSCl_3(dppe)]$ in order to probe the tantalum(V)-phosphine bonds.

5.2 Results and Discussion

5.2.1 Synthesis of $TaSCl_3$ thio- and seleno-ether complexes

Tantalum pentachloride was reacted with $S(SiMe_3)_2$ and a range of thioethers in anhydrous dichloromethane to form the unusual tantalum thioether complexes, $[TaSCl_3(L\text{-}L)]$ (L-L = $PhSCH_2CH_2SPh$, $MeSCH_2CH_2SMe$, $MeSCH_2CH_2CH_2SMe$, $^nBuSCH_2CH_2CH_2S^nBu$ or $^i PrSCH_2CH_2S^i Pr$). This range was chosen to allow for comparisons to the literature examples of $[NbSCl_3(L\text{-}L)]$ and to the known compound $[TaSCl_3\{PhSCH_2CH_2Ph\}]$.[29,32] The ligand $^n BuSCH_2CH_2CH_2S^n Bu$ was also targeted, with a view to testing the resulting tantalum complex as a single-source precursor for the deposition of thin films of TaS_2.

Addition of one mol. equivalent of the dithioethers to $TaCl_5$ in anhydrous CH_2Cl_2 gave bright yellow solutions. One mol. equivalent of $S(SiMe_3)_2$ in CH_2Cl_2 was then added dropwise to these solutions, causing the colour of the reactions to darken and some precipitate to form, most likely a polymeric tantalum decomposition product, which was filtered off and discarded. The filtrates yielded dark solids with microanalyses confirming the composition as $[TaSCl_3(L\text{-}L)]$. The colours of the solids varied, even when comparing two samples of the same species, with colours ranging from yellow to orange to brown to black. Similar colour variation has been observed in the $NbSCl_3$ systems and, in these systems, was attributed to the presence of small amounts of disulfide ($[S_2]^{2-}$) ligands in some samples, leading to the formation of complexes such as $[Nb_2Cl_4S_3(tht)_4]$ (tht = tetrahydrothiophene).[25,29,34] Although similar disulfide species have not been identified in the literature for these tantalum thiochloride systems, it is a likely explanation for the differences in colour amongst these samples. Infrared and NMR spectra indicated separate batches of the same complex with different colours were spectroscopically identical, and the microanalytical data were consistent with the desired products and thus impurities are likely very minor.

The solid complexes also darken and become sticky over time, even in inert and anhydrous conditions, with the long chain thioether complexes, such as $[TaSCl_3(^n BuSCH_2CH_2CH_2S^n Bu)]$, being particularly oily low-melting solids. For most of the complexes the single crystals selected for the X-ray analysis were also intensely coloured, e.g. orange-brown for $[TaSCl_3(MeSCH_2CH_2SMe)]$, purple for $[TaSCl_3(^i PrSCH_2CH_2S^i Pr)]$ and dark green for $[TaSCl_3(MeSCH_2CH_2CH_2SMe)]$. Attempts to prepare the complexes from $[TaSCl_3(MeCN)_2]$[32,35] were unsuccessful, with the MeCN competing with the thioether as shown by retention of MeCN in the ^1H NMR spectra and infrared spectra even after isolating and washing a solid product. These reactions were performed in acetonitrile and it is possible they may have been more successful if performed

in CH_2Cl_2 with the addition of a small amount of MeCN, however given the complexes formed readily in CH_2Cl_2 without the need for the acetonitrile adduct, this was not pursued. Crystals of [$TaSCl_3$(^{n}BuS$CH_2CH_2CH_2S^n$Bu)] were obtained from a CH_2Cl_2 solution layered with n-hexane. The structure, Figure 5.5, reveals six-coordinate tantalum in a pseudo-octahedal geometry, in a *meso*-conformation, with *mer*-chlorines and the dithioether *trans* to S/Cl, as is typical of these systems. Disorder of the S and Cl *trans* to the neutral ligands in these metal sulfide chlorides is common and due to the similar scattering power of S^{-2} and Cl^-, it is not possible to completely rule out disorder in such systems.[27,29,32,36] However, in the case of [$TaSCl_3$(^{n}BuS$CH_2CH_2CH_2S^n$Bu)], the structure appears disorder-free. The d(Ta1-S1) = 2.199(3) Å and d(Ta1-Cl2) = 2.283(3) Å are significantly different and are within the expected ranges for these bond types. It is notable that the Ta-$S_{thioether}$ distances are also significantly different d(Ta1–S3) = 2.684(2) and d(Ta1–S2) = 2.791(2) Å, which is attributed to the *trans* influence Ta=S > Ta-Cl also noted in similar systems. The axial Ta-Cl are also significantly longer, 2.360(2) and 2.345(2) Å than the equatorial chloride.

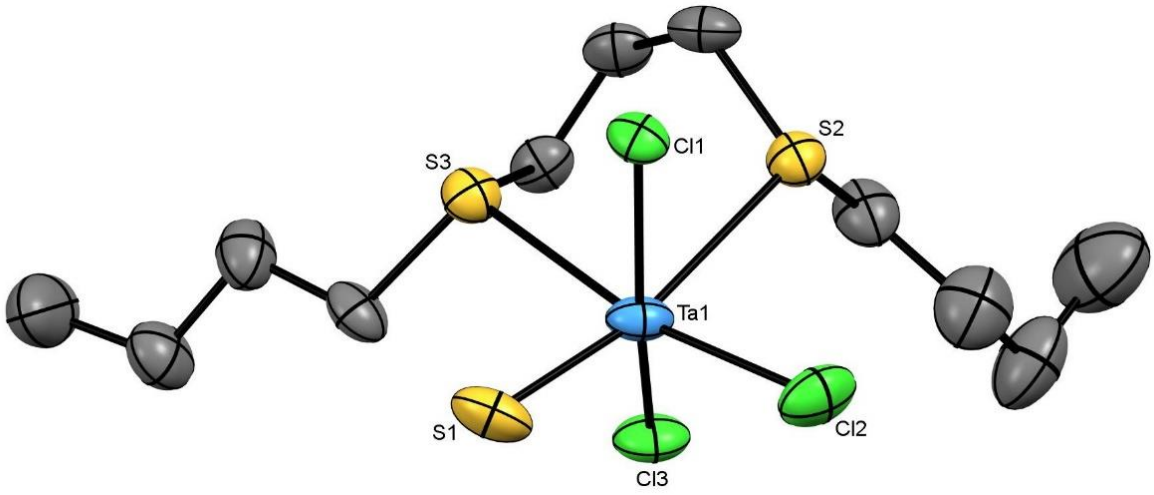

Figure 5.5. View of the structure of [$TaSCl_3$(^{n}BuS$CH_2CH_2CH_2S^n$Bu)] with atom numbering scheme. Ellipsoids are shown at the 50% probability level and H atoms are omitted for clarity. Selected bond lengths (Å) and angles (°): Ta1–Cl1 = 2.360(2), Ta1–S3 = 2.684(2), Ta1–Cl3 = 2.345(2), Ta1–S1 = 2.199(3), Ta1–S2 = 2.791(2), Ta1–Cl2 = 2.283(3), Cl1–Ta1–S3 = 82.12(7), Cl1–Ta1–S2 = 75.16(7), S3–Ta1–S2 = 80.59(7), Cl3–Ta1–Cl1 = 156.78(8), Cl3–Ta1–S3 = 82.87(8), Cl3–Ta1–S2 = 84.99(8), S1–Ta1–Cl1 = 97.24(8), S1–Ta1–S3 = 90.45(10), S1–Ta1–Cl3 = 100.49(9), S1–Ta1–S2 = 168.90(9), S1–Ta1–Cl2 = 103.81(11), Cl2–Ta1–Cl1 = 95.64(9), Cl2–Ta1–S3 = 165.74(9), Cl2–Ta1–Cl3 = 94.56(9), Cl2–Ta1–S2 = 85.22(9).

X-ray structures were also determined for [$TaSCl_3(MeSCH_2CH_2SMe)$] and [$TaSCl_3(^iPrSCH_2CH_2S^iPr)$] (Figures 5.6 and 5.7), and here the very similar bond lengths of d(Ta=S) and d(Ta-Cl2) and the similar Ta-S bond lengths to the dithioether ligands clearly show that disorder is present. For all the described thio- and seleno-ether structures, attempts were made to account for any S/Cl disorder, however, these did not significantly improve the model, and whilst the structures serve to confirm the basic geometries, comparisons of the geometric data are unreliable. The coordinated dithioethers in both structures are the *DL* diastereoisomer.

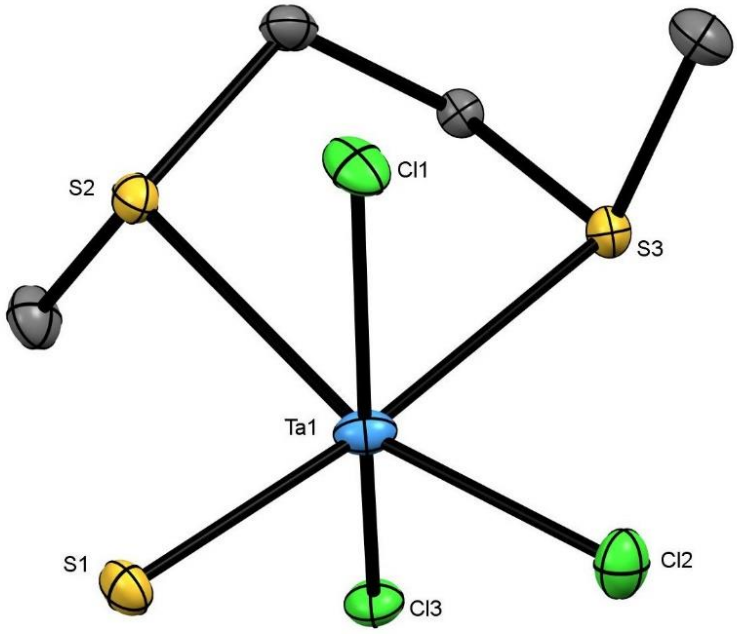

Figure 5.6. View of the structure of [$TaSCl_3(MeSCH_2CH_2SMe)$] with numbering scheme adopted. Ellipsoids are shown at the 50% probability level. Note that S1 and Cl2 are disordered. Selected bond lengths (Å) and angles (°): Ta1–S3 = 2.7243(13), Ta1–Cl3 = 2.3600(12), Ta1–S1 = 2.2301(13), Ta1–Cl2 = 2.2642(13), Ta1–S2 = 2.6993(12), Ta1–Cl1 = 2.3522(13), Cl3–Ta1–S3 = 76.71(4), Cl3–Ta1–S2 = 84.72(4), S1–Ta1–S3 168.01(5), S1–Ta1–Cl3 = 96.24(5), S1–Ta1–Cl2 = 105.79(5), S1–Ta1–S2 = 91.23(4), S1–Ta1–Cl1 = 97.98(5), Cl2–Ta1–S3 = 84.83(5), Cl2–Ta1–Cl3 = 96.45(5), Cl2–Ta1–S2 = 162.66(5), Cl2–Ta1–Cl1 = 96.37(5), S2–Ta1–S3 = 78.58(4), Cl1–Ta1–S3 = 86.10(4), Cl1–Ta1–Cl3 = 157.48(5), Cl1–Ta1–S2 = 77.61(4).

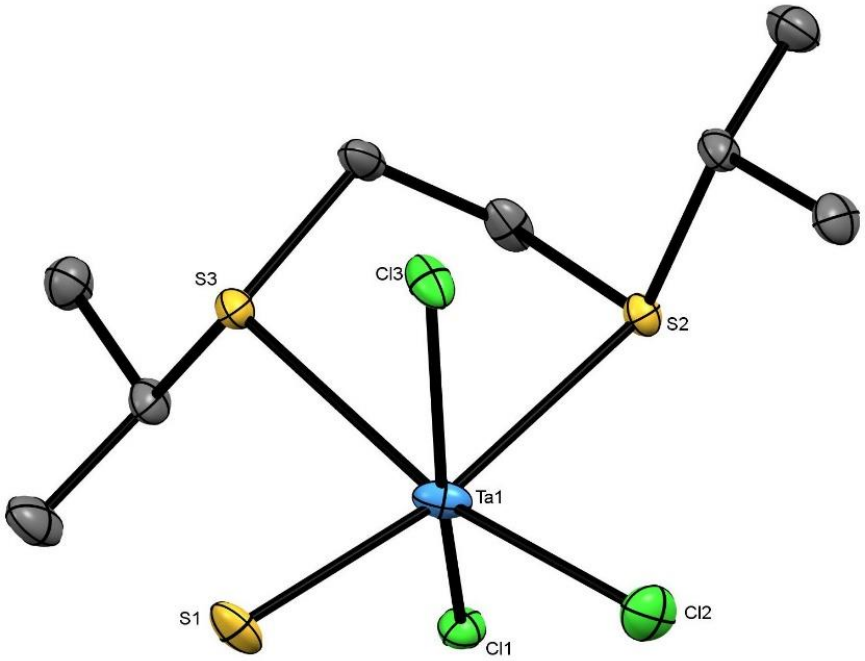

Figure 5.7. View of the structure of [TaSCl$_3$(^{i}PrSCH$_2$CH$_2$S^{i}Pr)] with numbering scheme adopted. Ellipsoids are shown at the 50% probability level and H atoms are omitted for clarity. Note that S1 and Cl2 are disordered Selected bond lengths (Å) and angles (°): Ta1–Cl1 = 2.3509(4), Ta1–Cl3 = 2.3559(5), Ta1–Cl2 = 2.2442(5), Ta1–S2 = 2.7487(5), Ta1–S3 = 2.7375(5), Ta1–S1 = 2.2339(5), Cl1–Ta1–Cl3 = 155.464(17), Cl1–Ta1–S2 = 76.447(15), Cl1–Ta1–S3 = 85.118(15), Cl3–Ta1–S2 = 83.485(15), Cl3–Ta1–S3 = 77.214(15), Cl2–Ta1–Cl1 = 97.282(17), Cl2–Ta1–Cl3 = 96.615(18), Cl2–Ta1–S2 89.812(17), Cl2–Ta1–S3 = 167.641(17), S3–Ta1–S2 = 78.929(14), S1–Ta1–Cl1 = 98.236(17), S1–Ta1–Cl3 = 97.905(18), S1–Ta1–Cl2 = 103.941(19), S1–Ta1–S2 = 165.867(16), S1–Ta1–S3 = 87.635(17).

In the IR spectra the ν(Ta=S) is found as a medium intensity feature ~ 505-510 cm^{-1}, except for [TaSCl$_3$(PhSCH$_2$CH$_2$SPh)] where there are two bands at 513, 519 cm^{-1}; neither corresponds to any dithioether ligand modes, and the splitting is presumably due to solid state effects. Importantly, Rice *et al.* also made note of two bands in the IR spectrum of [TaSBr$_3${PhS(CH$_2$)$_2$SPh}], noting that it was unusual as the crystal structure of the species might be expected to have shown if there were two distinct domains for the Ta=S groups, which would give rise to the two Ta=S stretches.[32] The ν(Ta-Cl) are assigned as two bands which lie in the range 305-360 cm^{-1}. The range of values is consistent with the values for the [NbSCl$_3$(L-L)] analogues, comparisons can be seen in Table 5.5. On the basis of the molecular symmetry, it would be expected that three Ta-Cl bands would be visible, however

the bands are broad and bands are likely overlapping. The ^{1}H NMR spectrum of [$TaSCl_3$(PhSCH_2CH_2SPh)] in CD_2Cl_2 at 295 K shows a single δ(CH_2) resonance indicating fast exchange, but upon cooling the solution to 223 K, two δ(CH_2) resonances are present, consistent with the expected structure, Figure 5.8. The ^{1}H NMR spectra of the dithioalkane complexes mostly show two RS- and two SCH_2 (backbone) resonances at room temperature as broad singlets distinguishing the donor groups which are inequivalent in these structures, and consistent with stronger donation in the alkyl substituted ligands. Cooling of the solutions, further results in the reversible appearance of more complex resonance patterns, no doubt due to the slowing of pyramidal inversion at the coordinated sulfur, Figure 5.8.

Table 5.5. A table of ν(Ta=S) and ν(Ta-Cl) bands for a series of tantalum thio-chlorides and some analogous niobium complexes for comparison.[29]

Compound	*ν*(M=S)/ cm^{-1} (IR/Nujol)	*ν*(M-Cl)/ cm^{-1} (IR/Nujol)
[$TaSCl_3${$MeS(CH_2)_2SMe$}]	508	352, 327
[$TaSCl_3${$PhS(CH_2)_2SPh$}]	519, 513[a]	360, 320
[$TaSCl_3${$^{i}PrS(CH_2)_2S^{i}Pr$}]	509	351, 329
[$TaSCl_3${$MeS(CH_2)_3SMe$}]	507	326 (br)
[$TaSCl_3${$^{n}BuS(CH_2)_3S^{n}Bu$}]	508	340, 328
[$TaSCl_3${$MeSe(CH_2)_2SeMe$}]	507	348, 326
[$TaSCl_3${$^{n}BuS(CH_2)_3Se^{n}Bu$}]	508	331, 307
[$NbSCl_3${$MeS(CH_2)_2SMe$}]	526	361, 349, 319
[$NbSCl_3${$MeS(CH_2)_3SMe$}]	524	369, 345, 323
[$NbSCl_3${$MeSe(CH_2)_3SeMe$}]	521	342, 320
[$NbSCl_3${$^{i}PrS(CH_2)_2S^{i}Pr$}]	527	365, 348, 318
[$NbSCl_3${$^{n}BuS(CH_2)_2S^{n}Bu$}]	529	349, 322

[a] *Two bands observed for this species, consistent with literature values.*[32]

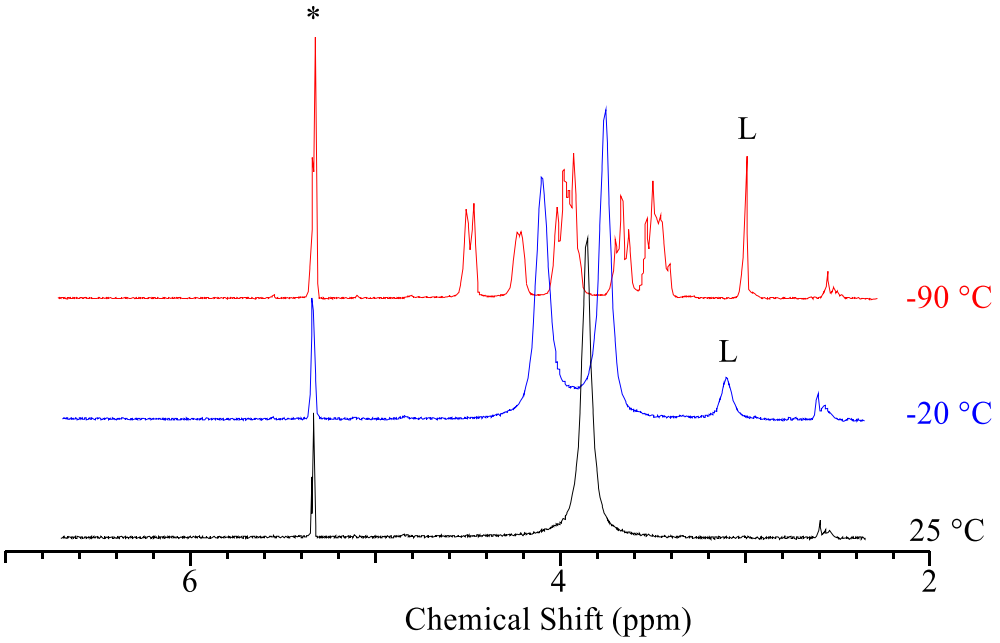

Figure 5.8. Three overlaid ^{1}H NMR spectra of [$TaSCl_3${$PhS(CH_2)_2SPh$}] in CD_2Cl_2 at 25 °C (black), -20 °C (blue) and -90 °C (red). The spectra show a splitting of the ethylene backbone proton resonances. The peak attributed to solvent, CD_2Cl_2 is shown (*) and upon cooling a peak attributed to free ligand appears (L).

In the case of the selenoether complexes, the diselenoethers, $MeSe(CH_2)_2SeMe$, $MeSe(CH_2)_3SeMe$ and $^{n}BuSe(CH_2)_3Se^{n}Bu$, were added to solutions of $TaCl_5$ in CH_2Cl_2, followed by one molar equivalent of $S(SiMe_3)_2$. For $MeSe(CH_2)_2SeMe$ and $^{n}BuSe(CH_2)_3Se^{n}Bu$, the resulting purple-black solids were [$TaSCl_3$(diselenoether)], and although [$TaSCl_3${$MeSe(CH_2)_3SeMe$}] is evident in the IR and ^{1}H NMR spectra, attempts to isolate the product cleanly were unsuccessful. Dark purple crystals of the diselenahexane complex [$TaSCl_3${$MeSe(CH_2)_2SeMe$}] were obtained by laying a dichloromethane solution of the product with hexane. Structural analysis via single crystal X-ray diffraction shows a similar geometry to the dithioether complexes, Figure 5.9, with a five-membered chelate ring formed by the neutral ligand and S/Cl disorder *trans* to the diselenoether. The IR and ^{1}H NMR spectra of [$TaSCl_3${$MeSe(CH_2)_2SeMe$}] are broadly similar to those of [$TaSCl_3${$MeS(CH_2)_2SMe$}] and the $^{77}Se\{^{1}H\}$ NMR spectrum (CD_2Cl_2, 295 K) of the product shows two resonances due to the two selenium environments, *trans* to Cl and S (144 and 186 ppm, respectively). A small amount of Me_2Se_2 is also evident (266 ppm); this is most likely a result of some elimination of $-CH_2CH_2-$ from the ligand backbone in solution.[7] However, the ^{1}H NMR spectrum of [$TaSCl_3$($^{n}BuSeCH_2CH_2CH_2Se^{n}Bu$)] is little different to that of the free diselenoether, with less splitting observed, the resonances are broader, likely

owing to the lability of the complex in solution. This complex does not show any resonances in the $^{77}Se\{^{1}H\}$ NMR spectrum, which is consistent with rapid dissociation in the case of the larger (six-membered) chelate ring complex.

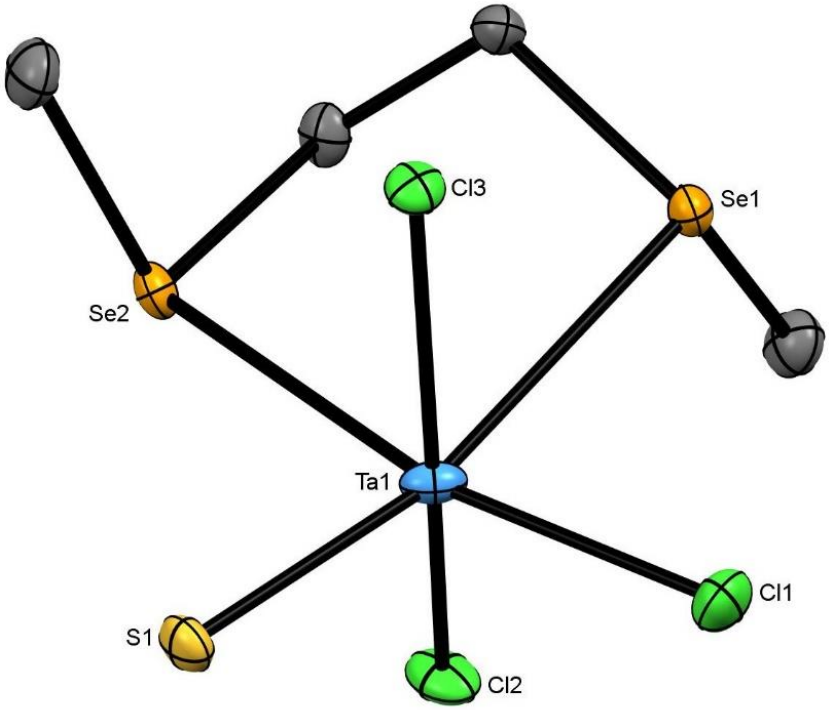

Figure 5.9. View of the structure of [TaSCl$_3$(MeSeCH$_2$CH$_2$SeMe)] with atom numbering scheme. Thermal ellipsoids are drawn at the 50% probability level and H atoms are omitted for clarity. Note that S1 and Cl1 are disordered Selected bond lengths (Å) and angles (°): Ta1–Se1 = 2.8412(5), Ta1–Se2 = 2.8050(5), Ta1–Cl3 = 2.3592(11), Ta1–Cl1 = 2.2671(12), Ta1–Cl2 = 2.3543(12), Ta1–S1 = 2.2293(12), Se2–Ta1–Se1 = 80.046(14), Cl3–Ta1–Se1 = 76.31(3), Cl3–Ta1–Se2 = 85.05(3), Cl1–Ta1–Se1 = 83.77(4), Cl1–Ta1–Se2 = 162.78(4), Cl1–Ta1–Cl3 = 96.85(5), Cl1–Ta1–Cl2 = 96.26(5), Cl2–Ta1–Se1 = 86.58(3), Cl2–Ta1–Se2 = 77.01(3), Cl2–Ta1–Cl3 = 157.11(4), S1–Ta1–Se1 = 168.12(3), S1–Ta1–Se2 = 90.35(3), S1–Ta1–Cl3 = 96.05(4), S1–Ta1–Cl1 = 106.41(5), S1–Ta1–Cl2 = 98.13(4).

Reactions of $TaCl_5$, $S(SiMe_3)_2$ and the monodentate ligands S^nBu_2 or Se^nBu_2 in anhydrous CH_2Cl_2 solution were also attempted, as it was anticipated that these products may be potential CVD precursors. However, unfortunately these reactions produced black powders with highly variable analytical composition, and importantly these lacked any IR spectral

evidence for a Ta=S feature. In solution, the ^{1}H spectra, and for the selenoether compound, the ^{77}Se NMR spectrum showed resonances only due the uncoordinated chalcogenoether, and the nature of these black products is unknown. Attempts to form these complexes via addition of a small amount of MeCN were not attempted due to competition of MeCN proving to be problematic in the bidentate systems. The niobium systems, $[NbSCl_3(SR_2)]$ (R = Me, ^{n}Bu) and $[NbSCl_3(Se^{n}Bu_2)]$ are discussed above, Section 5.1.2, and exist as dimers of the form $[Nb_2S_2Cl_4(\mu\text{-}Cl)_2(SMe_2)_2]$, with the sulfides terminal in plane and with *syn* axial SMe_2 ligands.[29] Also a red 2:1 complex $[TaSCl_3(SMe_2)_2]$ has been described in the literature, discussed in Section 5.1.3, although it has very limited characterisation.[32] As such it is possible these species could form either the mononuclear $[TaSCl_3(ER_2)_2]$ or the binuclear $[Ta_2S_2Cl_4(\mu\text{-}Cl)_2(ER_2)_2]$, however, to-date we have been unable to isolate either type.

5.2.2 Chemical Vapour Deposition Studies

Complexes with *n*-butyl substituents were targeted as potential single source CVD reagents since these can undergo β-hydride elimination on heating, Section 1.5.2, often providing a low energy pathway to the metal chalcogenide thin film material.[29,37–39] Low pressure CVD experiments were performed as described in Section 5.4.2 under guidance from Fred Robinson. Attempts to deposit TaE_2 thin films by low pressure CVD were carried out using $[TaSCl_3(^{n}BuSCH_2CH_2CH_2S^{n}Bu)]$ and $[TaSCl_3(^{n}BuSeCH_2CH_2CH_2Se^{n}Bu)]$ as precursors. LPCVD of $[TaSCl_3(^{n}BuSCH_2CH_2CH_2S^{n}Bu)]$ gave no deposit, and $[TaSCl_3(^{n}BuSeCH_2CH_2CH_2Se^{n}Bu)]$ gave a red coloured film. These red coloured films proved to be only elemental selenium, as demonstrated through grazing incidence X-ray diffraction (GIXRD), scanning electron microscopy (SEM) and energy dispersive X-ray (EDX) analysis, with no evidence for any TaE_2, Figures 5.10 - 5.12.

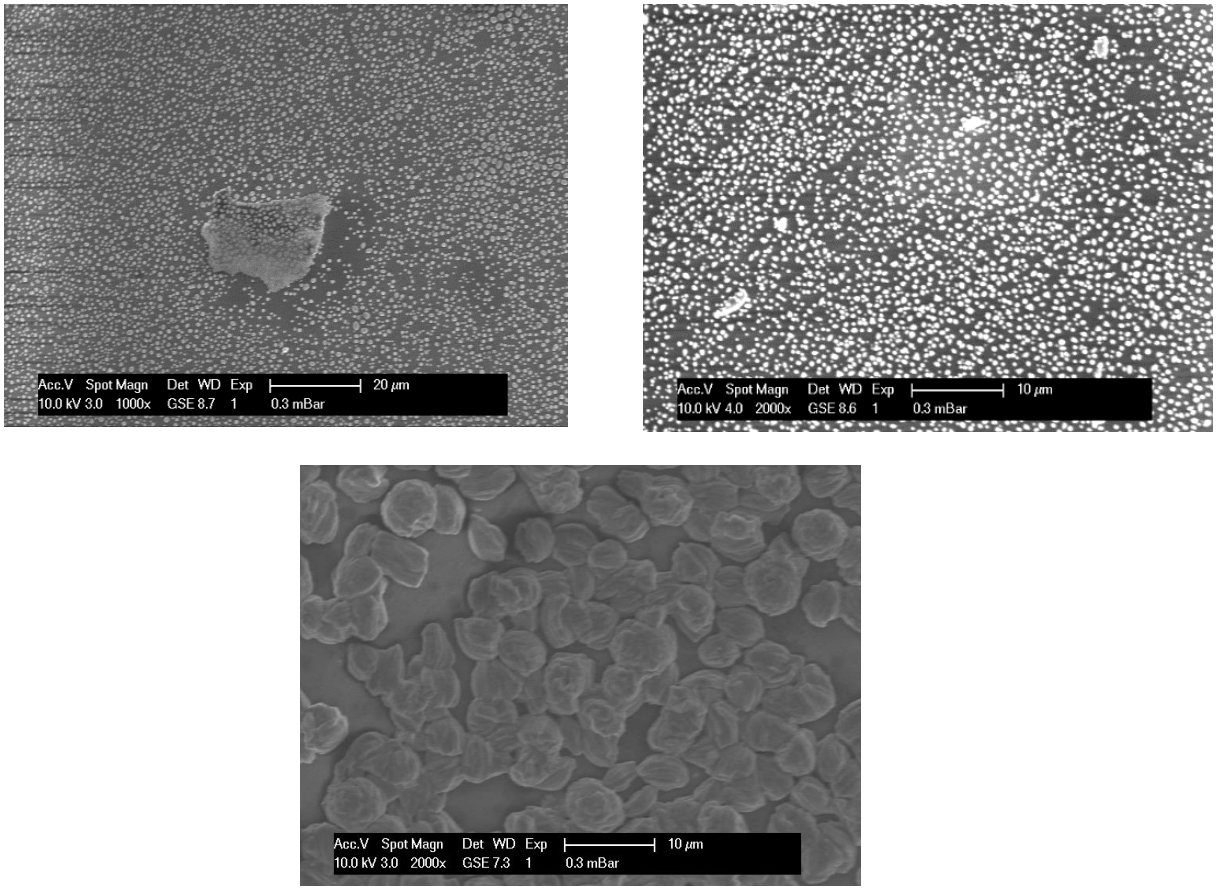

Figure 5.10. SEM analysis of the deposit grown onto SiO_2 substrates (elemental Se) via low pressure CVD using [$TaSCl_3(^nBuSeCH_2CH_2CH_2Se^nBu)$].

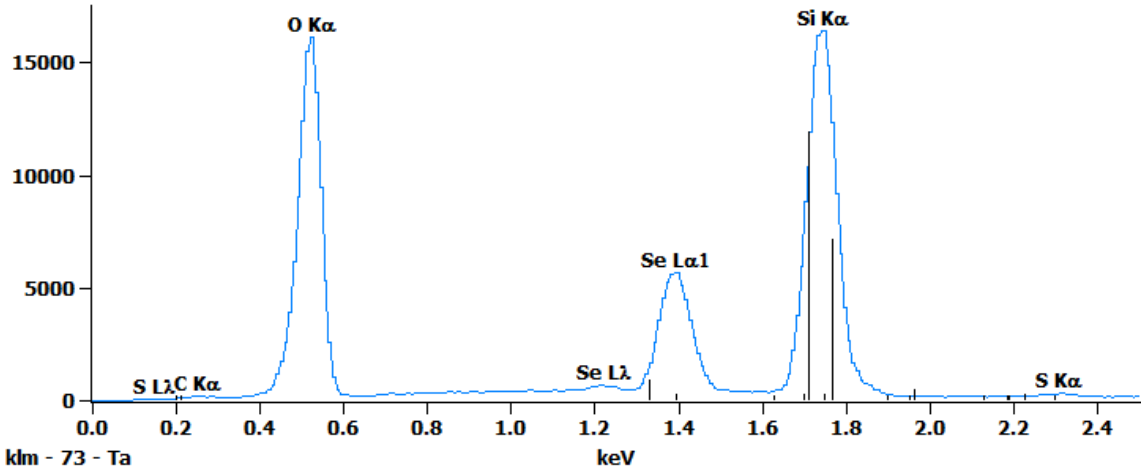

Figure 5.11. EDX analysis of the deposit grown onto SiO_2 substrates (elemental Se) via low pressure CVD using [$TaSCl_3(^nBuSeCH_2CH_2CH_2Se^nBu)$].

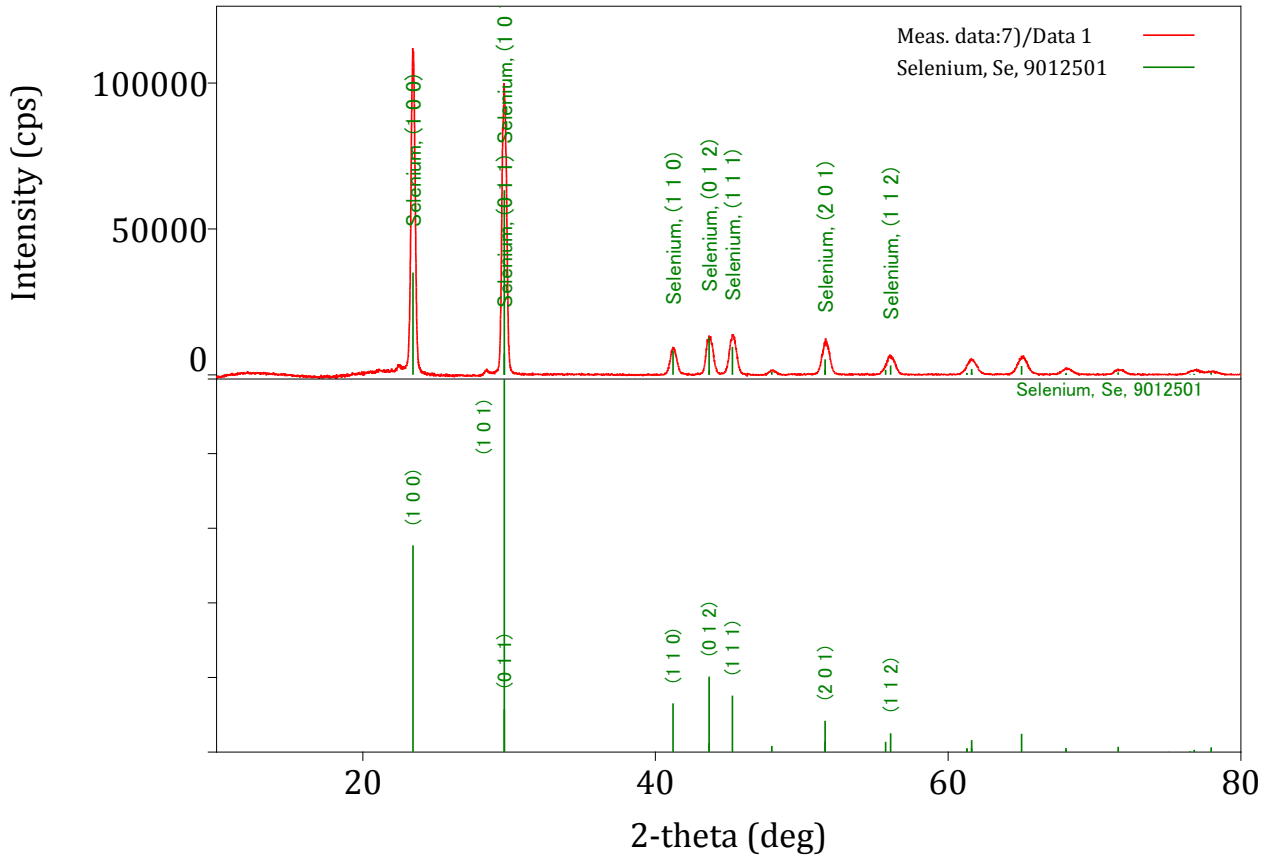

Figure 5.12. [$TaSCl_3(^nBuSeCH_2CH_2CH_2Se^nBu)$] GIXRD of the deposit grown onto SiO_2 substrates (Matched to DB card # 9012501 i.e. elemental selenium).

5.2.3 Attempted synthesis of [$TaSCl_3$(dppe)]

An initial attempt to synthesise [$TaSCl_3$(dppe)] (dppe = $Ph_2P(CH_2)_2PPh_2$) through the addition of one equivalent of dppe to $TaCl_5$, followed by one equivalent of $S(SiMe_3)_2$, in dichloromethane, instead led to the formation of the ionic species $[TaCl_4(dppe)_2][TaCl_6]$. The addition of a dppe solution to the colourless solution of $TaCl_5$ in dichloromethane, caused the solution to turn a vibrant yellow. The subsequent addition of $S(Me_3Si)_2$ did not lead to a further colour change even on prolonged stirring, suggesting no further reaction (in the chalcogenoether chemistry described above the addition of $S(SiMe_3)_2$ led to rapid colour changes). A single crystal was obtained by slow evaporation of a dichloromethane solution of the product, $[TaCl_4(dppe)_2][TaCl_6]\cdot CH_2Cl_2$, Figure 5.13. This structure unambiguously proves the existence of the 8-coordination dodecahedral anion $[TaCl_4(dppe)_2]^+$, despite the steric bulk of the dppe ligand. Elemental analysis (after drying in vacuo) was consistent with the unsolvated species, $[TaCl_4(dppe)_2][TaCl_6]$, and a $^{31}P\{^1H\}$ NMR spectrum showed a single resonance, shifted from free ligand -11.1 ppm, at 41.7 ppm, indicative of the deshielding effect of a phosphorus atom contained within a five-membered chelate

ring.(chem rev Garrou). Infrared spectroscopy confirmed the incorporation of the ligand, from the P-C band at 1091 cm^{-1} and the metal halide from the Ta-Cl band at 324 cm^{-1}.

A follow up experiment reacting one mol. equivalent of $TaCl_5$ with dppe in dichloromethane and isolating the product by concentrating the solution and precipitating a solid with hexane, also gave a yellow powder that was shown by elemental analysis, $^{31}P\{^1H\}$ NMR, ^1H NMR and infrared spectroscopy to be $[TaCl_4(dppe)_2][TaCl_6]$, and as such it was concluded that this was not a viable route to $[TaSCl_3(dppe)]$. The data obtained for $[TaCl_4(dppe)_2][TaCl_6]$ are in good agreement with those described by Jamieson and Lindsell for the complex described as "$[TaCl_5(dppe)]$" and, as such, it is likely they also formed the ionic species.[22] Structural characterisation of this species was imperative to the designation of the speciation provided as elemental analysis, ^1H NMR spectroscopy and $^{31}P\{^1H\}$ NMR spectroscopy alone would not lead to a definitive assignment.

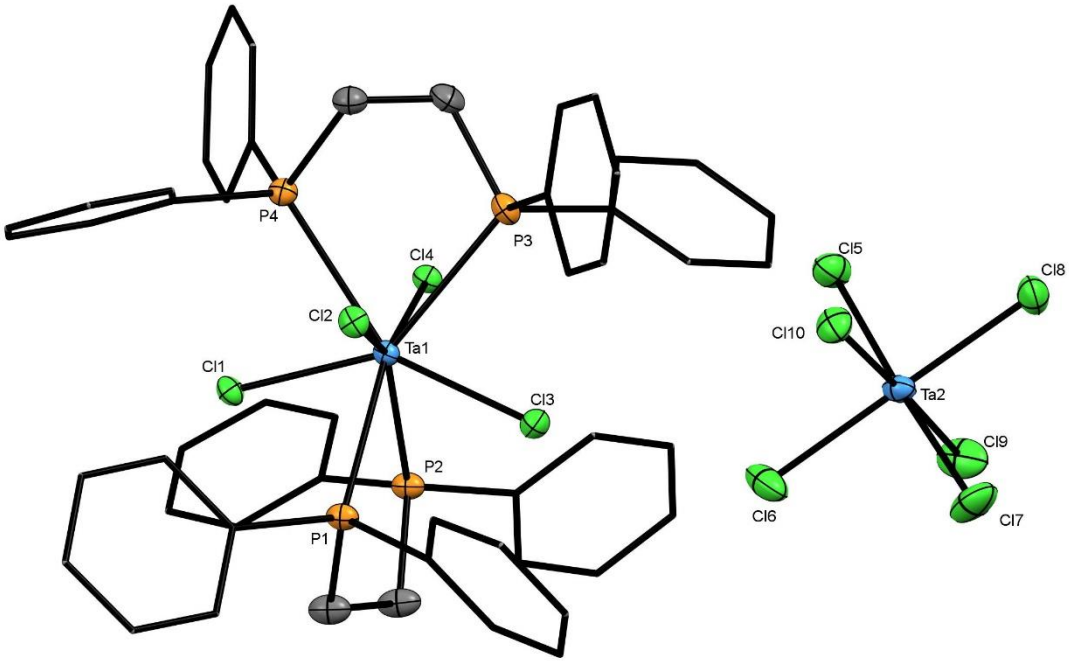

Figure 5.13. A crystal structure of the ionic species, $[TaCl_4(dppe)_2][TaCl_6)]\cdot 0.5CH_2Cl_2$ with atom numbering scheme. Thermal ellipsoids are drawn at the 50% probability level. H atoms and the solvent molecule are omitted, and phenyl rings depicted as wire frames for clarity. Selected bond lengths (Å) and angles (°) are: Ta1–Cl1 = 2.3986(12), Ta1–Cl2 = 2.4034(11), Ta1–Cl3 = 2.3930(11), Ta1–Cl4 = 2.3966(12), Ta1–P1 = 2.7430(13), Ta1–P2 = 2.7488(13), Ta1–P3 = 2.7278(13), Ta1–P4 = 2.7118(13), P1–Ta1–P2 = 72.62(4), P3–Ta1–P4 = 74.84(4), Cl1–Ta1–P1 = 71.89(4), Cl1–Ta1–Cl2 = 97.56(4).

A further experiment was performed in which the $S(SiMe_3)_2$ was added to the stirring solution of $TaCl_5$ first, in order to form the $TaSCl_3$ *in situ*. To this brown solution was added the dppe solution. The solution was stirred for 2 hours then filtered and the resulting brown solution was concentrated and layered with hexane, forming orange crystals. Single crystal X-ray analysis determined these crystals to be $[TaSCl_3(dppe)]\cdot CH_2Cl_2$, Figure 5.14. The crystal shows a *pseudo*-octahedral geometry, with the ligand in the usual *trans* S/Cl position. The Ta=S and Ta-Cl bond lengths are indicative of some S/Cl disorder, as with many of the structures described here. The elemental analysis was also consistent with the formation of $[TaSCl_3(dppe)]$. The Ta=S stretch cannot be unambiguously assigned in the infrared spectrum due to features from dppe present between 480 and 520 cm^{-1}. A $^{31}P\{^1H\}$ NMR spectrum showed a shift from free ligand (-11.1 ppm) to 9.5 ppm, although this is not as large a shift as would usually be expected for a diphosphine complex containing a five-membered chelate ring.[40] There is no evidence of any of the ionic salt, $[TaCl_4(dppe)_2][TaCl_6]$, (41.7 ppm) or $dppeS_2$ (44 ppm)[41] in the solution spectrum. However, $^{31}P\{^1H\}$ NMR experiments at -90 ˚C did not show the expected splitting of the resonance corresponding to the two P environments, suggesting a possible decomposition of the product in solution. As such the solid state data seems consistent with the proposed mononuclear complex, $[TaSCl_3(dppe)]$. The solution data, on the other hand, are more ambiguous and require further study and potentially other examples of similar species, which were beyond the scope of this work.

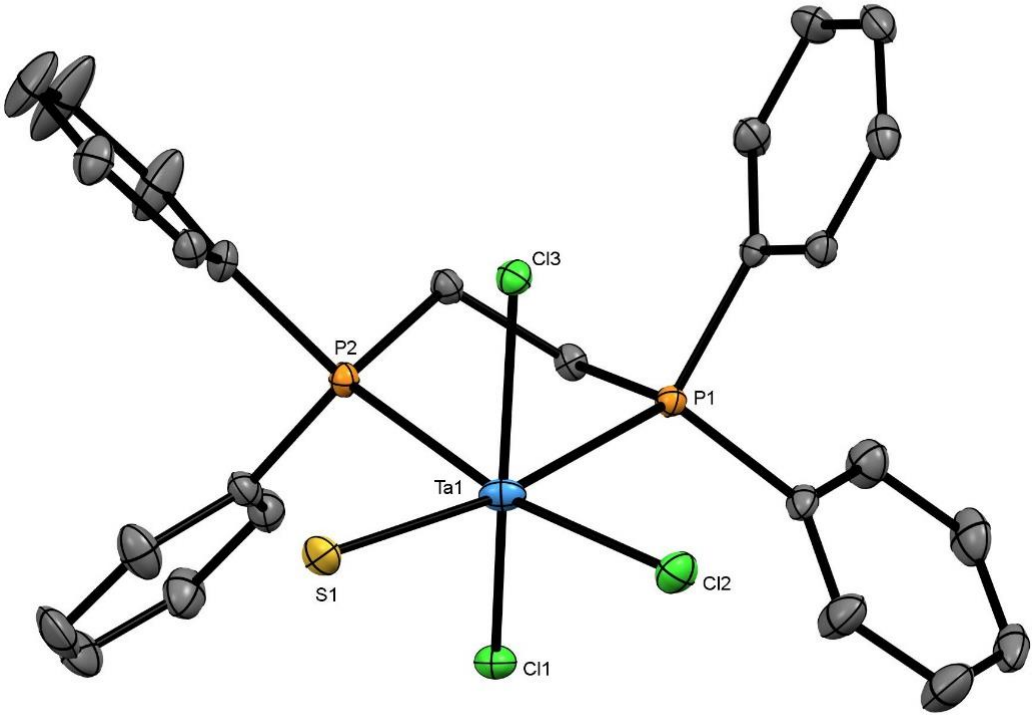

Figure 5.14. A crystal structure of [TaSCl$_3$(dppe)]·CH$_2$Cl$_2$ with the atom numbering scheme. Thermal ellipsoids are drawn at the 50% probability level. Hydrogen atoms and a disordered CH$_2$Cl$_2$ molecule are omitted for clarity. The structure does demonstrate some S/Cl disorder and attempts to model this made little difference to the structure solution. Selected bond lengths (Å) and angles (˚) are: Ta1–Cl1 = 2.3698(6), Ta1-Cl2 = 2.2798(6), Ta1–Cl3 = 2.3398(6), Ta1–S1 = 2.2589(6), Ta1–P1 = 2.7516(6), Ta1–P2 = 2.7201(6), P1–Ta1–P2 = 75.587(18), S1–Ta1–Cl1 = 97.12(2), S1–Ta1–Cl2 = 106.44(2), S1–Ta1–P2 = 88.32(2), S1–Ta1–P1 = 163.69, Cl2–Ta1–P1 = 89.66(2), Cl2–Ta1–P2 = 165.24(2).

The reaction of one mol. equivalent of $TaCl_5$ with dppm in dichloromethane led to the formation of the yellow powdered product, $[TaCl_4(dppm)_2][TaCl_6]$. Yellow crystals were isolated by slow evaporation of a dichloromethane solution, single crystal X-ray diffraction of these confirmed the ionic species, Figure 5.15. A $^{31}P\{^1H\}$ NMR study showed a shift from free ligand (-22.3 ppm) to -9.89 ppm, which is as expected for the four-membered chelating ring.[40] The ^1H NMR spectrum also shows a shift in the methylene protons from 2.83 ppm to 4.83 ppm. Infrared spectroscopy confirmed incorporation of the ligand, with the P-C band at 1094 cm^{-1} and the metal halide with the Ta-Cl band at 327 cm^{-1}, and elemental analysis confirmed the successful formation of $[TaCl_4(dppm)_2][TaCl_6]$.

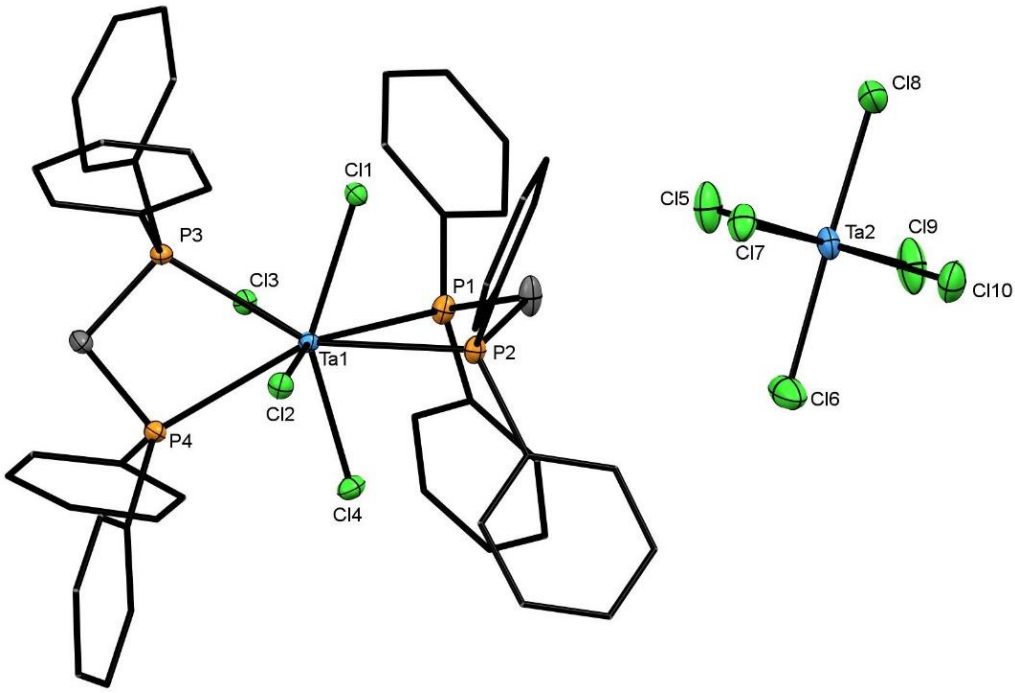

Figure 5.15. A crystal structure depicting the ionic species $[TaCl_4(dppm)_2][TaCl_6]$ with the atom numbering scheme. Only one unit is shown here, with two present in the crystal lattice. Thermal ellipsoids are drawn at the 50% probability level. Hydrogen atoms are omitted and the phenyl rings are shown as wire frames for clarity. A disordered dichloromethane molecule was treated using the SQUEEZE function. Selected bond lengths (Å) and angles (°) are: Ta1–Cl1 = 2.4207(9), Ta1–Cl2 = 2.3887(8), Ta1-Cl3 = 2.3999(8), Ta1–Cl4 = 2.3749(9), Ta1–P1 = 2.6894(10), Ta1–P2 = 2.7251(9), Ta1–P3 = 2.6841(9), Ta1–P4 = 2.7203(9), Ta2–Cl(5-10) = 2.3247(12) – 2.3617(11), P1–Ta1–P2 = 62.19(3), P3–Ta1–P4 = 63.36(3), Cl1–Ta1-Cl2 = 95.49(3), Cl1–Ta1-P1 = 75.27(3), Cl1–Ta1–Cl4 = 146.96(3).

5.3 Conclusions

The successful synthesis of a series of very unusual Ta(V) sulfide trichloride complexes; $[TaSCl_3(L\text{-}L)]$ (L-L = $MeSCH_2CH_2SMe$, $^{i}PrSCH_2CH_2S^{i}Pr$, $PhSCH_2CH_2SPh$, $^{n}BuSCH_2CH_2CH_2S^{n}Bu$, $MeSCH_2CH_2CH_2SMe$, $MeSeCH_2CH_2SeMe$ or $^{n}BuSeCH_2CH_2CH_2Se^{n}Bu$), are described. The products have been analysed with elemental analysis, infrared spectroscopy, ^{1}H NMR and $^{77}Se\{^{1}H\}$ NMR spectroscopy (where applicable). Crystal structures of representative examples, $[TaSCl_3(L\text{-}L)]$ (L-L = $MeS(CH_2)_2SMe$, $^{i}PrS(CH_2)_2S^{i}Pr$, $^{n}BuS(CH_2)_3S^{n}Bu$ or $MeSe(CH_2)_2SeMe$), all of which display distorted octahedral coordination with the bidentate ligand lying *trans* to S/Cl. Except where there is S/Cl disorder evident in the crystal structures, the higher *trans* influence of the sulfide vs. chloride is clearly manifested in the $Ta\text{-}S_{thioether}$ bond distances and the spectroscopic data are in accordance with the solid state structures. The products obtained from similar reactions with the monodentate ligands $E^{n}Bu_2$ (E = S, Se) were irreproducible and could not be identified.

Investigation of the ^{n}Bu-bearing dithioether and diselenoether complexes as potential CVD precursors for tantalum sulfide/selenide thin film growth proved unsuccessful. The thioether regent, $[TaSCl_3\{^{n}BuS(CH_2)_3S^{n}Bu\}]$ resulting in no deposit (contrasting with the corresponding niobium(V) complex, which gave NbS_2 films), while the selenoether complex, $[TaSCl_3\{^{n}BuSe(CH_2)_3Se^{n}Bu\}]$, yielded only elemental selenium. Introducing tantalum in place of niobium has the obvious consequence of increasing the molecular weight of the corresponding complex by 88 a.m.u.. However, this is unlikely to be the major cause of the failure of the Ta(V) complexes to function as CVD reagents for TaS_2, since, based upon the coordination chemistry, the $TaOCl_3$ and $TaSCl_3$ complexes generally appear to be significantly less stable than the niobium analogues, reflecting the harder Lewis acidity of Ta(V).[29,30,32,33,42]

Finally, initial attempts to synthesise $[TaSCl_3(dppe)]$, *via* the addition of dppe to $TaCl_5$ in dichloromethane followed by the addition of $S(SiMe_3)_2$, instead led to the ionic species $[TaCl_4(dppe)_2][TaCl_6]$. This speciation was confirmed by ^{1}H and $^{31}P\{^{1}H\}$ NMR spectroscopy, elemental analysis, infrared spectroscopy and a crystal structure was obtained. The unit cell was confirmed for a number of crystals in the batch. This species was also made by the direct reaction of the dppe ligand with $TaCl_5$ in dichloromethane, as was the analogous species $[TaCl_4(dppm)_2][TaCl_6]$, which was also confirmed by a crystal structure. On changing the order of addition of the starting materials, to first form $[TaSCl_3]$ appeared to give the desired $[TaSCl_3(dppe)]$ complex in the solid state. The speciation was consistent

with the elemental analysis, a Ta=S terminal stretch is present in the infrared spectrum and a single crystal was obtained for the species, confirming a mononuclear pseudo-octahedral formulation. However further experimentation would be required to fully characterise this spectroscopically.

5.4 Experimental

5.4.1 General Experimental

All preparations were carried out under rigorously anhydrous conditions *via* a dry dinitrogen atmosphere and standard Schlenk and glovebox techniques. $TaCl_5$ and $S(Me_3Si)_2$ were obtained from Sigma-Aldrich and used as received. The thioether and selenoether ligands were made as described.[43–46] For further details regarding the instrumentation see Appendix A.

5.4.2 Low Presure CVD Experiments

The selected precursor complex (*ca*. 50 mg) was loaded into the end of a silica tube in an N_2 purged glove box. Then the fused silica substrates (~1 x 8 x 20 mm^3) also were placed along the tube end-to-end. The tube was set in a furnace so that the substrates were in the heated zone and the precursor was *ca.* 2 cm away from the start of the heated zone. The tube was evacuated to 0.5 mm Hg, and the furnace was heated to the requisite temperature between 600 and 800^{o}C. The tube was then moved gradually into the furnace so that the precursor moved closer to the hot zone until it began to evaporate. The position of the sample was then maintained for 2 hours. The tube was then cooled to room temperature and the tiles were unloaded inside a dry N_2-purged glove box, where they were stored for further characterisation.

5.4.3 Analysis of Thin Films

Scanning electron microscopy (SEM) was performed on samples at an accelerating voltage of 15 kV using a Philips XL30 ESEM. Energy dispersive X-ray (EDX) data were obtained with a Thermofisher Ultradry NSS 3. X-Ray diffraction (XRD) patterns were collected in grazing incidence mode (θ_1 = 1°) or in-plane mode (θ_1 = 0.5°, $2\theta_\chi$ scan with the detector scanning in the film plane) using a Rigaku SmartLab diffractometer (Cu-K_α, λ = 1.5418 Å) with parallel X-ray beam and a DTex Ultra 250 1D detector. Phase matching used the PDXL2 software package[47] and diffraction patterns from ICSD.[48]

5.4.4 Tantalum Sulfide Chloride Chalcogenoethers

$[TaSCl_3(PhSCH_2CH_2SPh)]\cdot CH_2Cl_2$ - $TaCl_5$ (0.30 g, 0.84 mmol) was stirred in dichloromethane (5 mL). A solution of $PhSCH_2CH_2SPh$ (0.21 g, 0.84 mmol) in dichloromethane (1 mL) was added and stirred for 2 h, causing a colour change to yellow. $S(Me_3Si)_2$ (0.15 g, 0.84 mmol) dissolved in dichloromethane was then added to the reaction

mixture and stirred for 2 h, giving a dark orange solution. The solvent was removed *in vacuo* and the resulting orange-brown solid was washed with n-hexane (2 mL). Yield: 0.28 g, 59%. Required for $C_{14}H_{14}Cl_3S_3Ta{\cdot}CH_2Cl_2$ (650.7): C, 27.69; H, 2.48 %. Found: C, 27.78, 2.30 %. ^{1}H NMR (CD_2Cl_2): δ = 3.84 (br s, [4H], C***H₂***C***H₂***), 7.37-7.50 (m, [10H], Ph); (203 K): δ = 3.75 (br s, [2H], C***H₂***CH_2), 4.09 (br s, [2H], CH_2C***H₂***), 7.36-7.64 (m, [10H], Ph). IR spectrum (Nujol mull)/cm^{-1}: 519 s, 513 s (Ta=S), 360 br s, 320 m (Ta-Cl).

[TaSCl$_3$(MeSCH$_2$CH$_2$SMe)] - Method 1: $TaCl_5$ (0.30 g, 0.84 mmol) was stirred in anhydrous CH_2Cl_2 (5 mL). A solution of $MeSCH_2CH_2SMe$ (0.11 g, 0.84 mmol) in CH_2Cl_2 (5 mL) was added and the reaction stirred for 30 min., giving a yellow solution immediately on addition of the ligand. $S(SiMe_3)_2$ (0.15 g, 0.84 mmol) dissolved in CH_2Cl_2 (1 mL), was then added to the reaction mixture, causing a colour change from bright yellow to straw coloured with some solid precipitating. The reaction was stirred for a further 16 h, during which time the solid all dissolved and the solution became darker. The solution was filtered and then concentrated and a dark brown solid was precipitated with n-hexane (2 mL), collected by filtration and dried *in vacuo*. Yield 0.24 g, 66 %. Orange crystals were obtained by layering a dichloromethane solution of the product with n-hexane. Required for $C_4H_{10}Cl_3S_3Ta$ (441.3): C, 10.88; H, 2.28 %. Found: C, 11.23; H, 2.65 %. ^{1}H NMR (CD_2Cl_2): δ = 2.27 (s, [3H], Me), 2.89 (s, [3H], Me), 3.08 (br m, [2H], CH_2), 3.47 (br m, [2H], CH_2). IR (Nujol mull)/cm^{-1}: 508 s (Ta=S), 352 s, 327 m (Ta-Cl).

[TaSCl$_3$(*i*PrSCH$_2$CH$_2$S*i*Pr)]- $TaCl_5$ (0.30 g, 0.837 mmol) was stirred in CH_2Cl_2 (5 mL). A solution of ^{i}PrSCH$_2$CH$_2$S^{i}Pr (0.19 g, 0.84 mmol) in CH_2Cl_2 (5 mL) was added and stirred for 16 h, giving a yellow solution. $S(SiMe_3)_2$ (0.15 g, 0.84 mmol) dissolved in CH_2Cl_2 (1 mL) was then added to the reaction mixture and stirred for 2 days, during which the solution turned from yellow to brown to black. The solution was concentrated and the dark solid was precipitated with n-hexane, collected by filtration, washed with n-hexane and dried *in vacuo*. Yield 0.32 g, 77 %. Dark purple crystals were obtained by layering a solution of the product in CH_2Cl_2 with n-hexane. Required for $C_8H_{18}Cl_3S_3Ta$ (497.4): C, 19.30; H, 3.65 %. Found: C, 18.73; H, 3.50 %. ^{1}H NMR (CD_2Cl_2): δ = 1.34 (d, [6H], C***H₃***), 1.61 (d, [6H], C***H₃***), 3.05 (m, [2H], C***H₂***), 3.24 (septet, [1H], C***H***), 3.49 (m, [2H], C***H₂***), 3.58 (septet, [1H], C***H***). IR spectrum (Nujol mull)/cm^{-1}: 509 s (Ta=S), 351 m, 329 s (Ta-Cl).

[TaSCl$_3$(MeSCH$_2$CH$_2$CH$_2$SMe)] - $TaCl_5$ (0.30 g, 0.84 mmol) was stirred in CH_2Cl_2 (5 mL). A solution of $MeSCH_2CH_2CH_2SMe$ (0.115 g, 0.84 mmol) in CH_2Cl_2 (5 mL) was added and stirred for 4 h. The solution turned yellow on addition of the ligand. $S(SiMe_3)_2$ (0.149

g, 0.84 mmol) dissolved in CH_2Cl_2 (1 mL) was then added to the reaction mixture and stirred for 16 h. The solution turned from bright yellow to dark green. Dark green crystals were obtained from a CH_2Cl_2 solution of the product layered with n-hexane. Yield 0.243 g, 64 %. Required for $C_5H_{12}Cl_3S_3Ta$ (455.3): C, 13.18; H, 2.65 %. Found: C, 13.40; H, 2.64 %. ^{1}H NMR (CD_2Cl_2): δ = 2.08 (br s, [3H], C***H₃***), 2.24 (s, [3H], C***H₃***) 2.58 (br s, [2H], C***H₂***), 3.01 (br s, [2H], C***H₂***), 3.32 (br s, [2H], C***H₂***). IR spectrum (Nujol mull)/cm^{-1}: 507 m (Ta=S), 326 br s (Ta-Cl).

[TaSCl$_3$(^{n}BuSCH$_2$CH$_2$CH$_2$S^{n}Bu)]- $TaCl_5$ (0.30 g, 0.84 mmol) was stirred in CH_2Cl_2 (5 mL). A solution of ^{n}BuSCH$_2$CH$_2$CH$_2$S^{n}Bu (0.185 g, 0.84 mmol) in CH_2Cl_2 (5 mL) was added and stirred for 4 h. The solution turned yellow after stirring for 20 mins. $S(SiMe_3)_2$ (0.15 g, 0.84 mmol), dissolved in CH_2Cl_2 (1 mL) was then added to the reaction mixture and stirred for16 h; after 30 mins. the solution had turned from yellow to black. A dark solid was precipitated by the addition of n-hexane, collected by filtration, washed with n-hexane and dried *in vacuo*. Yield 0.211 g, 47 %. Required for $C_{11}H_{24}Cl_3S_3Ta$ (539.8): C, 24.47; H, 4.48 %. Found: C, 24.33; H, 4.70 %. ^{1}H NMR (CD_2Cl_2): δ = 0.91 (m, [3H], C***H₃***), 0.93 (m, [3H], ***CH₃***), 1.41 (vbr, m, [6H], C***H₂***), 1.55 (br, [4H], C***H₂***), 2.51 (m [2H], C***H₂***), 2.59 (br, [2H], C***H₂***), 3.07 (v br [2H], C***H₂***), 3.31 (v br [2H], C***H₂***). IR spectrum (Nujol mull)/cm^{-1}: 508 m (Ta=S), 340 w, 328 br m (Ta-Cl).

[TaSCl$_3$(MeSeCH$_2$CH$_2$SeMe)] - $TaCl_5$ (0.30 g, 0.837 mmol) was stirred in CH_2Cl_2 (5 mL). A solution of MeSeCH$_2$CH$_2$SeMe (0.181 g, 0.837 mmol) in CH_2Cl_2 (5 mL) was added and stirred for 3 h, giving a yellow solution. $S(SiMe_3)_2$ (0.149 g, 0.84 mmol) dissolved in CH_2Cl_2 (1 mL) was then added to the reaction mixture and stirred for 3 h, causing a colour change to brown then black. The solution was concentrated, and a black solid and dark purple crystals were formed by addition of a layer of n-hexane (2 mL). These were collected by filtration and dried *in vacuo*. Yield 0.37 g, 82 %. Required for $C_4H_{10}Cl_3SSe_2Ta.CH_2Cl_2$ (620.35): C, 9.68; H, 1.95 %. Found: C, 9.55; H, 1.94 %. ^{1}H NMR (CD_2Cl_2): δ = 2.15 (s, [3H], C***H₃***), 2.74 (s, [3H], C***H₃***), 3.13 (br m, [2H], CH$_2$C***H₂***), 3.63 (br m, [2H], C***H₂***CH$_2$). ^{77}Se{^{1}H} NMR (CD_2Cl_2): 144 (s, [Se]), 186 (s, [Se]). IR spectrum (Nujol mull)/cm^{-1}: 507 s (Ta=S), 348 m, 326 s (Ta-Cl).

[TaSCl$_3$(^{n}BuSeCH$_2$CH$_2$CH$_2$Se^{n}Bu)]- $TaCl_5$ (0.30 g, 0.84 mmol) was stirred in CH_2Cl_2 (5 mL). A solution of ^{n}BuSeCH$_2$CH$_2$CH$_2$Se^{n}Bu (0.26 g, 0.84 mmol) in CH_2Cl_2 (5 mL) was added and stirred for 4 h. The solution turned yellow after 30 mins. $S(SiMe_3)_2$ (0.15 g, 0.84 mmol) dissolved in CH_2Cl_2 (1 mL) was then added to the reaction mixture and stirred for 16

h, during which the solution turned from yellow to black. The solvent was removed *in vacuo* leaving a dark oil, which was washed with n-hexane and afforded a black solid. Yield 0.28 g, 52 %. Required for $C_{11}H_{24}Cl_3SSe_2Ta.CH_2Cl_2$ (718.5): C, 20.06; H, 3.65 %. Found: C, 19.86; H, 3.67 %. ^{1}H NMR (CD_2Cl_2): δ = 0.93 (t, [6H], C***H*₃**), 1.43 (m, [4H], C***H*₂**), 1.66 (m, [4H], C***H*₂**), 1.99 (br, [2H], C***H*₂**), 2.34 (br, [2H], C***H*₂**), 2.58 (br, [2H], C***H*₂**), 2.62 (br, [2H], C***H*₂**), 3.19 (br, [2H], C***H*₂**). ^{77}Se{^{1}H} NMR (CH_2Cl_2): no resonance. IR spectrum (Nujol mull)/cm^{-1}: 508 s (Ta=S), 331 m, 307 br s (Ta-Cl).

5.4.5 Tantalum Phosphine Complexes

[TaCl$_4$(dppe)$_2$][TaCl$_6$] – $TaCl_5$ (0.100 g, 0.279 mmol) was stirred in CH_2Cl_2 (5 mL). A solution of dppe (0.111 g, 0.279 mmol) in CH_2Cl_2 (5 mL) was added dropwise and the solution turned bright yellow immediately on addition. The solution was concentrated and n-hexane (1 mL) was added to the solution and a bright yellow precipitate formed, which was filtered and dried. Yield 0.171 g, 81 %. Crystals were grown from the slow evaporation of a dichloromethane solution of the product. Required for $C_{52}H_{48}Cl_{10}P_4Ta_2$ (1512.70): C, 41.25; H, 3.20 %. Found: C, 41.38, 3.13 %. ^{31}P{^{1}H} NMR (CD_2Cl_2): δ = 41.7. IR spectrum (Nujol mull)/cm^{-1}: 1095 m (P-C), 324 s (Ta-Cl).

[TaCl$_4$(dppm)$_2$][TaCl$_6$] – $TaCl_5$ (0.100 g, 0.279 mmol) was stirred in CH_2Cl_2 (5 mL). A solution of dppm (0.107 g, 0.279 mmol) in CH_2Cl_2 (5 mL) was added dropwise and the solution turned bright yellow immediately on addition. The solution was concentrated and n-hexane (1 mL) was added the solution and a bright yellow precipitate formed, which was filtered and dried. Yield 0.142 g, 69 %. Required for $C_{50}H_{44}Cl_{10}P_4Ta_2$ (1484.67): C, 40.41; H, 2.99 %. Found: C, 40.45, H, 3.07 %. ^{31}P{^{1}H} NMR (CD_2Cl_2): δ = -9.89. IR spectrum (Nujol mull)/cm^{-1}: 1094 m (P-C), 327 s (Ta-Cl).

[TaSCl$_3$(dppe)]·CH$_2$Cl$_2$ – To a stirring solution of $TaCl_5$ (0.200 g, 0.558 mmol) in CH_2Cl_2 (5 mL) was added $S(Me_3Si)_2$ (0.100 g, 0.558 mmol) dissolved in CH_2Cl_2 (0.5 mL). The mixture became yellow then brown as the solution stirred for 15 minutes. A solution of dppe (0.222 g, 0.558 mmol) in CH_2Cl_2 (5 mL) was added dropwise. The solution turned dark brown on stirring for 30 minutes and a small amount of dark precipitate formed. The reaction mixture was filtered and concentrated and a brown precipitate was formed by adding n-hexane (1 mL) on the concentrated solution, which was filtered and dried *in vacuo*. Yield 0.152 g, 38 %. Orange crystals were obtained from layering a dichloromethane solution of the product with n-hexane. Required for $C_{27}H_{24}Cl_6P_2STa$ (800.32): C, 40.48; H, 3.02 %.

Found: C, 40.26, H, 3.70 %. $^{31}P\{^{1}H\}$ NMR (CD_2Cl_2): δ = 9.5. IR spectrum (Nujol)/cm^{-1}: 1095 w (P-C), 515 s (Ta=S), 312 (Ta-Cl).

Table 5.6 X-ray crystallographic data[a]

Compound	[$TaSCl_3(MeSCH_2CH_2SMe)$]	[$TaSCl_3(MeSeCH_2CH_2SeMe)$]
Formula	$C_4H_{10}Cl_3S_3Ta$	$C_4H_{10}Cl_3SSe_2Ta$
M	441.60	535.40
Crystal system	monoclinic	monoclinic
Space group (no.)	$P2_1$ (4)	$P2_1$ (4)
a /Å	7.22174(15)	7.3780(3)
b /Å	11.36725(15	11.4853(4)
c /Å	7.93897(16)	8.0629(3)
α /°	90	90
β /°	115.595(3)	115.924(5)
γ /°	90	90
U /Å^3	587.77(2)	614.49(5)
Z	2	2
μ(Mo-K_α) /mm^{-1}	10.508	15.635
F(000)	412	484
Total number reflns	5355	12183
R_{int}	0.018	0.030
Unique reflns	2267	2412
No. of params, restraints	102, 1	102, 1
GOF	1.069	1.036
R_1, wR_2 $[I > 2\sigma(I)]$[b]	0.015, 0.034	0.012, 0.030
R_1, wR_2 (all data)	0.015, 0.034	0.012, 0.030

Table 5.6 continued.

Compound	**[TaSCl$_3$(^{i}PrSCH$_2$CH$_2$S^{i}Pr)]**	**[TaSCl$_3$(^{n}BuSCH$_2$CH$_2$CH$_2$S^{n}Bu)]**
Formula	$C_8H_{18}Cl_3S_3Ta$	$C_{11}H_{24}Cl_3S_3Ta$
M	497.70	539.78
Crystal system	monoclinic	tetragonal
Space group (no.)	$P2_1/c$ (14)	$P\,4_1$ (76)
a /Å	8.7703(2)	9.65170(10)
b /Å	9.1766(2)	9.65170(10)
c /Å	19.7147(4)	19.9311(3)
α /°	90	90
β /°	98.565(2)	90
γ /°	90	90
U /Å^3	1568.97(6)	1856.69(5)
Z	4	4
μ(Mo-K$_\alpha$) /mm^{-1}	7.886	6.672
F(000)	952	1048
Total number reflns	32686	40170
R_{int}	0.023	0.071
Unique reflns	3090	3642
No. of params, restraints	140, 0	165, 1
GOF	1.071	1.068
R_1, wR_2 [I > 2σ(I)][b]	0.011, 0.026	0.027, 0.064
R_1, wR_2 (all data)	0.013, 0.026	0.029, 0.065

Table 5.6 continued.

Compound	**$[TaCl_4(dppe)_2][TaCl_6]\cdot 0.5(CH_2Cl_2)$**	**$[TaSCl_3(dppe)]\cdot CH_2Cl_2$**
Formula	$C_{105}H_{98}Cl_{22}P_8Ta_4$	$C_{27}H_{26}Cl_5P_2STa$
M	3111.29	799.29
Crystal system	monoclinic	monoclinic
Space group (no.)	$P2_1/n$ (14)	$P2_1/c$ (14)
a /Å	16.84370(10)	11.3463(2)
b /Å	16.93130(10)	19.4065(2)
c /Å	20.67680(10)	14.4962(2)
α /°	90	90
β /°	101.0780(10)	107.929(2)
γ /°	90	90
U /Å^3	5786.85(6)	3036.94(8)
Z	2	4
μ(Mo-K_α) /mm^{-1}	12.851	4.231
F(000)	3028	1564
Total number reflns	104542	63802
R_{int}	0.0373	0.0382
Unique reflns	10973	5936
No. of params, restraints	640, 0	352, 18
GOF	1.216	1.074
R_1, wR_2 [$I > 2\sigma(I)$][b]	0.034, 0.087	0.020, 0.047
R_1, wR_2 (all data)	0.035, 0.087	0.022, 0.047

Table 5.6 continued.

Compound	**$[TaCl_4(dppm)_2][TaCl_6]$**
Formula	$C_{100}H_{88}Cl_{20}P_8Ta_4$
M	2970.26
Crystal system	monoclinic
Space group (no.)	I2/a (15)
a /Å	25.20060(10)
b /Å	16.42880(10)
c /Å	42.9282(3)
α /°	90
β /°	105.1120(10)
γ /°	90
U /Å^3	17158.32(19)
Z	6
μ(Mo-K$_\alpha$) /mm^{-1}	4.436
F(000)	8640
Total number reflns	182709
R_{int}	0.0519
Unique reflns	16847
No. of params, restraints	822, 0
GOF	1.036
R_1, wR_2 [$I > 2\sigma(I)$][b]	0.029, 0.066
R_1, wR_2 (all data)	0.034, 0.067

[a] Common items: T = 100 K; wavelength (Mo-K$_\alpha$) = 0.71073 Å; θ(max) = 27.5°;

[b] $R_1 = \Sigma||Fo|-|Fc||/\Sigma|Fo|$; $wR_2=[\Sigma w(Fo^2-Fc^2)^2/\Sigma wFo^4]^{1/2}$

5.5 References

1 M. Jura, W. Levason, R. Ratnani, G. Reid and M. Webster, *Dalton Trans.*, 2010, **39**, 883–891.

2 S. L. Benjamin, A. Hyslop, W. Levason and G. Reid, *J. Fluor. Chem.*, 2012, **137**, 76–83.

3 T. Waters and A. G. Wedd, in *Comprehensive Coordination Chemistry II - 4.5 Niobium and Tantalum*, eds. J. A. McCleverty and T. J. Meyer, Elsevier, Amsterdam, 2004, pp. 241–312.

4 S. L. Benjamin, A. Hyslop, W. Levason and M. Webster, *Acta Crystallogr. Sect. C*, 2011, **67**, m221–m223.

5 W. Levason, B. Patel, G. Reid, V. A. Tolhurst and M. Webster, *J. Chem. Soc. Dalton Trans.*, 2000, 3001–3006.

6 S. D. Reid, A. L. Hector, W. Levason, G. Reid, B. J. Waller and M. Webster, *J. Chem. Soc. Dalt. Trans.*, 2007, 4769–4777.

7 R. Hart, W. Levason, B. Patel and G. Reid, *J. Chem. Soc. Dalton Trans.*, 2002, 3153–3159.

8 M. D. Brown, M. B. Hursthouse, W. Levason, R. Ratnani and G. Reid, *Dalton Trans.*, 2004, 2487–2491.

9 M. F. Davis, W. Levason, M. E. Light, R. Ratnani, G. Reid, K. Saraswat and M. Webster, *Eur. J. Inorg. Chem.*, 2007, 1903–1910.

10 M. Jura, W. Levason, R. Ratnani and M. Webster, *Dalton Trans.*, 2010, **2**, 883–891.

11 M. F. Davis, W. Levason, J. Paterson, G. Reid and M. Webster, *Eur. J. Inorg. Chem.*, 2008, 802–811.

12 A. L. Hector, M. Jura, W. Levason, S. D. Reid and G. Reid, *New J. Chem.*, 2008, **33**, 641–645.

13 K. H. Grundy, A. Thompson and F. Fairbrother, *J. Chem. Soc.*, 1965, 765–770.

14 H. Vanni and A. E. Merbach, *Inorg. Chem.*, 1979, **18**, 2758–2762.

15 R. Good and A. E. Merbach, *Inorg. Chem.*, 1975, **14**, 1030–1034.

16 A. E. Merbach, *J. Chem. Soc., Chem. Commun.*, 1974, 163–164.

17 L. G. Hubert-Pfalzgraf, in *Encyclopedia of Inorganic Chemistry*, eds. R. B. King, R. H. Crabtree, C. M. Lukehart, D. A. Atwood and R. A. Scott, American Cancer Society, 2006, p. 3.

18 R. Haiges, P. Deokar and K. O. Christe, *Angew. Chemie Int. Ed.*, 2014, **53**, 5431–5434.

19 F. A. Cotton, L. R. Falvello and R. C. Najjar, *Inorg. Chem.*, 1983, **22**, 770–774.

20 S. L. Benjamin, Y.-P. Chang, C. Gurnani, A. L. Hector, M. Huggon, W. Levason and G. Reid, *Dalton Trans.*, 2014, **43**, 16640–16648.

21 W. Levason, M. E. Light, G. Reid and W. Zhang, *Dalton Trans.*, 2014, **43**, 9557–9566.

22 G. Jamieson and W. E. Lindsell, 1978, **28**, 113–118.

23 L. G. Hubert-Pfalzgraf, M. Postel and J. G. Riess, in *Comprehensive Coordination Chemistry*, eds. G. Wilkinson, R. D. Gillard and J. A. McCleverty, Pergamon, Oxford, 3rd edn., 1987, p. 585.

24 D. A. Rice, *Coord. Chem. Rev.*, 1978, **25**, 199–227.

25 M. G. B. Drew, D. A. Rice and D. M. Williams, *J. Chem. Soc., Dalton Trans.*, 1983, 2251 – 2256.

26 M. G. B. Drew, D. A. Rice, G. W. A. Fowles and R. J. Hobson, 1976, **20**, 35–36.

27 M. G. B. Drew and R. J. Hobson, *Inorg. Chim. Acta*, 1983, **72**, 233–237.

28 A. Bashall, V. C. Gibson, T. P. Kee, M. McPartlin, O. B. Robinson and A. Shaw, *Angew. Chemie Int. Ed.*, 1991, **30**, 1990–1992.

29 Y.-P. Chang, A. L. Hector, W. Levason and G. Reid, *Dalton Trans.*, 2017, **46**, 9824–9832.

30 K. Behzadi and A. Thompson, *J. Less Common Met.*, 1987, **128**, 195–206.

31 V. C. Gibson, A. Shaw and D. N. Williams, *Polyhedron*, 1989, **8**, 549–550.

32 M. G. B. Drew, D. A. Rice and D. M. Williams, *Dalton Trans.*, 1984, 845–848.

33 M. G. B. Drew, D. A. Rice and D. M. Williams, *J. Chem. Soc., Dalton Trans.*, 1983, 2251 – 2256.

34 I. Nowak, E. M. Page, D. A. Rice, A. D. Richardson, R. J. French, K. Hedberg and J. S. Ogden, *Inorg. Chem.*, 2003, **42**, 1296–1305.

35 R. D. Bannister, W. Levason, M. E. Light, G. Reid and W. Zhang, *Polyhedron*, 2019, **167**.

36 A. Noll and U. Müller, *Z. Anorg. Allg. Chem.*, 1999, **625**, 803–805.

37 C. J. Carmalt, T. D. Manning, I. P. Parkin, E. S. Peters and A. L. Hector, *J. Mater. Chem.*, 2004, **14**, 290.

38 A. C. Jones and M. L. Hitchman, *Chemical Vapour Deposition - Chapter 1*, The Royal Society of Chemistry, 2009.

39 Y.-P. Chang, W. Levason, M. E. Light and G. Reid, *Dalton Trans.*, 2016, **5**, 16262–16274.

40 P. E. Garrou, *Chem. Rev.*, 1981, **81**, 229–266.

41 J. Uziel, C. Darcel, D. Moulin, C. Bauduin and S. Jugé, *Tetrahedron: Asymmetry*, 2001, **12**, 1441–1449.

42 R. D. Bannister, W. Levason, G. Reid and F. Robinson, *Polyhedron*, 2019, **169**, 129–134.

43 F. R. Hartley, S. G. Murray, W. Levason, H. E. Soutter and C. A. McAuliffe, *Inorg. Chim. Acta*, 1979, **35**, 265–277.

44 D. J. Gulliver, E. G. Hope, W. Levason, S. G. Murray, D. M. Potter and G. L. Marshall, *J. Chem. Soc., Perkin Trans. II*, 1984, 429–434.

45 C. Gurnani, S. L. Hawken, A. L. Hector, R. Huang, M. Jura, W. Levason, J. Perkins, G. Reid and G. B. G. Stenning, *Dalton Trans.*, 2018, **47**, 2628–2637.

46 C. H. De Groot, C. Gurnani, A. L. Hector, R. Huang, M. Jura, W. Levason and G. Reid, *Chem. Mater.*, 2012, **24**, 4442–4449.

47 S. Grazulis, D. Chateigner, R. T. Downs, A. F. T. Yokochi, M. Quirós, L. Lutterotti, E. Manakova, J. Butkus, P. Moeck and A. Le Bail, *J. Appl. Crystallogr.*, 2009, **42**, 726–729.

48 *ICSD Inorganic Crystal Structure Database Fachinformationszentrum Karlsruhe (FIZ), accessed via the EPSRC funded National Database Service hosted by the Royal Society of Chemistry.*

Chapter 6 Summary and outlook

The work described in this thesis has considerably advanced the coordination chemistry of lanthanide halide and high oxidation state tantalum oxychloride and thiochloride.

The successful synthesis of the lanthanum and lutetium complexes; $[La(dppmO_2)_4]Cl_3$, $[La(dppmO_2)_4][PF_6]_3$, $[La(dppmO_2)_4]I_3$, $[LaCl_3(dppeO_2)_{1.5}]_n$, $[LaCl_2(PPO_2)_2(H_2O)_2]Cl$, $[LaCl_2(PPO_2)_2(H_2O)_2][PF_6]$, $[LuCl_2(dppmO_2)]Cl$, $[LuI_2(dppmO_2)]I$, $[LuCl(dppmO_2)_2(H_2O)][PF_6]_2$, $[LuCl_2(PPO_2)_2]Cl$, $[LuI_2(PPO_2)_2]I$ have been described. This work took an in depth look at the effect of metal ion radius, counter ion and ligand architecture in the resulting speciation of trivalent lanthanide phosphine oxide complexes. The larger lanthanum ion can achieve much greater coordination numbers than the smaller lutetium ion. Whilst $dppmO_2$ readily formed six-membered chelate rings with the lanthanide metal centres, the more flexible $dppeO_2$ instead formed polymeric chains of $[LaCl_3(dppeO_2)_{1.5}]_n$, when reacted with $LaCl_3{\cdot}7H_2O$. In order to produce a seven-membered chelate ring, the more rigid PPO_2 ligand was utilised. The complexes formed through the reaction of lanthanum salts with PPO_2 also formed eight-coordinate species, however only adopted two PPO2 ligands, however due to the size and steric bulk of the ligand, the eight-coordinate geometry is instead achieved with the small monodentate ligands, Cl^- and water.

Further studies into the reaction of lanthanide salts with $dppmO_2$ produced the complex $[Ce(dppmO_2)_4]Cl_3$ and complexes of the form $[LnCl(dppmO_2)_3]Cl_2$ (Ln = Sm, Eu, Gd, Tb, Ho, Yb). These reactions were performed in attempt to study the boundaries in coordination of each of the metal centres. The samarium metal centre is large enough to accommodate four $dppmO_2$ ligands as shown by the crystal structure of $[Sm(dppmO_2)_4]Cl_3$. Elemental analysis of the bulk product, however, suggests a 1:3 ratio of metal to ligand. A crystal structure of $[YbCl(dppmO_2)_3]Cl_2$ shows a seven-coordinate geometry. Addition of excess ligand to a solution of $[YbCl(dppmO_2)_3]Cl_2$ afforded a crystal, which on structure solution was determined to be solvated $[Yb(dppmO_2)_3(H_2O)]Cl_3{\cdot}(dppmO_2)$, which is strong evidence that the metal centre is likely not large enough to accommodate a fourth $dppmO_2$ ligand.

A series of the first examples of Ln(II) phosphine oxide complexes were successfully isolated and characterised. The complexes, $[LnI_2(OPR_3)_4]$ (Ln = Sm, Eu or Yb; R = Me or Ph) and $[EuBr_2(OPR_3)_4]$ (R = Me or Ph), were produced by the reaction of the divalent lanthanide halide with the relevant phosphine oxide in anhydrous MeCN and under an inert

atmosphere. Crystal structures of the octahedral species *cis*-[$EuI_2(OPPh_3)_4$] and *trans*-[$EuBr_2(OPPh_3)_4$] show that both the *cis*- and *trans*- geometries are accessible and are likely a result of crystallisation effects. Infrared spectroscopy indicates the [$LnX_2(OPPh_3)_4$] bulk solid adopts a *cis*- geometry, whereas the [$LnX_2(OPMe_3)_4$] adopt a *trans*- geometry in the bulk. The divalent species are incredibly difficult to handle, readily oxidising to form $[LnX_2(OPR_3)_4]^+$. The successful synthesis of these species indicates that further investigation into Ln(II) complexes with other phosphine oxides, such as $dppmO_2$, $dppeO_2$, PPO_2, or other oxygen donor ligands such as $OAsR_3$ or O_2SR_2 could yield more divalent lanthanide complexes.

A family of lanthanide iodide macrocyclic complexes, of the general form [$LnI_2([18]aneO_4X_2)$] (Ln = Sm or Eu; X = NH, O, S or Se) and [$EuI_2(Me_6[18]aneN_6)$], were synthesised via the addition of the macrocyclic ligand to an acetonitrile solution of EuI_2 or a THF solution of SmI_2. Spectroscopic analysis of the samples was particularly difficult. Though this was in part due to the sensitivity of the compounds to air and moisture, but also the paramagnetic metal centre and a lack of an NMR active nuclei for most species meant NMR spectroscopy was not viable. UV-vis spectroscopy was used to confirm the presence of a divalent metal centre for the powdered products [$EuI_2([18]aneO_4S_2)$], [$SmI_2([18]aneO_4S_2)$] and [$SmI_2([18]aneN_2O_4)$], showing the presence of f-d transitions typical of these divalent lanthanide metal centres. Infrared spectroscopy showed an absence of water and acetonitrile in the bulk solids, whilst elemental analysis was used to confirm the formulation. A crystal structure of $[Eu(Me_6[18]aneN_6)(MeCONH_2)][I]_2 \cdot 3MeCN$ was obtained from a solution of [$EuI_2(Me_6[18]aneN_6)$] in an acetonitrile solution cooled in the freezer, with the acetamide likely formed by adventitious water. These complexes demonstrate the first examples of Eu(II) and Sm(II) selenoethers. Further work towards structural characterisation of these species, along with expanding this series to include examples of other divalent lanthanides, such as Nd(II) or Tm(II) warrants investigation.

Two series of complexes, derived from $TaECl_3$ (E = O or S), with $dppmO_2$, $dppeO_2$, PPO_2 and $OPPh_3$, 1,10-phen and 2,2'-bipy have been synthesised. The crystal structures of show rare octahedral monomeric structures. Also a series of tantalum complexes of the general form [$TaSCl_3$(L-L)], where (L-L) is a neutral chalcogenoether, were successfully synthesised. Although CVD experiments proved ultimately unsuccessful with the given reaction conditions, future work could involve establishing the conditions required to deposit TaS_2 utilising the precursor candidates described within.

Appendix A General Experimental Techniques

Where required all preparations were carried out under rigorously anhydrous conditions *via* a dry dinitrogen atmosphere and standard Schlenk and glovebox techniques. Solvents were dried and degassed prior to use. All commercial reagents (obtained from Sigma-Aldrich or Alfa Aesar) were used as received. THF was distilled over Na/benzophenone ketyl, n-hexane was distilled over over Na wire, CH_2Cl_2 and MeCN were distilled over CaH_2 and MeOH was dried over Mg/I_2.

Infrared spectra were recorded as Nujol mulls between CsI plates using a Perkin-Elmer Spectrum 100 spectrometer over the range 4000–200 cm^{-1}. UV–Vis spectra were recorded from sealed PTFE cell with silica window on neat samples, using the diffuse reflectance attachment, in a Perkin Elmer 750S spectrometer. NMR spectra were recorded on a Bruker AV400 or DPX400 spectrometers. ^{1}H NMR spectra were referenced to the solvent resonances. $^{31}P\{^{1}H\}$ NMR spectra were recorded using a Bruker AV400 spectrometer and are referenced to external 85% H_3PO_4. Microanalyses were undertaken by London Metropolitan University or Medac Ltd.

Data collections for single crystal X-ray analyses used a Rigaku AFC12 goniometer equipped with an enhanced sensitivity (HG) Saturn724 + detector mounted at the window of an FR-E + SuperB- right molybdenum (k = 0.71073) rotating anode generator with VHF Varimax optics (70 micron focus) with the crystal held at 100 K (N_2 cryostream). Structure solution and refinement were performed using SHELX(S/L)97, SHELX-2014/7, H atoms were added and refined with a riding model.[1] Where additional restraints were required, details are provided in the cif file for each structure, or are discussed in the text.

References

1 G. M. Sheldrick, *Acta Crystallogr. Sect. C*, 2015, **71**, 3–8.

Appendix B Crystallographic Information Files

Cif files are located on a CD attached to the back of the thesis.

The filenames correspond to the complexes as follows:

Chapter 2.

$[La(dppmO_2)_4][PF_6]_3 \cdot 2EtOH$	2016rrdb38c
$[LaCl_3(dppeO_2)_{1.5}]_n \cdot EtOH$	rdb31a
$[LaCl(PPO_2)_3][PF_6]_2 \cdot 3.5EtOH \cdot 2.8H_2O$	2016rrdb55
$[LaCl_2(PPO_2)_2(H_2O)(EtOH)]Cl \cdot 3.5EtOH$	2016rrdb54a
$[Ce(dppmO_2)_4]Cl_3 \cdot 4H_2O$	RDBCe2
$[YbCl(dppmO_2)_3]Cl_2$	RDB203E
$[Yb(dppmO_2)_3(H_2O)]Cl_3 \cdot dppmO_2$	RDBybL4
$[LuCl_2(PPO_2)_2]Cl$	2016rrdb79

Chapter 3.

$[EuBr_2(OPPh_3)_4]$	RDB172Eu1
$[EuI_2(OPPh_3)_4] \cdot MeCN$	2017kRDB116_twin1_hklf4
$[EuI_2(OPPh_3)_4][I_3]$	RDBEuI2OPPh3I3
$[Eu(Me_6[18]aneN_6)(MeCONH_2)]3I \cdot 3MeCN$	RDB33

Chapter 4

$[TaOCl_3(1,10\text{-phen})]$	TaOCl3phen
$[TaOCl_3(PPO_2)]$	TaOCl3PPO2
$[TaOCl_3(OPPh_3)_2]$	TaOCl3OPPh3
$[TaSCl_3(MeCN)_2]$	TaSCl3(MeCN)2
$[TaSCl_3\,(1,10\text{-phen})]$	TaSCl3phen
$[Cl_3(1,10\text{-phen})Ta(\mu\text{-}O)Ta(1,10\text{-phen})Cl_3].2CH_2Cl_2$	Ta2Cl6O(phen)2
$[TaSCl_3\,(dppeO_2)]$	TaSCl3dppeO2
$[TaSCl_3\,(OPPh_3)_2]$	TaSCl3OPPh3

Chapter 5

$[TaSCl_3(MeSCH_2CH_2SMe)]$	TaSCl3dithiahexane
$[TaSCl_3(MeSeCH_2CH_2SeMe)]$	TaSCl3MeSeC2SeMe
$[TaSCl_3(^{i}PrSCH_2CH_2S^{i}Pr)]$	TaSCl3iPrSC2SiPr
$[TaSCl_3(^{n}BuSCH_2CH_2CH_2S^{n}Bu)]$	TaSCl3nBuSC3
$[TaCl_4(dppe)_2][TaCl_6]\cdot 0.5(CH_2Cl_2)$	RDB171
$[TaSCl_3(dppe)]\cdot CH_2Cl_2$	RDB206a
$[TaCl_4(dppm)_2][TaCl_6]$	RDB210_sq